AD-A061 404 ARMY ENGINEER WATERWAYS EXPERIMENT STATION VICKSBURG MISS F/G 8/6
STUDY OF CLAY SHALE SLOPES ALONG THE PANAMA CANAL. SUPPLEMENTAL--ETC(U)
AUG 78 D C BANKS

UNCLASSIFIED WES-TR-S-70-9 NL

1 OF 3
ADA
061404

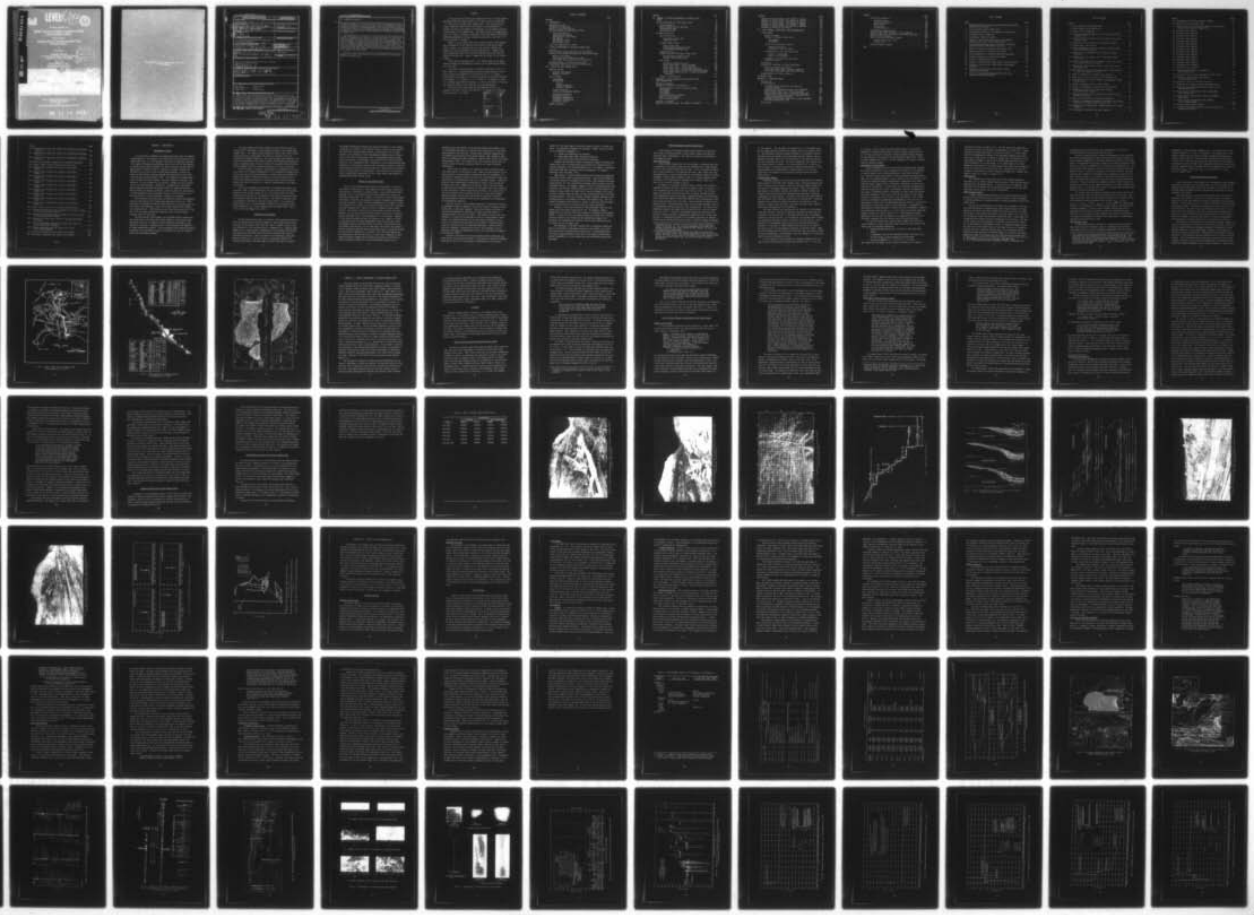

LEVEL II

TECHNICAL REPORT S-70-9

STUDY OF CLAY SHALE SLOPES ALONG THE PANAMA CANAL

Supplemental Report

A REANALYSIS OF THE EAST CULEBRA SLIDE PANAMA CANAL

by

Don C. Banks

Geotechnical Laboratory
U. S. Army Engineer Waterways Experiment Station
P. O. Box 631, Vicksburg, Miss. 39180

August 1978
Supplemental Report to a Series

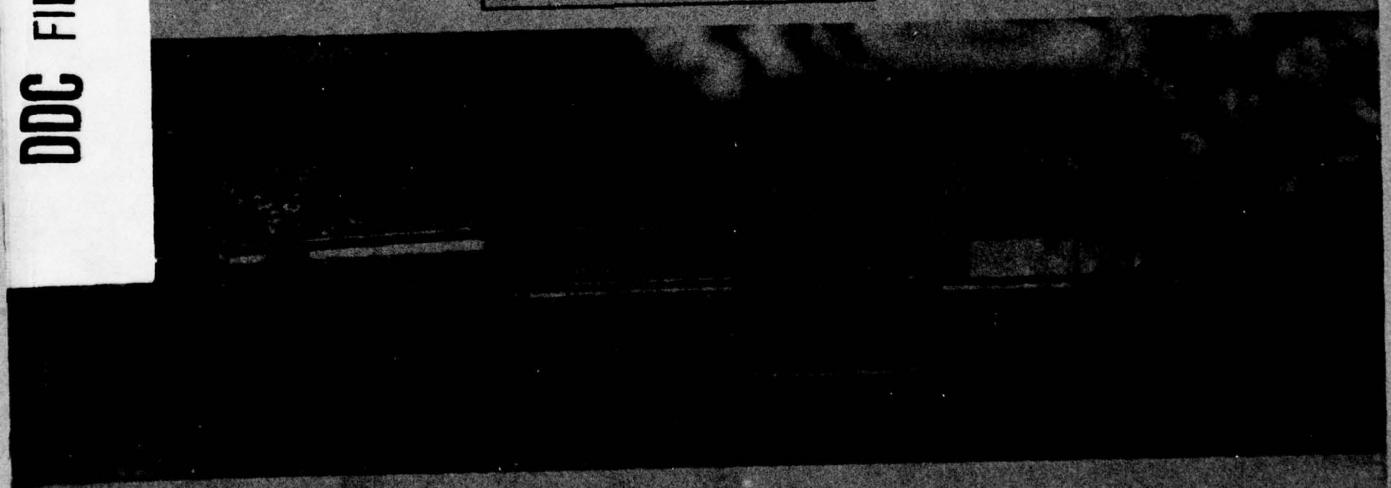

Prepared for Office, Chief of Engineers, U. S. Army
Washington, D. C. 20314
and
The Panama Canal Company, Balboa Heights, Canal Zone

Destroy this report when no longer needed. Do not return
it to the originator.

Unclassified

SECURITY CLASSIFICATION OF THIS PAGE (When Data Entered)

REPORT DOCUMENTATION PAGE

READ INSTRUCTIONS BEFORE COMPLETING FORM

1. REPORT NUMBER: Technical Report S-70-9
2. GOVT ACCESSION NO.:
3. RECIPIENT'S CATALOG NUMBER:

4. TITLE (and Subtitle): STUDY OF CLAY SHALE SLOPES ALONG THE PANAMA CANAL; Supplemental Report, A REANALYSIS OF THE EAST CULEBRA SLIDE, PANAMA CANAL.

5. TYPE OF REPORT & PERIOD COVERED: Supplemental report to a series

6. PERFORMING ORG. REPORT NUMBER:

7. AUTHOR(s): Don C. Banks

8. CONTRACT OR GRANT NUMBER(s):

9. PERFORMING ORGANIZATION NAME AND ADDRESS:
U. S. Army Engineer Waterways Experiment Station
Geotechnical Laboratory
P. O. Box 631, Vicksburg, Miss. 39180

10. PROGRAM ELEMENT, PROJECT, TASK AREA & WORK UNIT NUMBERS:

11. CONTROLLING OFFICE NAME AND ADDRESS:
Office, Chief of Engineers, U. S. Army
Washington, D. C. 20341 and The Panama Canal Company, Balboa Heights, Canal Zone

12. REPORT DATE: August 1978

13. NUMBER OF PAGES: 260

14. MONITORING AGENCY NAME & ADDRESS (if different from Controlling Office): Technical Reports

15. SECURITY CLASS. (of this report): Unclassified

15a. DECLASSIFICATION/DOWNGRADING SCHEDULE:

16. DISTRIBUTION STATEMENT (of this Report)

Approved for public release; distribution unlimited.

12 265 p.

17. DISTRIBUTION STATEMENT (of the abstract entered in Block 20, if different from Report)

14 WES-TR-S-70-9

18. SUPPLEMENTARY NOTES

19. KEY WORDS (Continue on reverse side if necessary and identify by block number)

Clay shales	Shear strength
East Culebra Slide	Slides
Panama Canal	Slope failures

20. ABSTRACT (Continue on reverse side if necessary and identify by block number)

This report was previously submitted (April 1978) by the author to the University of Illinois in partial fulfillment or requirements for the degree of Doctor of Philosophy in Civil Engineering. The reported work was conducted as an adjunct study to a long-term and broad effort entitled "Study of Clay Shale Slopes Along the Panama Canal" conducted by personnel of the U. S. Army Engineer Waterways Experiment Station under the author's supervision. The work consists of a documentation of a case history in which the (Continued)

DD FORM 1 JAN 73 1473 EDITION OF 1 NOV 65 IS OBSOLETE

Unclassified

SECURITY CLASSIFICATION OF THIS PAGE (When Data Entered)

20. ABSTRACT (Continued).

CONT'

occurrence and nature of initial failures or "breaks" were described and pinpointed with respect to time, location, and extent; the geological setting and groundwater conditions were described; physical tests, with emphasis on laboratory determination of strength parameters, were conducted; and back analyses were conducted along nine cross sections constructed through six initial breaks to compare the required field strength parameters with parameters determined in laboratory tests.

The importance of the study lies in the conclusion that the initiation of the East Culebra Slide is an example of a first-time failure of a slope, comprised of clay shale strata, that failed during construction or under short-term conditions. The significance of the study lies in the agreement of the strength parameters determined by back analyses with parameters determined from tests on slickensided samples of Cucaracha clay shale. In particular, it is shown that required strength parameters operative at the time of the initial breaks compared favorably with laboratory determined parameters that described the effective peak shear strength of undisturbed slickensided specimens taken from Cucaracha clay shale strata.

Important results and conclusions from this Supplemental Report as well as Reports 1, 2, and 3 of the series will be presented in Report 4, which summarizes the overall study.

PREFACE

The study described herein was conducted at the U. S. Army Engineer Waterways Experiment Station (WES) for the Office, Chief of Engineers, U. S. Army, and the Panama Canal Company (PCC). This report was previously submitted (April 1978) by the author to the University of Illinois in partial fulfillment of requirements for the degree of Doctor of Philosophy in Civil Engineering. The report, which is a supplemental report to a series, presents a reanalysis of the East Culebra Slide with particular emphasis on strength parameters operative at the time of the initial failures or "breaks."

Report 1 of the series deals with the major activity and engineering considerations of the East and West Culebra Slides and the Model Slope. Report 2 is concerned with the slide history, geology, and mechanics of slide development along the Gaillard Cut. Report 3 presents engineering studies of clay shale materials and slope stability along the Gaillard Cut. Report 4 summarizes the results of the overall studies.

This report was prepared by Dr. D. C. Banks, Chief of the Engineering Geology and Rock Mechanics Division of the Geotechnical Laboratory (GL), WES.

The work was performed under the general supervision of Mr. J. P. Sale, Chief, GL. Valuable guidance was given during planning, conduct of the study, and preparation of the report by Mr. S. J. Johnson, former Special Assistant, GL. Detailed technical direction was provided by Professors A. J. Hendron, Jr., A. S. Nieto, H. O. Ireland, G. Mesri, E. J. Cording, and Professor Emeritus R. B. Peck, University of Illinois, who served as members of the Committee on Final Examination.

Directors of the WES during the investigation were BG E. D. Peixotto, CE, COL G. H. Hilt, CE, and COL J. L. Cannon, CE. Technical Director was Mr. F. R. Brown.

TABLE OF CONTENTS

CHAPTER		Page
I:	INTRODUCTION	1
	Background of Study	1
	Definition of Clay Shale	2
	Failure of Clay Shale Slopes	3
	Previous Analyses of East Culebra Slides	6
	Third Lock Studies	6
	Isthmian Canal Studies	7
	Development of slope charts	8
	MIT analysis	9
	WES analyses (1970)	9
	WES analyses (1975)	10
	Scope and Organization of Study	11
II:	INITIAL DEVELOPMENT OF THE EAST CULEBRA SLIDE	17
	Location	18
	Slide Activity During Construction by the French	18
	Slide Activity During Construction by the United States	20
	Nature of the breaks	20
	Slide dates from literature accounts	22
	Slide dates from construction cross sections	24
	Excavation Rates at the East Culebra Slide	29
	Slope-Height Relations at the East Culebra Slide	30
III:	GEOLOGY OF EAST CULEBRA SLIDE	45
	Regional Geology	45
	Regional stratigraphy	45
	Regional structure	46
	Local Geology	46
	Physiography	47
	Stratigraphy	47
	General	47
	Culebra formation	48
	Cucaracha formation	48
	Primary structure	51
	Joint and slickensided features	52
	Groundwater Conditions	55
	Boring observations	56
	Piezometer observations	58
	Piezometer installations	58
	Piezometer results	58
	Summary statement	60

CHAPTER Page

IV: SUMMARY OF PHYSICAL PROPERTIES OF CUCARACHA CLAY SHALE 97

General Properties and Consolidation Data 98

Slaking behavior 98
Water contents and dry densities 98
Classification data 99
Consolidation data 100

Strength Properties 101

Third Locks Study 102

Field direct shear tests 103
Laboratory tests 104

Isthmian Canal Studies 105

Direct shear tests 105
Unconsolidation-undrained tests 105
Consolidated-undrained tests 106

Hodges Hill Study 106
Atlantic-Pacific Interoceanic Canal Study 107

Unconsolidated-undrained tests 107
Residual direct shear tests 107

WES studies 107

Unconfined compression tests 108
Direct shear tests - precut specimens 108
Direct shear tests - intact specimens 108
Direct shear tests - slickensided specimens 109
Direct shear tests - slurry-consolidated specimens. . 110
Consolidated-undrained tests - slurry-consolidated specimens 110

Summary of strength data 111

V: ANALYSES OF INITIAL BREAKS AT THE LOCATION OF THE EAST CULEBRA SLIDE 125

Methods of Analyses 126
Assumptions Involved in the Analyses 128

Slope geometry at time of individual break. 128
Stratigraphy 128
Groundwater 128
Unit weights 129
Location of failure surfaces 129
Base of resistive wedge 129
Base of active wedge 129

Approach of Analyses 130
Analysis of Initial Break - Sta 1938+10 to 1940+60 136

CHAPTER Page

Analysis of Initial Break - Sta 1940+60 to 1944+10 138
Analysis of Initial Break - Sta 1944+10 to 1947+60 139
Analysis of Initial Break - Sta 1947+60 to 1949+60 140
Analysis of Initial Break - Sta 1949+60 to 1956+60 141
Analysis of Initial Break - Sta 1956+60 to 1960+60 144
Discussion of Results of Analyses 145

VI. STUDY SUMMARY, CONCLUSIONS, AND RECOMMENDATIONS 176

Study Summary 176

Nature of breaks 176
Geology of the East Culebra Slide 177

Stratigraphy 178
Groundwater 178

Nature of the Cucaracha formation 179

General description 179
Properties of the clay shale 180

Slickensiding in the clay shale strata 180

Origin of slickensides 180
Extent of slickensides 181

Strengths of the Cucaracha clay shale 181
Stability analyses 182

Conclusions 183
Application of Results to Future Excavations 186

Slides on preexisting surfaces 186
First-time slides under long-term conditions 186
First-time slides under short-term conditions 188

Recommendations for Future Research 188

LITERATURE CITED 191

APPENDIX A: LABORATORY TESTS 198

Introduction 198
Test Procedures 198

Atterberg limits, grain-size, and specific gravity analyses 198
Consolidation and swell pressure tests (combined) 199
Drained direct shear tests, intact specimens 201
Drained direct shear tests, slickensided specimens . . . 201
Drained direct shear and triaxial compression tests, slurry-consolidated specimens 202
Repeated drained direct shear tests, precut specimens . . 203
Unconfined compression tests 204

Test Results 204

CHAPTER Page

Descriptive properties 205

Atterberg limits. 205
Grain-size analyses 206
Water content 206
Dry density 206
Specific gravity 206

Consolidation characteristics 206
Effective peak shear strengths, intact specimens 207
Effective peak shear strengths, slickensided specimens . . 208
Residual shear strengths 209
Tests on slurry-consolidated samples 210

Drained direct shear tests 210
Triaxial tests 211

Undrained shear strengths 211

VITA 250

LIST OF TABLES

Table		Page
1	Geological Factors Controlling Slope Stability and Their Engineering Consequence	13
2	Dates of Breaks, East Culebra Slide	32
3	Stratigraphic Relations of Formations in Gaillard Cut	62
4	Piezometer Data in Study Area	63
5	Piezometers, Hodges Hill Area	64
6	Results of Field Direct Shear Tests, Slickensided Cucaracha Clay Shale, Third Locks Project	113
7	Consolidated-Undrained Tests on Cucaracha Clay Shale, Harvard University 1948 (Second Series)	114
8	Results of Stability Analyses, East Culebra Slide	149
9	Average Properties of Cucaracha Clay Shale	190
A1	Test Assignments for Cucaracha Clay Shale Specimens	212
A2	General Properties of Cucaracha Clay Shale	213
A3	Results of Consolidation Tests	214
A4	Results of Drained Direct Shear Tests, Intact Specimens	215
A5	Results of Drained Direct Shear Tests, Slickensided Specimens	216
A6	Results of Drained Direct Shear Tests, Slurry-Consolidated Specimens	217
A7	Results of Consolidated-Undrained Triaxial Tests, Slurry-Consolidated Specimens	218

LIST OF FIGURES

Figure		Page
1	Map of Canal Zone and Panama Canal	14
2	Slide locations along Gaillard Cut	15
3	General plan of study area	16
4	A view of the eastern bank of the Cut north of Gold Hill (December 1904)	33
5	A view of the eastern bank of the Cut north of Gold Hill (February 1907)	34
6	Construction cross section at sta 1952+60 (1785+00)	35
7	Planned Canal cross section	36
8	Slope configuration by years, from end of 1905 through 1913 at selected stations	37
9	Positions of the elevation 260- and 200-ft contours with time	38
10	A slide on the east bank of the Cut opposite Culebra (June 1910)	39
11	A mound of upheaval, 18 ft in height, in the floor of the Cut, north of Gold Hill (1910)	40
12	Break in east bank opposite Culebra, view to the south (February 1912)	41
13	East Culebra Slide area indicating break in bank adjacent to Gold Hill (February 11, 1912)	42
14	Areas of excavation at selected cross sections	43
15	Slope chart for initial failure, East Culebra Slide	44
16	Surface profiles at various stages of development of East Culebra Slide	65
17	Original topography at East Culebra (1884)	66
18	Geology and topography at East Culebra Slide (1908)	67
19	Geological sections at sta 1950+10 and 1952+60 (sta 1782+50 and 1785+00)	68
20	Geological sections below original ground surface along French center line	69
21	Logs of recent borings into Cucaracha formation	70
22	Composite stratigraphic columns for Cucaracha (and Culebra) formations in Culebra Reach (Gaillard Cut)	71
23	Detailed section through East Culebra Slide at sta 1957+60 (1790+00)	72
24	Photographs of Cucaracha clay shale samples	73

Figure		Page
25	Radiographs of Cucaracha clay shale samples	74
26	Yearly and monthly rainfall data	75
27	Composite plot of recorded water levels in open borings, east and west sides of Panama Canal	76
28	Piezometer data, WEC-P1A	77
29	Piezometer data, WEC-P1B	78
30	Piezometer data, WEC-P1C	79
31	Piezometer data, WEC-P1D	80
32	Piezometer data, WEC-P1E	81
33	Piezometer data, WEC-P1F	82
34	Piezometer data, WMS-P1A	83
35	Piezometer data, WMS-P1B	84
36	Piezometer data, WMS-P1C	85
37	Piezometer data, WMS-P1D	86
38	Piezometer data, WMS-P1E	87
39	Piezometer data, WMS-P1F	88
40	Piezometer data, WCSE-P1A	89
41	Piezometer data, WCSE-P1B	90
42	Piezometer data, WCSE-P1C	91
43	Piezometric head profile, piezometers in East Culebra Slide	92
44	Piezometric head profile, piezometers in Model Slope	93
45	Piezometric head profile, piezometers in South Cucaracha Slide	94
46	Piezometric levels in Cucaracha formation	95
47	Comparison of piezometric levels and water levels	96
48	Boring log and classification data, boring 14-D-37, East Culebra Slide	115
49	Boring log and classification data, boring WEC-1, East Culebra Slide	116
50	Boring log and classification data, boring WMS-1, Model Slope	117
51	Boring log and classification data, WCSE-1, South Cucaracha Slide	118
52	Drained residual shear strength	119
53	Effective peak shear strength for intact specimens of Cucaracha clay shale	120

Figure		Page
54	Effective peak shear strength for slickensided specimens of Cucaracha clay shale	121
55	Effective peak shear strength for slurry-consolidated specimens of Cucaracha clay shale	122
56	Results of $\overline{R}$ triaxial compression tests for slurry-consolidated specimens of Cucaracha clay shale	123
57	Summary of strength data - Cucaracha clay shale	124
58	Method of analyses for initial breaks	150
59	Conditions surrounding the May 1908 break at sta 1944+60 (1777+00)	151
60	Investigation of magnitude of effective interwedge force E'_{a-n} for initial break (May 1908) at sta 1944+60 (1777+00) (α_n = 24 deg; δ = 10 deg; α = 45 deg)	152
61	Investigation of magnitude of effective interwedge force E'_{a-n} for initial break (May 1908) at sta 1944+60 (1777+00) (α_n = 24 deg; δ = 10 deg; α = 30 deg)	153
62	Investigation of the effect of varying angle of inclination (δ) of effective interwedge force E'_{a-n} for initial break (May 1908) at sta 1944+60 (1777+00) (α_n = 24 deg; α = 45 deg)	154
63	Investigation to determine required angle of obliquity, α_n, assuming vertical water-fill cracks intersecting bedding planes for initial break (May 1908) at sta 1944+60 (1777+00)	155
64	Investigation to determine required angle of obliquity, α_a, for different base plans of active wedge for initial break (May 1908) at sta 1944+60 (1777+00)	156
65	Results of analyses for initial break (May 1908) at sta 1944+60 (1777+00)	157
66	Conditions surrounding the December 1909 break at sta 1939+60 (1772+00)	158
67	Results of analyses for initial break (December 1909) at sta 1939+60 (1772+00)	159
68	Conditions surrounding the January 1909 break at sta 1942+60 (1775+00)	160
69	Results of analyses for initial break (January 1909) at sta 1942+60 (1775+00)	161
70	Conditions surrounding the May 1908 break at sta 1946+10 (1778+50)	162
71	Results of analyses for initial breaks (May 1908) at sta 1946+10 (1778+50)	163

Figure		Page
72	Conditions surrounding the January 1909 break at sta 1948+60 (1781+00)	164
73	Results of analyses for initial break (January 1909) at sta 1948+60 (1781+00)	165
74	Conditions surrounding the January 1912 break at sta 1950+10 (1782+50)	166
75	Results of analyses for initial break (January 1912) at sta 1950+10 (1782+50)	167
76	Conditions surrounding the January 1912 break at sta 1952+60 (1785+00)	168
77	Results of analyses for initial break (January 1912) at sta 1952+60 (1785+00)	169
78	Conditions surrounding the January 1912 break at sta 1955+10 (1787+50)	170
79	Results of analyses for initial break (January 1912) at sta 1955+10 (1787+50)	171
80	Conditions surrounding the September-November 1908 break at sta 1958+60 (1791+00)	172
81	Results of analyses for initial break (September-November 1908) at sta 1958+60 (1791+00)	173
82	Required shear strength along bedding, initial breaks, East Culebra Slide	174
83	Required shear strength across bedding, initial breaks, East Culebra Slide	175
A1	Plasticity chart	219
A2	Drained direct shear tests: examples of time-compression curves for intact specimens, Series B	220
A3	Drained direct shear test results for intact specimens, Series A and B	221
A4	Drained direct shear test results for intact specimens, Series C	222
A5	Drained direct shear test results for intact specimens, Series C, concluded	223
A6	*Effective peak shear strength for intact specimens*	224
A7	Time-compression curves for slickensided specimens, Series D	225
A8	Time-compression curves for slickensided specimens, Series E	226
A9	Time-compression curves for slickensided specimens, Series F	227

Figure		Page
A10	Drained direct shear test results for slickensided specimens, Series D	228
A11	Drained direct shear test results for slickensided specimens, Series E	229
A12	Drained direct shear test results for slickensided specimens, Series F	230
A13	Effective peak shear strength for slickensided specimens.	231
A14	Change in water content during direct shear tests	232
A15	Residual shear strength test results, boring WEC-1, Sample 5	233
A16	Residual shear strength test results, boring WEC-1, Sample 6	234
A17	Residual shear strength test results, boring WEC-1, Sample 10	235
A18	Residual shear strength test results, boring WMS-1, Sample 4	236
A19	Residual shear strength test results, boring WMS-1, Sample 6	237
A20	Residual shear strength test results, boring WMS-1, Sample 10	238
A21	Residual shear strength test results, boring WMS-1, Sample 12	239
A22	Residual shear strength test results, boring WMS-1, Sample 14	240
A23	Residual shear strength test results, boring WCSE-1, Sample 8	241
A24	Water content profile for slurry-consolidated sample	242
A25	Scanning electron microscope photograph of horizontal surface of slurry-consolidated sample	243
A26	Scanning electrom microscope photograph of vertical surface of slurry-consolidated sample	244
A27	Drained direct shear test results for slurry-consolidated specimens	245
A28	Effective peak shear strength for direct shear tests on slurry-consolidated specimens	246
A29	Triaxial compression test ($\overline{R}$) results for slurry-consolidated specimens	247
A30	Unconfined compression test results, boring WEC-1	248
A31	Unconfined compression test results, boring WMS-1	249

CHAPTER I: INTRODUCTION

Background of Study

In the history of mankind, few engineering feats rival the singular accomplishment of the joining of the Atlantic and Pacific Oceans via the Panama Canal (Fig. 1). The opening of the Canal to commercial shipping on 15 August 1914 marked a significant point in the life of the project--a project that had been envisioned for almost 400 years and had required approximately 35 years of labor to complete; a project in which over 232 million cu yd of soil and rock had been excavated; a project in which over $675 million had been expended and during which over 12,000 lives had been sacrificed (Mack, 1944). The opening of the Canal signified a triumph over many problems - political, medical, financial, and technical - but the opening did not signify a triumph over the long nemesis of the Canal builders - landslides. Throughout the construction period numerous landslides had plagued efforts to complete the Canal. Even following the opening, landslides closed the Canal for short periods of time necessitating the additional removal of over 50 million cu yd of slide material to date to maintain a channel for shipping.

Both during and following Canal construction the most consequential slides occurred within the 8.5-mile-long Gaillard Cut (Fig. 2). While more than 50 individual slides have been identified, the largest and, for that reason, most important slides are the East Culebra, West Culebra, and Cucaracha Slides. These Slides occurred near the deepest part of the Cut in the Cucaracha and Culebra formations, both of which contain numerous strata of clay shale.

The East Culebra, West Culebra, and Cucaracha Slides occurred during construction of the Canal and caused changes in construction plans, additional costs for the removal of slide material, and delays in the opening of the Canal. Continued motion of slide material has impeded or at times stopped Canal traffic. Such consequences have required continued observation of slope behavior along the Gaillard Cut, and, as required, additional maintenance dredging.

The understanding of factors leading to slope failures along the Gaillard Cut is important to the operating officials of the Panama Canal Company (PCC). For example, large cracks and fissures have been recently observed along the slopes where the Canal cuts through or into the Cucaracha and Culebra formations. But, more broadly, case histories, such as the one contained in this thesis, provide the engineering profession a means of gaining insight into the behavior of clay shale slopes with particular emphasis upon the strengths operative at the time of failure.

Previous studies, referenced appropriately in subsequent portions of this thesis, have provided documentation of the engineering geology of the area as well as the history and nature of sliding along the Gaillard Cut. While these studies contained descriptions of the East Culebra, West Culebra, and Cucaracha Slides, the descriptions were broad and did not present the detail necessary for a complete understanding of the important slides.

This thesis documents and evaluates the engineering geology, construction events, field observations, and test results and also provides analyses of the initial failure of one of the large slides. The East Culebra Slide was chosen as the subject of this thesis because more data were available than for the other slides. The thesis concentrates upon the initiation of failure at the East Culebra Slide, i.e., during the period 1908 to 1912. The development from 1912 to the present is presented elsewhere, e.g., Binger (1948); Lutton and Banks (1970); Lutton et al. (1975); and Banks et al. (1975).

Definition of Clay Shale

The East Culebra Slide (Fig. 3) occurred in the Cucaracha formation, which is underlain by the Culebra formation. Both formations have been described as clay shales (PCC, 1942; PCC, 1947). However, since no precise definition of the term clay shale is available (e.g., Johnson, 1969; Gamble, 1971), indiscriminate comparisons of the Cucaracha (and Culebra) clay shales with materials called clay shales elsewhere may result in misleading conclusions. While the nature of the materials, along with physical properties, is given in detail in subsequent chapters, the Cucaracha and Culebra clay shales may be briefly described as follows.

The bedded Cucaracha and Culebra clay shales are Middle to Late Tertiary in age and, as a result of the intense volcanic activity in the region at that time, are derived, either directly or indirectly, from volcanic sources. The alteration of very fine-grained, somewhat basic, volcanic ash, in the case of the Cucaracha, and of fine-grained andesitic materials, in the case of the Culebra, has resulted in silt- and clay-sized particles rich in montmorillonite. Materials in both formations have been subjected to consolidation loads from past overburden greatly in excess of loads resulting from their present overburden. Many strata are characterized by a random system of slickensides. Intact pieces of the material tend to expand when unrestrained and will slake rapidly when exposed to alternate wetting and drying cycles.

Failure of Clay Shale Slopes

One of the more interesting aspects of the behavior of slopes in clay shales is the ability of some apparently stable slopes to stand for long periods of time before a failure occurs. Scott and Brooker (1968) prepared a list of contributing factors that influence the failure of clay shale slopes (Table 1). Several of the factors involve depositional environment, lithology, and geological processes operating over extremely long time intervals. They indicated diagrammatically how change in some of the factors could operate to increase the shear stress and to decrease the shear strength over a period of time to ultimately cause a slope failure. The factors listed by Scott and Brooker can cause the slope material to be in such a condition that failure can occur as a result of natural processes, such as the downcutting of a river valley. Examples of this natural process are given by Peterson et al. (1960) for slopes in clay shale along the South Saskatchewan River and by Knight (1963) and Fleming, Spencer, and Banks (1970) for slopes in clay shales along the Missouri River Valley. On the other hand, the factors can operate to produce conditions such that when an artificial slope is produced, failure can occur almost immediately or, because of new conditions imposed by the construction, failure can occur at a later time. Examples of slope failures during or immediately following construction activities are given by Palladino (1971) for the overconsolidated Lawton clay in

connection with construction of the Seattle Freeway and by Hamel (1973) for the Bearpaw clay shale in connection with construction of the powerhouse slopes at Fort Peck Dam. Several slope failures, exemplified by the Northolt and the Kensel Green Slides (Henkel, 1957; Skempton, 1964) and by the Sudbury Hill Slide (Skempton, 1964 and 1977) and the Wood Green Slide (Henkel, 1957), all located in the stiff fissured London clay, illustrate cases of failures occurring from 19 to 55 years following construction.

Once a slope is created, pore pressures within individual strata start adjusting to the new stress state. While the time required for the pore pressures to adjust depends considerably upon the permeability of the materials contained within the slope, for overconsolidated clays, and clay shales, the equilibrating time can be extremely lengthy. Bishop and Bjerrum (1960) schematically illustrated the trend of the varying pore pressures with time. Skempton and Hutchinson (1969) termed the stage at which the pore pressures caused by the excavation were fully developed as the short-term or end-of-construction condition. The stage at which the pore pressures were in equilibrium with the steady state seepage conditions within the new slope was termed the long-term condition. The short-term and long-term conditions are separated by an intermediate or equilibrating condition.

The use of more or less standard approaches to assess the stability of embankment slopes of compacted clay and cut slopes in normally consolidated clays is generally adequate. Much poorer results have been obtained when assessing the stability of slopes containing strata of overconsolidated clays and clay shales. The degree with which the stratigraphy of a slope can be described, as well as the groundwater conditions, is of primary importance in the successful assessment of stability, but other factors that affect the strength of overconsolidated clays and clay shales are of significant importance. Several factors, such as disturbance, orientation and size of test specimens, rate of shearing, softening, and progressive failure, were discussed by Skempton and Hutchinson (1969).

Because of the poorer success in assessing slopes containing clay shale strata, much use has been made of case records in which the strength operating at the time of the failure is determined from a stability

analysis of the slope under the condition that the factor of safety was unity. As suggested by Skempton and Hutchinson (1969), the case records can be considered as examples of:

a. Slides on preexisting slip surfaces.

b. First-time slides under long-term conditions.

c. First-time slides under short-term conditions.

Skempton and Hutchinson (1969) illustrated by means of several case studies that slides on preexisting slip surfaces are controlled by the residual strength of the overconsolidated clay or clay shale. Confirming conclusions have been reached by other investigators, for example, Palladino (1971) and Hamel (1973).

Many studies of slopes containing clay shale strata have emphasized first-time failures under long-term conditions. These studies generally confirm the concept of softening within the mass from nonuniform swelling along fissures (as first described by Terzaghi, 1936) as being the cause of delayed failure. For example, Skempton (1970) in discussing first-time failures in the overconsolidated London clay concluded from numerous case studies by DeLory (1957) and James (1970) that the strength at the time of failure tended toward, and does not fall significantly below, the fully softened strength. The fully softened strength, Skempton reasoned, could be represented by the strength of normally consolidated clay. The discussion by Skempton was restricted to cases of long-term stability (failures occurring from 16 to 81 years after the slope excavation).

Studies of first-time failures in overconsolidated clays and clay shales under short-term conditions are few. The Bradwell example (Skempton and La Rochelle, 1965) was discussed by Skempton and Hutchinson (1969). In that case, the discrepancy between calculated field strength and that obtained in the laboratory was explained by Skempton and Hutchinson by considering the influence of pore water migration toward the shear zone and by sample size.

The reanalysis of the East Culebra Slide is important because the Slide, as developed in subsequent portions of this thesis, is a first-time failure that developed during construction. The determination of the field strength operative at the time of the failure is made after proper documentation of field observations and construction events has been made.

Previous Analyses of East Culebra Slide

Slope analyses of the East Culebra Slide (usually in conjunction with studies including analyses of other nearby slopes) have been performed by other investigators. The results of previous investigations are summarized below.

Third Lock Studies

Collins (1942) stated that the first attempt to determine the order of magnitude of the shear strength of the Cucaracha was a rough analysis of one of the initial slides along the Canal. Little discussion is given and no other reference to the analysis was found. Most likely the slope was hypothetical. Collins stated that for the assumed condition of sudden drawdown, a uniform shear strength of about 1.2 tsf was computed (factor of safety = 1.0) using Taylor's stability chart (Taylor, 1948) for a slope of 3V to 2H and a height of 100 ft.

An analysis of the Model Slope* was made to obtain the "cohesive" component of shear resistance required to produce a factor of safety = 1.0 for an assumed friction angle of 10 deg (Collins, 1942). The friction angle was determined from laboratory tests on precut polished surfaces. A three-dimensional analysis was made, assuming incipient sliding between sta** 1961+60 and 1969+60 (1974+00 and 1802+00) and considering the resistance along the south side of the mass. These stations correspond to the southern limit of the West Culebra Slide and the assumed northern limit of the agglomerate forming Contractors Hill, respectively. The limit of possible deep slides in the Model Slope was placed 100 ft below the channel bottom (el -60 ft). While the stratigraphy within the section was described as being comprised of agglomerate, weathered rock, residual clay, and ash, no accounting was made for the probable variations in strength afforded by the different materials; rather a uniform strength was assumed

---

* The Model Slope is located opposite and to the south of the East Culebra Slide (Fig. 3). The area was designated as the Model Slope because no failures have ever occurred at the location; in short, the area behaved in a model manner.

** Several stationings have been used at the study area in the past (Lutton and Banks, 1970). The present stationing is preferred in this thesis, but since many records are referenced to an older system in use during construction, where used, the older stationing is shown in parentheses.

for the analyses. The ash layer was assumed to act as a drainage layer, and the sudden drawdown condition was applied only to the material below it. The resistance along the southern boundary of the possible slide in the Model Slope was assumed to be contributed only by cohesion, and assumptions were made that 0, 50, and 100 percent of the end area were effectively resisting the slide. For these assumptions, the required cohesion values (factor of safety = 1.0) varied from 0.68 to 1.4 tsf for a friction angle of 10 deg acting along the assumed failure surface. From these analyses of the Model Slope, a cohesion value of 1.15 tsf was adopted for slope design in the Cucaracha formation during the Third Locks Project.

Isthmian Canal Studies

Additional analyses of the study area were made during the Isthmian Canal studies of 1947 (PCC, 1947; Binger, 1948). Stability analyses were made at selected cross sections of the East and West Culebra Slides for the purpose of modifying existing slope charts. Canal cross sections were taken at sta 1950+10, 1952+60, and 1955+10 (1782+50, 1785+00, and 1787+50) where the most detailed information was available on geology, topography, and slide history. The records indicated that these sections were essentially free from major slides prior to January 1912. Stability analyses by a circular arc method were made at each section as they existed in January 1912, June 1912, July 1915, and March 1947, the first three dates preceding major slide movements.

The slope failures were considered to be confined to the Cucaracha formation; failures occurring in materials bordering the Cucaracha were considered, for the most part, as secondary failures and not originally involved in the major slides. In the analyses, the average shear strength was computed for the most critical circular arc at each section. The elevation of the groundwater table at the time of sliding was unknown; therefore, a condition of sudden drawdown from the top of the slope to the bottom of the cut was assumed for analyses of the 1912 slides. Water was first admitted in the Gaillard Cut in October 1913, and for all slides occurring subsequently, the groundwater table was assumed to be horizontal and at the level of water in the Cut.

For his analysis, Binger assumed the strength parameters were the same as those deduced from the Third Locks studies (i.e., c = 1.15 tsf;

ϕ = 10 deg). For the initial failure (January 1912) at the sections analyzed at the East Culebra Slide, factors of safety varying from 0.76 to 0.83 were calculated to indicate a larger required average strength. For the analysis of the sections as they existed in March 1947, factors of safety varying from 2.48 to 4.07 were calculated to indicate a smaller required average strength.

Development of slope charts

Since the heights of cuts in the Cucaracha formation were variable for the 1947 proposed sea level alignment of the Canal, it was desirable to develop design curves relating permissible slope angle to depth of cut. MacDonald (1913) had prepared a table proposing a decreasing slope angle for an increasing depth of cut as a function of rock condition. The values were apparently drawn from MacDonald's experiences with slopes along the Canal, tempered with a qualitative assessment of factors contributing to instability. A slope chart was constructed by MacDonald in 1939 and revised by him in 1940. The original curve was recommended in the report, "Preliminary Report on Estimates for Safe Slopes for Pacific Side Canal Excavation" (file 9-L-3, PCC, 26 June 1939), but the report contains no information as to how the curve was obtained. The revised curve was contained in a memorandum from MacDonald to the Engineer of Maintenance, 18 July 1940; the memorandum indicates that the revised curve was based on an empirical study of actual landslides. Casagrande and Middlebrooks reviewed MacDonald's revised curve and recommended a slightly more conservative design curve, i.e., one in which the required slope was slightly flatter for a given depth of cut. Later Thompson extended MacDonald's revised curve for depths of cut ranging from 350 to 700 ft. Published literature does not indicate how the extension was made.

For the 1947 Interoceanic Canal Studies, Binger (1948) used stability analyses to develop new slope design curves for the Cucaracha formation with the following assumptions:

a. Sudden drawdown from the top of the cut to the Canal water surface.
b. A homogeneous section with weathered material near the top of the cut having the same strength as the Cucaracha.
c. Strength parameters of c = 1.15 tsf, ϕ = 10 deg.

Two curves were developed, one for a factor of safety of 1.1 and the

second for a factor of safety of 1.3. The two curves were arbitrarily flattened for lower cuts to agree with MacDonald's revised curve. Binger thought the design curve based on a factor of safety of 1.3 was conservative for designing safe slopes in the Cucaracha formation but stated that once a slope fails as a result of having been cut oversteep, it will then assume an "angle of repose" much flatter than would have been required originally for a safe design. It is interesting to note from MacDonald's 1913 table of slope inclinations that values were included for depths of cut up to 656 ft and further that inclinations for rocks described as "the material in motion toward the Culebra Cut," compare with Binger's curve for a factor of safety of 1.1.

MIT* analysis

In a reanalysis of slope design charts and strength parameters, Hirschfeld et al. (1965) compared slopes existing in 1947 with the various empirical and 1947 design curves. On the basis of this comparison, they indicated (not concluded) that the MacDonald-Thompson and the 1947 Isthmian Canal studies design curves were conservative.

WES** analyses (1970)

A simple wedge analysis was made at four sections through the East Culebra and West Culebra Slides at different stages of their development to provide estimates of average effective strengths parameters (Lutton and Banks, 1970).

The toe and the backscarp of the slides were estimated at each section from descriptions of upheaval and cracks along the slope. The base angles of the passive and active wedges were varied as well as the depth of the base of the neutral block until a critical surface (i.e., the surface having the largest average shear stress) was found. Once found, the average effective normal stress was determined for the surface. The base of the neutral block was assumed to be parallel with the dip of strata, but in the absence of stratigraphic detail, no attempt was made to position the base of the neutral block in clay shale strata or at interfaces between clay shale strata and stiffer silty clay or sandstone strata. Once the critical positions of the base angles of the active and passive wedges were found, the average shear and effective normal stresses were

---

* Massachusetts Institute of Technology, Cambridge, Mass.
** U. S. Army Engineer Waterways Experiment Station, Vicksburg, Miss.

determined along a second surface that corresponded to the depth of sliding indicated by recent slope indicator data.

Critical surfaces (and the surface corresponding to the slope indicator data) were determined at each section and each stage of sliding for several simple assumptions of pore water pressure acting within the slope. First, the groundwater surface was assumed to lie below the surface of the slopes at a position corresponding to the base of the weathered clay. The pore pressures were assumed to vary directly with the distance below the phreatic surface. Second, for analyses of the initial failure, the pore pressures were assumed to be reduced from the hydrostatic values as a result of Canal excavation. The degree to which the pore pressures could have been reduced was speculative; therefore, various assumed reductions were used. The pore pressure was computed along each trial failure surface but was included in the stability analysis as a single variable (pore pressure ratio, r_u ; Bishop, 1955) using the computational procedure suggested by Bishop and Morgenstern (1960).

The average shear and effective normal stress on each critical surface were plotted, and a strength envelope was fitted to the data. The results indicated that average strength envelopes for the initial failure were defined by strength parameters varying from $\phi'_{avg} \simeq 21$ deg, $c'_{avg} \simeq 0$ to $\phi'_{avg} \simeq 15$ deg, $c'_{avg} \simeq 0$. These results were encouraging, in spite of the inadequacy of the wedge method used* and the simple pore pressure assumption, in that a single strength envelope was shown to approximate the calculated stresses and that the calculated average effective friction angle was only slightly lower than the effective friction angles established from drained direct shear tests on slickensided specimens (Lutton and Banks, 1970).

WES analyses (1975)

A simple wedge analysis was made at a single section through the East Culebra Slide at different stages of development using the two-dimensional method of slices developed by Morgenstern and Price (1965).

---

* In a review of the results, Hutchinson (1970) pointed out an error in the derivation of the equations used in the stability analyses. The error was such that the average effective normal stresses were overestimated; the average shear stresses were unaffected. Thus, the effect of the error was to cause the value of ϕ'_{avg} to be smaller than if the error had not been made.

Assumptions of pore pressures, geometry, etc., as described above, were followed (Banks et al., 1975). The purpose of the analysis was to determine average shear and effective normal stresses acting along the critical failure surface. Those stresses, determined for the initial failure at the section being analyzed and when plotted with the results of analyses of other sections in the Cucaracha formation for similar conditions, suggested that the average effective strength envelope could be defined by $\phi'_{avg} = 18$ deg and $c'_{avg} \simeq 0$ (lower limit) to $c'_{avg} \simeq 0.65$ tsf (upper limit).

Scope and Organization of Study

Since the purpose of this thesis is to determine the field strength operative at the time of the initial failure of the East Culebra Slide, extensive efforts were made to date the initiation of the Slide and to describe those engineering geology features that contributed to the development of the Slide.

Most descriptions of the East Culebra Slide relate that the Slide developed over a period of time by the joining of several individual slides or, as they were termed by construction engineers and geologists, "breaks." These descriptions do not clearly state where or when individual breaks occurred. Further, past analyses have been made only at sections involved in the last stages of development of the Slide. Thus, a major effort was expended in this thesis in reviewing contemporary accounts of the East Culebra Slide and construction-day cross sections to provide as complete as possible description of the Slide development. The development of the East Culebra Slide is described in Chapter II.

The geology of the Gaillard Cut is relatively complex. However, because of the importance of the East Culebra Slide, geologists working for the PCC during construction documented important observations of major geologic features, such as stratigraphy, lithology, and locations of faults, in the area of the Slide. Unfortunately, only minimal attention was given to such important geologic features, such as joints and slickensides. Since the mass involved originally in the Slide has now been removed, the nature of the joints and slickensides was inferred from observations obtained elsewhere in the Cucaracha formation. Since little,

if any, documentation exists on the groundwater conditions existing at the Slide, inferences must be made from present-day observations that were obtained elsewhere along the Canal. Much of the geologic work has been described elsewhere and is appropriately referenced in the summary presented in Chapter III.

Samples of Cucaracha clay shale were tested in the laboratory as part of this thesis. Particular efforts were made to determine effective strength parameters of intact, slickensided, and slurry-consolidated samples. The results of the laboratory strength tests are presented in Chapter IV.

Six individual initial breaks were identified in the development of the East Culebra Slide. A single cross section was prepared for four of the initial breaks; two cross sections were prepared for one break and three cross sections for the major break that developed last. An analytical study using a wedge analysis was made to determine the field shear strength parameters operative at the time of the breaks. The results of these analyses are presented in Chapter V.

Chapter VI contains a discussion of the study, conclusions gained therefrom, and recommendations.

Table 1. Geological Factors Controlling Slope Stability and Their Engineering Consequence*

Geological Factors		Influence	Engineering Consequence
1. Depositional environment	(a) Marine deposition	High sodium concentrate in pore fluid	High osmotic swelling potential
	(b) Fine-grained clastic sediments and volcanic ash	Clay sizes dominant, montmorillonite abundant	High plasticity soils
	(c) Slow rate of sedimentation	Sediments generally of uniform texture and structure	Low permeability
	(d) Relatively shallow depth of burial	Lithification incomplete, interparticle bonds weak	Low shear strength, high rehydration swelling potential
2. Lithology and stratigraphy	(a) Bentonite layers interstratified with clay shales	Retards downward movement of groundwater; leaching along top of bentonite layers	Zones of high plasticity, high swelling pressure, low shear strength
	(b) Fine-grained sandstone layers widely spaced	Drainage layers widely spaced	Layers of relatively high shear strength related to distribution of sandstone
3. Stress history	(a) Loading by younger sediments	Consolidation	Increase in shear strength with loading
	(b) Diastrophism and preglacial erosion	Removal from marine environment, leaching, dilatancy, sediments in condition of overconsolidation	Residual stresses relieved only in near surface zone
	(c) Glacial erosion and loading	In some areas consolidation loads may exceed those imposed by sediments	May cause increase in overconsolidated ratio
	(d) Glacial unloading	Initiation of residual stress relief; sediments in condition of over-consolidation	Residual stress concentrations
	(e) Postglacial rebound	Terrain uplift--erosion base level lowering, increase in groundwater gradients	Stream erosion accelerated; downcutting exceeds rate of residual stress relief
	(f) Valley erosion	Exposure of zone of high residual stress. Fracture development parallel with the valley	High lateral stresses in valley walls
4. Structure	(a) Attitude of bedding	Controls outcrop width of formation	Older beds of formation may occur below near-surface zone of stress relief
	(b) Fracture development	Vertical planes of weakness	Loss in mass shear strength
5. Climate	(a) Precipitation	Affects rate of groundwater movement and leaching	Seasonal pore pressure fluctuations; leaching may decrease shear strength
	(b) Temperature	Alternate wetting and drying produces fractures. Freeze/thaw action in fractures	Decrease in shear strength in near-surface fracture zone
6. Geomorphology	(a) Position of base level	Controls depth of valley and, in part, rate of erosion	Failures occur only where base level of erosion is below critical height of slope. Critical height, however, is not constant
	(b) Stream channel configuration	Asymmetrical cross valley profile, steep undercut slopes, toe erosion	Decrease in shearing resistance of slope
	(c) Terrace development	Reduction in effective slope height	Decrease in shear stresses
	(d) Rate of erosion	Rate of downcutting may exceed rate of residual stress relief in valley walls	Increase in shear stresses
	(e) Slope exposure	Exposure to insolation may depress groundwater flow regimen	Increase in effective stress due to decrease in neutral stresses
7. Groundwater	(a) Quantity	Seasonal variations in flow may increase leaching and pore pressures	Decrease in shear resistance
	(b) Quality	Differences between groundwater chemistry and pore-water chemistry can create osmotic swelling pressures	Decrease in shear resistance

* From Scott and Brooker (1968).

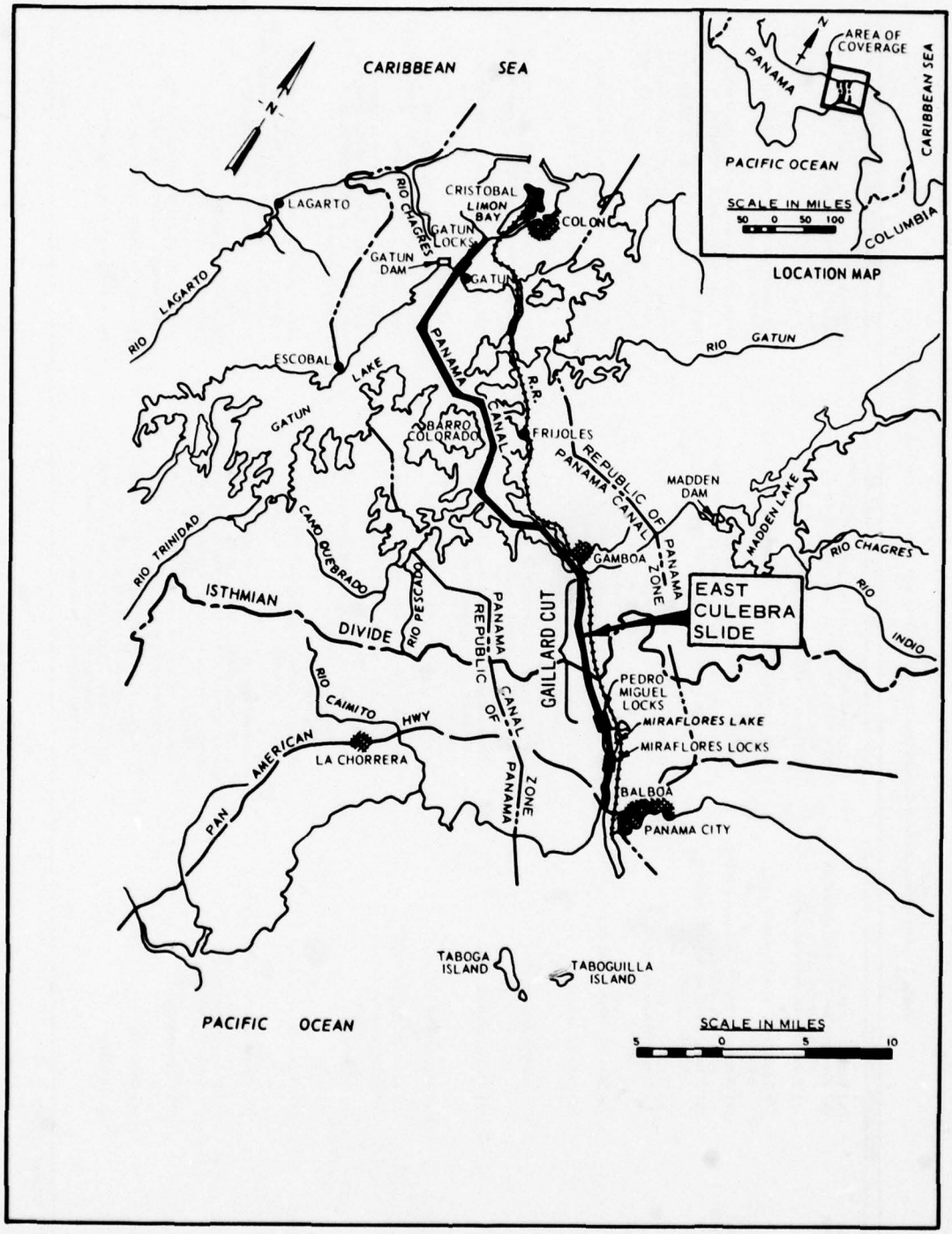

Fig. 1. Map of Canal Zone and Panama Canal (from Banks et al., 1975)

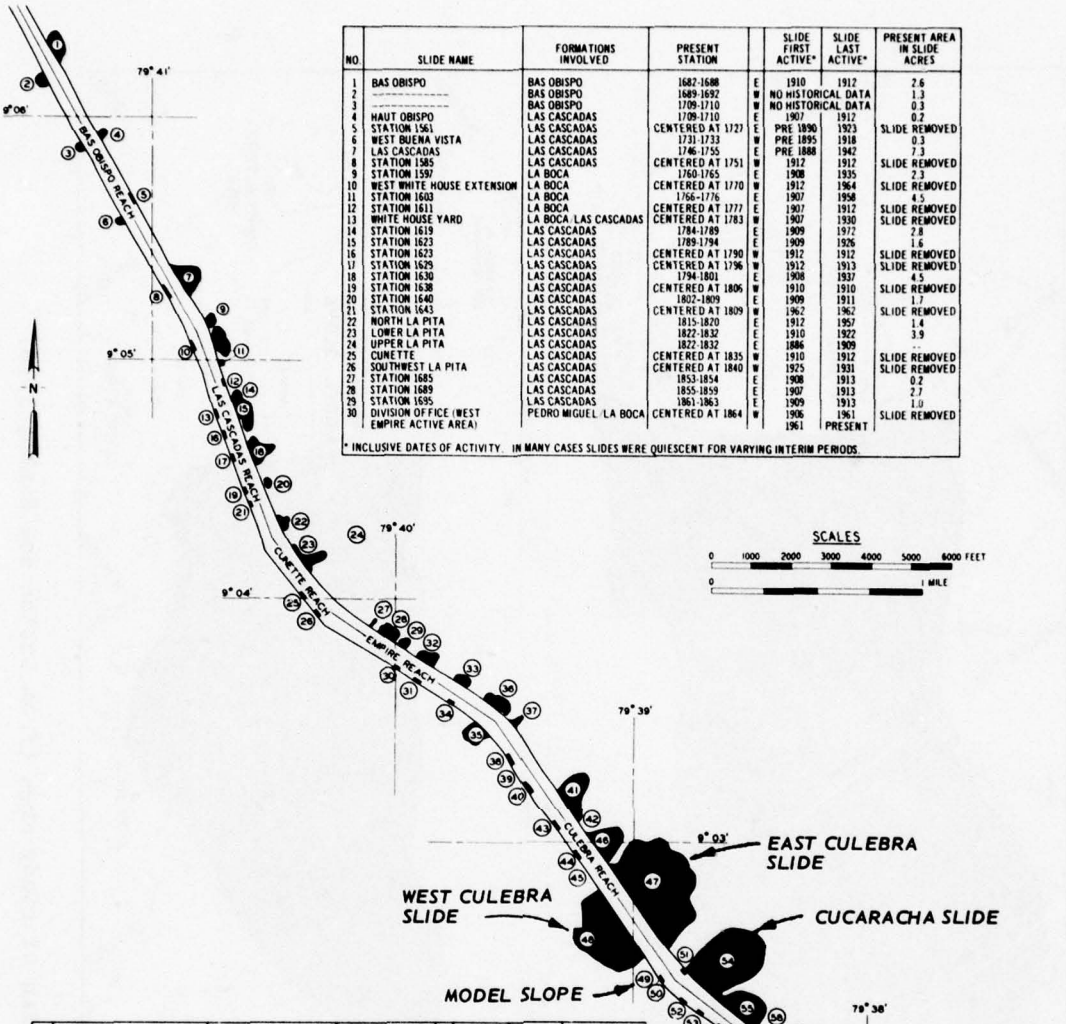

NO.	SLIDE NAME	FORMATIONS INVOLVED	PRESENT STATION		SLIDE FIRST ACTIVE*	SLIDE LAST ACTIVE*	PRESENT AREA IN SLIDE ACRES
1	BAS OBISPO	BAS OBISPO	1682-1688	E	1910	1912	2.6
2	----------	BAS OBISPO	1689-1692	W	NO HISTORICAL DATA		1.3
3	----------	BAS OBISPO	1709-1710	W	NO HISTORICAL DATA		0.3
4	HAUT OBISPO	LAS CASCADAS	1709-1710	E	1907	1912	0.2
5	STATION 1561	LAS CASCADAS	CENTERED AT 1727	E	PRE 1890	1923	SLIDE REMOVED
6	WEST BUENA VISTA	LAS CASCADAS	1731-1733	W	PRE 1895	1918	0.3
7	LAS CASCADAS	LAS CASCADAS	1746-1755	E	PRE 1888	1942	7.3
8	STATION 1585	LAS CASCADAS	CENTERED AT 1751	W	1912	1912	SLIDE REMOVED
9	STATION 1597	LA BOCA	1760-1765	E	1908	1935	2.3
10	WEST WHITE HOUSE EXTENSION	LA BOCA	CENTERED AT 1770	W	1912	1964	SLIDE REMOVED
11	STATION 1603	LA BOCA	1766-1776	E	1907	1958	4.5
12	STATION 1611	LA BOCA	CENTERED AT 1777	E	1907	1912	SLIDE REMOVED
13	WHITE HOUSE YARD	LA BOCA-LAS CASCADAS	CENTERED AT 1783	W	1907	1930	SLIDE REMOVED
14	STATION 1619	LAS CASCADAS	1784-1789	E	1909	1972	2.8
15	STATION 1623	LAS CASCADAS	1789-1794	E	1909	1926	1.6
16	STATION 1623	LAS CASCADAS	CENTERED AT 1790	W	1912	1912	SLIDE REMOVED
17	STATION 1629	LAS CASCADAS	CENTERED AT 1796	W	1912	1913	SLIDE REMOVED
18	STATION 1630	LAS CASCADAS	1794-1801	E	1908	1937	4.5
19	STATION 1638	LAS CASCADAS	CENTERED AT 1806	W	1910	1910	SLIDE REMOVED
20	STATION 1640	LAS CASCADAS	1802-1809	E	1909	1911	1.7
21	STATION 1643	LAS CASCADAS	CENTERED AT 1809	W	1962	1962	SLIDE REMOVED
22	NORTH LA PITA	LAS CASCADAS	1815-1820	E	1912	1957	1.4
23	LOWER LA PITA	LAS CASCADAS	1822-1832	E	1910	1922	3.9
24	UPPER LA PITA	LAS CASCADAS	1822-1832	E	1886	1909	--
25	CUNETTE	LAS CASCADAS	CENTERED AT 1835	W	1910	1912	SLIDE REMOVED
26	SOUTHWEST LA PITA	LAS CASCADAS	CENTERED AT 1840	W	1925	1931	SLIDE REMOVED
27	STATION 1685	LAS CASCADAS	1853-1854	E	1908	1913	0.2
28	STATION 1689	LAS CASCADAS	1855-1859	E	1907	1913	2.7
29	STATION 1695	LAS CASCADAS	1861-1863	E	1909	1913	1.0
30	DIVISION OF FICE (WEST EMPIRE ACTIVE AREA)	PEDRO MIGUEL-LA BOCA	CENTERED AT 1864	W	1906 1961	1961 PRESENT	SLIDE REMOVED

* INCLUSIVE DATES OF ACTIVITY. IN MANY CASES SLIDES WERE QUIESCENT FOR VARYING INTERIM PERIODS.

NO	SLIDE NAME	FORMATIONS INVOLVED	PRESENT STATION		SLIDE FIRST ACTIVE*	SLIDE LAST ACTIVE*	PRESENT AREA IN SLIDE ACRES
31	STATION 1703	PEDRO MIGUEL	CENTERED AT 1870	W	1912	?	SLIDE REMOVED
32	STATION 1702	LA BOCA	1867-1872	E	1907	?	2.7
33	STATION 1712	PEDRO MIGUEL	1878-1882	E	1910	1912	1.2
34	STATION 1713	PEDRO MIGUEL	CENTERED AT 1881	W	1912	1930	SLIDE REMOVED
35	OLD LIRIO	PEDRO MIGUEL, CULEBRA?	1888-1896	W	1912	1932	5.8
36	EAST LIRIO	CULEBRA?	1887-1893	E	1909	1935	5.2
37	----------	CULEBRA?	1894-1896	E	NO HISTORICAL DATA		1.4
38	STATION 1735	CULEBRA?	CENTERED AT 1902	W	1923	1960	SLIDE REMOVED
39	1910-1920 PROBLEM AREA	CULEBRA	1910-1920	W	?	?	--
40	CULEBRA VILLAGE	CUCARACHA CULEBRA	CENTERED AT 1910	W	1899	1934	SLIDE REMOVED
41	HAGAN'S SLIDE	CULEBRA	1915-1923	E	1910	1946	10.0
42	1925 EAST ACTIVE AREA	CULEBRA	1922-1930	E	1929	PRESENT	--
43	NEW TOWN	CULEBRA	CENTERED AT 1920	W	PRE 1908	1911	SLIDE REMOVED
44	OLD HODGES HILL	PEDRO MIGUEL CUCARACHA CULEBRA	CENTERED AT 1930	W	1908	1961	SLIDE REMOVED
45	HODGES HILL ACTIVE AREA	PEDRO MIGUEL CUCARACHA CULEBRA	CENTERED AT 1932	W	CRACKS IN 1968 STABILIZED IN 1969		--
46	EAST CULEBRA EXTENSION	CUCARACHA CULEBRA	1928-1936	E	1910	1964	7.8
47	EAST CULEBRA	CUCARACHA CULEBRA	1938-1963	E	PRE 1886	PRESENT	78.0
48	WEST CULEBRA	CUCARACHA	1946-1962	W	1900	PRESENT	41.0
49	MODEL SLOPE	CUCARACHA CULEBRA	1962-1971	W	?	?	--
50	N. CONTRACTORS HILL	PEDRO MIGUEL CUCARACHA	CENTERED AT 1970	W	1907	1943	SLIDE REMOVED
51	STATION 1804	PEDRO MIGUEL CUCARACHA	CENTERED AT 1971	E	1884	1910?	SLIDE REMOVED
52	CONTRACTORS HILL FISSURED	PEDRO MIGUEL CUCARACHA	CENTERED AT 1976	W	1954	1954	SLIDE REMOVED
53	S. CONTRACTORS HILL	PEDRO MIGUEL CUCARACHA	CENTERED AT 1982	W	1908	1913	SLIDE REMOVED
54	CUCARACHA	CUCARACHA CULEBRA	1972-1983	E	1884	PRESENT	52.0
55	SOUTH CUCARACHA	CUCARACHA CULEBRA	1983-1992	E	1885	PRESENT	13.0
56	CUCARACHA SIGNAL STA.	CUCARACHA	CENTERED AT 1985	W	1908	1941	SLIDE REMOVED
57	STATION 1823	CUCARACHA	CENTERED AT 1991	W	1901	1910	SLIDE REMOVED
58	STATION 1830	CUCARACHA CULEBRA	1996-2000	E	1909	1954	2.3
59	CUCARACHA VILLAGE	CUCARACHA CULEBRA	2007-2010	E	1907	1930	3.2
60	PARAISO	CUCARACHA CULEBRA	2040-2048	E	1898	1913	9.7
61	CARTAGENITA	PEDRO MIGUEL	2065-2070	W	1936	1936	1.3
62	CARTAGENA MUD FLOW	PEDRO MIGUEL	2070-2073	W	?	?	13.6
63	CARTAGENA	LA BOCA	2073-2080	W	1889	1931	2.0
64	CARTAGENA EXTENSION	LA BOCA	2080-2085	W	1964	1964	1.4

* INCLUSIVE DATES OF ACTIVITY. IN MANY CASES SLIDES WERE QUIESCENT FOR VARYING INTERIM PERIODS.

Fig. 2. Slide locations along Gaillard Cut (from Banks et al., 1975)

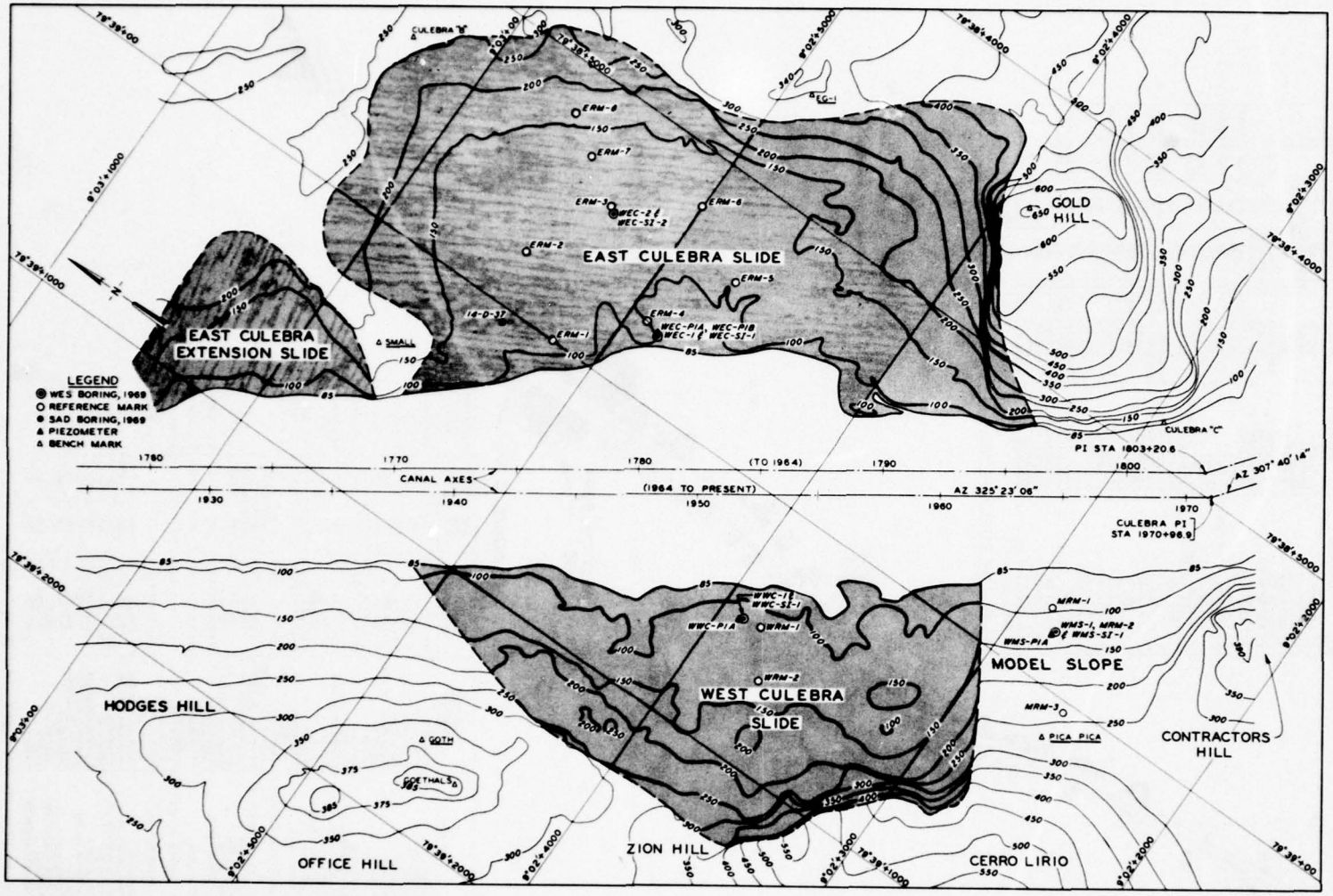

Fig. 3. General plan of study area (from Lutton and Banks, 1970)

CHAPTER II: INITIAL DEVELOPMENT OF THE EAST CULEBRA SLIDE

Since the slides in the Gaillard Cut were the focus of attention during construction and for the several subsequent studies of sliding (e.g., Goethals, 1916a and 1916b; Cross, 1924; Binger, 1948; Hirschfeld et al., 1965; Lutton and Banks, 1970; Lutton et al., 1975; Banks et al., 1975), quite vivid descriptions exist, many with accompanying photographs and cross sections, from which an account of the initial development of the East Culebra Slide may be reconstructed. The purposes of the studies by Goethals, Cross, and Hirschfeld et al. were general in nature; accounts of slides were descriptive, and although photographs and cross sections were given, few data were presented from which information could be drawn concerning the dates when sliding started at a given station along the Canal, the extent of a given sliding activity, or the slope geometry existing at the time of failure. In the study by Binger, simplified cross sections through the last portion of the East Culebra Slide to be involved in sliding and the results of rudimentary analyses were presented. In later studies, attention was given to the evolution of the East Culebra Slide. Lutton and Banks presented a review of previous information, developed the geologic setting, and described the development of the Slide from its initiation to its present form; preliminary analyses were performed to determine strength parameters likely to be acting along failure surfaces at stages during Slide development. Later, Lutton et al. expanded their study to include the geological setting of the entire Gaillard Cut, i.e., descriptions of individual slides, slide characteristics, and sliding mechanisms. In the study, a description was given of the sliding experienced by the French in overburden or weathered clay materials along with further involvement of underlying materials caused by continuing excavation at one cross section through the Slide. Analyses of the Slide at this cross section were made by Banks et al.

The information contained in these previous descriptions was reviewed to determine, as nearly as possible, the dates and nature of failures that first occurred in connection with construction activities at the site. Particular attention was paid and heavy reliance given to construction-day photographs and records, particularly those contained

in the Annual Reports (1905-1916) of the Isthmian Canal Commission, the Canal Record (1907-1932), a weekly information bulletin published by the PCC, and PCC files containing construction cross sections through the Canal at 50-ft stations (PCC Vault File 288). This review, as discussed in this chapter, indicated that the East Culebra Slide did not develop along a broad front but rather as individual breaks concentrated in small reaches to later unite and increase in size by incorporating additional area further back in the slope. More importantly, this review allowed a positioning of these individual breaks to be made, along with their extent and date of occurrence.

Location

The East Culebra Slide is located in the Culebra Reach of the Gaillard Cut. At the present time, the Slide encompasses some 75 acres; it lies between sta 1935+00 and 1964+00 (1767+40 and 1796+40) and extends some 2000 ft from the present Canal axis, as shown in Fig. 3. Gold Hill, to the south, and Zion Hill, to the southwest, two topographic features once establishing the Isthmian Divide in the area are at the boundary of the Slide. The Slide is located some 10 miles northwest of Panama City, the Pacific terminus of the Panama Canal, and is accessible by two unimproved roads - one leading from the Summit Naval Station, and the other from the Gaillard Highway.

Slide Activity During Construction by the French

The earliest reported landslides along the Panama Canal occurred in 1884, soon after the commencement of excavation by the first French company (Cross, 1924). While these slides were particularly troublesome, according to Cross, the importance was expressed in terms of the inconvenience, delay, and expense caused. Few descriptions of the slides exist, but they were important enough to be mentioned in the historical essays of Mack (1944), Hammond and Lewin (1966), Cameron (1971), and McCullough (1977). Although the early slides were not adequately documented to allow their exact locations to be determined, Cross placed them all in the region south of Gold Hill, i.e., across the Isthmian

Divide from the East Culebra Slide. The slides occurred principally in the rainy season and apparently involved the 20- to 30-ft-thick surficial zone of dark red, weathered clayey soil. Cross stated that the sliding surface was located at the base of the weathered clay.

The French geologist Bertrand and the Swiss engineer Zurcher, who were attached to the Second Technical Commission of the second French company, made a detailed geological study of the Canal area in about 1898 (Bertrand and Zurcher, 1899). They made no mention of sliding at the site of the East Culebra Slide although the potential for sliding was recognized.

> This inclination *of bedding toward the Canal* creates from the point of view of the stability of the layer of red clay on the left (*East*) bank, unfavorable conditions that have already caused the sliding at Cucaracha.*

A topographic map prepared near the end of French construction indicated that a large area immediately north of Gold Hill had been modified between sta 1952 and 1960 (1785 and 1793). The French evidently had excavated beyond their intended prism line for some 400 ft on a gentle slope in contrast to their usual practice of excavating steep slopes. The base of the excess excavation lay some 30 ft below the original ground surface. This information led Lutton and Banks (1970) to infer that before the French efforts had ceased and possession had passed to the United States, some surficial slides, as anticipated by Bertrand and Zurcher, had occurred at the East Culebra Slide.

The extent of sliding during the French construction activities at the present East Culebra Slide was studied more thoroughly by Lutton et al. (1975). In that study, a review of French maps indicated that surficial slides (i.e., those involving the weathered clay) had appeared by September 1885. Further study indicated that the extent of these surficial slides may have been greater than generally recognized since, according to the interpretation of French maps by Lutton et al., by 1890 they involved material along a 2000-ft front and extended back from the center line to distances ranging from 1150 to 1300 ft.

---

* Italicized words and phrases in this quotation, as well as others to follow, are provided by the author to aid in the clarity of the quotation.

The apparent discrepancy between the report by Bertrand and Zurcher (as quoted above) and the conclusions reached by Lutton et al. (1975) in their study of French maps is puzzling. Cross (1924) in his description of sliding following the French efforts stated:

> ...For some years before *the United States took possession of the Canal Zone on 8 May 1904*, there had been no new excavation work; the banks of the French cut had become overgrown with jungle vegetation and such slides as may have occurred during this period have not been recorded.

Few, if any, slides involving the material underlying the weathered clay could have occurred at the site of the East Culebra Slide, judging from the appearance of the bank in December 1904 (Fig. 4). Thus it is concluded that up until the United States started construction all sliding activity involved only surficial materials.

Slide Activity During Construction by the United States

Nature of the breaks

In the literature describing slide occurrences at later dates, the writers usually were specific in classifying the slides into one of three types as follows (NAS, 1924):

> *Type* I. Movements of rock masses on a preexisting plane or zone of weakness, inclined toward the canal.
> *Type* II. Movements along newly-formed fractures or by flowage or the two combined. These slides, which are of the greatest importance, are now called "breaks" by the Canal engineers. (*The East Culebra Slide was placed into this category.*)
> *Type* III. Movements of surface material:
> (a) Soil with associated rock debris and vegetation.
> (b) Dump material, talus, etc.

The distinction between slide types was definitively made by MacDonald in 1912 although he also included a fourth class of weathering or surface erosion (Canal Record, 6 November 1912, and Annual Report, 1912). The term "breaks" apparently had been used with the meaning given above for a few years previous to MacDonald's discussion. The first usage of the term to describe a slide movement was made in the 8 December 1909 Canal Record although a previous Canal Record (24 November 1909) spoke of a

slide as having "broke back" from the edge of the cut. References prior to these dates were merely to "slides." Thus, the character of the slides occurring from 1904 through 1909 is not clearly distinguished in the contemporary reports.

The following discussion of slide development can be better appreciated by a review of the description of the typical sequence of events surrounding a break (MacDonald, 1915). This description is particularly pertinent since MacDonald's assignment during construction was to study the slides and to recommend remedial measures. He states:

> These deformations first manifested themselves by the appearance of one or of a set of cracks or fissures parallel or somewhat oblique to the edge of the cut, and from a few yards to some hundreds of yards back from it and from each other. Some of them were traceable on the surface for several hundred yards and gradually developed into perpendicular crevices up to one-third of a yard wide and many yards deep. The second stage of this phenomenon consisted in the settling or tilting of these big block masses that had been divided from each other by the fissures. This movement was a slight and almost even settling (0.1 to 1 yard) of the block or blocks, or a tilting of them toward the excavation, or both. Some of the blocks sank a little in front and tilted up in the rear so that they were a yard above the front part of the block behind. The third and last stage consisted in the dropping downward of the front block, owing to the failure, and squashing out of its base. The whole block then disintegrated and sloughed down into the excavation. This last stage ran its course in a few hours to a few days; the other stages required some months or more than a year to reach completion. The movements of the last and of the second stages were often accompanied by bulging at the bottom and at the lower slopes of the excavation.

The cause of failure for the breaks was not known at the time; however, discussions by MacDonald (1915) cited either "deformation by rupture or deformation by plastic flow" as being the cause. While MacDonald's explanation may be questionable in terms of present knowledge, his description of the events involved in a slide indicates that vertical, open cracks formed during the first stage and grabens during the second stage. The formation of grabens at the slide scarp has been noted in descriptions of translational slides, e.g., Hutchinson (1967)

and Seed (1968), suggesting that shear along a weak layer was probably involved. The bulging at the toe of the slide suggests that the weak bed participating in sliding was at times some distance below the bottom of the cut. On more than one occasion, the upheaval at the toe was large. Perhaps the most striking occurrence was in 1915 when, following large movements by the East Culebra Slide, the West Culebra Slide experienced a large movement, and the toes of the two opposing slides met to form a large "mound."

Slide dates from literature accounts

The East Culebra Slide area apparently was relatively free of slides of any type from 1904 through at least mid-1907. Those that may have occurred were too small to be of significance to Howe, the Isthmian Canal Commission geologist, who made a thorough report in the Annual Report (1907). Mr. Howe's reference to landslides states*...

> From near Empire southward the cutting will be in the Culebra formation....Several small faults do occur in the Culebra beds between Culebra and Empire and cross the canal in an east and west direction; they will have no effect on excavation nor upon the stability of the slopes....The physical character of the Culebra beds, consisting as they do of alternating layers of sandstone and shale, is peculiarly favorable to landslides. Structurally, however, the strata are so nearly horizontal, or have such low southerly dips north of Gold Hill, that movements involving large masses of rock are improbable, while slopes of suitable angles will do away with the danger of minor slips....In Contractors Hill...if the Culebra beds...are inclined in the direction of the cut, as the surface indications suggest, it will be necessary to make comparatively low slopes to avoid any possibility of landslides. This is the only point along the Canal where such movements are at all possible.

The Annual Report (1908) describes four specific slides, none being at the East Culebra site, as the "only ones causing any trouble in the canal since the United States assumed control of the Canal." The Annual

---

* Howe described the material from Empire southward (i.e., the Culebra Reach) as being the Culebra formation. The distinction of the Cucaracha formation was not made until later, specifically, by MacDonald in the Annual Report (1913).

Report (1909) again describes specific slides but with no mention of any occurring within the East Culebra Slide area.

The Annual Report (1910) made a distinction between slides and breaks as discussed previously. The Annual Report states...

> Three bad breaks occurred during the year. *The largest occurred* on the west bank of the Canal at the town of Culebra....The second largest break, directly opposite that just described, covers an area of 11-1/2 acres on the east side of the Canal; during the *fiscal* year, 314,184 cu yd were removed making a total from this locality of 480,202 cu yd.

Thus, the Annual Report of 1910, while the first to specifically mention the breaks and more particularly the first to mention the East Culebra Slide, does not agree with previous Annual Reports in that evidently some 166,000 cu yd of material had been excavated prior to the 1910 fiscal year, i.e., before 1 July 1909. As indicated above, no description of these movements exists; the first description of motion was made during the fiscal year of 1910 in the Canal Record of 8 December 1909...

> The east bank of the cut opposite Culebra Village has broken 90 ft back from the top of the slope and a quantity of material is moving into the prism of the Canal. This slide is small compared to that of the west bank.

The Annual Report (1911) emphasized the sliding in the area. Whereas previous reports tended to largely dismiss the importance of the slides, since the estimated volume of slide material was within the contingency allowed for total excavation, by mid-1911 the slides had increased in size such that the estimates had to be revised upward. A table in the Annual Report indicated that the East Culebra Slide encompassed 31.6 acres. Significantly, in the table, the "date when slide first developed" was shown as January 1908. The table further indicated that 1,454,081 cu yd were excavated from 1 July 1910 to 30 June 1911, bringing the total excavation to 2,329,784 cu yd. Thus, it appears that the start of sliding was backdated to January 1908 and 395,501 cu yd were added to the amount of material stated as being previously derived from the East Culebra Slide.

The Annual Report (1912) again emphasized the seriousness of slides by revising upward the estimated excavation required for completion of

the Canal. The East Culebra Slide was listed as encompassing 50.7 acres from which 1,960,000 cu yd of material were removed during the fiscal year to bring the total to 4,290,000 cu yd. Significantly, in this report the start of the East Culebra Slide was stated to be January 1907. Whether or not this date was a typographical error is unknown, but the date was continued in subsequent reports and papers on the East Culebra Slide.

General Goethals, writing later, recalled the January 1907 date as the start of the sliding at the East Culebra site (Goethals, 1916b).

> ...In October 1907, a crack developed 50 or more feet from the face of the bank on the west side of the Canal near...Culebra....Subsequently new cracks developed further back, followed by similar settlements and movements into the cut, involving large masses of new materials; the same condition developed on the east side.

Elsewhere the slide initiation was described as (Goethals, 1916a)

> ...In January 1907, a slide occurred on the east side opposite Culebra....

In commenting on Goethals' descriptions, Cross (1924) stated:

> ...It is not clear from available data as to how much sliding took place in the East Culebra area in 1907, nor what its character may have been.... No other references to slides in this area *other than those quoted above* have been found....

The area referred to by Goethals was perhaps just north of Gold Hill at about sta 1957 (1790) as shown on a construction photograph taken in February 1907 (Fig. 5). If, as Goethals stated, the slide was located opposite Culebra, it must have been north of sta 1947 (1780) since the benches southward appear undisturbed to the slide just north of Gold Hill. Evidence presented subsequently tends to support early sliding north of sta 1947 (1780).

Slide dates from construction cross sections

Some additional information is available from which dating of failure can be inferred. The PCC files contain construction cross sections through the Canal at 50-ft stations (PCC Vault File 288). A copy of the construction cross section through sta 1952+60 (1785+00) is shown in Fig. 6 to illustrate the type data from which inferences of failure dates can be made. The center line in Fig. 6 is the so-called cross section

or construction center line and corresponds to the French center line. The first American center line to which the Canal was constructed is located 80 ft to the west, i.e., to the right on Fig. 6. Data contained on these cross sections show the excavation progress from the time of early American excavation in the Culebra Reach (circa 1905) through the end of the steam shovel operations in mid to late 1913. The cross section of the Panama Canal through Gaillard Cut, as planned by the Isthmian Canal Commission, is presented in Fig. 7, and the excavation progress at selected stations in Fig. 8. For reference, the original ground surface and the ground surface in 1969 are designated in Fig. 8; shaded areas indicate the material removed by year. Dates at which the actual excavation encroached the planned excavation can be determined by superimposing the planned Canal cross section from Fig. 7 on Fig. 8. Dates so determined can be taken as indicative of some type of failure.

The sections in Fig. 8, particularly at sta 1952+60 (1785+00) and 1957+60 (1790+00), show that the ground surface at the end of 1905 was lower than the original ground surface for several hundred feet beyond the design line. Whether the lowered surface represents excavation by the French or pre-1906 excavation by the Americans is not known, although it was previously inferred that the lowered surface resulted from surficial sliding. The depth of excavation corresponds roughly to the depth of weathering in the Cucaracha formation, i.e., 20 to 30 ft. In 1906, material was excavated near the projected design slope. On sections at sta 1952+60 (1785+00) and 1957+60 (1790+00), a berm was created at the 295-ft level during 1906. The creation of the berm is not taken as indicative of failure, but rather an area for catching surficial material that might be washed or otherwise moved toward the Canal prism. During 1907 the major effort was in deepening the Canal prism, and the creation of the planned berm at the 245-ft level. Figure 9 shows the 260- and 200-ft contours at times of important changes in their configuration. The position of the 260-ft contour indicates that by June 1907 the berm at the 245-ft level had been made almost over the entire width of the future Slide. The fact that the contour position was so uniform along the cut slope strongly suggests that failures had not affected the berm. In Fig. 8 the berm created in 1907 at sta 1939+60 (1772+00) extended further beyond the design line than at the other sections in the figure,

and additionally the back slope was flatter than at other locations. If this location is the area referred to by Goethals (1916a and 1916b) and the change in berm slope represents failure, then most likely the mass was confined to the weathered upper materials as judged from the depth of the berm below the original ground surface.

During 1908, as indicated in Fig. 8, the Canal was deepened, but importantly, the Canal was widened beyond the design line at several locations, e.g., note the change in section at sta 1957+60 (1790+00). At sta 1939+60 (1772+00) in Fig. 8, the 1908 excavation extended slightly beyond the design line, especially near the 245-ft berm. The encroachment probably represents a continuation of surficial movements similar to those described above. Figure 9 shows a change of position for the 260-ft contour between sta 1944+10 and 1947+60 (1776+50 and 1780+00) in May 1908. Although no change is noted in the position of the 200-ft contour, possibly indicating that the movement was surficial, the relatively large amount of material removed cannot be overlooked, and May 1908 will be taken as the date when failure in connection with construction activities first occurred between these stations. A change in position of both the 260- and 200-ft contours is shown in Fig. 9 between sta 1956+60 and 1960+60 (1789+00 and 1793+00) during the period September to December 1908. These dates will be taken as the time of failure in connection with construction activities between these stations. Failure at this location during early 1907 was mentioned previously and shown in Fig. 5. Failure during 1907 at this location will be taken, as at other stations, to be surficial.

The change in position of the 200-ft contour (Fig. 9) between sta 1940+60 and 1949+60 (1773+00 and 1782+00) indicates that by January 1909 a substantial portion of the bank at the site of the present East Culebra Slide was being affected. Since a portion of this reach had evidently experienced failure in May 1908, failure resulting from construction activities in January 1909 will be ascribed only to the portion from sta 1940+60 to 1944+10 (1773+00 to 1776+50) and from sta 1947+60 to 1949+60 (1780+00 to 1782+00). It should be reiterated here that the contemporaneous descriptions did not mention these dates nor make reference to slides or breaks in the area, possibly because the sections affected were not extensive in length nor were the slides or breaks particularly

large. Significantly, the first contemporaneous description of slope failure was made in December 1909 (quoted previously). A study of the positioning of the 200-ft contour (Fig. 9) indicates a large change (on the order of 90 ft, as described) from sta 1938+10 to 1940+60 (1770+50 to 1773+00) in February 1910. Most likely, the description and change in contour are reflective of the same break; thus, December 1909 can be taken as the date of the first construction-related failure between these stations. No other changes in positions are noted for either the 260- or 200-ft contours during 1910. The lack of data from excavation cross sections agrees generally with descriptions contained in the Canal Record (1910) where the activities described were concerned either with renewed motions or with removal of the slide debris. Figure 10 is a photograph of the site of the East Culebra Slide taken in June 1910. A large lateral movement is indicated just above the bottom of the cut and a general breakdown of the bank above. Figure 11 is another photograph of the site, again taken in June 1910. The two photographs were not taken on the same day, judging from the amount of water in the cut. Also, the photographs were obviously not taken at the same locations, judging from the haulage track configuration. Figure 11 shows an upheaval amounting to some 18 ft in the floor of the cut. The proximity of Gold Hill in the background of the mound suggests a position to the south of the area previously noted as in motion during 1910 (Fig. 9).

During February 1911, a major break, some 1100 ft in length, occurred between sta 1937+60 and 1948+60 (1770+00 and 1781+00). The Canal Record for 15 February 1911 states:

> ...on...February 9, a section of the east bank of the Canal, 1,100 feet in length, opposite the Y.M.C.A. clubhouse at Culebra, broke away and settled almost vertically for a distance of 30 feet, carrying away the berm below it on the 135-foot level, and displacing laterally this berm and all material west of it up to the pioneer drainage cut which was almost completely closed. The berm on the 135-foot level, below the break, varied in width from about 20 feet at the south end to 100 feet in the middle of the break, and 50 feet on the north limit of the break. All loose or broken material lying above this berm had been entirely cleared away by steam shovel only a few days previously.

The location of the break is shown by the change in position of both the

260- and 200-ft contours for March 1911 (Fig. 9). Although this motion is important to analyses of subsequent movements and evolution of the East Culebra Slide, the slope for the entire width (with the possible exception near sta 1937+60 (1770+00)) had previously exhibited movement. The widening during 1911, shown for the section at sta 1957+60 (1790+00) in Fig. 8, was only a local modification and is not presented in Fig. 9. As indicated in Fig. 9, an appreciable portion of the East Culebra Slide was in motion.

During 1912 the entire width of the present East Culebra Slide was to come into motion as indicated by the large change in sections (Fig. 8) and change in position of both the 260- and 200-ft contours (Fig. 9). In part, the indicated modifications were caused by excavations, following the by then established policy of removing material to lighten the load on the slopes. The Canal Record of 14 February 1912 stated:

> ...on...February 10 a portion of the bank of Culebra Cut below the old French 90-meter *(295-ft)* level, on the east side of the cut, opposite the village of Culebra and about 500 yards north of Gold Hill, broke off, carrying away the 95-foot berm and partly closing the recently completed drainage ditch in the locality....Other cracks have opened to the south and east of the broken mass, on the old French 90-meter *(295-ft)* level, which apparently indicate that there will be considerable addition in the near future....

The excavation cross sections from which Figs. 8 and 9 were prepared (Fig. 6) contain areas denoted as the January slide. While no written description was found of such a slide or break, the date conflicts only by days with the description given above. Figure 9 indicates that the change in position of the contours occurred along stations previously affected by slides with the exception that the cross section was widened between sta 1949+60 and 1956+00 (1782+00 and 1789+00). January 1912 will be taken as the date when construction activity first caused failure between these stations. Figure 12 is a construction photograph of the break in which bottom upheaval is suggested by the ridge formed about 40 ft in front of the toe of the slide. Figure 13 shows the slope configuration at the location of the February break and farther southward.

By January 1912, the entire width of the East Culebra Slide had experienced failure. The position of contour lines (Fig. 9) indicates

that the most active portion of the Slide was in the northern part. Subsequent changes in position of the contour lines are concentrated in this area also, although their repositioning was in part caused by steam shovel excavations to lighten the slope loads.

The contour positions shown in Fig. 9 indicate a large change from late 1912 or early 1913 to their present locations. For the most part, this change had occurred by early 1916. While the full development of the East Culebra Slide between 1913 and 1916 is the most dramatic, necessitating drastic action on the part of the builders, the development is beyond the scope of this study.

The dates of individual breaks are summarized by station in Table 2. As shown, no failure is associated with the January 1907 date commonly ascribed to the East Culebra Slide. Slope failures noted on that date, and as discussed above, were mostly surficial. The contour positions indicated in Fig. 9 show clearly that the East Culebra Slide did not develop at one time or over a large front but rather resulted from the union of several small breaks. For that reason, the station bounds indicated in Table 2, while reasonable, are somewhat approximate. Finally, the data from which Table 2 was compiled were taken from excavation cross sections intended to show volumes of materials removed and not locations of individual breaks and dates as inferred. The dates shown in the tabulation appear reasonable based on descriptive accounts contained in the Annual Reports of the Isthmian Canal Commission and Canal Records of the time.

Since dates and extent of individual breaks have been established, the construction cross sections (illustrated in Fig. 6) can be used to construct applicable before- and after-failure slope profiles for analyses. Such profiles are shown in Chapter V along with applicable geologic features.

Excavation Rates at the East Culebra Slide

Information of the form shown in Fig. 6 can be used to indicate the quantity of material excavated with time at various cross sections. The cumulative change in area as determined for several cross sections at dates of change between early 1906 and late 1912 was used as an index of the quantity of excavation (Fig. 14).

The data indicate that in the period 1906 to 1908 excavation proceeded at a fairly uniform and relatively rapid rate. Near the end of 1908, failures had occurred at sta 1942+60, 1944+60, 1946+60, and 1958+60 (1775+00, 1777+00, 1779+00, and 1791+00, respectively). The failure dates were followed by a two- or three-year period, i.e., until near the beginning of 1911, in which relatively small amounts of material were removed. The February 1911 movements, described previously between sta 1937+60 and 1948+60 (1770+00 and 1781+00), in effect caused a large increase in the amount of material removed. The failures were not responsible for the total change indicated in Fig. 14 since, because of the failures, operations were begun to flatten and unload the uppermost portions of the slope. Data from cross sections at sta 1950+10, 1952+60, and 1955+10 (1782+50, 1785+00, and 1787+50, respectively) show a similar excavation history as at other sections (Fig. 14), although failure did not occur at these stations until early 1912. The similarity of quantities of excavation indicates that the work at the unfailed sections was adversely affected by the failure at other sections.

Slope-Height Relations at the East Culebra Slide

The data presented in Fig. 14 effectively show the work activities but does not give a complete picture of the nature of the excavations. The cross sections, illustrated in Fig. 6, can be interpreted to give slope-height relationships to determine whether the excavation essentially steepened the slope angle or whether the excavation essentially deepened the cut to cause an increase in slope height. The overall shape of the cross sections at any stage requires considerable judgment to obtain a representative slope height and average slope inclination (Fig. 15).

The path shown for each station starts about June 1906 and is drawn through points for end of 1906, end of 1907, etc., until initial failure occurred. For reference, the slope inclination at 3V to 2H, as originally planned (Fig. 7), is shown in Fig. 15. The dashed line represents a reasonable average of the slope-height inclination relationship at failure.

The paths at the various stations are particularly revealing.

Excavation activities at sections experiencing early failures apparently were concentrated more upon steepening the slopes toward the planned inclination than upon deepening the cut. For slope heights on the order of 75 to 150 ft, the relationship presented in Fig. 15 would indicate that slope angles on the order of 45 to 35 deg produced a critical situation. Sections experiencing later failures, when at comparable heights, were somewhat flatter with slope angles on the order of 25 to 30 deg. Some of the early excavations caused an increase in inclination but not nearly as steep as at sections experiencing early failure. After the early failures, it appears that no attempt was made to steepen the inclination but that most excavation caused a deepening of the cut.

Table 2. Dates of Breaks, East Culebra Slide

Date	Stationing			
	Present		First American	
	From	To	From	To
Dec 1909	1938+10	1940+60	1770+50	1773+00
Jan 1909	1940+60	1944+10	1773+00	1776+50
May 1908	1944+10	1947+60	1776+50	1780+00
Jan 1909	1947+60	1949+60	1780+00	1782+00
Jan 1912	1949+60	1956+60	1782+00	1789+00
Sep-Nov 1908	1956+60	1960+60	1789+00	1793+00

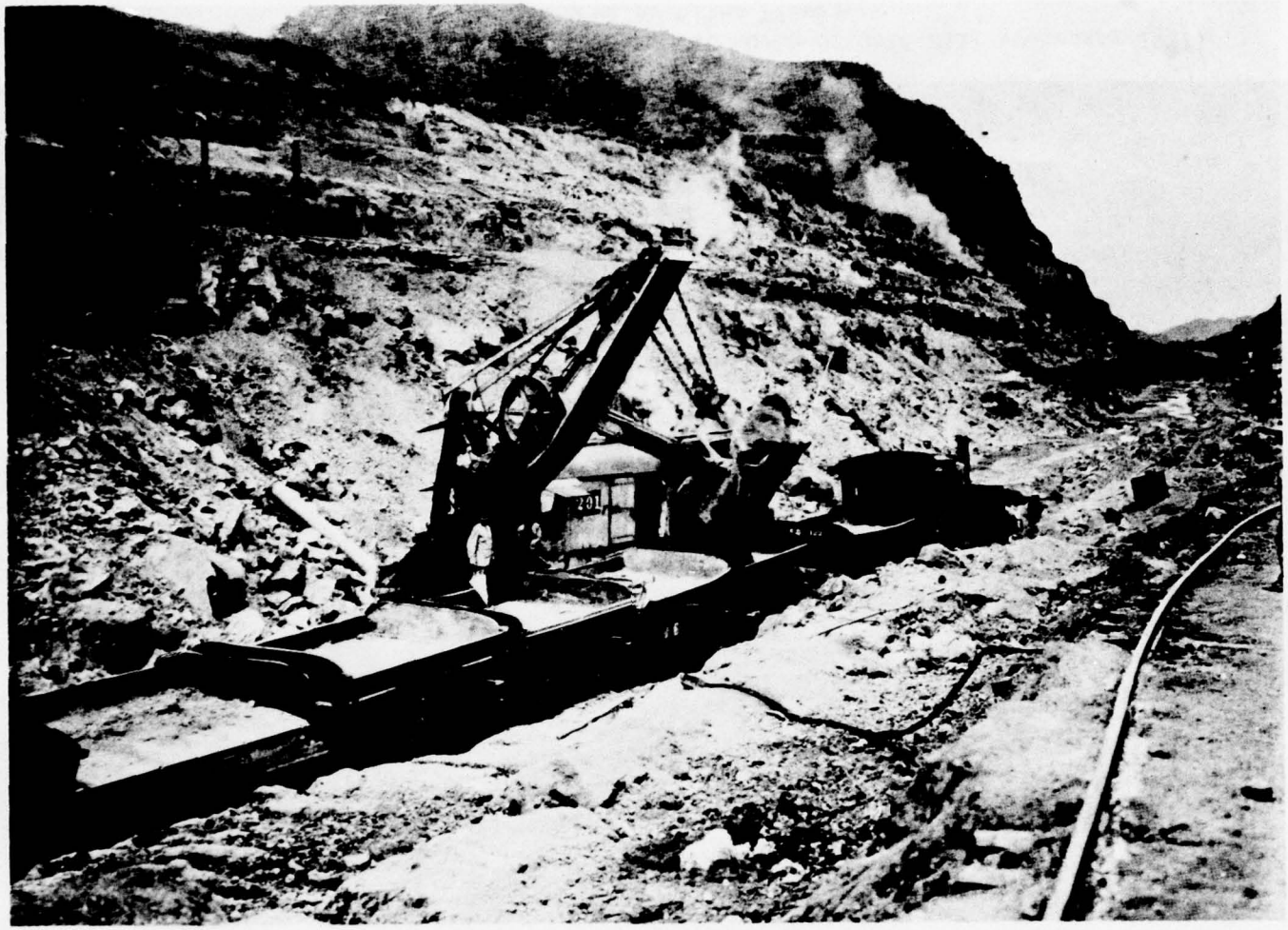

Fig. 4. A view of the eastern bank of the Cut north of Gold Hill (December 1904) (from NAS, 1924; Plate 27)

Fig. 5. A view of the eastern bank of the Cut north of Gold Hill (February 1907)
(from National Archives Files)

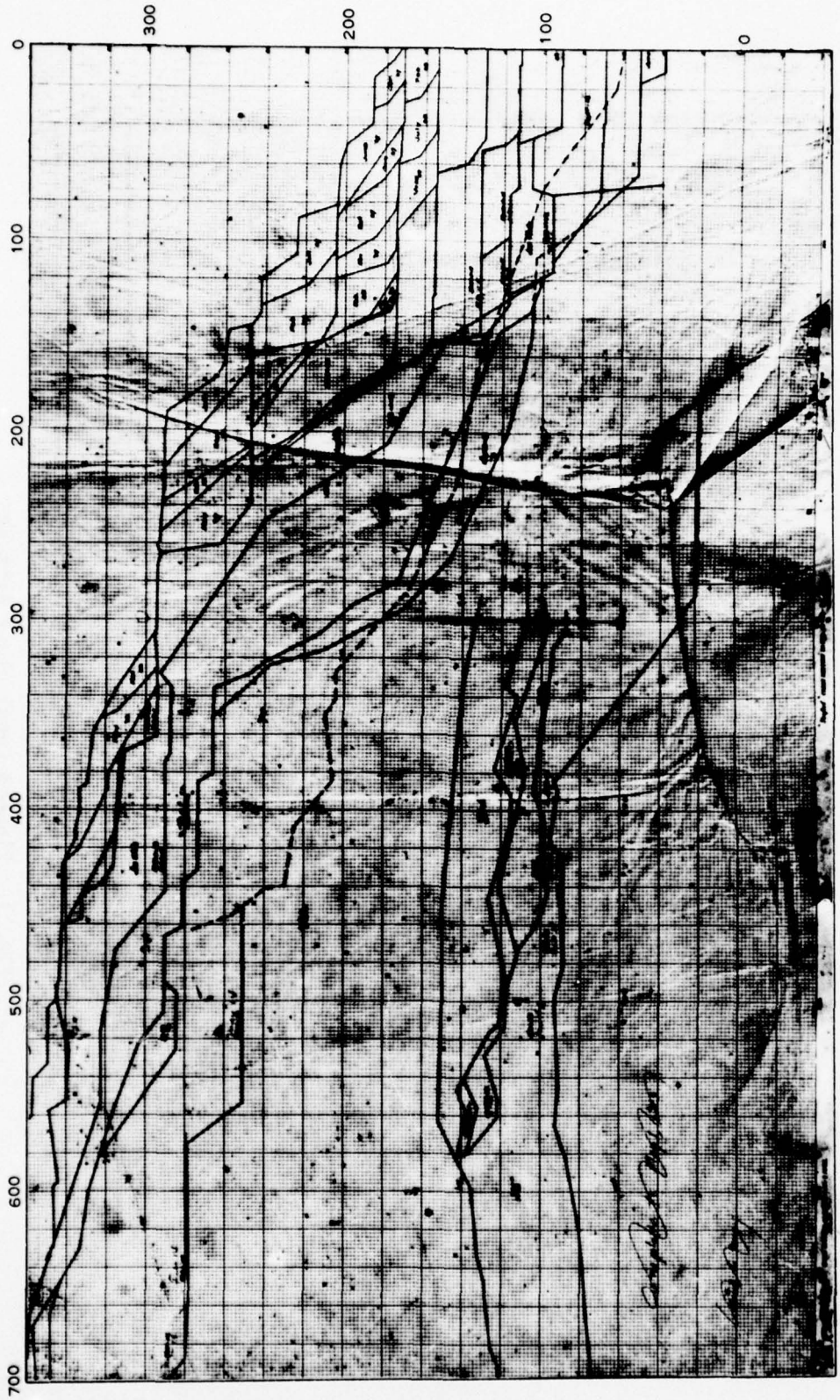

Fig. 6. Construction cross section at sta 1952+60 (1785+00)
(from FCC Vault File 288)

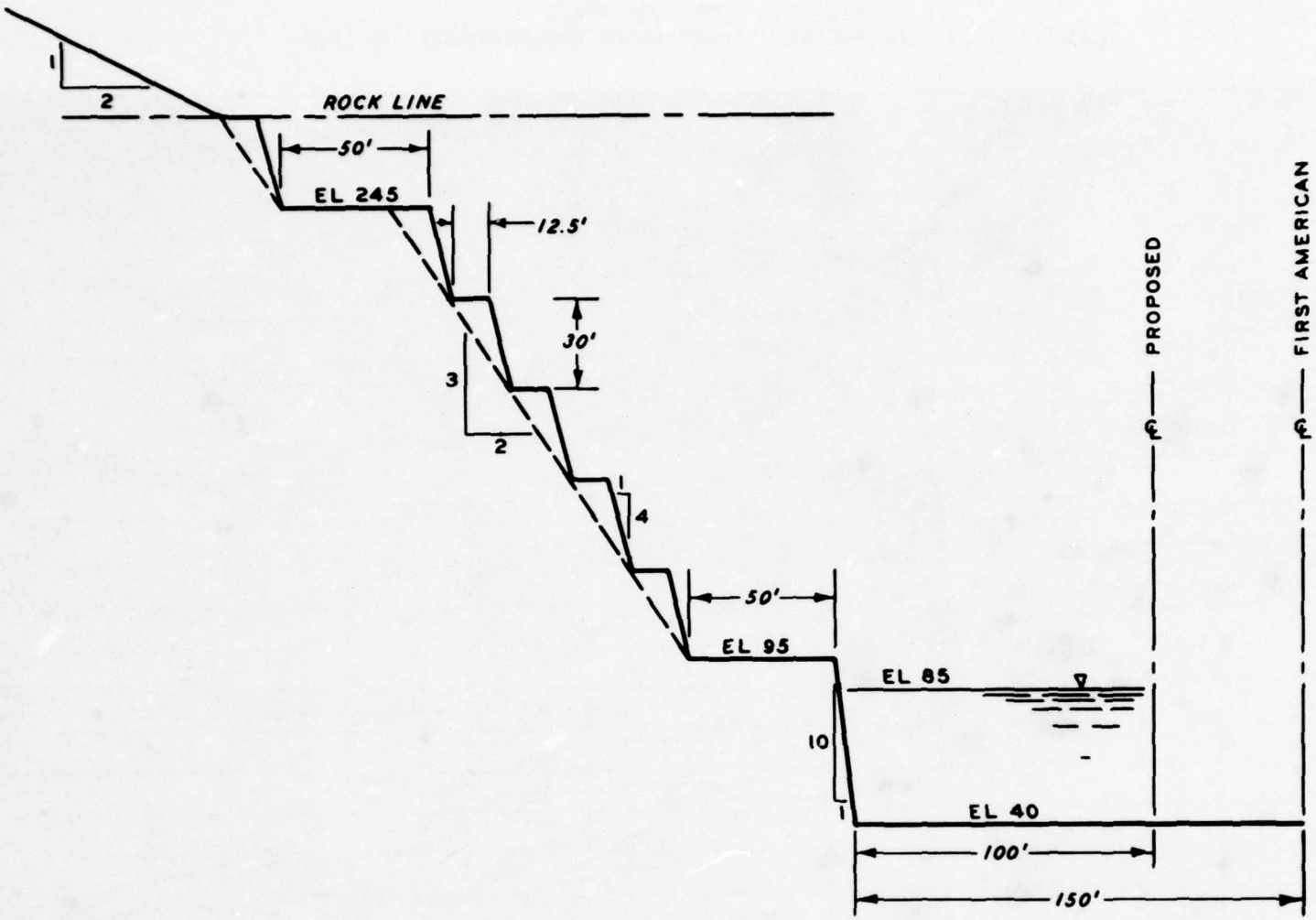

Fig. 7. Planned Canal cross section

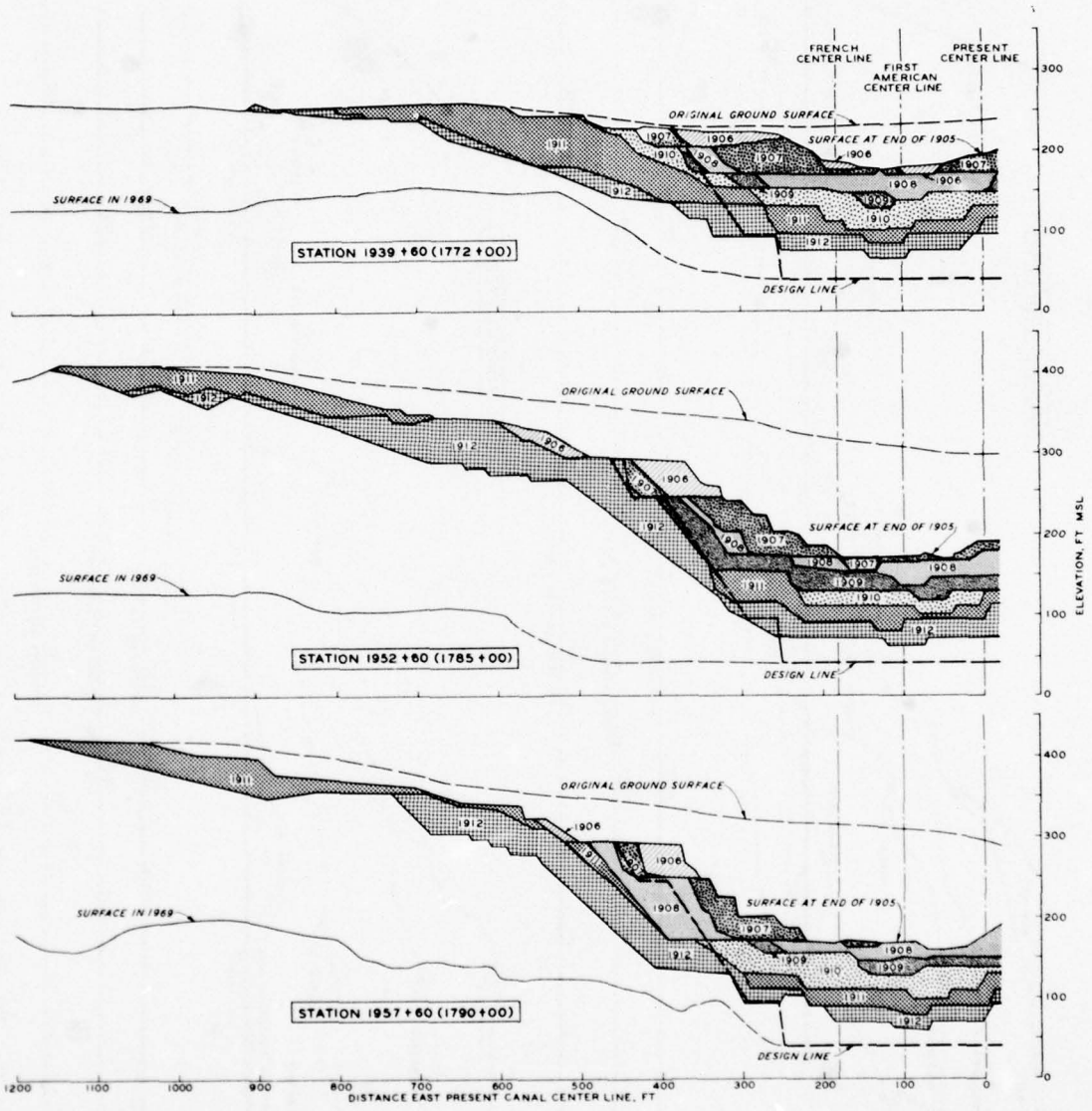

Fig. 8. Slope configuration by years, from end of 1905 through 1913 at selected stations

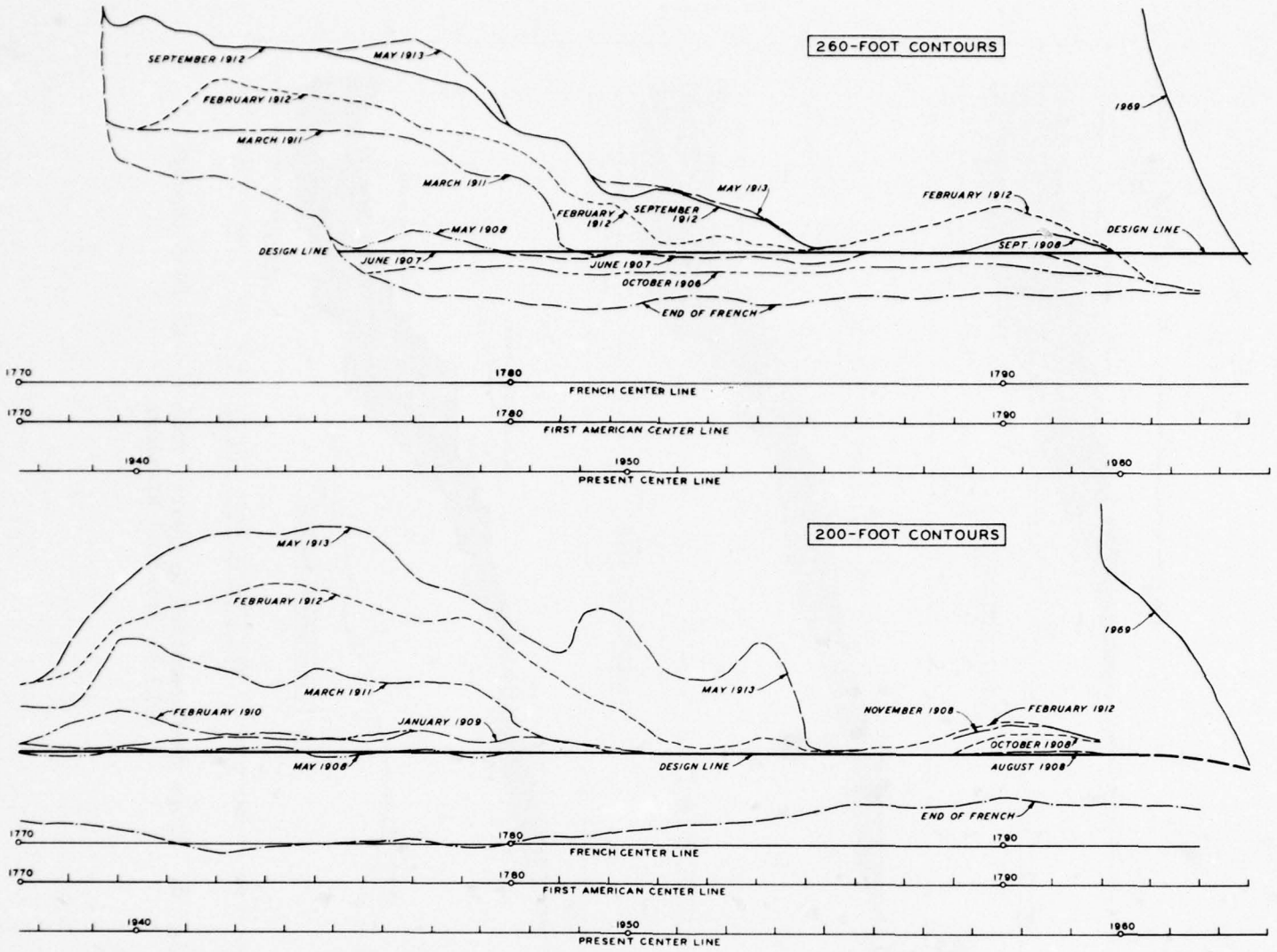

Fig. 9. Positions of the elevation 260- and 200-ft contours with time

Fig. 10. A slide on the east bank of the Cut opposite Culebra (June 1910) (from NAS, 1924; Plate 28)

Fig. 11. A mound of upheaval, 18 ft in height, in the floor of the Cut, north of Gold Hill (1910) (from NAS, 1924; Plate 29)

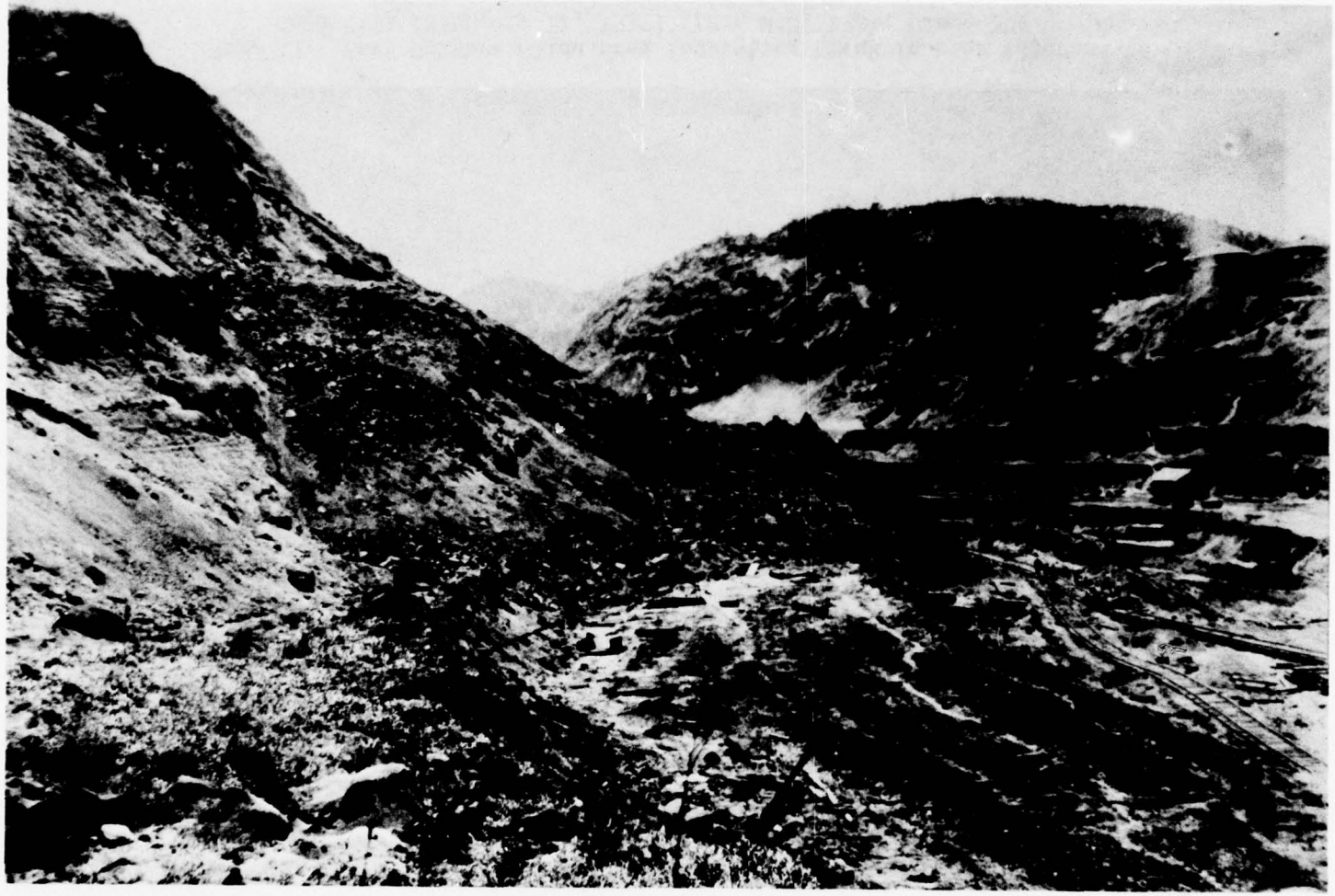

Fig. 12. Break in east bank opposite Culebra, view to the south (February 1912)
(from National Archives Files)

Fig. 13. East Culebra Slide area indicating break in bank adjacent to Gold Hill (February 11, 1912) (from NAS, 1924; Plate 30)

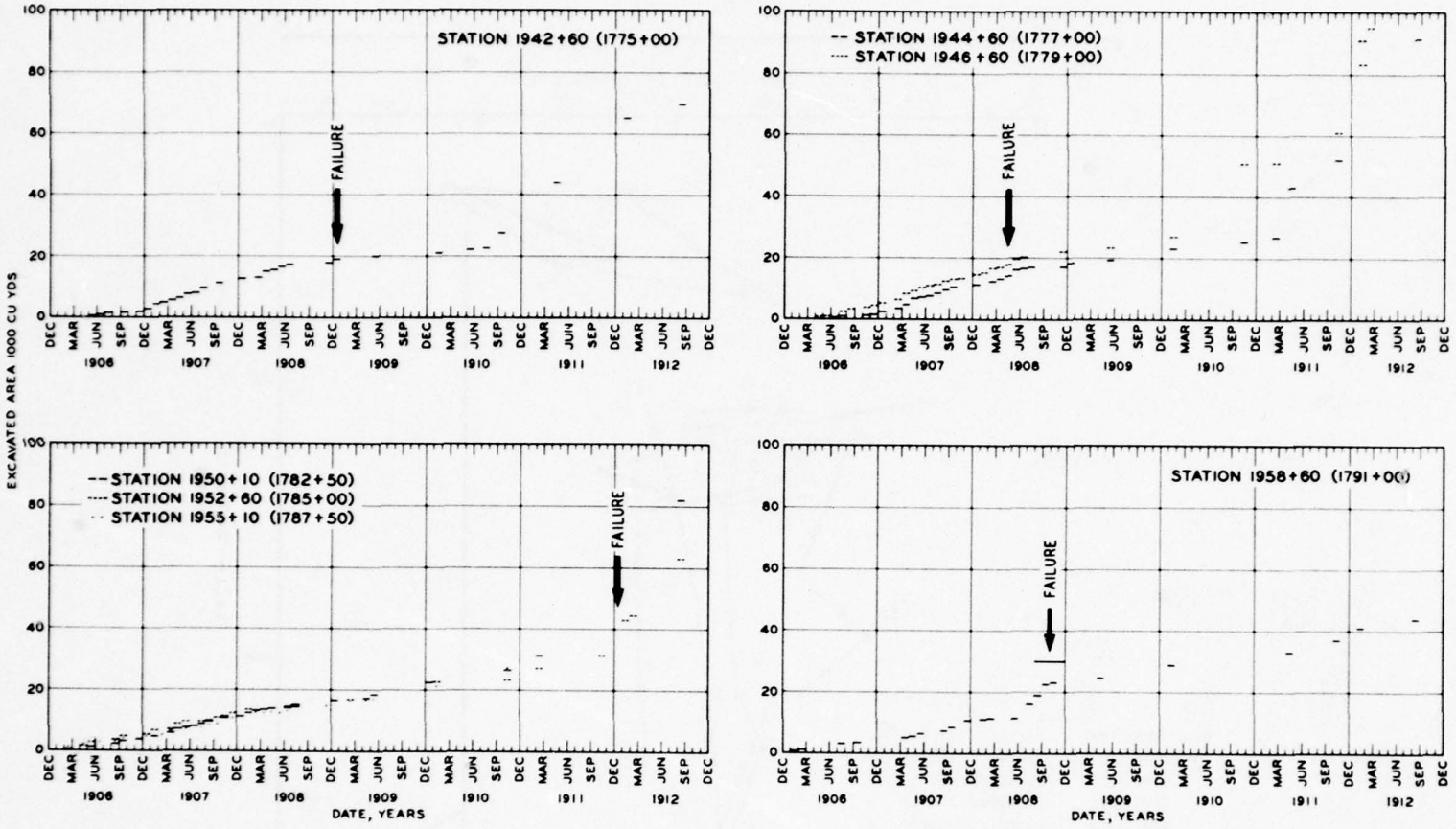

Fig. 14. Areas of excavation at selected cross sections

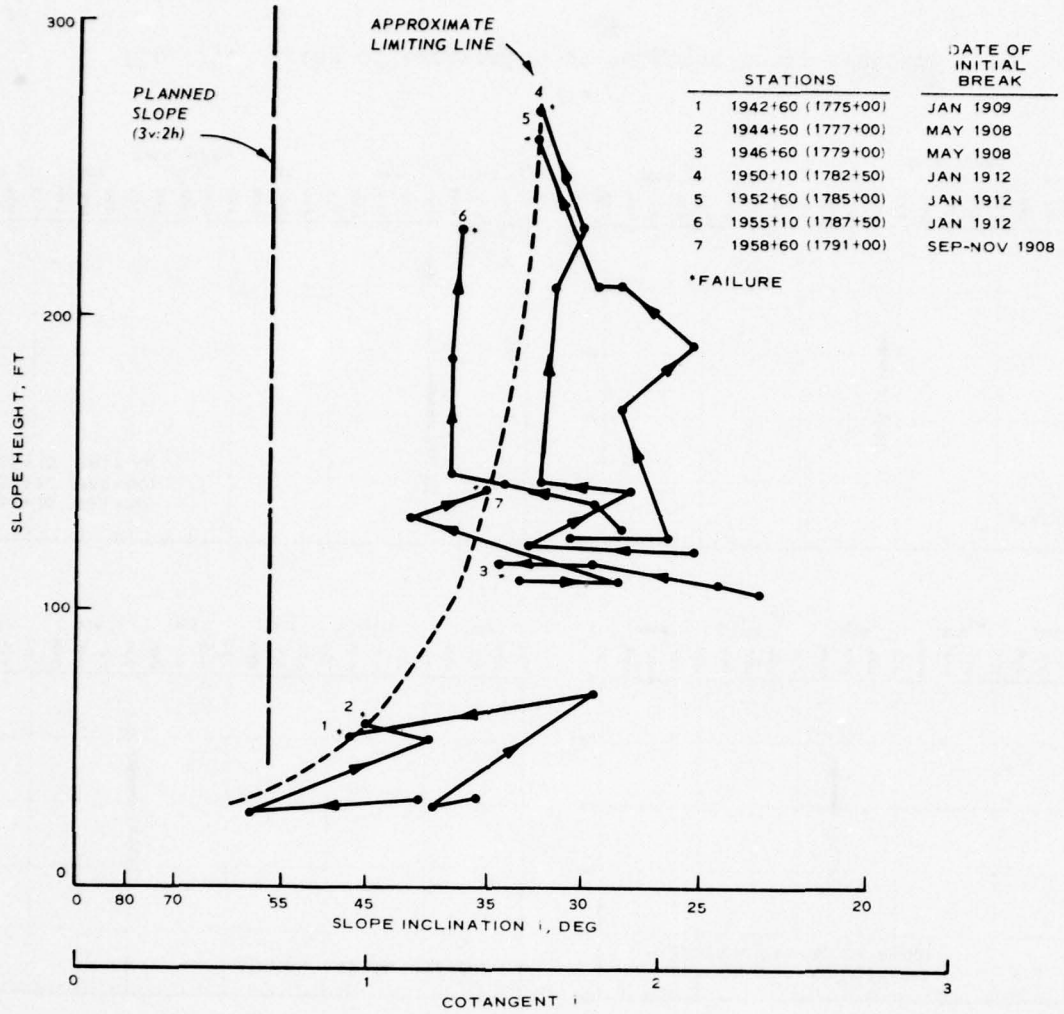

Fig. 15. Slope chart for initial failure, East Culebra Slide

CHAPTER III: GEOLOGY OF EAST CULEBRA SLIDE

The geology of the Panama Canal area has been studied by MacDonald (1924), Woodring (1957), Lutton and Banks (1970), and Lutton et al. (1975). MacDonald described general geologic features, and Woodring described the extent and characteristics of the various formations found in the Canal area. Lutton and Banks summarized previous work but more importantly used French and United States construction-day maps and recent borings to describe the geology in the immediate vicinity of the East Culebra Slide. More recent work by Lutton et al. described important geologic features to slides occurring throughout the Gaillard Cut. A most important contribution of the study by Lutton et al. was the development of a stratigraphic column through the Cucaracha formation. Studies by Banks et al. (1975) included a description of piezometric levels in the Cucaracha formation.

The previous work was reviewed in this Chapter to summarize those geologic features of importance to the occurrence of the initial slides or as they were termed, breaks, at the East Culebra Slide. In the review, emphasis was placed on the stratigraphic sequence, character of clay shale strata, location and extent of faults, and the groundwater conditions.

Regional Geology

Regional stratigraphy

Materials exposed in the banks of the Canal through the Gaillard Cut are believed to range in age from Eocene to Pliocene. All materials resulted from volcanic activities, either directly or in combination with sedimentary and weathering processes. The latest, most definitive, published regional geological data are those of Woodring (1957). The stratigraphic relationship within the Gaillard Cut, as presented by Woodring, is shown in Table 3. More recent work by R. H. Stewart, PCC geologist, has indicated that the Gatuncillo formation unconformably lies beneath the Culebra formation particularly at the East Culebra Slide (Table 3). Differences in the stratigraphic correlations are important only for regional studies; for this particular study, the East Culebra Slide involves only

the Cucaracha formation and the overlying residual, weathered clay.

Regional structure

The structure of the Isthmus, in a broad sense, is anticlinal with local intrusions of igneous rocks. Near the intrusions, the dip of beds may be quite steep; near the flanks of the anticline the dips are comparatively flat and continuous except for local folds and faults (MacDonald, 1924). In the study area, a downfold, or syncline, trends across the Gaillard Cut to take the stronger strata of the Culebra formation below the bottom of the Canal for a horizontal distance of more than a mile and to leave the weaker strata of the Cucaracha formation to form the sides of the Cut near its deepest point. The bedding in the area dips gently toward the south or oblique to the Canal, but is intersected by numerous local faults to produce graben-horst features in the Culebra Reach. The faults apparently are part of a regional system of faults that divide the Isthmus into a group of N-S- to NNE-SSW-trending fault blocks. The geologic structure has been shown to be important to the occurrence of slides in the Gaillard Cut and is discussed subsequently for the East Culebra Slide.

Local Geology

Figure 16 shows sections through the present East Culebra Slide. The original ground surface, ground surface at the time of the initial breaks, present ground surface, and present depth of sliding are shown. As was developed in Chapter II of this thesis, the initial breaks occurred during construction--at times before the Canal had been excavated to its full prism dimensions (bottom el +40 ft). As shown in Fig. 16, the present ground surface is approximately 250 ft lower than the ground surface that existed at the time of breaks. Most of the material originally involved in the sliding has been removed; material that is still present has been reworked and exists only as slide debris. Thus information on those local geologic features of importance to the initial development of the East Culebra Slide must be obtained from construction-day records, or from mapping or borings in nearby areas, or, if in the area of the East Culebra Slide, beneath the present slide surface.

Physiography

The study area, prior to construction, exhibited a moderately hilly topography (Fig. 17). The headwaters of the Rio Obispo and its tributaries had incised shallow, broad valleys to the north. The east and west bounds of the study area once were dominated by the topographic expressions of Gold Hill (el +660 ft) and Zion Hill (el +550 ft), respectively. These features formed the Isthmian Divide and were separated by a saddle (approximate el +360 ft) on the Canal line. Lower hills--Contractors Hill to the south, Cerro Lirio to the southwest, the Office Hill or Hodges Hill to the northwest--completed the relief at the bounds of the study area. Generally, the hills are composed of durable basalts or breccia masses, possibly localized over volcanic vents.

Presently, the Canal and subsequent slide developments are the most conspicuous changes noticed in the study area. These changes are illustrated by Fig. 16. Areas now lying within the East Culebra Slide and along the lower end and back side of the low ridge extending northwest from Gold Hill were used as dumps for the material excavated by the French. The dumps are visible today but are largely covered by vegetation. The dump, el +246 ft (75-metre level), and its continuation to the northwest covered large portions of the Rio Obispo drainage basin in the area (Fig. 18). These dumps diverted the surface waters from the construction area, but formed a reservoir, the Lirio Lagoon, fed by surface runoff. The reservoir existed during the American construction days, until 1923, when drainage operations were started.

Stratigraphy

General. The surficial geology as exposed in January 1908, or about the beginning of major sliding, is shown in Fig. 18. The geological data were based largely on numerous cross sections made during construction. As shown on the map, the Cucaracha formation (overlain by residual soil and spoil material) formed the upper portion of the East Culebra Slide. Sectional views through the Slide (Fig. 19) and a longitudinal view (Fig. 20) indicate the general stratigraphic sequence in the Cucaracha and underlying Culebra formations. As was developed in Chapter II and shown on appropriate cross sections in Chapter V, the initial sliding at the East Culebra Slide involved only the Cucaracha formation. Thus, the

stratigraphy of the Cucaracha formation is of primary importance and will be discussed in detail. The stratigraphy of the underlying Culebra formation is summarized for completeness.

Culebra formation. Oysters, crabs, and other marine fossils found in the Culebra formation indicate the environment of deposition to be nearshore marine and the age to be early Miocene (Woodring, 1957). The formation has been generally considered to consist of upper and lower portions (MacDonald, 1924, Woodring, 1957). The lower portion of the formation contains soft, thin-bedded or laminated beds of carbonaceous or lignitic shales, carbonaceous silty mudstones, and shaly siltstones with subordinate tuffaceous and calcareous sandstone and conglomerate. The upper portion consists of strata varying from sandy limestone to calcareous sandstone with fairly abundant calcareous concretions. The strata in the upper half are commonly from 3 to 10 ft thick and are separated by thin partings of soft carbonaceous shale and laminated tuffaceous siltstone. The shale and siltstone crumble after a year or so of exposure to the atmosphere. A few thin basalt layers interpreted tentatively as sills have been intercepted in borings. Recent borings indicate the Culebra is about 350 ft thick.

Cucaracha formation. This formation overlies the Culebra formation. The contact is marked by one or more unconformities. The Cucaracha formation consists of clay shale with subordinate layers of siltstone, sandstone, and conglomerate. The unit is tuffaceous in nature, and its high clay content results from the breakdown of volcanic materials that once constituted a major part of individual strata.

The Cucaracha formation has been regarded as terrestrial in origin, mainly because of the presence of mammal and plant remains. The presence of marine fossils in the lower Cucaracha, however, suggests that the contact between the Cucaracha and the Culebra is in part transitional, with marine conditions existing intermittently during deposition. A transition zone has been delineated within the Cucaracha on the geological sections (Figs. 19 and 20) to include characteristics of both the Cucaracha and Culebra formations. The upper limit of the transition zone was based on the arrangement of sandstone and conglomerate strata and the position of calcareous concretions in the shale. The thickness of the transition

zone ranges from 130 to 150 ft at the location of the East Culebra Slide.

The upper part of the Cucaracha formation has been altered by weathering. The action of acidic water on the shale above the water table forms a residual, weathered clay. The clay is yellow and red in color, indicating oxidation of iron. Below the water table, the shale is greenish-gray in color. Certain strata, a few feet thick, are brown to maroon in color (termed red beds), and elsewhere the shale may be mottled and crisscrossed with maroon-colored material.

The Cucaracha formation contains a hard and resistant layer of welded tuff (also referred to as andesite and dacite breccia), from 10 to 20 ft thick, lying about 300 ft above its base (Figs. 19 and 20). The welded tuff layer is persistent in the area of the East Culebra Slide and is useful in establishing the detailed stratigraphic sequence in the Cucaracha formation as well as in determining the continuity of strata between borings.

Four recent borings have been made in the general area. Boring WEC-1 was made into material presently underlying the East Culebra Slide; boring WMS-1 was made in the Model Slope, about 2000 ft south of boring WEC-1; boring WWC-1 was made into material presently underlying the West Culebra Slide at a location about 1200 ft southwest of boring WEC-1. Locations of borings WEC-1, WMS-1, and WWC-1 are shown in Fig. 3. Boring WCSE-1 was made at the site of the Cucaracha Slide (Fig. 2). The borings were continuously sampled and described in detail. Logs of the borings are shown in Fig. 21. Although the ground surface elevations at the top of the borings were comparable, faulting in the area has caused the borings to encounter the same strata at different depths. As a consequence, a composite stratigraphic column (Fig. 22) of the Cucaracha and underlying Culebra formations can be established (Lutton et al., 1975). When the composite stratigraphic column was constructed, logs of borings, other than those shown in Fig. 21, were reviewed for confirming information.

The composite column indicates the alternation of sandstone and shale layers below the welded tuff in the Cucaracha formation. A brown or black lignitic shale layer commonly (but not always) occurs at the top of each shale layer. Grain size increases more or less gradually downward through a sedimentary cycle of shale, silty shale, siltstone,

sandstone, and conglomerate. A marked change in grain size exists at the base of the conglomerate, and the sedimentary cycle is repeated. At least eight such sedimentary cycles are shown on the composite stratigraphic column, Fig. 22 (Lutton et al., 1975).

Figure 23 shows the detailed stratigraphy along a section within the Cucaracha formation (Lutton et al., 1975). The section uses data from three French borings (K54.550-II, -V, -VIII) and two PCC borings (SC-15 and -21) made long after the sliding activity had ceased. A gap in information between the two sets of borings was completed with data from the log of boring GH-10 located about 1200 ft to the southeast. The stratigraphic sequence depicted in Fig. 23 compares closely with the composite stratigraphic column (Fig. 22). The correspondence of the data between the two sources is important since for the purposes of analyses (Chapter V), it will be possible to determine the sequence of materials encountered at any section once the locations of marker beds are established.

As indicated on the section shown in Fig. 23, the strata correlate extremely well between the French borings to show continuous beds dipping toward the Canal at 2 to 4 deg. While no stratigraphic data exist between boring K54.550-VIII and the major fault shown beyond the boring, it is reasonable to assume (in the absence of faults, as discussed subsequently) that the individual layers are continuous at least to the fault contact.

Figure 20 shows the general stratigraphic sequence along the French center line. Although the present East Culebra Slide extends from sta 1935+00 to 1964+00 (1767+40 to 1796+40), discussions presented in Chapter II of this thesis showed the early breaks occurred between sta 1938+10 to 1960+60 (1770+50 to 1793+00). The welded tuff layer varied some in thickness between sta 1946+60 and 1957+60 (1779+00 and 1790+00), but the base of the layer is located between el +210 and +230 ft. Between sta 1946+60 and 1957+60 (1779+00 and 1790+00) the stratigraphic sequence can be established with respect to the welded tuff layer. The welded tuff layer daylights at sta 1946+60 (1779+00); therefore, between sta 1938+10 and 1946+60 (1770+50 and 1779+00) the conglomeratic sandstone layer lying about 100 ft beneath the welded tuff layer

can be used to establish the stratigraphic sequence. Between sta 1957+60 and 1960+60 (1790+00 and 1793+00) the welded tuff layer is present, but the elevation of its base decreases from about +210 to +110 ft. Additionally, between these stations the stratigraphic sequence evidently differs from those presented by the composite column (Fig. 22) and on the detailed section at sta 1957+60 (1790+00) (Fig. 23). Thus, while the one section required for analysis between sta 1957+60 and 1960+60 (1790+00 and 1793+00) will contain a sequence of materials with respect to the welded tuff, the stratigraphic sequence is only approximate.

Primary structure

The discussion above has indicated that the Cucaracha formation contained relatively flat-lying continuous strata. Before the continuity of the beds can be accepted, the nature of faults in the area must be investigated.

The geological structure in the study area (Fig. 18) was reconstructed largely from geological sections (PCC Vault File 903-1 and 902-1) prepared during American construction and from boring logs prepared since about 1940 (Lutton and Banks, 1970). The geological map, Fig. 18, compares closely with an earlier published map (MacDonald, 1915), but differs slightly from later maps (e.g., MacDonald, 1947). The major difference is in the trend of faults in the area; on the earlier maps the faults trended about N-S, whereas in later maps the trend was more NE-SW. The earlier work possibly benefitted from fresh exposures and therefore presented a more representative indication of structure at the East Culebra Slide (Lutton and Banks, 1970).

One zone of several small faults (marked A-1, A-2, and A-3, Fig. 18) crosses the Canal center line near sta 1937 (near sta 1770). These faults are vertical or dip westward, but the down-thrown side is on the east, so that they apparently are reverse faults. The fault marked A-1 in Fig. 18 is shown on the longitudinal section (Fig. 20) as it crosses the French center line. The strata are apparently offset about 20 ft. The faults marked A-2 and A-3 are discontinuous with neither crossing the French center line. However, their alignment strongly suggests that they are the same fault. In any event, the longitudinal section shows no offset in the strata where they approach

the center line. The faults in this zone trend toward the north and were traced until they were obscured by the French dumps. Their location corresponds roughly to the present scarp of the East Culebra Slide in that area.

A vertical fault (labeled B, Fig. 18) crosses the center line at about sta 1955+10 (1787+50) (Fig. 20). The strata apparently are offset about 15 ft downward to the east of the fault. The fault extended to the north until it also was obscured by the French dumps. The fault was assumed to continue its northward trend beneath the dumps, since some sections constructed for analyses (Chapter V) cross the projected fault.

The largest fault (marked C, Fig. 18) trends about N20°W from the north flank of Gold Hill. The fault is normal with a dip of approximately 60°W. The fault is shown in Figs. 19 and 23. The beds are offset as much as 300 ft vertically at the fault. Although its extension beyond the East Culebra Slide is open to question, the present backscarp of the Slide is largely bounded by the fault. With the removal of material through sliding, strata of the Culebra formation now stand exposed in the slide scarp.

The irregular mass of basalt forming Gold Hill on the south of the East Culebra Slide is similar to other basalt masses in the region. The flow structure is funnel-shaped. The prominent columnar jointing, oriented normal to the contact and flow structure, appears to dip outward in all directions from the center of the mass to indicate that the mass is intrusive. Although extensive deformations occurred near the extremities of Gold Hill, apparently the Cucaracha and Culebra strata were not deformed extensively. The fault (marked D, Fig. 18) separated the subsiding basalt mass from the Cucaracha and Culebra formations. The beds immediately adjacent to the fault show some drag features, but the effect is minimal. Over distances of a few tens of feet the bedding is again nearly horizontal.

Joint and slickensided features

Joints and slickenslides are important geologic features in the materials in the study area. No efforts have been made to obtain joint data (i.e., spacing, opening, continuity, or spatial distribution) within the Cucaracha formation. The Annual Report (1912), apparently to dispel

the notion that the Cucaracha was soft and mudlike, specifically described the material heaved up at the toe of the East Culebra Slide as being

> ...composed of pieces of argillaceous sandstone varying in volume from a few cubic inches to 20 or 30 cubic yards and averaging from 1 to 3 cubic yards.

Although the joint data might prove enlightening and useful in understanding the slide behavior, apparently the presence of numerous slickensides in certain horizons was more readily observed and was described in detail. These slickensides, according to Thompson (1947),

> ...are relatively short (averaging less than 3 in.) curved surfaces that do not exhibit any pattern of orientation or appreciable continuity, except locally where their disposition has been influenced by faulting.

Thompson quotes from a letter report on Cucaracha shale by a Bailey Willis:

> All specimens exhibit an internal structure, a sheared structure similar to that of serpentine. The spacing of major shears is such as to divide the mass into fragments which are from 1/10 to 3/10 of an inch on the side, but the shearing is in fact microscopic in dimensions.

Thompson continues:

> There can be no doubt as to the weakening in resistance to shear due to numerous polished surfaces represented by slickensides within a stratum or series of strata of the Cucaracha formation. This has been proved by many tests on samples that, with the exception of degree of slickensiding, were of an apparently identical nature. The weakest materials to compressive stresses were those showing most pronounced slickensiding. However, the fact of disorientation of the slickensides should not be overlooked, in that incipient sliding of a bank along any failure arc would follow either around the solid pieces of Cucaracha via the existing slickensided surfaces or shear through them. It follows that their weakening effect is not as great as would be the case if they were parallel to potential slide shear planes.

Thompson concluded that:

(a) The slickensided horizons are found throughout the Cucaracha formation in clay shale members, and to a lesser degree in some of its other component beds.

(b) These are not of the conventional type induced by fault movement that characteristically show orientation of the polished and striated surfaces. The Cucaracha slickensides are short, interconnected, highly polished surfaces of arcuate configuration.

(c) Their origin is attributed to a change in volume when the original ashy materials of the formation underwent hydration and chemical alteration, with accompanying swelling. Since this alteration took place at a time when the formation was under considerable load, shearing stresses were set up, the clayey beds squeezed and shifted, and the polished surfaces now observable were created.

(d) The effect of slickensides on test samples or cut slopes is one of weakening. The extent of weakening is a function of the intensity of slickensiding, as reflected by polishing, and the closeness of slickenside spacing.

(e) The slickensides offer the easiest means by which free water within the formation can migrate. It is partially through these minute voids that hydrostatic forces are transmitted. They also store water, the weight of which adds to the load applied at the toe of a cut, but their presence facilitates the escape of free water by offering easier, interconnected drainage paths when the water table is drawn down by excavation than would be the case if they were not present.

Thompson restricted his discussion to slickensides found in the Cucaracha formation. The abundance of slickensides in the clay shale portions of the Cucaracha formation has been confirmed in studies by the WES (Lutton and Banks, 1970), as well as others. For example, in logging the recent borings (Fig. 21), the frequency of slickensides was denoted by the symbols SLK for one to three slickensides per foot and V SLK for more than three slickensides per foot. Absence of these symbols indicated that no slickensides were observed in the field. However, experience proved that many samples of material, immediately upon extraction from the sampling tube, may only exhibit a few prominent slickensides (Fig. 24a). With time, the samples expand (Fig. 24b) and completely

fall apart along numerous slickensides (Fig. 24c). The sample shown in Fig. 24a was waxed and stored in a humid room for approximately two months before being reopened (Fig. 24b). Without this precaution, many samples exhibit the same behavior within perhaps 5 to 10 min when exposed to the atmosphere.

Recent developments in radiography have provided means of viewing the internal structure of the Cucaracha clay shale (Krinitzsky, 1970). Radiography uses penetrating radiation, either X-rays or gamma rays, to produce shadow images of areas of varying densities. Figure 25 shows radiographs of several samples taken above and below the present depth of sliding at the East Culebra Slide. Numerous discontinuities are noted in each of the radiographs. A horizontal slice from Sample 4 in the slide debris shows many curved surfaces, suggesting the material had been heavily fractured and reworked almost to the state of remolding. Sample 5, nearer the failure surface but still in the slide debris, shows several major throughgoing discontinuities and many shorter and smaller discontinuities. The larger fractures apparently have been healed to some extent with a secondary mineral. Sample 6, taken slightly below the failure surface, shows several large nearly horizontal fractures, suggesting that the sample had experienced horizontal shear. Samples 10 and 17 are taken well below the sliding surface but indicate the continued presence of fractures even at depth. The fractures at depth are almost always slickensided and polished to a high gloss.

Groundwater Conditions

The groundwater conditions existing at the time of the initial failure of the East Culebra Slide are most important to the proper analysis of the Slide. Unfortunately those conditions were not documented and must be inferred. The NAS (1924) report discussed the interrelation of water and general slide activity and emphasized the beneficial effects of surface drainage by diversion ditches. Insofar as future observation and investigation, the NAS report stated:

> As underground water is of great importance in promoting slides in various ways, it should be carefully

> studied in the Canal Zone. These studies should be carried on in undisturbed areas of each of the formations which have been involved in important slides....A fully satisfactory investigation of this subject would require work in the following directions:
>
> (a) Determination of water-table in various rocks in the wet and dry seasons.
>
> (b) Rate of transmission of water through various rocks under different pressures.

The NAS report stated that during the committee's visit to the Canal no studies concerning the groundwater had been made but that arrangements were made for such a study. However, according to the report (NAS, 1924): "...the...investigations of the underground water...*were* suspended by action of the Canal authorities." This lack of data led to the NAS recommendation for future observation and investigation. No records exist that such a study was ever completed.

Present data come from two principal sources: observation of water levels in borings and observation of piezometric levels. In either case, it is important to delineate the rainfall pattern at the Slide. The mean annual rainfall is about 70 in.; however, as indicated by Fig. 26, most of the rain falls between May and November. As a consequence, water levels in borings and piezometers tend to be higher between these months than between December and April.

Boring observations

Previous discussions indicated that the uppermost portion of the Cucaracha formation was weathered, residual clay, colored yellow and red, indicating oxidation of iron. The thickness of the weathered clay varied from about 90 ft on the side of Gold Hill to about 10 ft on gentle topography (Fig. 20). Although the groundwater level varies seasonally throughout the weathered zone, the base of the weathered clay gives an approximate lower limit of the groundwater table that existed in unfailed areas. Numerous observations of water levels in open borings have verified this relationship (Lutton and Banks, 1970). An example is illustrated on the detailed stratigraphic cross section (Fig. 23).

Figure 27 shows a composite plot of water levels recorded in open borings on both the east and west sides of the Canal. (The data are tabulated in Tables 6 and 7, in the report by Lutton and Banks (1970).)

The ground surface, bottom of boring, and elevation (and dates) of water levels are shown. The water level observations on the east side of the Canal were made in separate borings in 1916, the mid-1940's, and the late 1960's - long after major sliding activity had ceased and the ground surface had been reduced in elevation to about that of today. As shown in Fig. 27, the groundwater levels are at or near the ground surface. The water level observations for the borings on the west side of the Canal are from the Hodges Hill area, northwest of the East Culebra Slide (Fig. 3). The Hodges Hill area has not been affected by slides, and ground surface elevations are similar to or slightly in excess of those existing at the East Culebra Slide before the initial breaks. As shown in Fig. 27, the groundwater levels are high and in almost all cases within the previously stated depths of 10 to 90 ft below the ground surface. Since the data shown in Fig. 27 were not recorded continuously over a long period of time, they do not represent maximum or minimum elevations, and it is possible that during periods of high or sustained rainfalls the groundwater levels were higher.

No records exist of artesian flow in the East Culebra Slide or Hodges Hill area. However, borings made beyond the crest of the Model Slope, near the base of Zion Hill, have produced artesian flows during and shortly following periods of high rainfall. Since the artesian flows result from the proximity of the topographic high, the presence of Gold Hill to the south of the East Culebra Slide (Fig. 3) may have produced similar conditions prior to the initiation of breaks at the site.

Two observations were made at dates long after the initial breaks to indicate that the groundwater table was high in the area, with the Lirio Lagoon (Fig. 18) being a prime source of groundwater. As developed in Chapter II, the East Culebra Slide had approximately reached its present dimensions by 1916, with only intermittent and smaller breaks adding additional area. One such addition occurred on 20 December 1922 when a break reestablished the backscarp of the Slide about 110 ft beyond the old scarp. A report of the break (Canal Record, 31 January 1923) stated:

> A survey made at the back of the slide...revealed numerous seepage streams...approximately 75 feet

> below the surface of the ground, over practically the entire distance of the new break. (*The description indicated that the new break was about 1800 ft in length.*) The direction was from Lirio Lagoon, the drainage surface of which is on an elevation approximately that of the seepage streams (*approximate el. +210 ft; see Fig. 18).* It is believed that the seepage from the lagoon, intensified by the torrential rains of the past few months...is accountable in no small part for...slides at this point.

Later a report (Canal Record, 25 July 1923) stated:

> Seepage streams at the plus 185-foot elevation on the north end of the slide...increased in numbers and volume as the Lirio Lagoon and swamp behind the slide area filled with water, as a result of heavy rains....

This discussion on groundwater conditions provides little quantitative data relating to the initial breaks but qualitatively suggests that the groundwater table was quite high and possible at times almost reached the ground surface.

While a knowledge of the position of the groundwater table is important, additional information is required to determine the water pressures existing at depth within individual strata. That information was sought from a review of recent piezometer data.

Piezometer observations

Piezometer installations. Fifteen Casagrande open-system piezometers were placed in borings clustered around reference borings WEC-1, WMS-1, and WCSE-1 (Fig. 21). The installation procedures have been described by Banks et al. (1975).

Piezometer results. The piezometric results are shown in Figs. 28-42; inserts on each figure show the detailed stratigraphy in the vicinity of each piezometer tip. Results are given in Table 4.

After installation, the piezometer riser pipes were filled with water and readings taken over a period of time sufficient for the piezometers to reach equilibrium. The rates at which the water levels fell in the piezometers were used to compute field permeabilities by the method suggested by Hvorslev (1951). The field coefficients of permeability varied from 10^{-9} to 10^{-6} cm/sec. Generally, the lower values are associated with the clay shale layers, whereas the higher values are

associated with the clayey sandstone layers.

Figures 28-42 show the piezometric levels for a period of approximately 16 months. The piezometer levels behaved in one of three distinctive manners. First, some piezometers indicated levels responsive to the more or less constant water level in the Canal. Second, some piezometers indicated levels that were higher than the Canal water level and varied seasonally with the rainfall. Third, some piezometers indicated levels lower than Canal water level. The indicated piezometric levels are summarized for each installation in Figs. 43-45. At the East Culebra Slide installation (Fig. 43), three piezometers indicate a piezometric level coincident with the Canal water level; the other three piezometers show levels substantially lower than the Canal water level. At the Model Slope installation (Fig. 44), three piezometers indicated a level coincident with the Canal water level. Two piezometers showed a level lower than the Canal water level, while the upper piezometer, WMS-P1B (Fig. 35) was strongly influenced by rainfall. At the South Cucaracha installation (Fig. 45), the three piezometers showed levels higher than the Canal water level; Figs. 40-42 indicated that the levels vary in response to the rainfall trends (Fig. 26).

The only additional source of information concerning piezometric levels in the Curaracha formation is the Hodges Hill piezometric data (Table 5). In Fig. 46, the locations of piezometers are shown (with respect to the offset distance from the Canal center line) as well as the tip elevation, piezometric level (in January 1971), and the ground surface. Inserts in Fig. 46 show, firstly, the piezometric level to be higher than the Canal water level except in a few cases for piezometers near the Canal edge and, secondly, that piezometric levels average about 8 ft and increase to about 57 and 118 ft above the Canal water elevation in piezometers placed approximately 400, 650, and 1050 ft, respectively, from the Canal center line. The range of piezometer levels and water levels in adjacent open-cased borings is plotted on the inserts; as shown, both levels are comparable in elevation. The piezometer data from the East Culebra Slide, Model Slope, and South Cucaracha Slide are shown in Fig. 46 for comparison to the Hodges Hill data. The piezometers at the East Culebra Slide and at the Model Slope indicated a

lower piezometric level than for those at Hodges Hill; the piezometric levels at the South Cucaracha Slide were comparable with those in Hodges Hill. A review of information in Tables 4 and 5 indicates that for piezometers exhibiting low piezometer levels, typically the tips were located in deep strata of predominately clay shales. Those piezometers exhibiting high piezometric levels were typically located in shallow predominately clay shale strata or in sandstone/siltstone strata.

Reasons for the low piezometric levels have been investigated by Lutton and Banks (1970) and Banks et al. (1975). It was concluded from those investigations that the low piezometric level reflected a reduction in pore pressure in the deep clay shale strata caused by removal of overburden by Canal excavation, sliding, and slope maintenance. The investigations further concluded that the low piezometric levels would increase slowly with time as the stresses in the shale strata reach equilibrium with the present stress conditions.

Since the interface between clay shales and sandstone/siltstone strata is a probable location of failure surfaces, it is important specifically to determine the extent to which piezometric levels within the sandstone/siltstone layers reflect groundwater levels indicated by open-cased borings. Those data, plotted in Fig. 47, indicate that piezometric levels in sandstone strata are more or less equal to water levels in open borings.

Summary statement

Inferences must be drawn from observations presented above relative to groundwater conditions likely to have existed at the time of slide development. Table 2 indicated dates of sliding; as shown, the slides developed during or shortly following the rainy season. Previous discussions indicated that the groundwater table could be assumed to be high with near coincidence with the ground surface existing at the time of failure. The discussion further indicated that while the clay shale layers are slow to respond to changes in stress conditions, the clayey sandstone or siltstone layers readily respond and do in fact exhibit water pressures directly relatable to the groundwater table. Piezometers in upper clay shale layers indicate responsiveness to rainfall. It is assumed that for the early breaks, piezometric levels in clay shale

strata to the rear of the breaks would have been equally responsive. The clay shale layers presently exhibiting low piezometric levels are located at depths near and below the present Canal bottom where lateral expansion has been inhibited. Such restraints did not exist during early sliding since, as discussed in Chapter II, the slides developed on weak beds that were daylighted by excavation. Since the potential sliding mass was largely unrestrained, it no doubt expanded to open cracks or joints or to produce fissures that allowed communication of groundwater between the more pervious sandstone layers through the shale layers. Even if the mass did not expand to allow access of groundwater, low piezometric levels would exist only near the toe of the slope near active construction and not to the rear of the potential slide mass. Along the base of the potential slide mass, the weak strata were in contact with the more permeable strata (for example, Fig. 22) such that pore pressures at the contact would be the same as those existing in the more permeable layers.

Table 3. Stratigraphic Relations of Formations in Gaillard Cut

Geologic Times	Woodring, 1957	R. H. Stewart, PCC Geologist (Lutton and Banks, 1970)
Cenozoic		
Quaternary		
Tertiary		
Pliocene		
Miocene		
Upper		Basalt
Lower	Panama formation	Pedro Miguel agglomerate*
	Cucaracha formation	Cucaracha formation
	Culebra formation**	Culebra formation**
Oligocene		
Upper	Hiatus	Hiatus
	Las Cascadas agglomerate	
Lower	Bas Obispo formation	
Eocene		
Upper		Gatuncillo
Lower		
Paleocene		
Mesozoic		

* Included as a member of the Panama formation by Woodring, 1957.
** Samples identified as Culebra formation have been dated variously on the basis of fossils from Upper Oligocene to Middle Miocene.

Table 4. Piezometer Data in Study Area

Piezometer	Date Installed	Tip Elevation ft msl	Local Stratigraphy	Basic Time Lag days	Horizontal Coefficient of Permeability* cm/sec	Elevation of Piezometric Surface** ft msl	Remarks
			East Culebra Piezometers, Referenced to Boring WEC-1				
WEC-P1A	22 Mar 69	-7.0	Blue-green clay shale, massive with few prominent slickensides	11.1	10^{-9}	83.7	Canal water elevation
WEC-P1B	28 Mar 69	-72.0	Layered clay shale with some sandy phases and many slickensides	--	--	54.0	
WEC-P1C	1 Apr 71	+18.0	Blue-green clay shale, massive with few prominent slickensides; layers of lignite and breccia	0.06	10^{-6}	85.0	Canal water elevation
WEC-P1D	22 Mar 71	-42.0	Blue-green clay shale, massive with many slickensides	276.0	10^{-10}	(23.6)	Methane liberated
WEC-P1E	30 Mar 71	-97.0	Interbedded limestone and clay shale	33.5	10^{-9}	84.2	Methane liberated; canal water elevation
WEC-P1F	26 Mar 71	-141.1	Interbedded sandstone and sandy shale	25.1	10^{-9}	45.6	
			Model Slope Piezometers, Referenced to Boring WMS-1				
WMS-P1A	11 Apr 69	+0.5	Blue-green clay shale with many slickensides	29.5	10^{-9}	59.8	
WMS-P1B	20 Apr 71	+78.6	Blue-green clay shale with few slickensides	2.4	10^{-8}	(101.1)	Varies; reflects rainfall data
WMS-P1C	7 Apr 71	+34.0	Conglomerate with some lignite and clay shale layers	0.5	10^{-7}	87.8	Methane liberated; varies slightly; may reflect rainfall data
WMS-P1D	24 Apr 71	-36.0	Blue-green clay shale with few slickensides; streaks of sand, silt, and lignite	242.0	10^{-10}	(85.4)	
WMS-P1E	19 Apr 71	-77.7	Sandstone with layers of lignitic clay shale	7.2	10^{-8}	61.0	
WMS-P1F	14 Apr 71	-178.0	Sandstone with clay shale	0.37	10^{-7}	86.3	Methane liberated
			South Cucaracha Piezometers, Referenced to Boring WCSE-1				
WCSE-P1A	7 Apr 72	+79.6	Greenish-gray clay shale, very slickensided	0.09	10^{-6}	--	Varies; reflects rainfall data
WCSE-P1B	6 Apr 72	+57.2	Slickensided clay shale, thin layers of fine-grained sandstone	0.27	10^{-7}	--	Varies; reflects rainfall data
WCSE-P1C	4 Apr 72	-12.2	Blue-green clay shale, slickensided	3.9	10^{-8}	--	Varies; reflects rainfall data

* Reported to order of magnitude only.
** Equilibrium position, except as noted by parentheses.

Table 5. Piezometers, Hodges Hill Area

Piezometer	Date Installed	Station	Offset from Axis, ft	Tip Elevation ft msl	Local Stratigraphy	Elevation of Piezometric Surface* ft msl	Remarks
CRW-1A 1	23 Jul 68	1937+95	403	-139.9	Sandstone	100.4	
2	23 Jul 68	1937+95	403	-39.9	Sandstone	90.1	
3	23 Jul 68	1937+95	403	+10.1	Sandstone	99.6	
CRW-4A 1	17 May 68	1931+98	424	-123.0	Siltstone	--	Inoperative
2	18 May 68	1931+98	424	-23.0	Sandstone	85.1	
3	18 May 68	1931+98	424	+27.0	Sandstone	93.0	
CRW-7A 1	7 Jun 68	1924+00	420	-117.1	Sandy siltstone	119.8	
2	7 Jun 68	1924+00	420	-17.1	Siltstone	134.9	
3	10 Jun 68	1924+00	420	+32.9	Siltstone	77.9	
CRW-9A 1	18 Jun 68	1918+00	401	-110.8	Siltstone	89.0	
2	19 Jun 68	1918+00	401	-20.8	Sandstone	88.5	
3	20 Jun 68	1918+00	401	+39.2	Sandstone	--	Inoperative
CRW-12A 1	28 Jun 68	1899+97	419	-124.5	Siltstone	93.8	
2	28 Jun 68	1899+97	419	-24.5	Sandy siltstone	96.7	
3	28 Jun 68	1899+97	419	+25.5	Sandy siltstone	93.7	
CRW-2A	15 Jun 68	1938+01	648	+76.8	Sandstone	103.9	
CRW-8A 1	11 Jun 68	1924+00	667	-105.6	Siltstone	--	Inoperative
2	11 Jun 68	1924+00	667	+54.4	Sandstone	138.4	
3	12 Jun 68	1924+00	667	+114.4	Sandstone	124.1	
CRW-10A 1	25 Jul 68	1918+00	656	-118.1	Siltstone	142.1	
2	26 Jul 68	1918+00	656	+41.9	Sandstone	131.7	
3	26 Jul 68	1918+00	656	+101.9	Sandstone	123.6	
CRW-13A 1	6 Jul 68	1900+00	655	-117.0	Tuffaceous sandstone	180.6	
2	10 Jul 68	1900+00	655	+33.0	Siltstone	154.8	
3	10 Jul 68	1900+00	655	+93.0	Sandstone	151.8	
CRW-11 R	28 Jun 68	1931+87	1051	-10.5	Clay shale	190.4	
C	28 Jun 68	1931+87	1051	+41.5	Clay shale	204.6	
CRW-14 1	2 Jul 68	1900+00	1040	-108.2	Sandstone	--	Inoperative
2	2 Jul 68	1900+00	1040	+59.8	Sandstone	208.9	
3	2 Jul 68	1900+00	1040	+119.8	Sandstone	210.1	

* During January 1971.

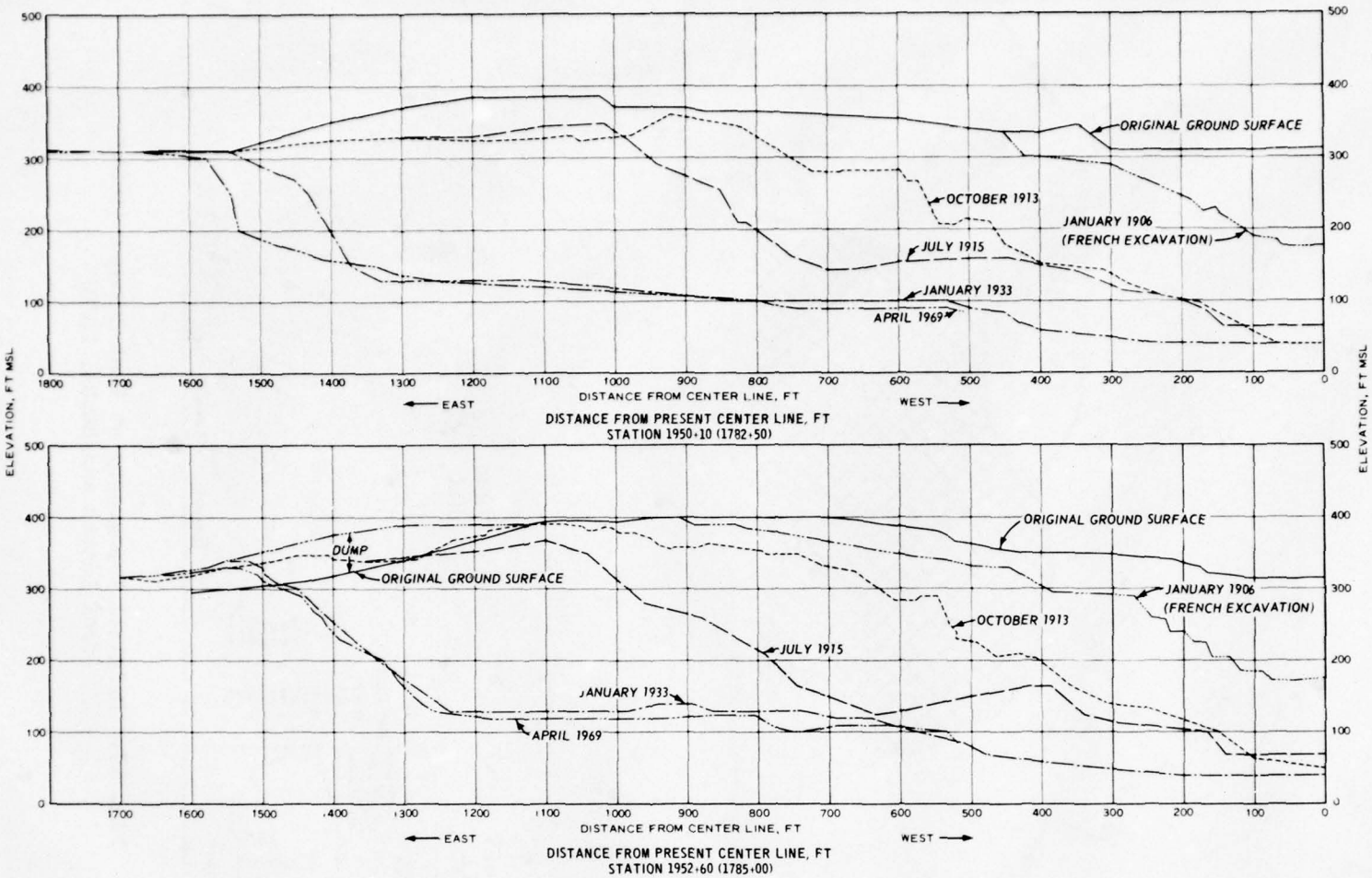

Fig. 16. Surface profiles at various stages of development of East Culebra Slide (from Lutton and Banks, 1970)

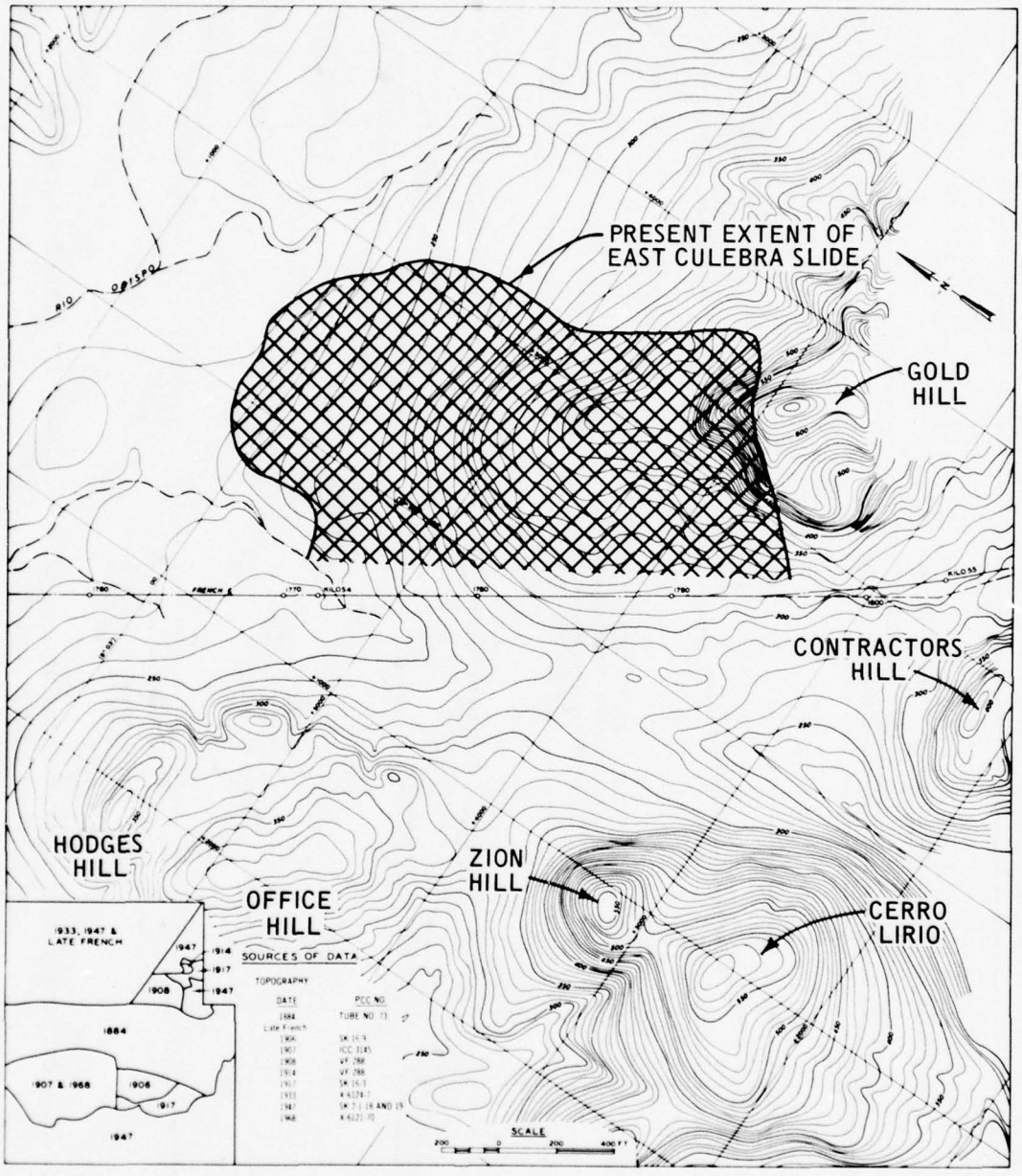

Fig. 17. Original topography at East Culebra (1884)
(from Lutton and Banks, 1970)

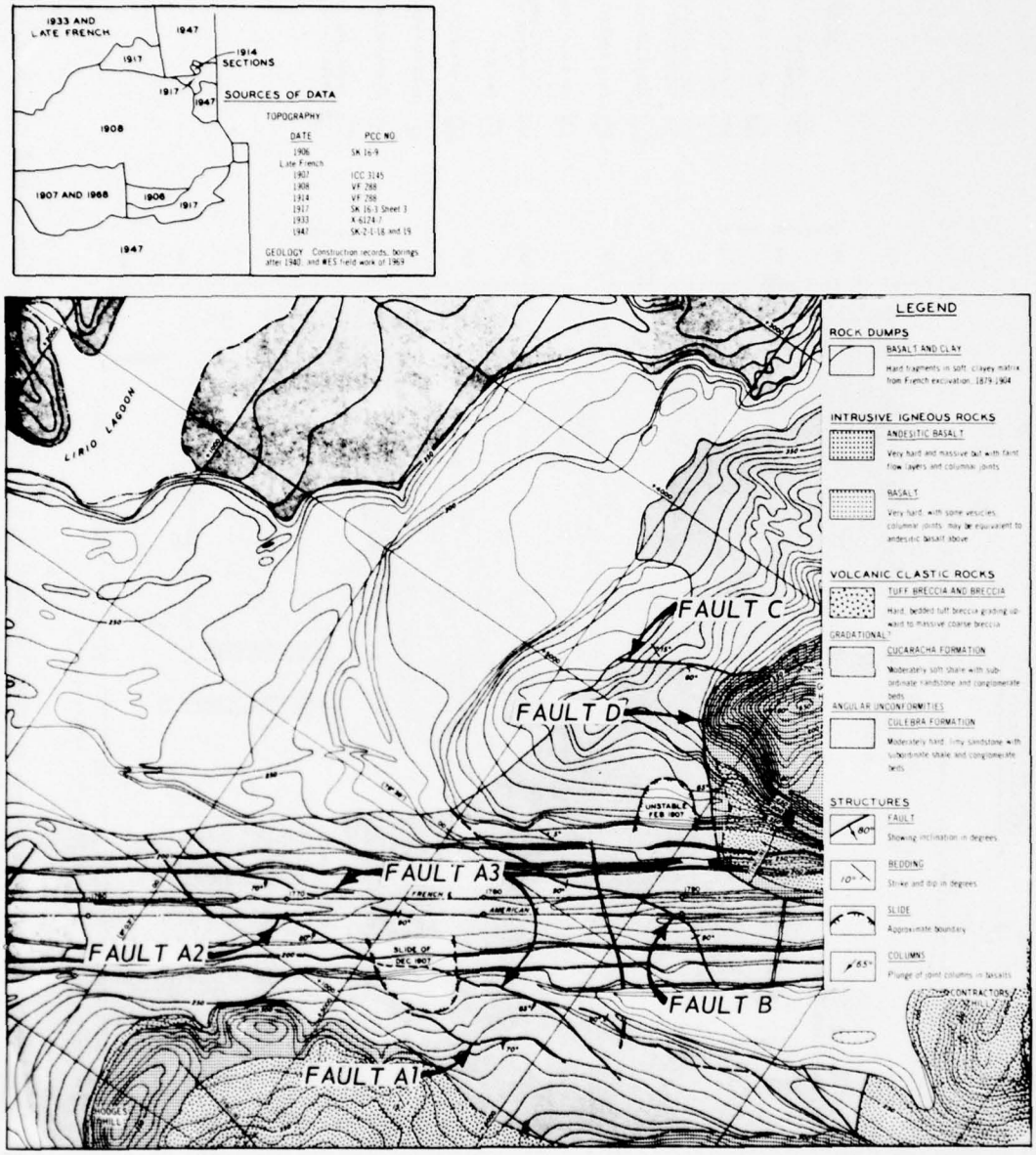

Fig. 18. Geology and topography at East Culebra Slide (1908) (from Lutton and Banks, 1970)

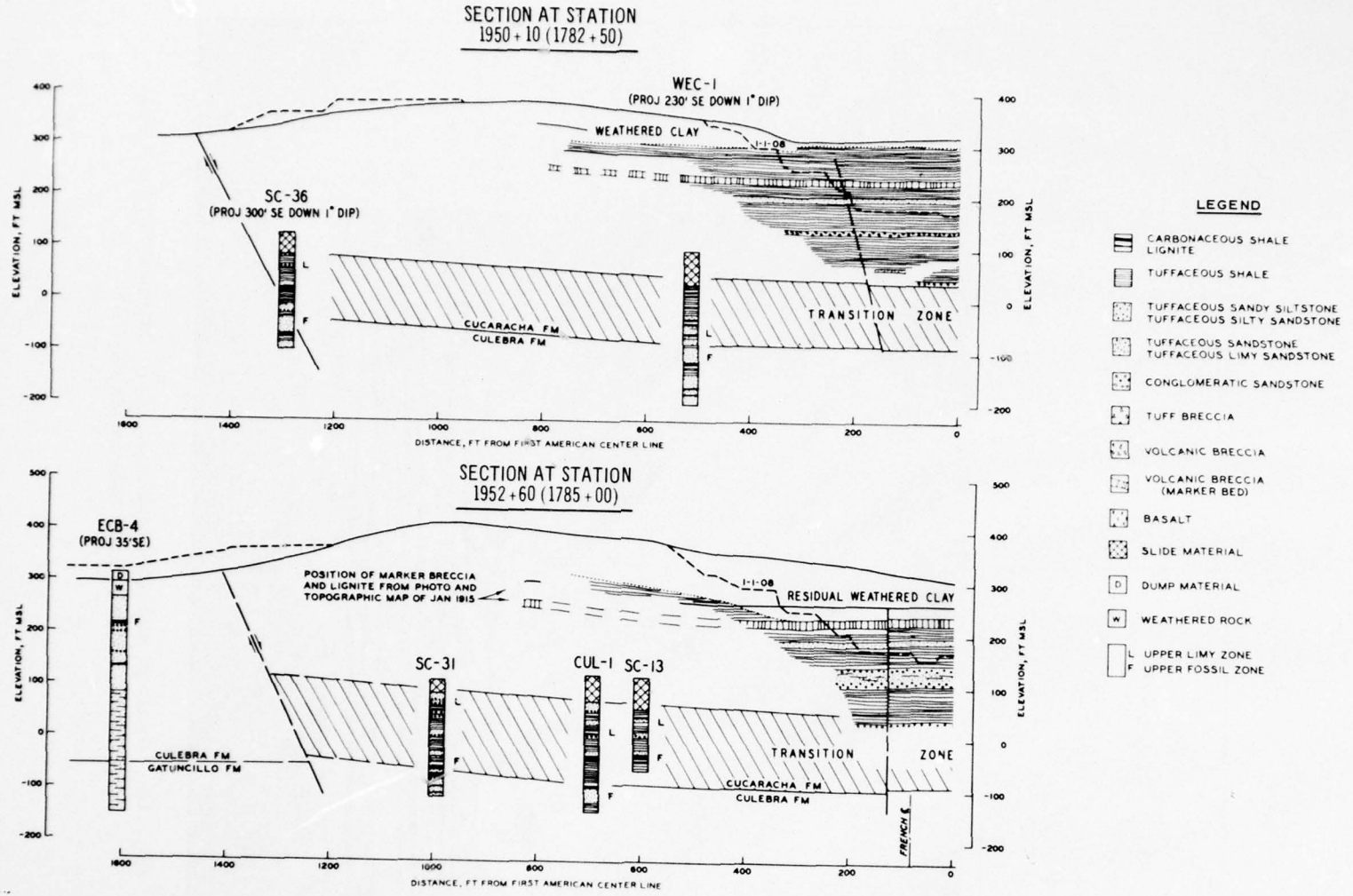

Fig. 19. Geological sections at sta 1950+10 and 1952+60 (sta 1782+50 and 1785+00) (from Lutton and Banks, 1970)

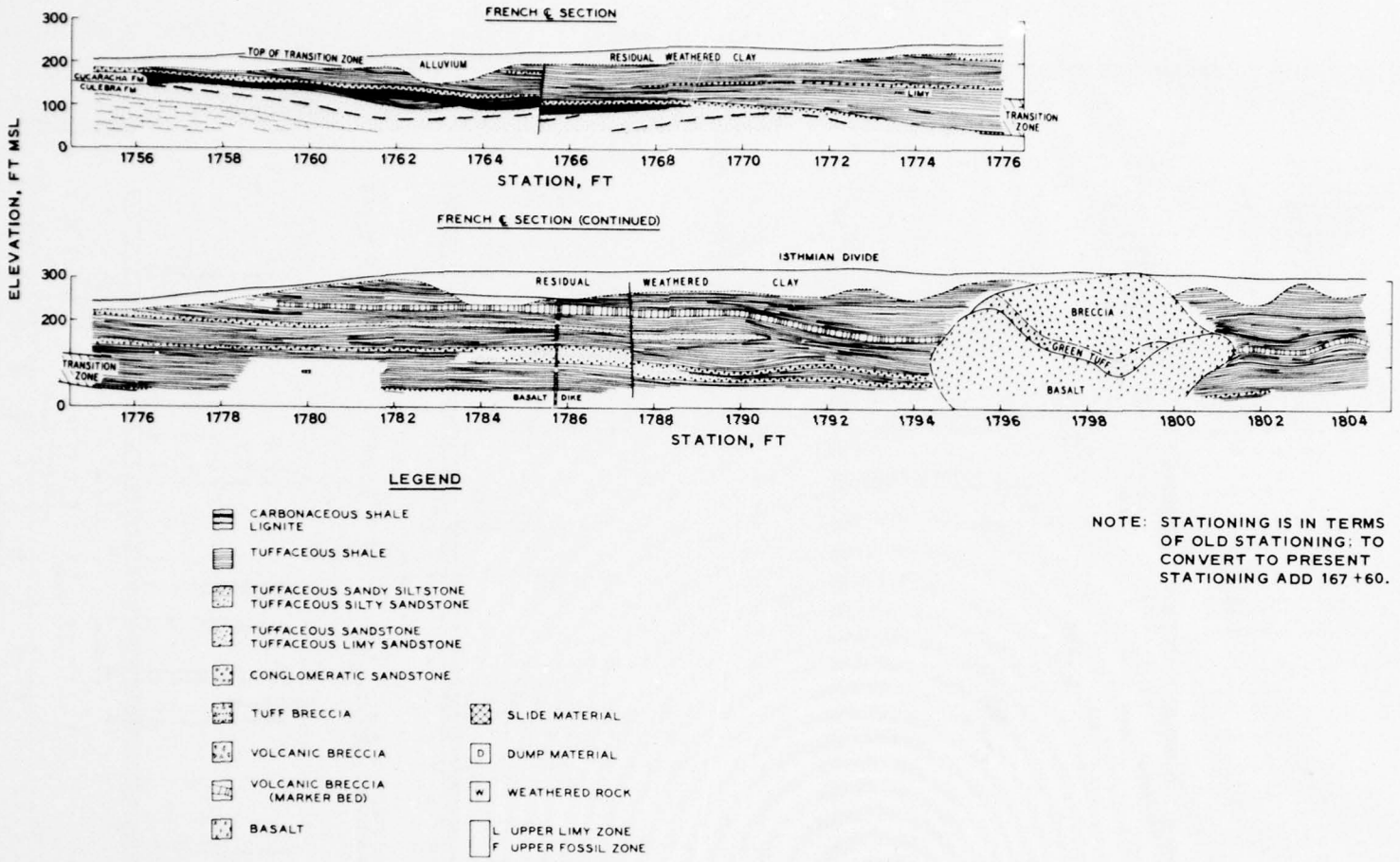

Fig. 20. Geological sections below original ground surface along French center line (from Lutton and Banks, 1970)

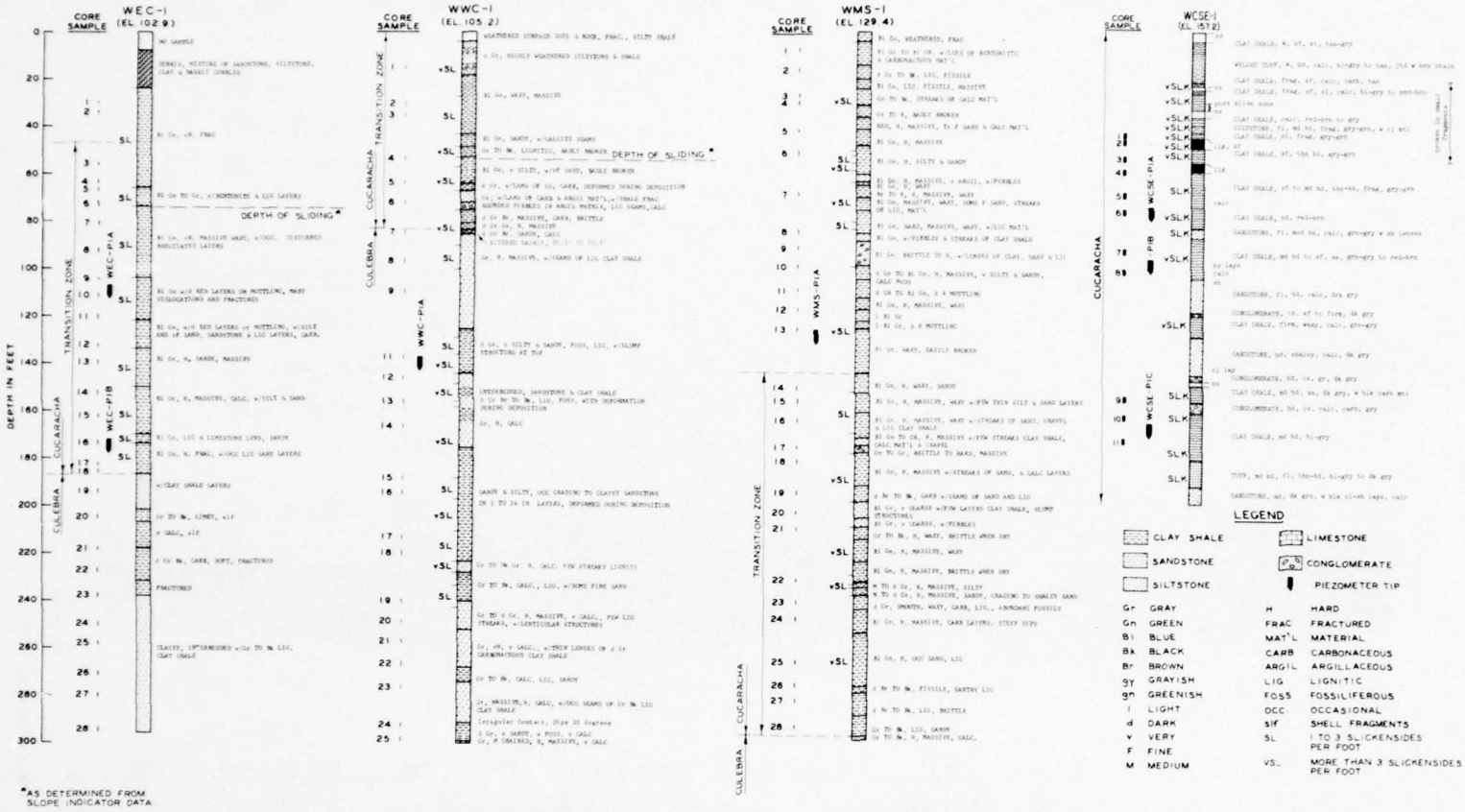

Fig. 21. Logs of recent borings into Cucaracha formation (from Lutton and Banks, 1970; Banks et al., 1975)

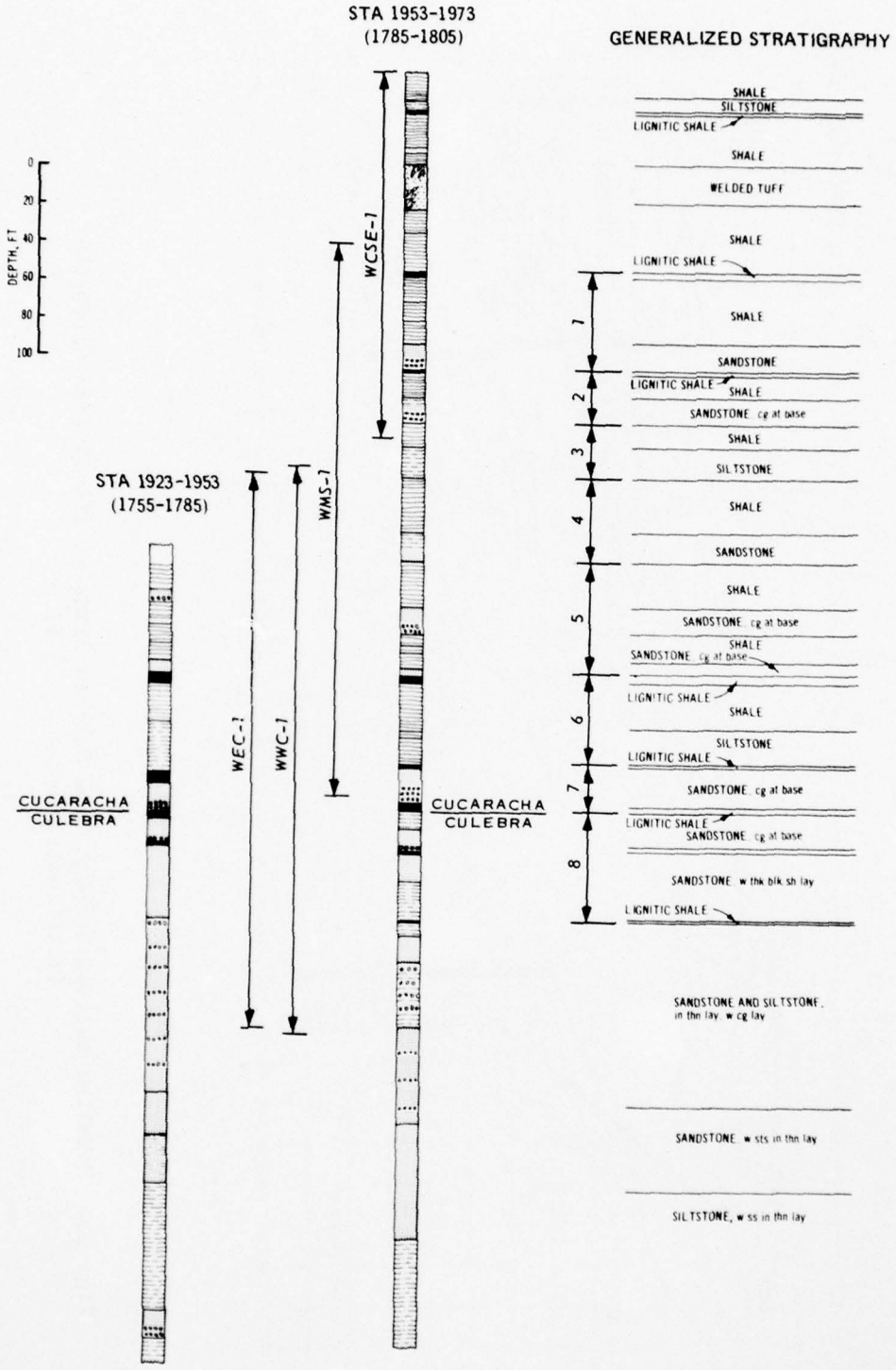

Fig. 22. Composite stratigraphic columns for Cucaracha (and Culebra) formations in Culebra Reach (Gaillard Cut) (from Lutton et al., 1975)

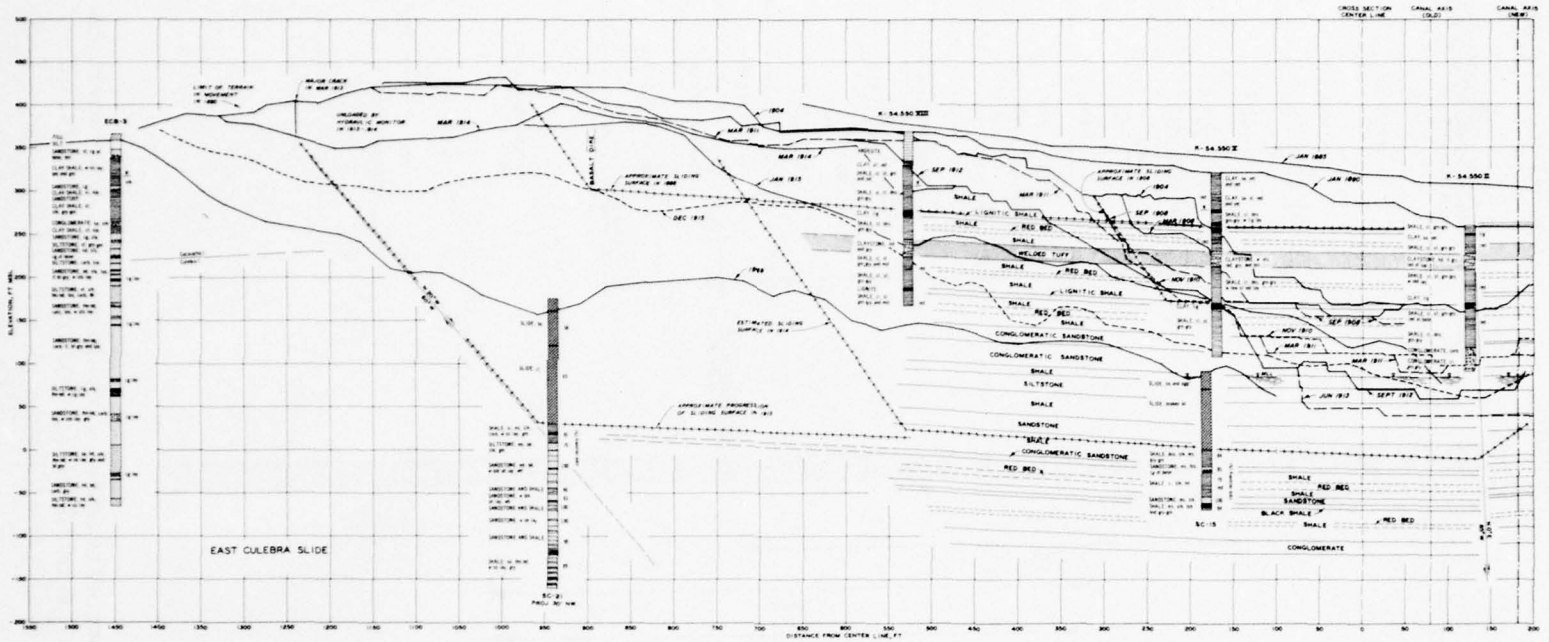

Fig. 23. Detailed section through East Culebra Slide at sta 1957+60 (1790+00) (from Lutton, et al., 1975)

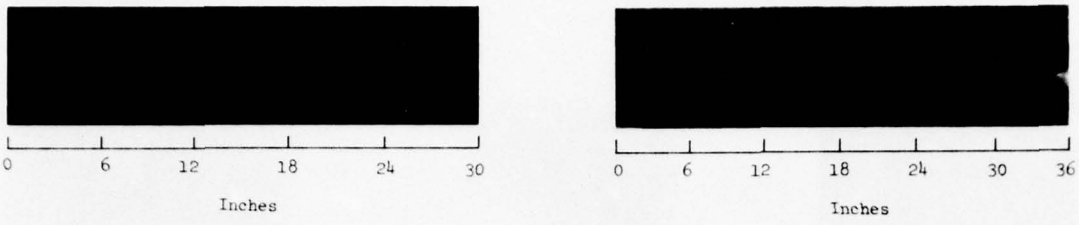

a. Sample condition upon extraction from sampling tube

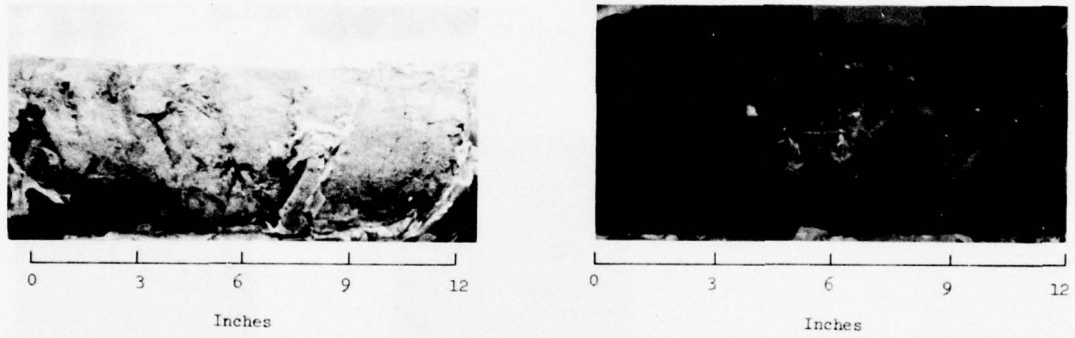

b. Sample condition after 5 to 10 minutes following extraction

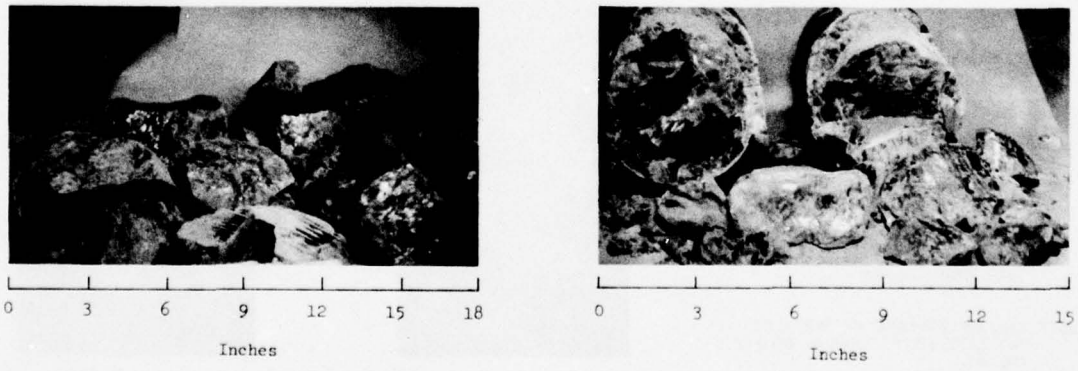

c. Sample condition after 10 minutes following extraction

Fig. 24. Photographs of Cucaracha clay shale samples

SAMPLE 4
DEPTH 62.0 - 63.2 FT
(VERTICAL VIEW)

SAMPLE 5
DEPTH 65.0 - 66.4 FT

SAMPLE 6
DEPTH 72.4 - 74.2 FT

a. SAMPLES ABOVE FAILURE SURFACE

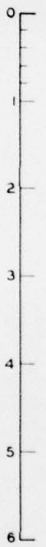

SCALE IN INCHES FOR
ALL RADIOGRAPHS

NOTE: FAILURE SURFACE AT DEPTH OF 74 FT (EL + 30 FT : BORING WEC-1, FIG. 49)

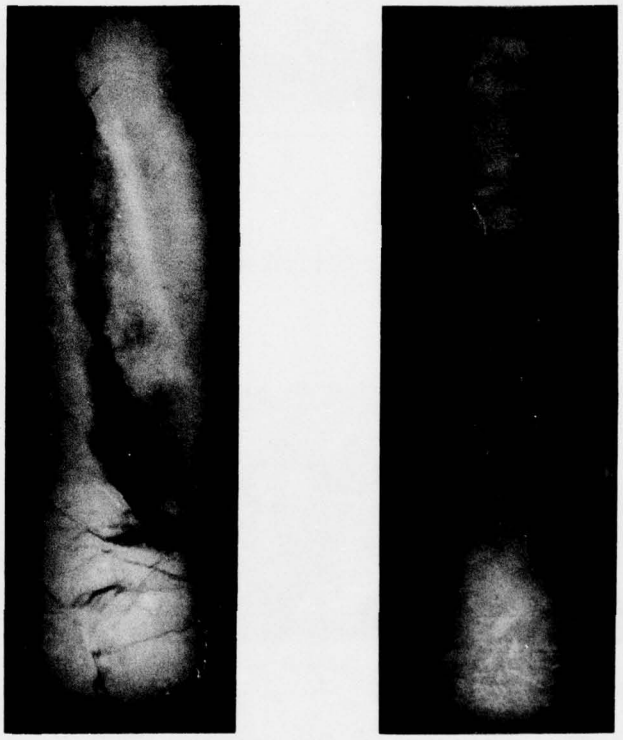

SAMPLE 10
DEPTH 112.3 - 114.1 FT

SAMPLE 17
DEPTH 181.7 - 183.5 FT

b. SAMPLES BELOW FAILURE SURFACE

Fig. 25. Radiographs of Cucaracha clay shale samples

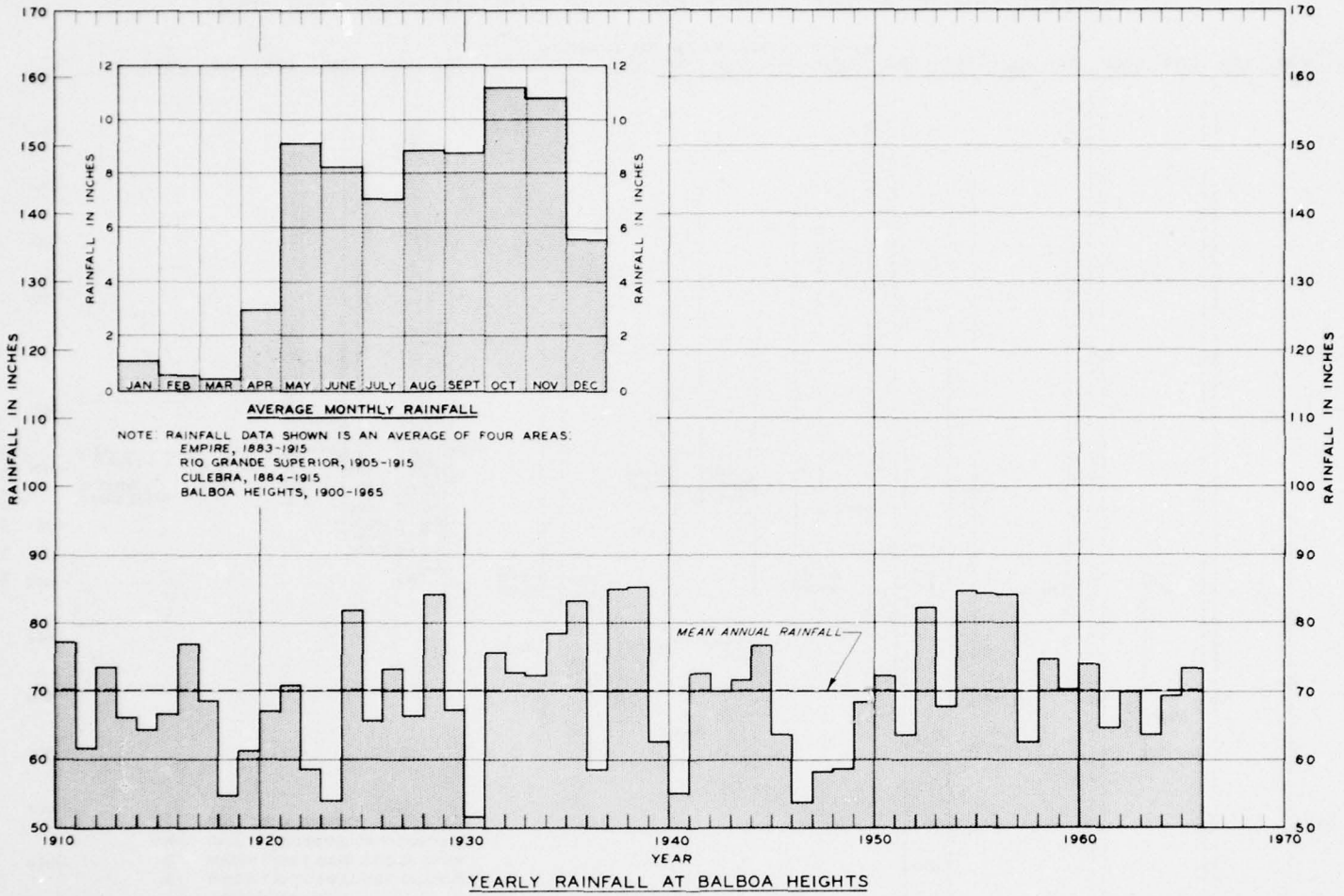

Fig. 26. Yearly and monthly rainfall data (from Lutton and Banks, 1970)

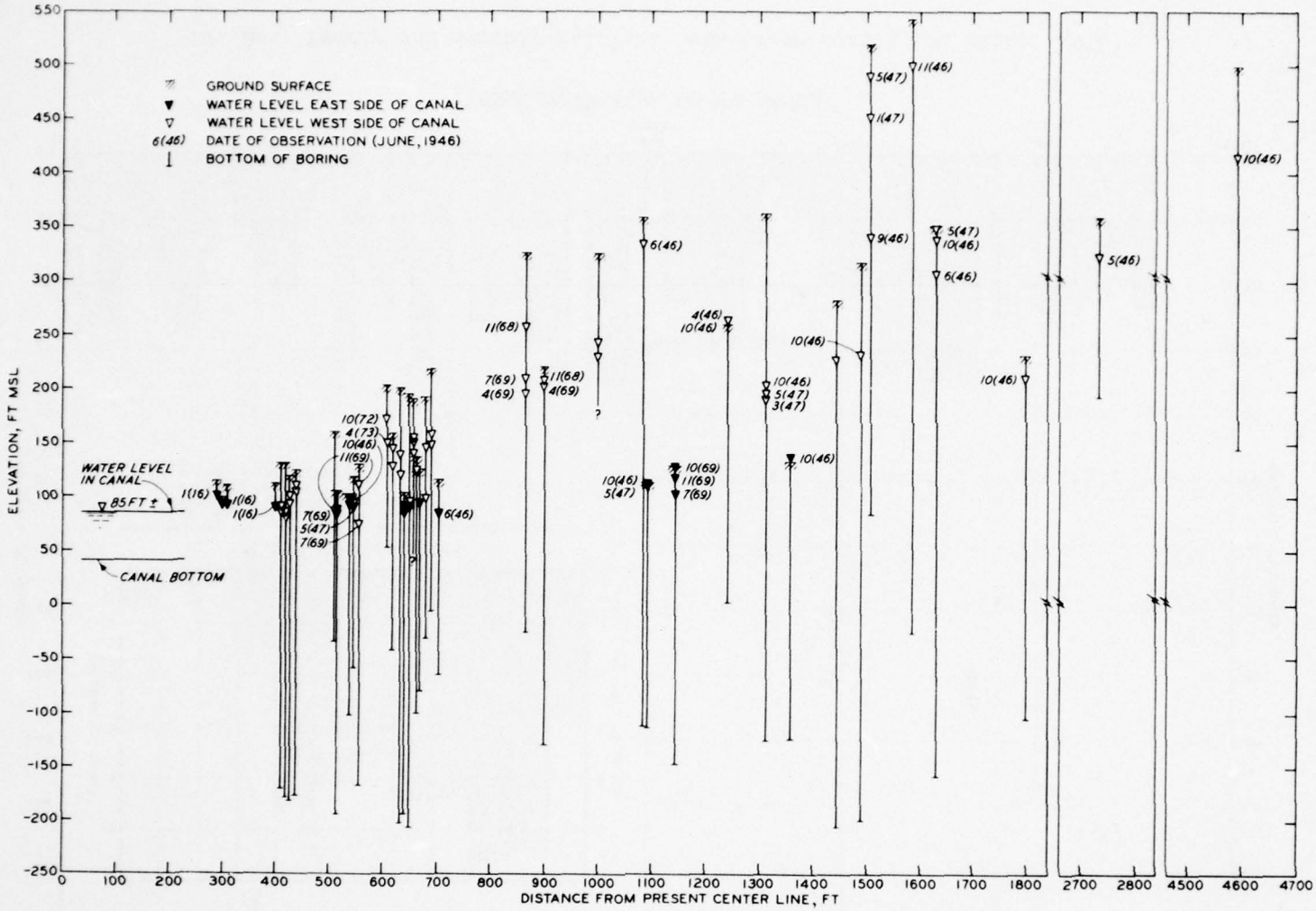

Fig. 27. Composite plot of recorded water levels in open borings, east and west sides of Panama Canal

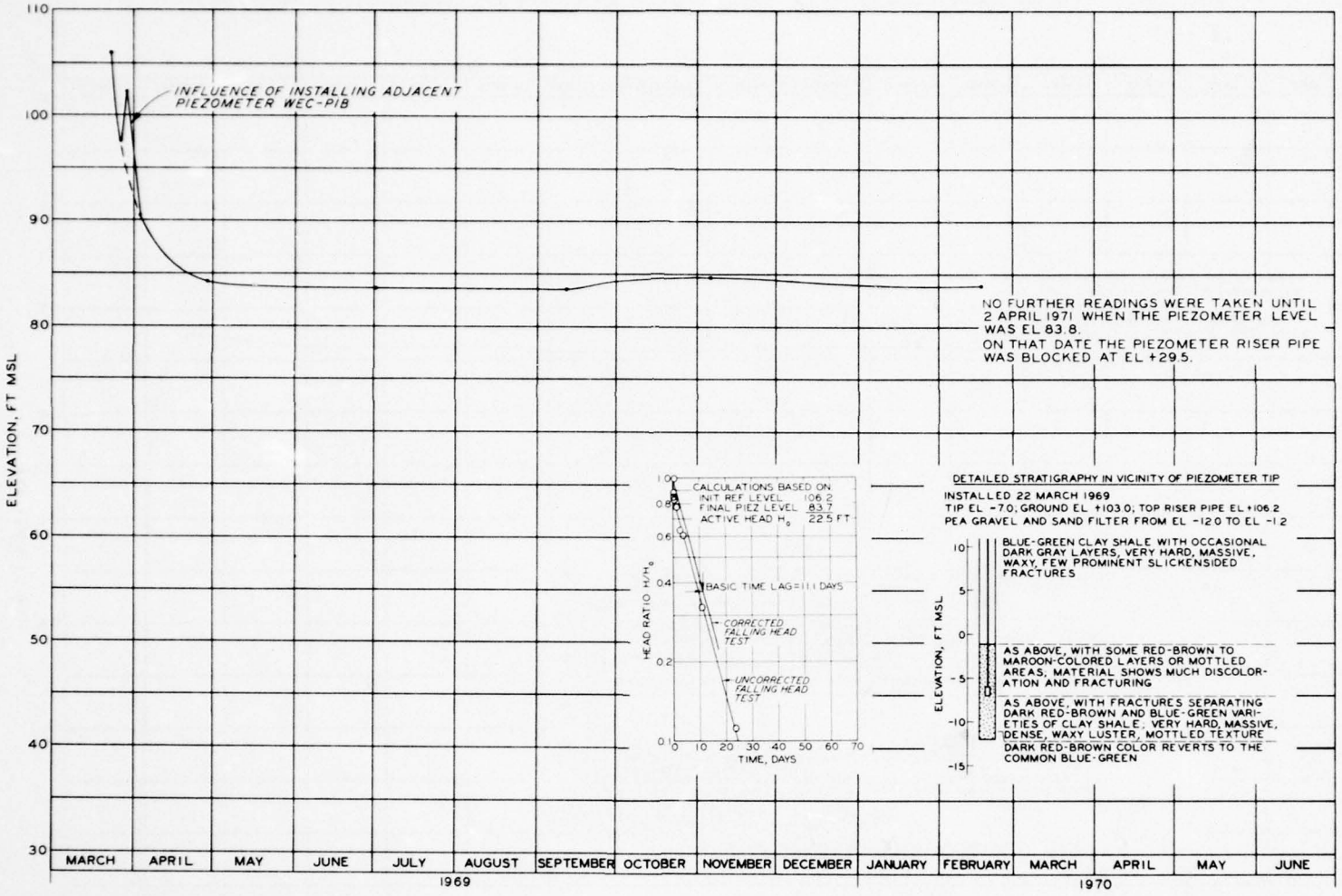

Fig. 28. Piezometer data, WEC-P1A (see Fig. 21.) (from Banks et al., 1975)

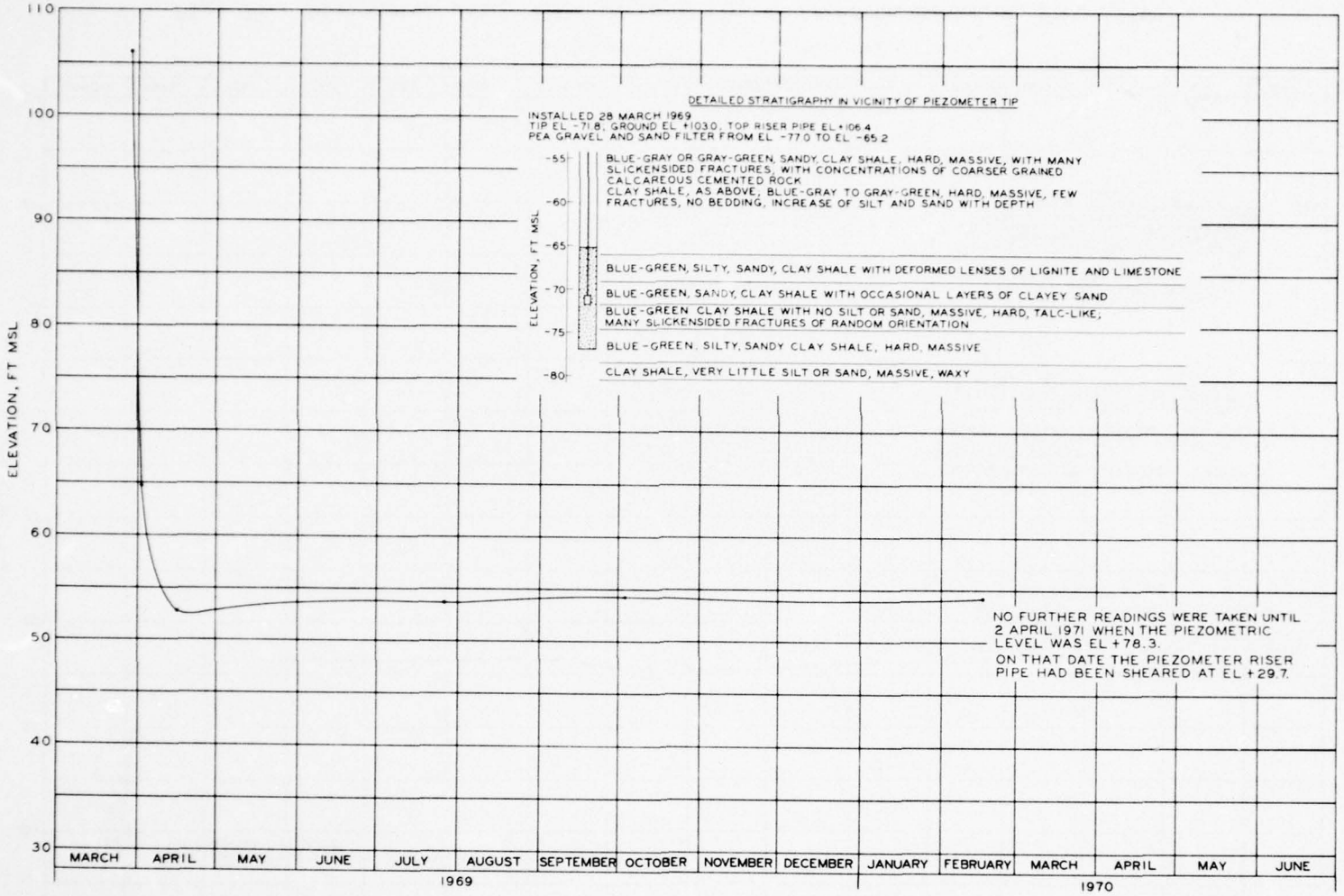

Fig. 29. Piezometer data, WEC-P1B (see Fig. 21.) (from Banks et al., 1975)

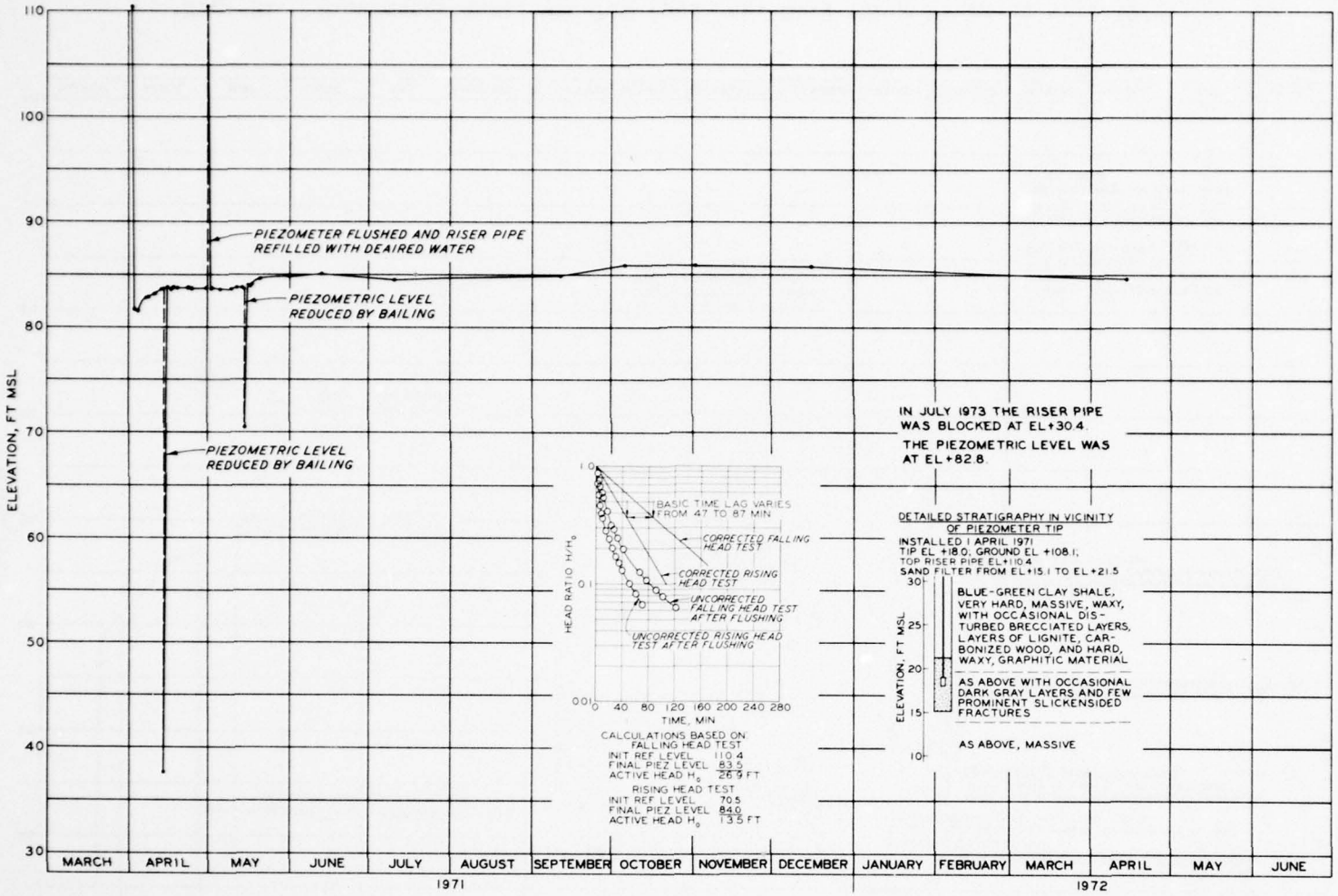

Fig. 30. Piezometer data, WEC-P1C (see Fig. 21.) (from Banks et al., 1975)

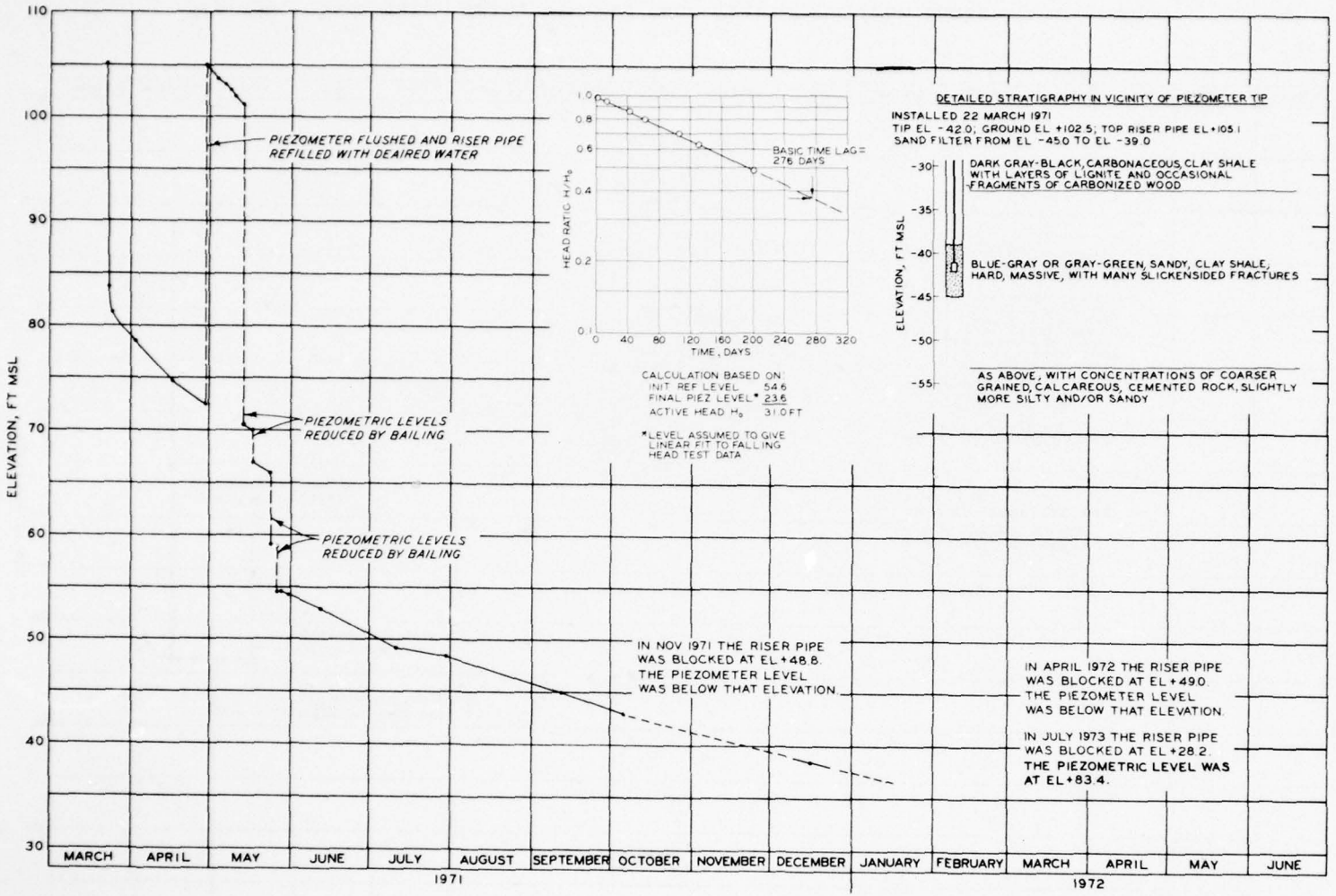

Fig. 31. Piezometer data, WEC-P1D (see Fig. 21.) (from Banks et al., 1975)

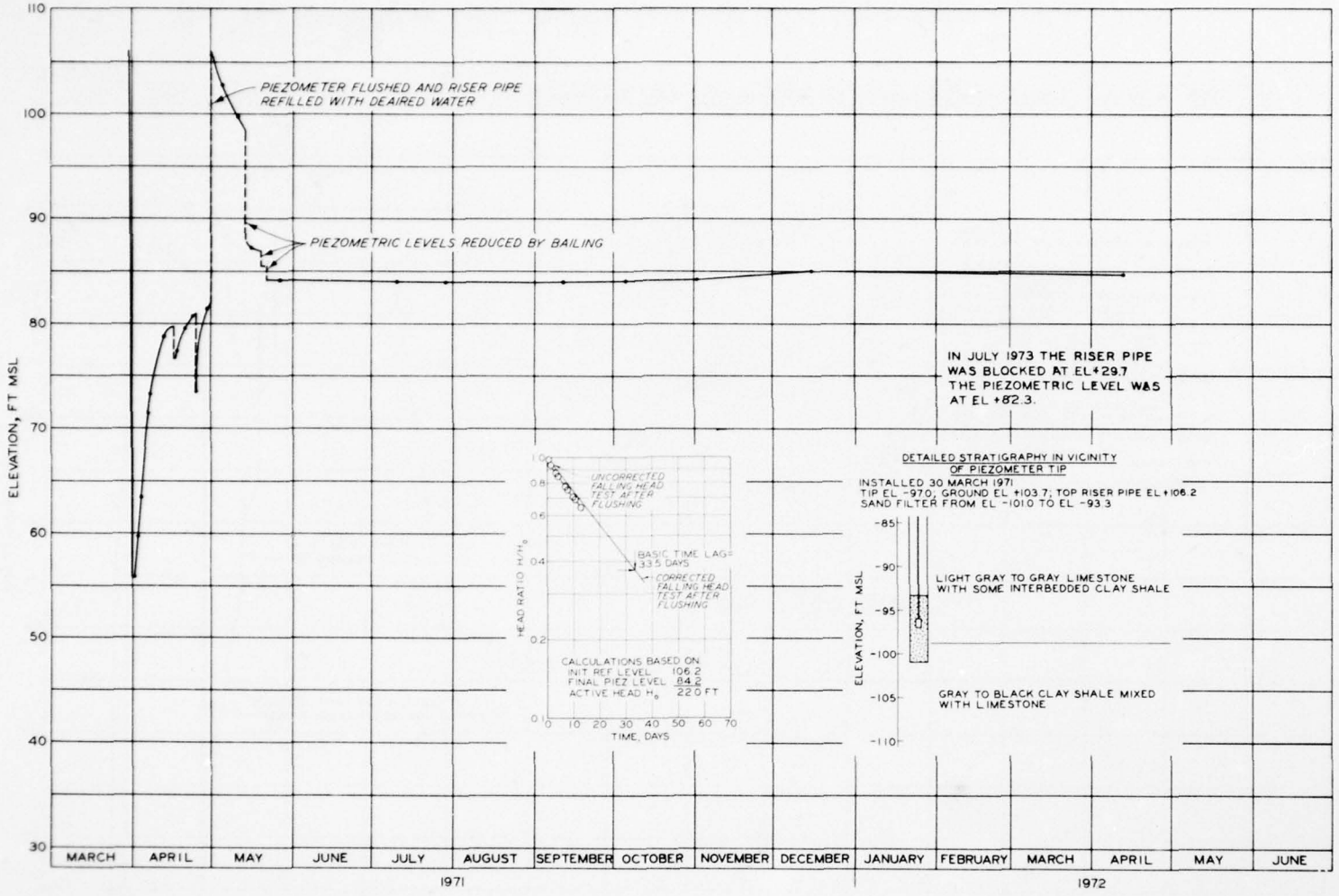

Fig. 32. Piezometer data, WEC-P1E (see Fig. 21.) (from Banks et al., 1975)

AD-A061 404 ARMY ENGINEER WATERWAYS EXPERIMENT STATION VICKSBURG MISS F/G 8/6
STUDY OF CLAY SHALE SLOPES ALONG THE PANAMA CANAL. SUPPLEMENTAL--ETC(U)
AUG 78 D C BANKS

UNCLASSIFIED WES-TR-S-70-9 NL

2 OF 3
ADA
061404

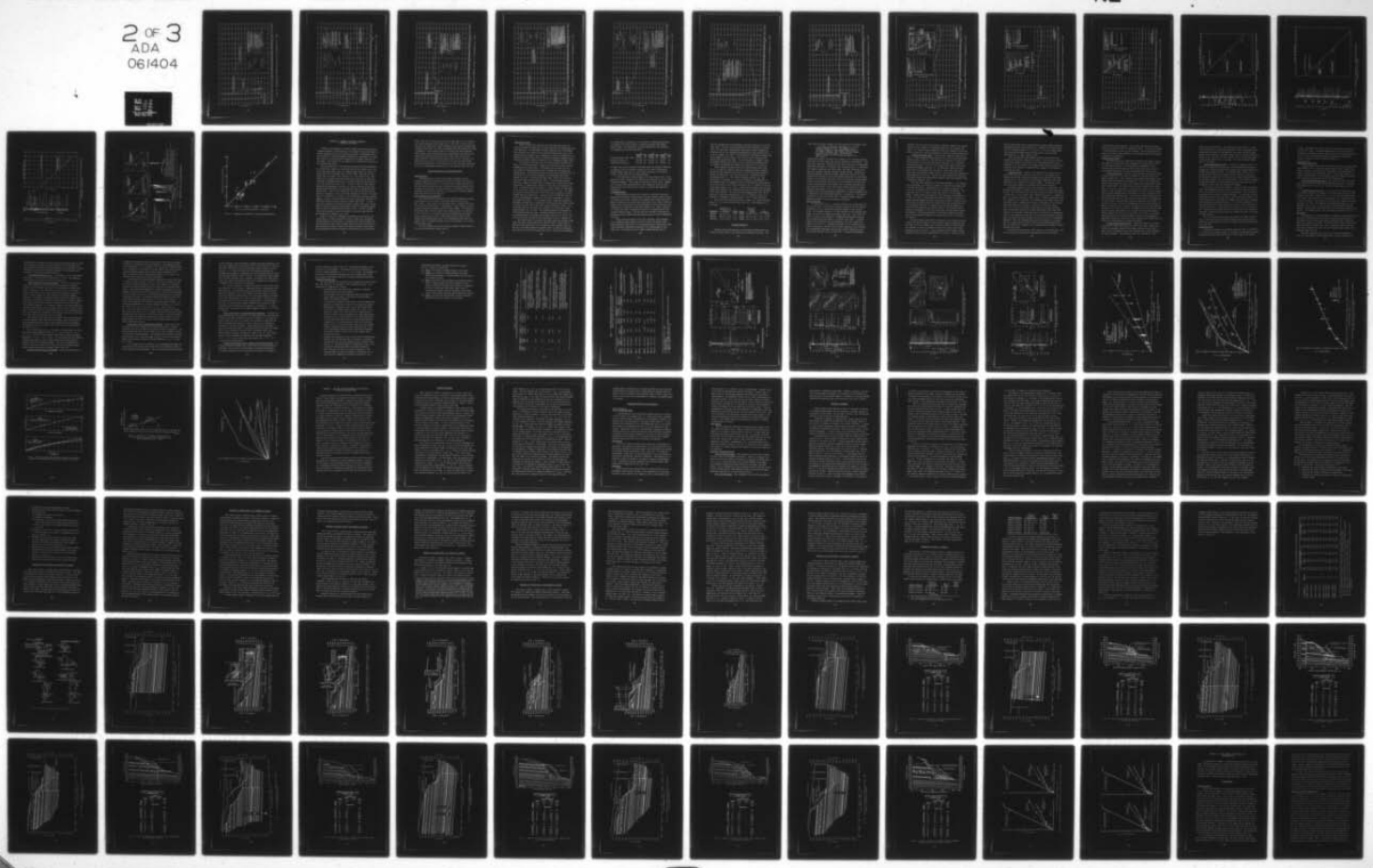

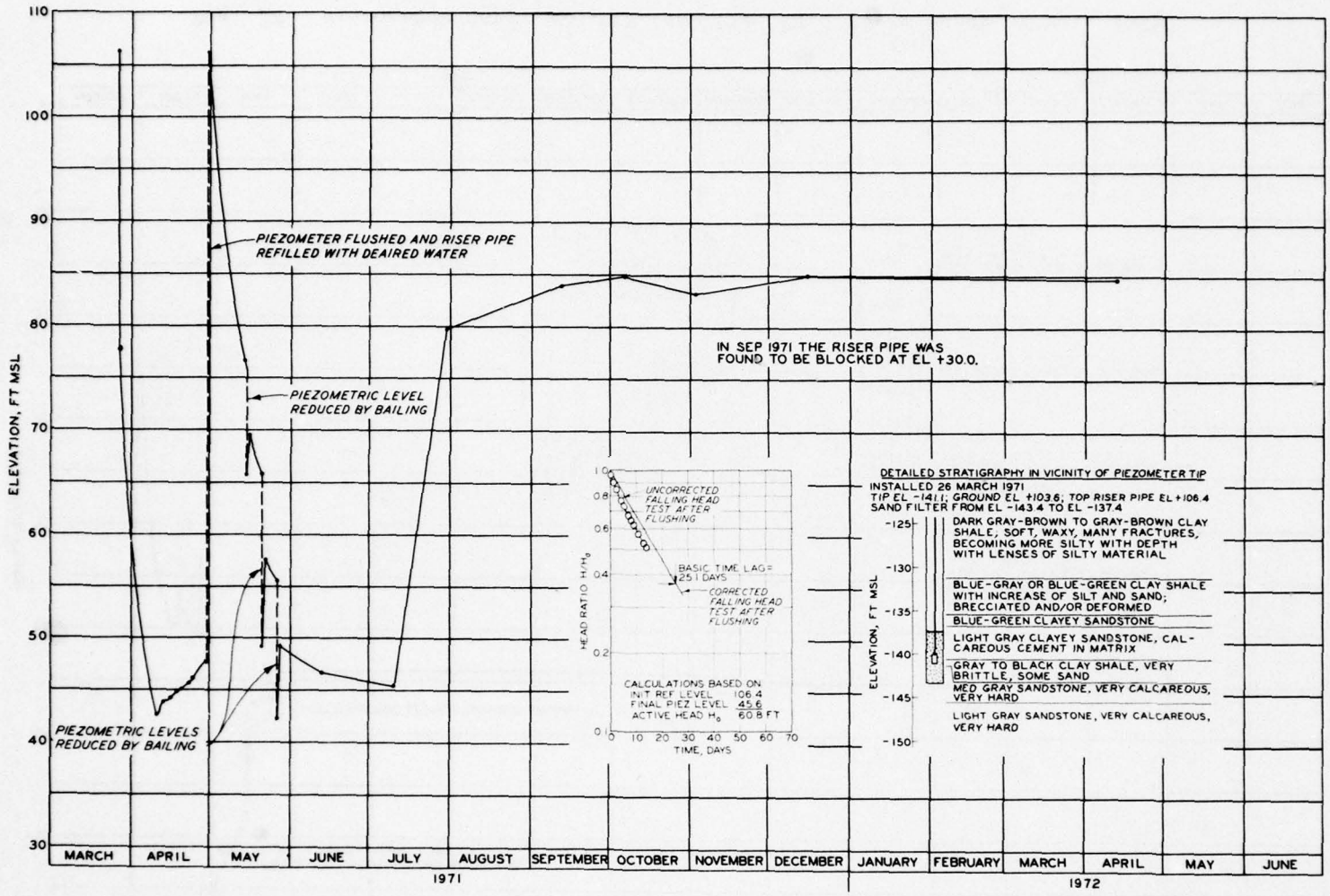

Fig. 33. Piezometer data, WEC-P1F (see Fig. 21.) (from Banks et al., 1975)

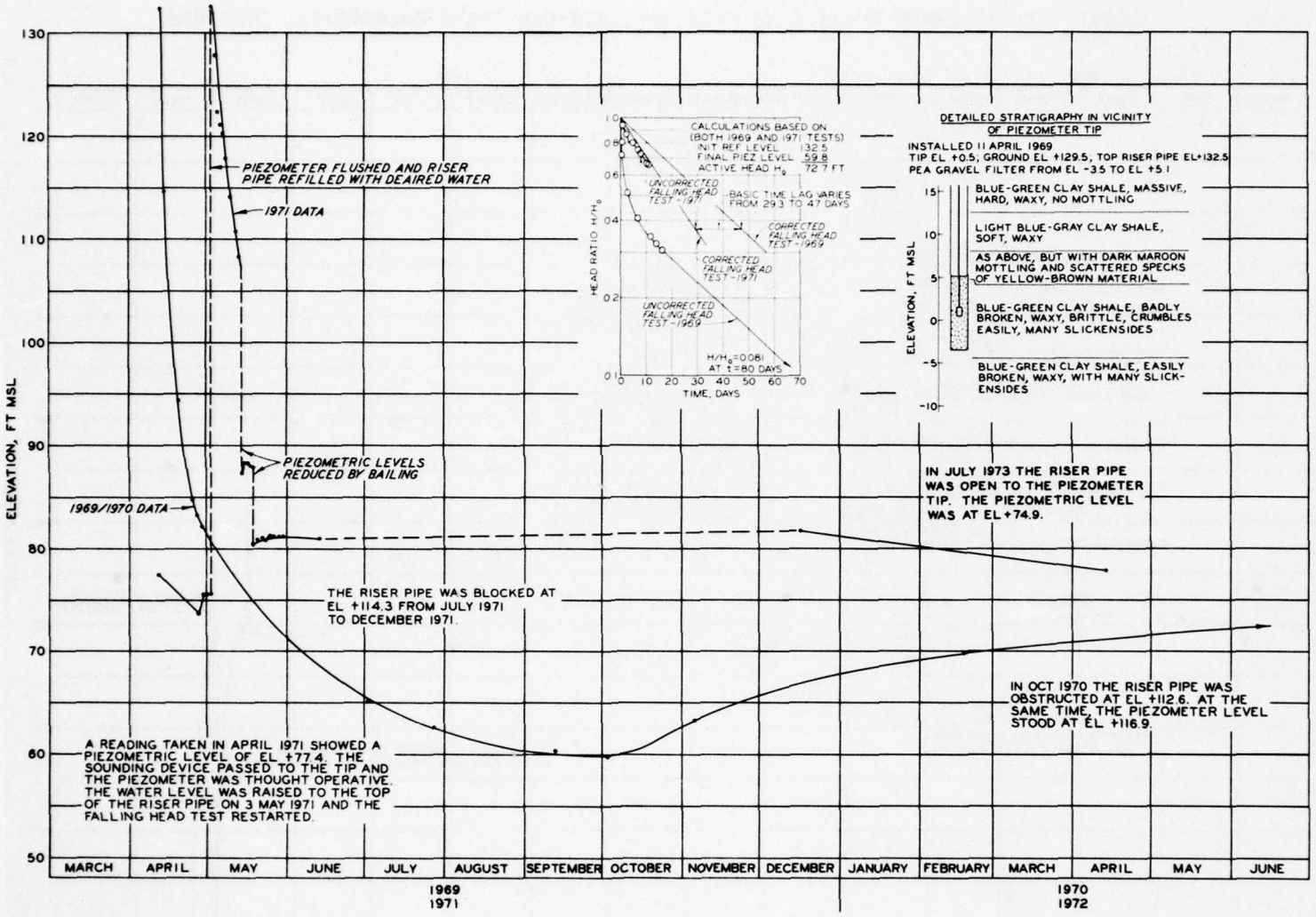

Fig. 34. Piezometer data, WMS-P1A (see Fig. 21.) (from Banks et al., 1975)

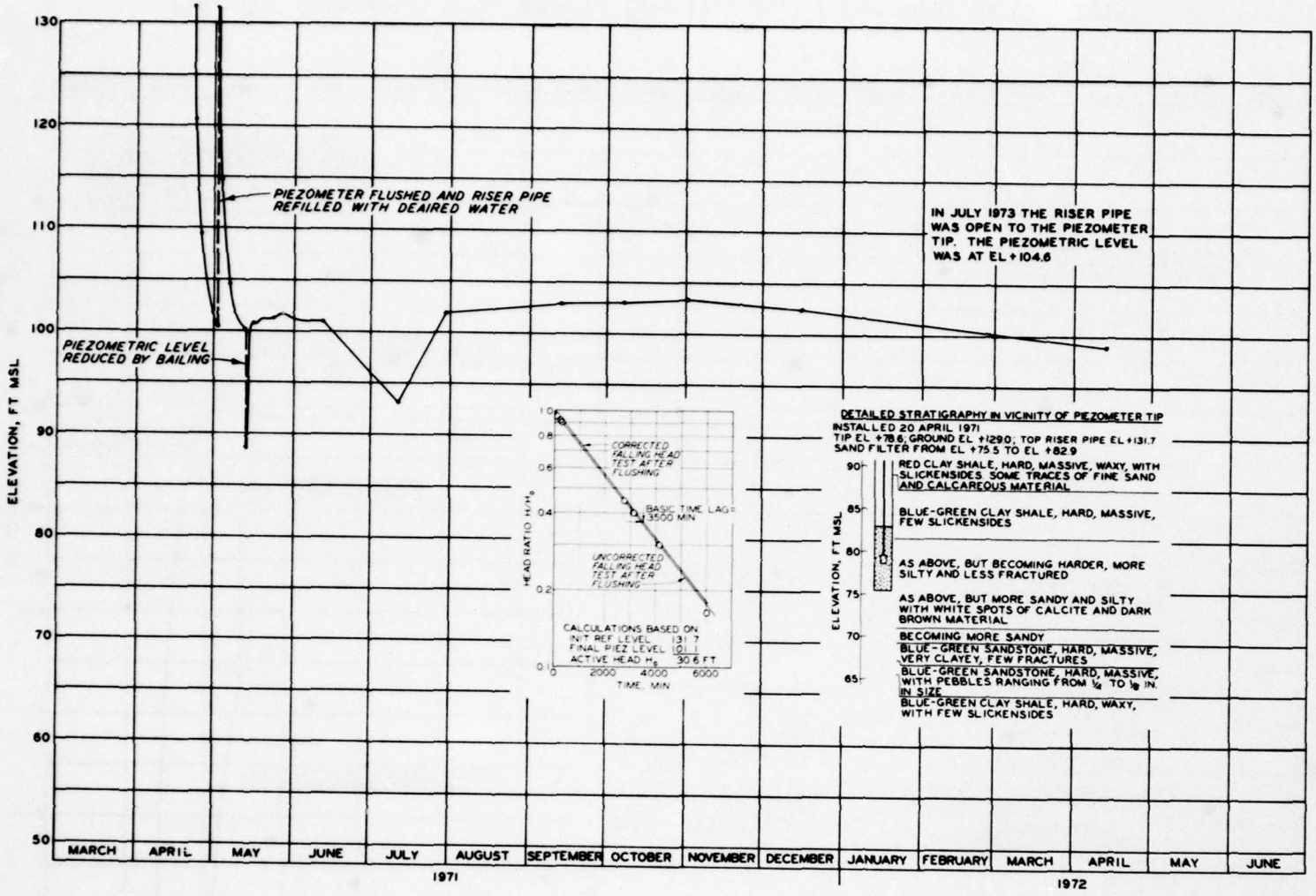

Fig. 35. Piezometer data, WMS-P1B (see Fig. 21.) (from Banks et al., 1975)

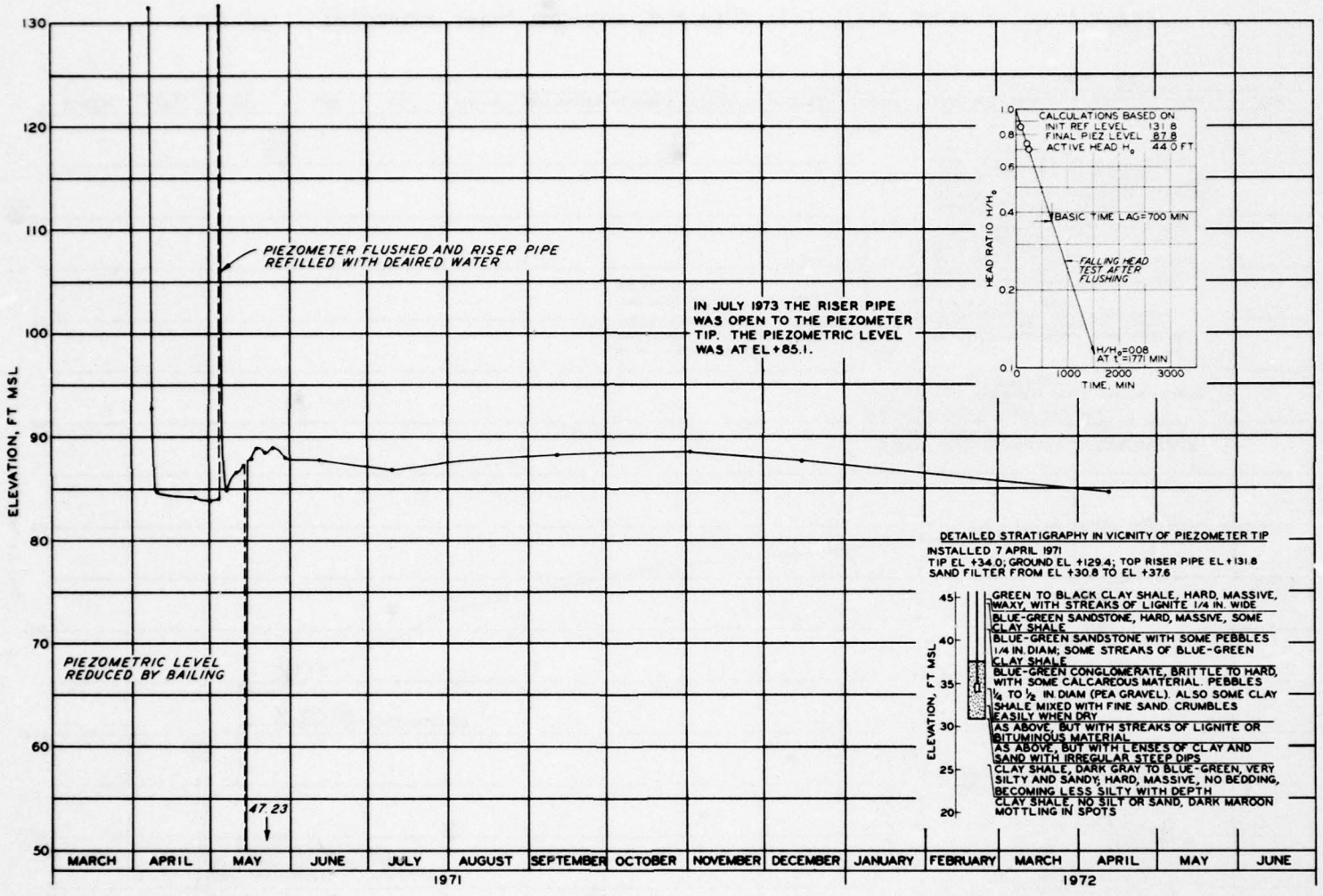

Fig. 36. Piezometer data, WMS-P1C (see Fig. 21.) (from Banks et al., 1975)

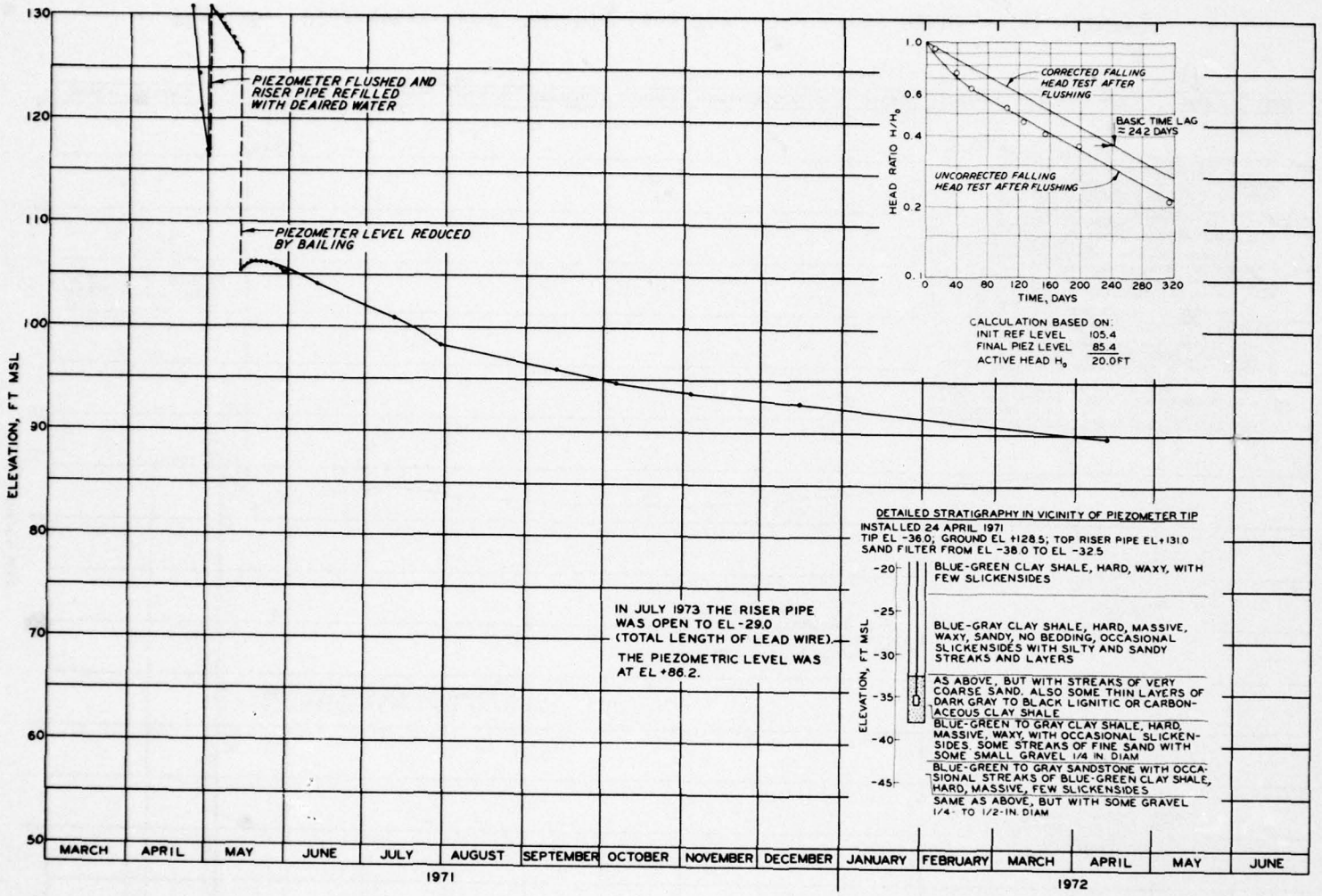

Fig. 37. Piezometer data, WMS-P1D (see Fig. 21.) (from Banks et al., 1975)

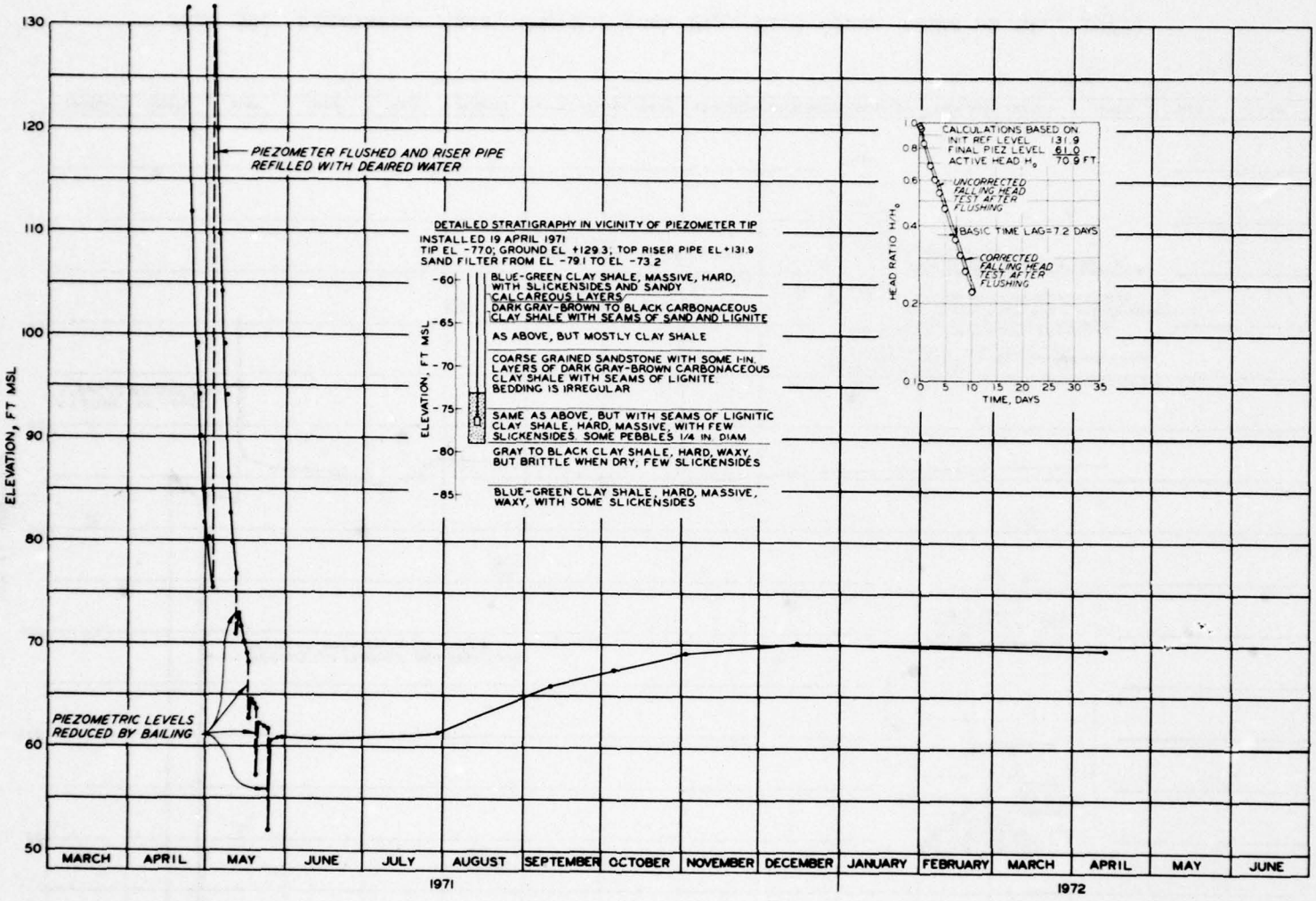

Fig. 38. Piezometer data, WMS-P1E (see Fig. 21.) (from Banks et al., 1975)

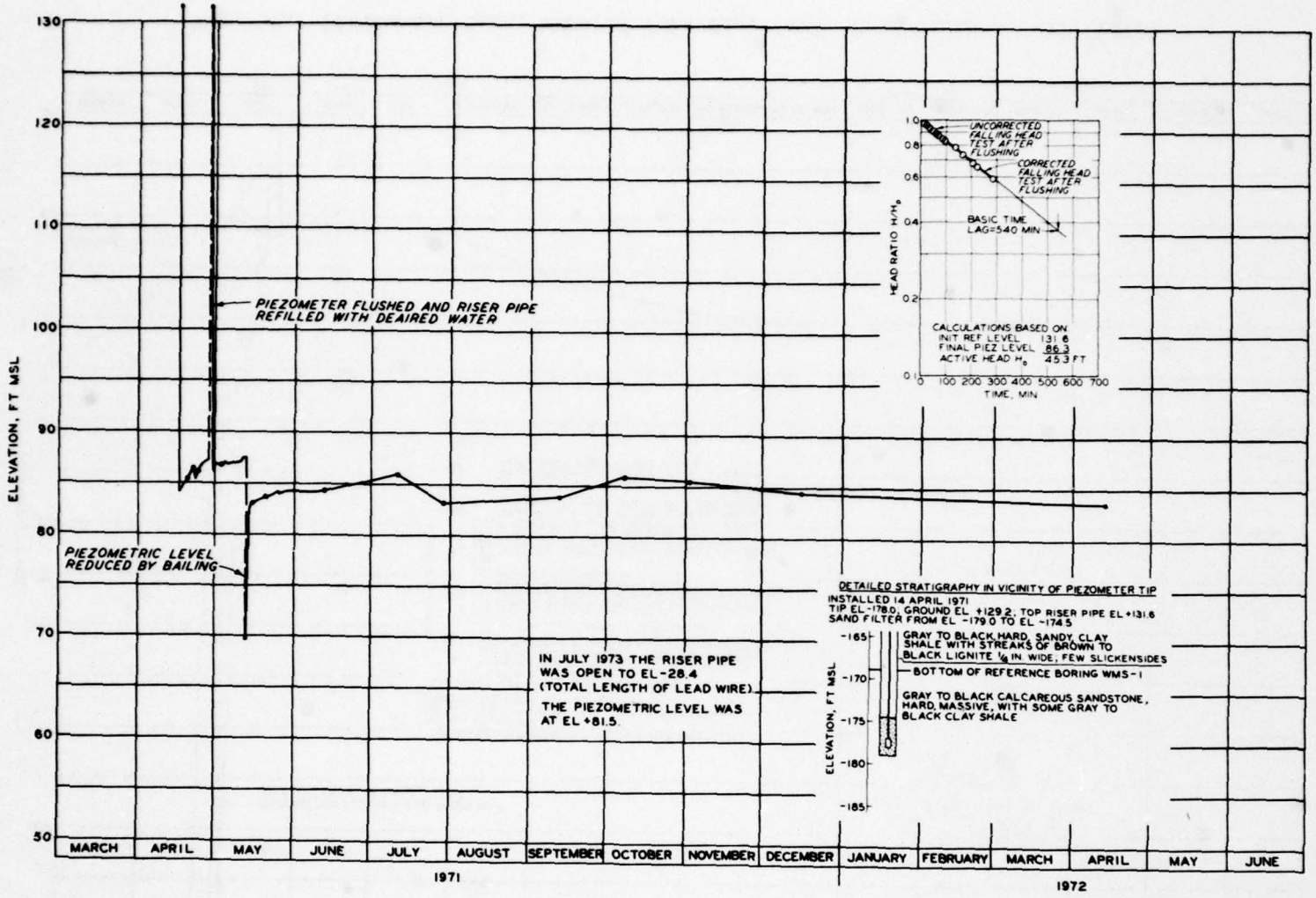

Fig. 39. Piezometer data, WMS-P1F (see Fig. 21.) (from Banks et al., 1975)

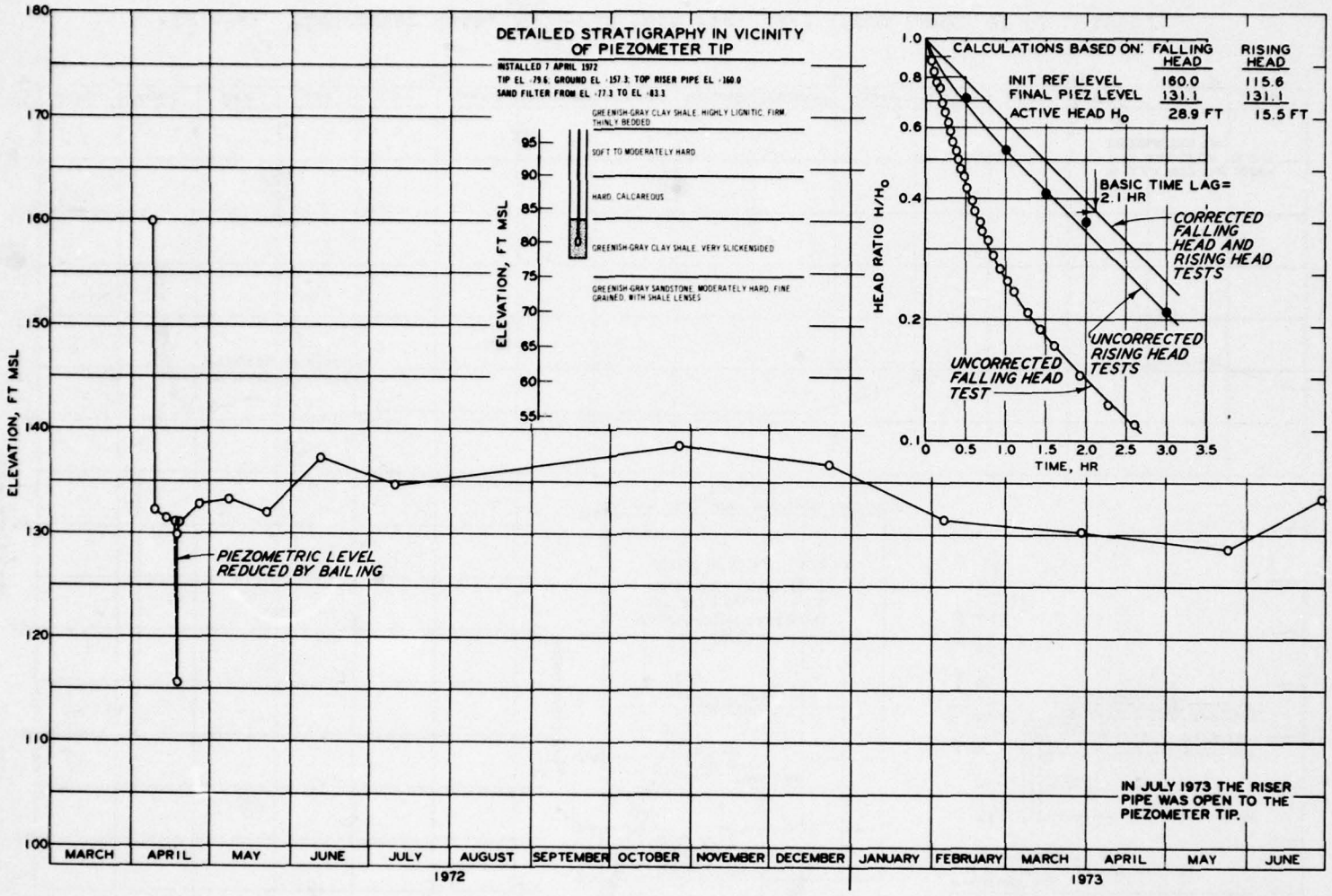

Fig. 40. Piezometer data, WCSE-P1A (see Fig. 21.) (from Banks et al., 1975)

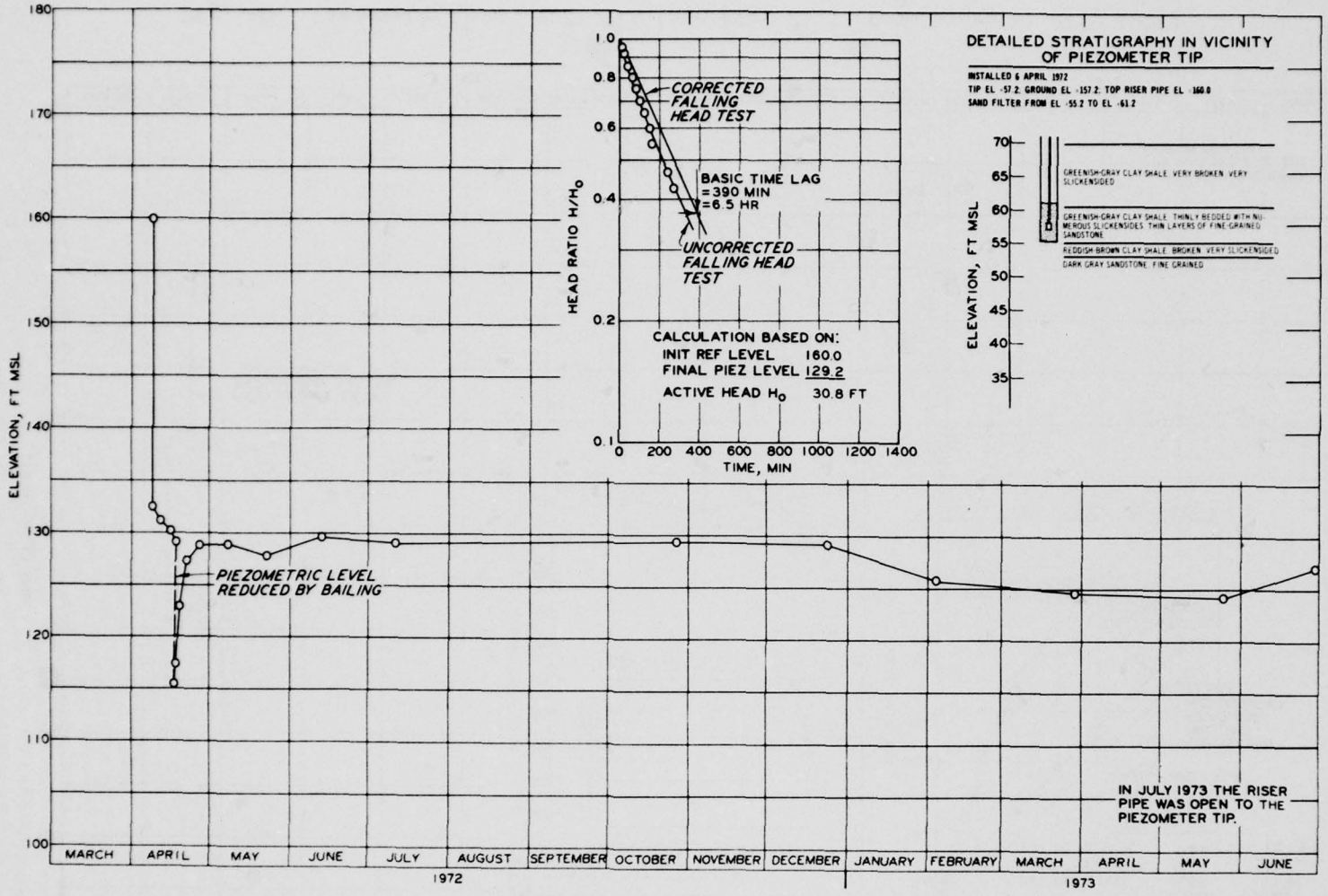

Fig. 41. Piezometer data, WCSE-P1B (see Fig. 21.) (from Banks et al., 1975)

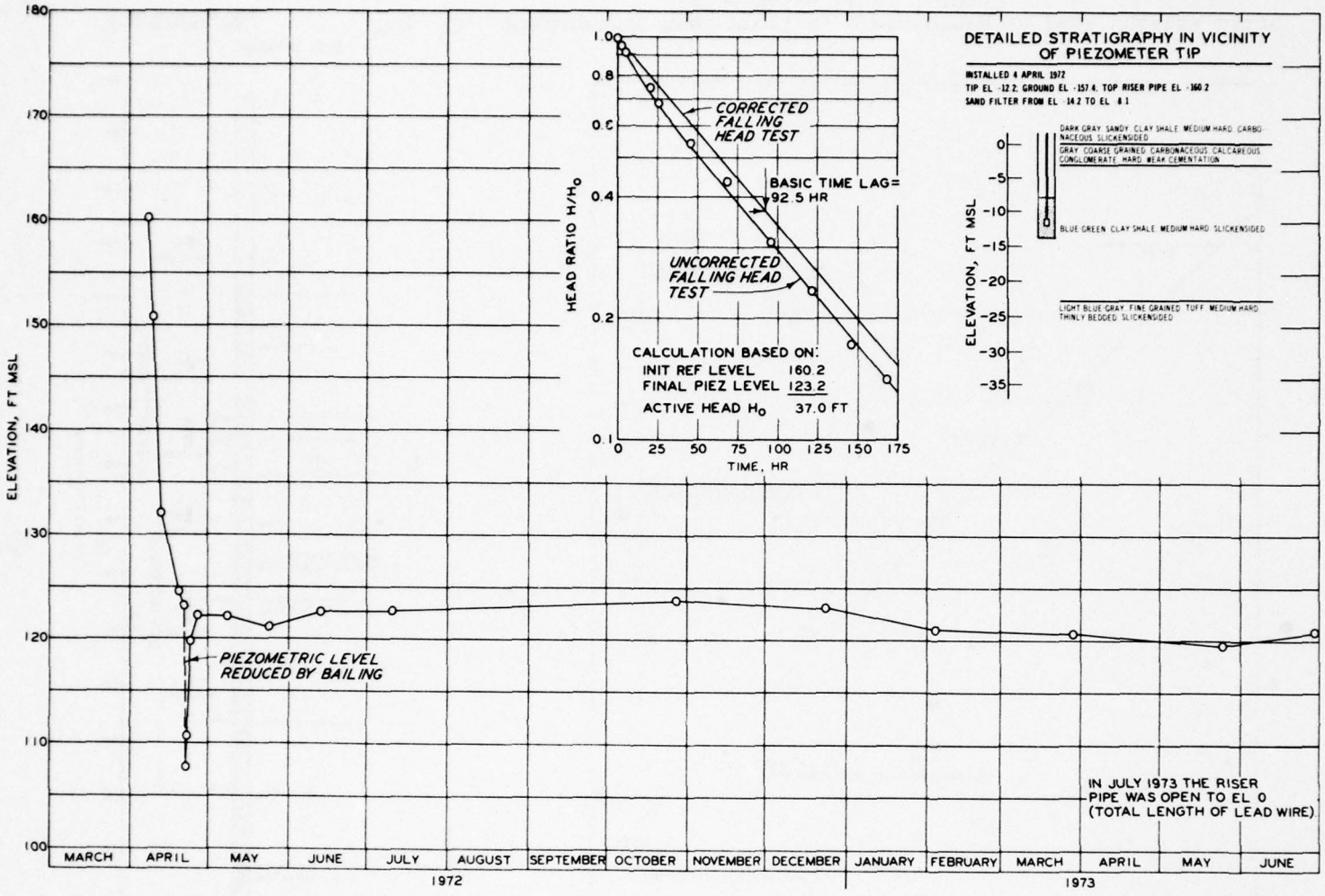

Fig. 42. Piezometer data, WCSE-P1C (see Fig. 21.) (from Banks et al., 1975)

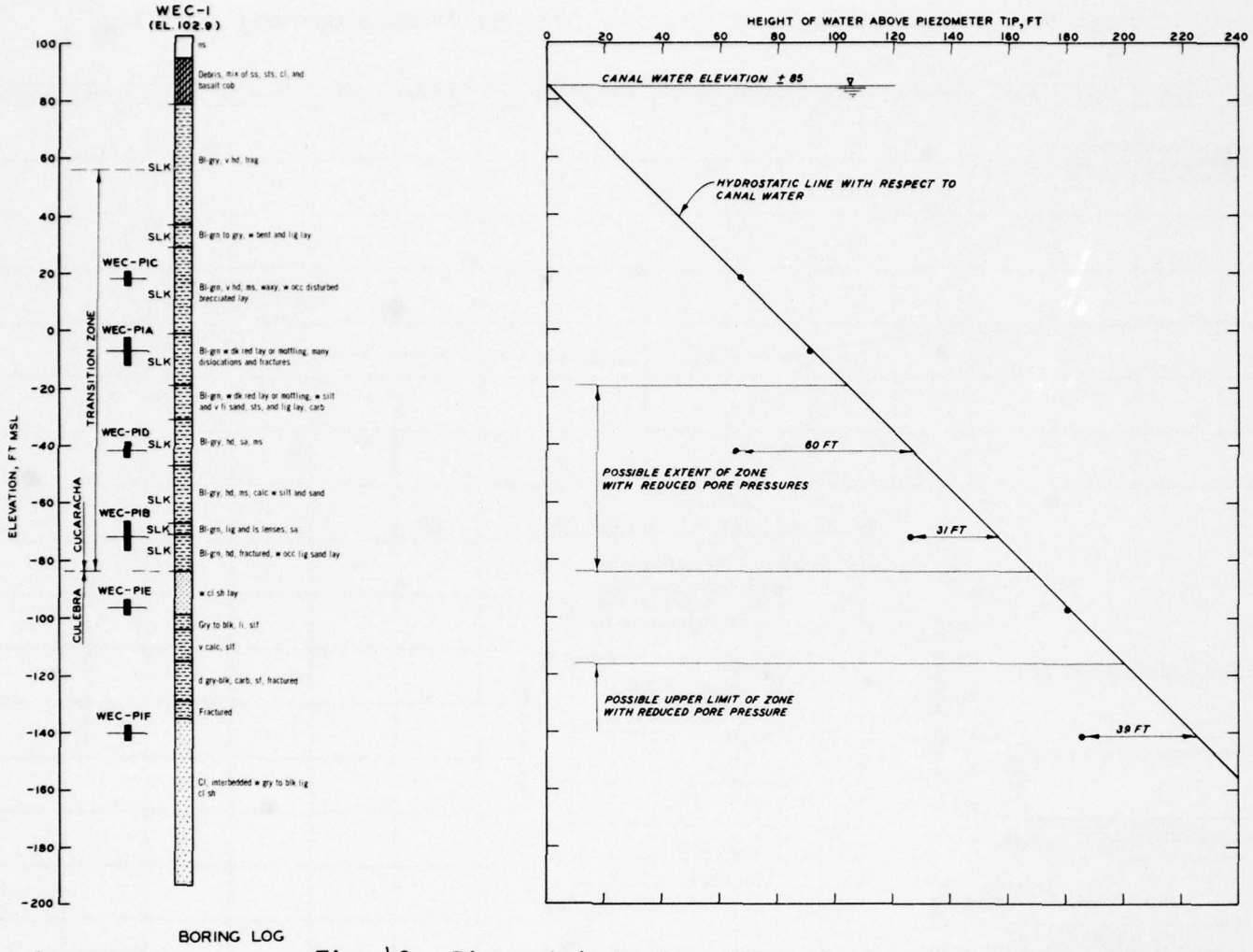

Fig. 43. Piezometric head profile, piezometers in East Culebra Slide (from Banks et al., 1975)

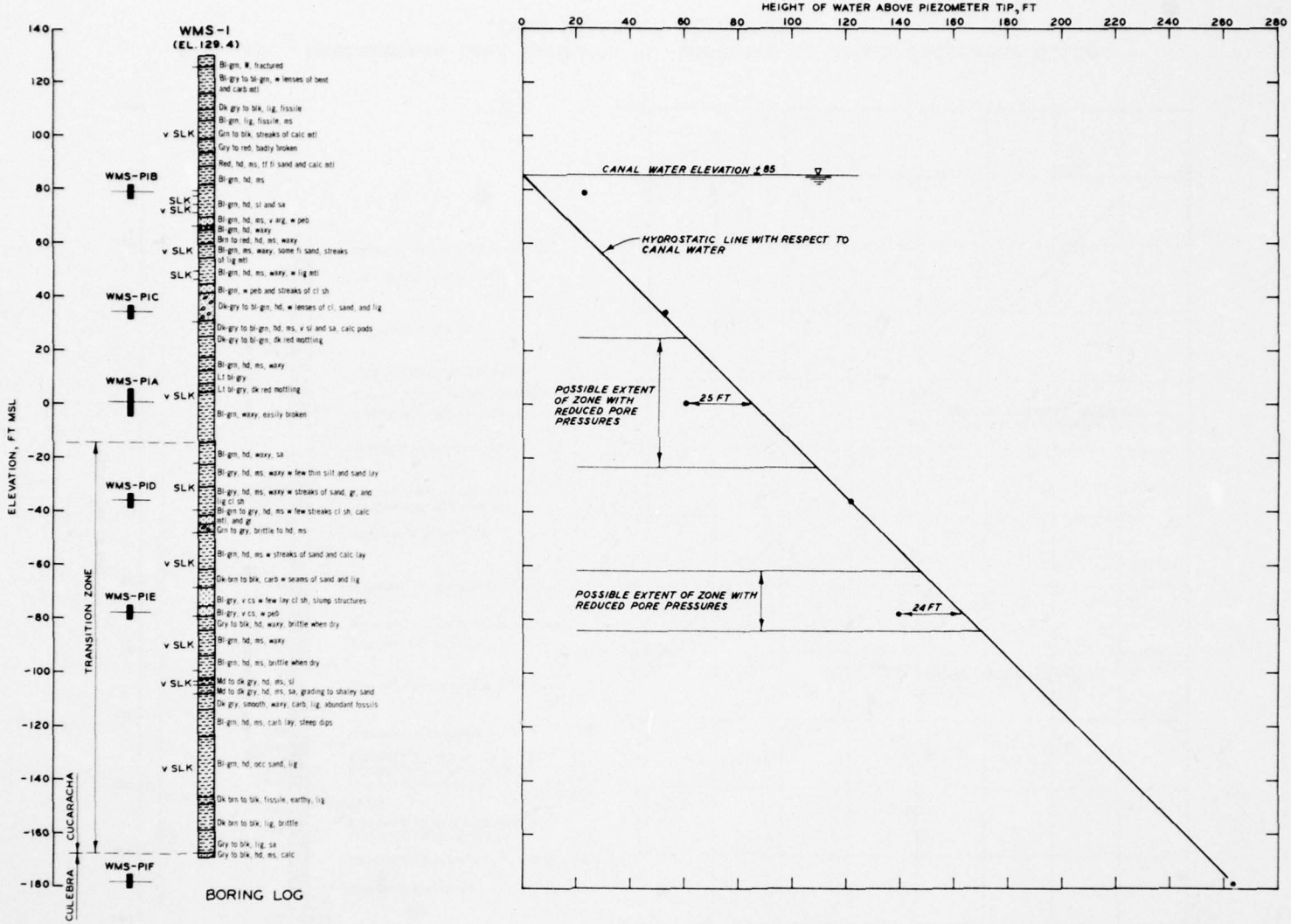

Fig. 44. Piezometeric head profile, piezometers in Model Slope (from Banks et al., 1975)

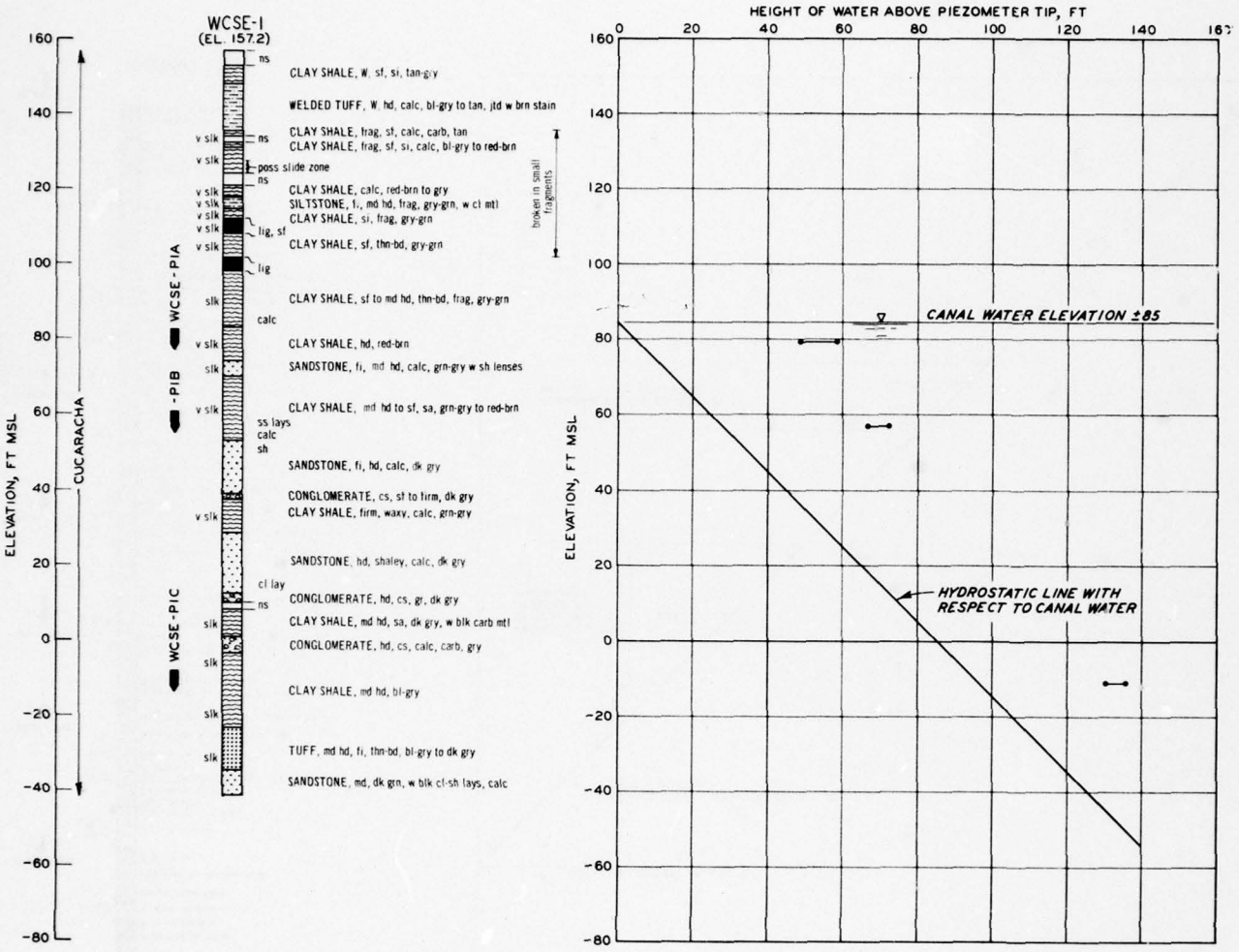

Fig. 45. Piezometric head profile, piezometers in South Cucaracha Slide (from Banks et al., 1975)

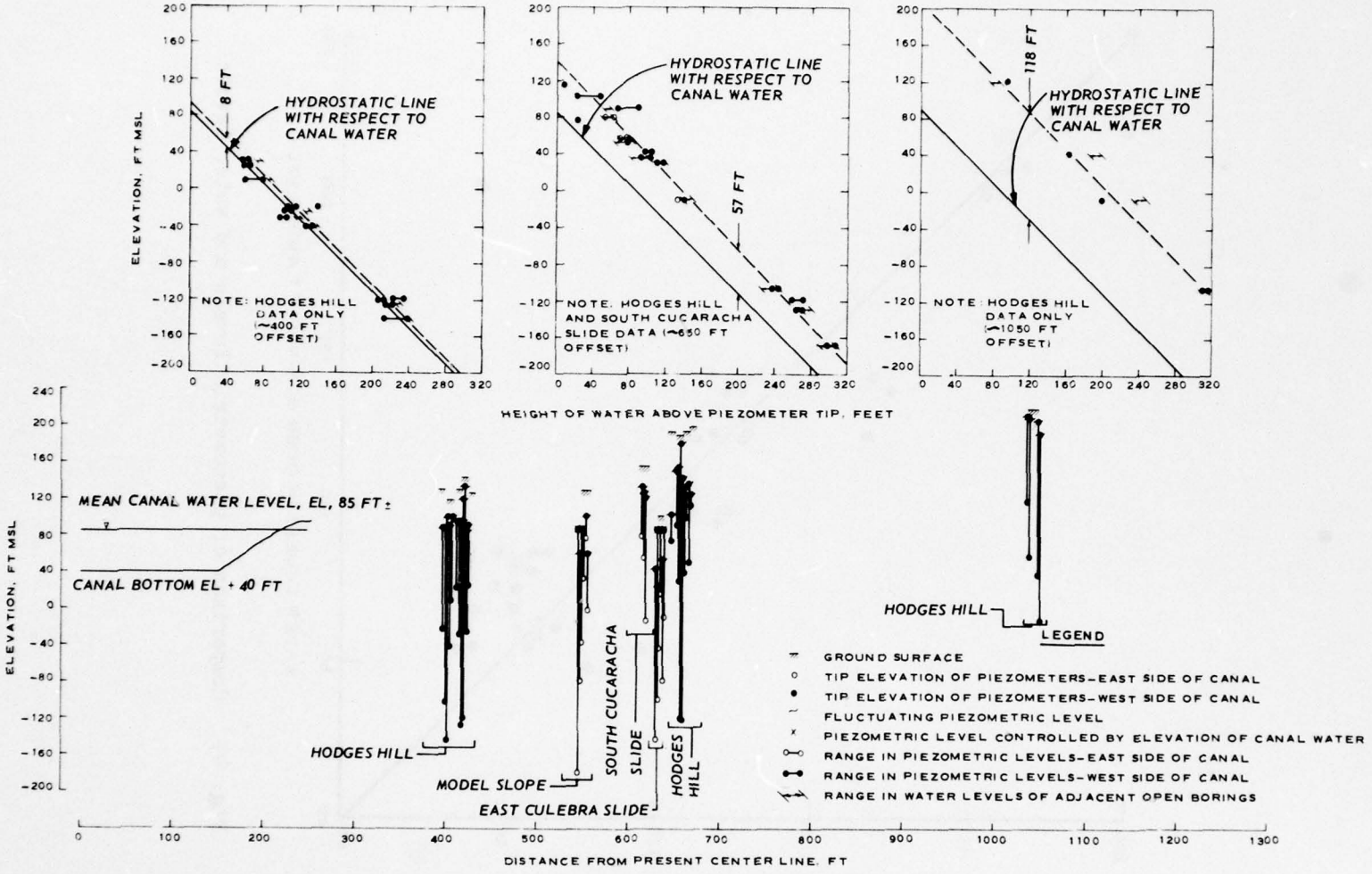

Fig. 46. Piezometric levels in Cucaracha formation

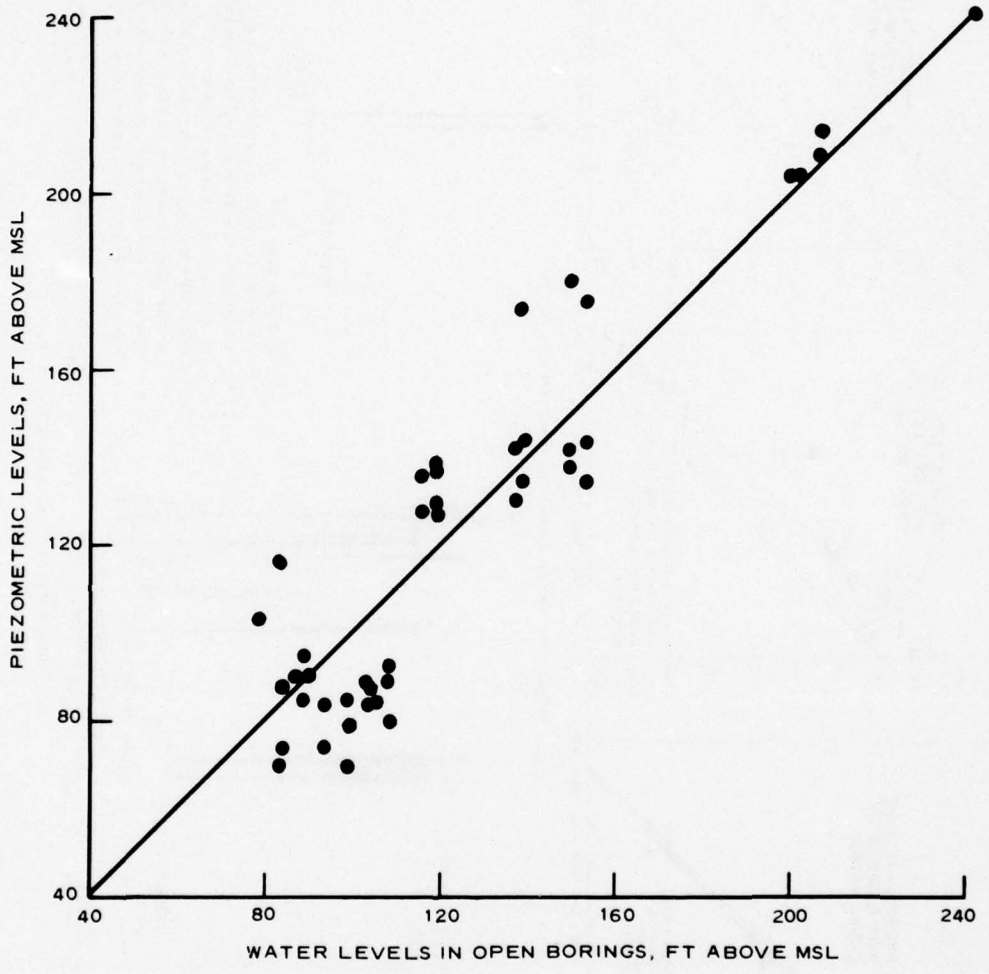

Fig. 47. Comparison of piezometric levels and water levels

CHAPTER IV: SUMMARY OF PHYSICAL PROPERTIES OF CUCARACHA CLAY SHALE

Because the development of the East Culebra Slide involved only the Cucaracha formation, the discussion in this chapter will be restricted to results obtained from tests on Cucaracha materials. Furthermore, since the description of Slide development indicated the importance of the weak shale layers, the discussion will emphasize the strength properties of the shales. Other properties are summarized to indicate the character of the Cucaracha clay shale.

Physical properties of the Cucaracha formation have been determined at various times, usually in connection with special studies such as the Third Locks Study (PCC, 1942), the Isthmian Canal Study (PCC, 1947), the Atlantic-Pacific Interoceanic Canal Study (APICSC, 1970), and the WES study (Lutton and Banks, 1970; Lutton et al., 1975; Banks et al., 1975). Field tests, including plate bearing and direct shear tests, have been conducted in Cucaracha materials at a location other than the study site (PCC, 1942; Smith and Lutton, 1974). The PCC, as part of their normal operation and maintenance activities, at various times has drilled and sampled areas underlain by the Cucaracha clay shale, including the East Culebra Slide. Logs of such borings and such test results as exist are generally contained in files and internal memoranda of the PCC. The USAE District, Jacksonville, in support of the APICSC Study, obtained borehole samples in 1969 at the East Culebra Slide; the samples were tested by the USAE South Atlantic Division Laboratory (SADL), SAD (1969). In 1969, tests were conducted by the WES on Cucaracha samples taken from a boring (WEC-1) drilled at the East Culebra Slide as well as on borehole samples taken at other locations (Lutton and Banks, 1970). In 1972, the WES tested Cucaracha shale taken from borings at locations other than the East Culebra Slide (Banks et al., 1975).

Details of early test procedures are generally only cursorily described and, as a result, uncertainty exists in many cases concerning the applicability of test results. Descriptions of test procedures and results obtained by the SADL on samples taken from boring 14-D-37 at the East Culebra Slide (Figs. 3 and 48) are given in detail in SAD (1969). Test procedures and results obtained by the WES are given by Lutton and

Banks (1970) for a first series of tests on clay shales of the Cucaracha and Culebra formations and by Banks et al. (1975) for a second series of tests on clay shales from several formations found along the Panama Canal. Procedures and results for tests on Cucaracha clay shale samples are given in Appendix A of this thesis; Table A1 indicates the tests conducted. Water content, grain-size analyses, and classification data obtained on samples from recent borings in the East Culebra Slide are shown in Figs. 48 and 49. Similar data are shown in Fig. 50 for a boring in the Model Slope and in Fig. 51 for a boring in the South Cucaracha Slide. Materials encountered in the borings shown in Figs. 48-51 are representative of the stratigraphy existing prior to the initial breaks (Fig. 22).

General Properties and Consolidation Data

Slaking behavior

Slaking reactions occurred very rapidly on samples from the Cucaracha formation, including the transition zone, when air-dried and immersed in distilled water. For the most part, slaking was complete. Material from the transition zone indicated some slight reactions to HCl at natural water content on discrete fossils or microfossils scattered throughout the material as opposed to no reactions on Cucaracha samples taken from above the transition zone.

Water contents and dry densities

The natural water content within the Cucaracha formation typically ranged from 10 to 25 percent on clay shale samples (Table A2 and Figs. 48-51). Higher values were generally found in samples taken from the near-surface slide debris. Occasionally, a large increase in water content was noted in highly fractured or broken layers. For example, in boring WEC-1 (Fig. 49), the water content almost doubled at a depth of 74 ft (el +29 ft) in a slickensided layer associated with the present depth of sliding at the Slide. From values listed in Table A2, the natural water content varies from 2 to 16 percentage points below the plastic limit on a sample-to-sample basis; on the average, it is 10 percentage points lower.

The dry densities within the Cucaracha formation ranged from 90 to 130 pcf with an average of about 110 pcf.

Classification data

Several studies have shown that both the Atterberg limits and grain-size analyses depend upon the effort expended in breaking down clay shale materials. All available Atterberg limit data for the Cucaracha clay shale were not obtained with consistent methods since much of the testing either preceded or was concurrent with research performed at the WES over the past several years to establish acceptable standard Corps of Engineers procedures (Heley and MacIver, 1971; Townsend and Banks, 1974).

The Atterberg limit data (Fig. 48) were determined at SADL (SAD, 1969). In the SADL procedure a sample was broken down by hand into approximately 1-in.-diam pieces. The material was air-dried for 48 hr, then slaked in distilled water for 48 hr through ten such drying and slaking cycles. The resulting material was wet-sieved through the No. 40 sieve with the limits being determined on the material that passed through the sieve. Atterberg limit data (Figs. 49 and 50) were determined at the WES (Lutton and Banks, 1970). In the procedure used at that time a sample was broken down at natural water content by the shaving action of a salad grater, spread in a flat tray, and air-dried for 48 hr. The material was then ground in a mortar, using a rubber-tipped pestle to produce a powder that would pass the No. 40 sieve. The powder was slaked in distilled water for 48 hr and then dried back to a water content above the liquid limit. Research work at the WES has since led to three standardized procedures for the Corps of Engineers to use in processing clay shales. In the primary method, termed the blenderized procedure, the material is broken down at its natural water content, then air-dried (at least 48 hr) and slaked in distilled water (48 hr). The resulting slurry is then worked in a blender for 10 min before being washed through a No. 40 sieve. The Atterberg limits are determined on the material passing the sieve. Atterberg limit data shown in Fig. 51 were determined by the blenderized procedure (Banks et al., 1975). Discussion of results from the two WES procedures is given in Appendix A.

The liquid limits of Cucaracha clay shale showed an extremely large range with only a small range for the plastic limit. Limits from the SADL cycled procedure (Fig. 48), the WES air-dried procedure (Figs. 49 and 50), or the WES blenderized procedure (Fig. 51) plot near and generally above the A-line on the plasticity chart. Thus from the standpoint

of classification, according to the Unified Soil Classification System, for example, the limits indicate a consistent category (CH--highly plastic clay). The differences in limits obtained for each procedure are exemplified by values shown below:

	LL		PL		PI	
	Range	Avg	Range	Avg	Range	Avg
Air-dried-cycled (SAD, 1969)	(50-260)	77	(25-63)	40	(18-215)	37
Air-dried (Table A2)	(48-116)	68	(19-42)	29	(19-78)	39
Blenderized (Table A2)	(59-120)	86	(26-46)	32	(32-81)	54

No doubt some of the differences indicated above are caused by variation in materials from the different borings, but the trend, indicated by average values, shows that the liquid limit increases with increased effort to break down the clay shale materials.

In the discussion of the geology of the area (Chapter III), it was pointed out that a transition zone marked the bottom 130 to 150 ft of the Cucaracha formation. These zones are indicated in Figs. 49-51. Comparison of liquid limits from materials in the transition zone with those obtained above the transition zone failed to indicate any significant differences.

Consolidation data

Preconsolidation loads did not indicate a consistent trend with depth below the present ground surface, nor with distance above and below the bottom of the Canal. Rather, low preconsolidation loads were determined for samples with initial high void ratios; for a series of tests on samples from a given boring, the preconsolidation loads increased in correspondence to a decrease in void ratio (Banks et al., 1975). However, at a given void ratio, considerable variation in preconsolidation load occurred between borings. The test data were reviewed to determine explanations for the variable preconsolidation load; no obvious explanation was found.

Initial WES consolidation tests were conducted, using equipment with a maximum loading capacity of 200 tsf (Lutton and Banks, 1970). Preconsolidation loads could not be established since pressure-void ratio curves indicated considerable curvature at the maximum applied load (Table A3). Consolidation tests by SADL (maximum applied load of

350 tsf) indicated the preconsolidation load may vary from 95 to 245 tsf (SAD, 1969). The more recent consolidation tests conducted by the WES (Table A3) that used a high-capacity consolidation device (maximum applied load of 500 tsf) indicated preconsolidation loads varying from 11 to 98 tsf (Banks et al, 1975). The maximum past overburden thickness has been estimated to be as much as 2500 to 3000 ft from formation thicknesses given by Woodring (1957). If the overburden is assumed to have an average saturated unit weight of 150 pcf with the groundwater near the surface, the maximum past loading is estimated at 110 to 130 tsf.

Swell pressures increased with depth and generally ranged from 0.8 to 1.3 times the computed effective overburden pressure, assuming hydrostatic pore pressures with respect to the present ground surface. Because the materials in the study area are in a rebounding stage, the swelling index C_s, the time at 50 percent rebound t_{50}, the coefficient of swelling c_s, and the coefficient of permeability k were computed from the unloading portion of consolidation curves between the 16- and 0.02-tsf load (Lutton and Banks, 1970) or between the 20- and 10-tsf loads (Banks et al., 1975). These stresses bracket loads existing before Canal excavation was commenced and those now existing at the depth of the test specimens. The swelling index averaged about 0.05; the coefficient of swelling averaged about 0.24×10^{-4} cm^2/sec; and the coefficient of permeability averaged about 1×10^{-10} cm/sec (Table A3).

Only limited data exist from which to compare k_h (from field data, Table 4) to k_v (from laboratory data, Table A3). That comparison is as follows:

Piezometer	Elevation of of Sand Filter ft msl	k_h cm/sec	Sample	Elevation of Sample ft msl	k_v cm/sec
WEC-P1A	-12.0 to -1.2	10^{-9}	WEC#10	-10.5 to -8.7	0.5×10^{-10}
WMS-P1C	+30.8 to +37.6	10^{-7}	WMS#10	+30.6 to +31.3	0.8×10^{-10}
WCSE-P1B	+55.2 to +61.2	10^{-7}	WCSE#8	+55.3 to +56.3	0.07×10^{-10}

Strength Properties

Although certain descriptions of the strength characteristics can be found in early reports, only qualitative assessments are given. The

first report of actual strength test data was given by MacDonald (1924):

> ...The Bureau of Standards, Washington, D. C., made crushing strength tests on seven samples of the Cucaracha formation....The weakest sample tested of the typical Cucaracha rocks crushed at 41,184 pounds per square foot *(20.6 tsf)*....The strongest sample...crushed at 70,272 pounds per square foot *(35.1 tsf)*....

Conscientious efforts to measure the strength of the Cucaracha materials began with the Third Locks Study and has continued to the present. A few field tests have been conducted, but the bulk of the tests was made under laboratory conditions for different test configurations, i.e., unconfined and triaxial compression and direct shear, and under differing, and in many cases unknown, drainage conditions during testing. Although the different drainage conditions no doubt caused large variations in the reported test results, an additional complicating factor to a consistent analysis of the strength data arose from the variability between samples. Previous discussions have indicated that the Cucaracha clay shales are heavily overconsolidated and, further, that the weaker materials, and thus those most likely to fail under field loading conditions, contain numerous slickensides. Thus, it is important to review the available strength data to determine whether representative strength parameters can be obtained for the slickensided materials. In addition, it is equally important to review the strength data to determine whether effective strength parameters have been adequately determined.

Third Locks Study

In August 1939, the U. S. Congress authorized the construction of a third set of locks to be located at varying distances from the existing structures and to be connected by approach channels to the existing Canal. The proposed lock was to be built parallel to the existing Pedro Miguel Lock and to be founded on Cucaracha clay shale. Tests were conducted to verify design parameters recommended by engineers and geologists concerned with this phase of the design (PCC, 1947). A limited number of field bearing tests and laboratory tests were conducted on samples from Test Pit 2. Although the details of the laboratory tests were not discussed in reports of the project, apparently they consisted of one unconfined compression test and two triaxial compression tests (as inferred from Fig. 5-121, in PCC, 1947). Continued investigation

indicated that the tests were conducted on material judged to be unrepresentative of the weakest or slickensided phases of the Cucaracha clay shale. As a result, several additional tests were conducted in both the field (in Test Pit 3) and the laboratory to verify or provide design data.

Field direct shear tests. The tests were conducted along the invert of a drift excavated between depths of 30 to 36 ft below the ground surface (invert el +29 ft). The drift was 6 ft high by 5 ft wide and was excavated 45 ft into the north wall of Test Pit 3 in a stratum of Cucaracha clay shale. Test Pit 3 was located about 4000 ft west of the present Pedro Miguel Lock (Fig. 1). The material in which the direct shear tests were conducted was described as "clay shale, purple with green bands, slickensided, soapy, brittle." Water inflow was experienced during excavation of the pit. Most of the flow originated in fractures with gouge filling, but an appreciable quantity came from seemingly tight slickensides (Thompson, 1947).

Six tests were conducted on 1-ft-square specimens. In the preparation of specimens, the floor was leveled, a grooved surface formed, and a concrete cap poured. Immediately prior to testing, a channel 1 by 1 in. was cut around the base to allow for specimen displacement. Two tests were run at 4 tsf and the other four tests at 7.5-tsf normal stress. Normal stresses were applied to the specimens in increments of 1.0 tsf per 2 min. No description was found to indicate how long the normal load was maintained before shearing was started. Although in four of the tests the normal loads were cycled twice, the inference from the test description was that the shearing force was applied immediately after the final application of normal stresses. The stresses were increased in increments of 0.25 tsf per min until the peak shear strength was obtained. Following attainment of peak shear strength, the shear stress was released and reapplied on each specimen until a second peak was obtained.

The test results, along with a description of the observed failure surface, are given in Table 6. Since the data showed considerable scatter under the 7.5-tsf normal load, the failure surface of each specimen was examined in detail to determine whether there existed some visual explanation for the scatter. It was concluded that the range in values indicated by the tests was characteristic of the mass. Therefore, each

test was given equal value in establishing the peak strength envelopes determined from the first loading cycle. Although the strength parameters as originally deduced (c = 0.65 tsf, ϕ = 21.6 deg) appear reasonable, alternate interpretations have from time to time been made (Hirschfeld et al., 1965; Johnson, 1968).

While the specimens were probably saturated during shear, the drainage conditions are unknown for the tests. The tests were of relatively short duration, but because of the slickensided nature of the specimens, it is not possible to determine whether the test results give a measure of the drained or undrained shear strength of slickensided Cucaracha clay shale.

Laboratory tests. Samples of the Cucaracha clay shales were obtained from cores in the vicinity of Test Pit 3. Also samples were obtained by drilling cylindrical specimens from irregular blocks taken from Test Pit 3. Both triaxial and unconfined compression tests were conducted on 2-in.-diam by 5-in.-high specimens. In addition, direct shear tests were conducted on specimens with polished surfaces.

Unconfined compression tests were conducted on 34 specimens. The specimens were loaded to failure by either "slow" or "quick" application of load. For the "slow" tests, loads were applied in increments of about 1 tsf per day; for the "quick" tests, loads were applied in increments of about 1 tsf per min (Smith and Lutton, 1974). Triaxial compression tests were conducted on 18 specimens. The loading rate was termed "quick," but the actual times of loading and conditions of drainage for the triaxial compression tests were not given. The source of the test results (Fig. 5-125, in PCC, 1947) also included the shear strength obtained from five specimens described as being "single shear tests under quick loading." The specimens tested were known to represent the stronger portions of the Cucaracha and even prior to testing were expected to yield higher strengths than were obtained from the field tests on slickensided materials. While the drainage conditions are not known, it is assumed that the triaxial tests were most likely unconsolidated-undrained and that the results give a measure of the undrained shear strength of intact Cucaracha clay shale.

Friction tests were made on short lengths of 2-in.-diam cores. The test surfaces were polished with Carborundum stones and by rubbing

opposing shale pieces together. During shear, the pieces were held in place in a direct shear box with plaster of paris. No data are available to indicate number of tests or test procedure. The friction angle was found to be about 10 deg; apparently, the polishing removed any cohesion possessed by the material.

Isthmian Canal Studies

Additional tests were conducted on Cucaracha clay shale in connection with the proposed sea level realignment of the Canal (PCC, 1947). All tests were conducted in the laboratory and consisted of both strain-controlled and stress-controlled direct shear tests as well as unconsolidated-undrained and consolidated-undrained triaxial tests.

Direct shear tests. Hand-cut cubical specimens were obtained from a depth of from 6 to 10 ft below the surface of the west bank of the Canal at Hodges Hill. After sampling, the specimens were wrapped in wet burlap sacks and returned to the laboratory. While in the laboratory, before being prepared for testing, the samples were stored under a cover kept wet with water. The direct shear tests were conducted on a pedestal, 2 to 2-1/2 in. high and 6 in. on each side, carved on top of each sample. Normal stresses varied from about 1.5 to 25 tsf, but no information was given regarding rate of application or time of application before applying the shearing load. Two tests were conducted under stress-controlled conditions by the application of shear force in increments of 0.4 tsf per min. The peak shear stress was reached in 6 and 9 min. In the other 20 tests, the rate of displacement was controlled between the range of 0.006 and 0.22 in. per min; the bulk of the tests was conducted at either 0.01 or 0.02 in. per min. Although the time to reach the maximum shear stress varied from 1.0 to 29.5 min for the extreme loading rates, generally the times varied from about 4 to 24 min. The complete loading history for the tests is unknown. However, the attainment of peak shear stresses on the order of a few minutes would indicate that the results are representative of undrained strengths.

Unconsolidated-undrained tests. Samples for triaxial tests were obtained from borings made during the Third Locks Study. Samples were coated with paraffin, wrapped in wax paper, and again covered with a thick coating of paraffin, and in this condition were stored underwater for about 15 months. Some confusion exists as to whether all test

specimens came from borings. The tabulation of data (Table 9, in PCC, 1947) indicates that ten specimens came from "cubic ft" specimens; these samples may have come from the Hodges Hill pit where the direct shear specimens were obtained. Confining stresses equal to the overburden were applied to each specimen from core samples, with no attempt being made to consolidate samples prior to testing. The times to failure ranged from 1.3 to 20 min.

Consolidated-undrained tests. Several core samples (2-1/8 in. in diameter) of Cucaracha clay shale were tested at Harvard University to determine the consolidated-undrained strength under varying loading rates (Casagrande and Shannon, 1948). The specimens were divided into two general groups, "those with a soapy feel and those with a sandy feel." The distinction between the two groups was not always sharply defined, and jointing, hardness, and color were variable. All specimens contained slickensided surfaces of varying dimensions, some relatively open and uncemented, others closed and apparently recemented.

Two series of tests were conducted. Severe air leaks through the lapped rubber membrane strips enclosing the specimens made the reliability of the results of the first series questionable. The second series successfully used cylindrical rubber membranes. All specimens were consolidated from two to five days under a lateral pressure of about 6 tsf. Volume changes during consolidation depended upon the relative soundness of the specimen and varied from about 1 cc for intact specimens to 5 cc for specimens that were badly fractured, jointed, or that contained uncemented slickensides. Strain rates varied from 0.002 to 31 percent per sec. Although free drainage from both the cap and base was maintained throughout consolidation and testing, the loading rates were fast enough to limit drainage.

The test results from the second test series are shown in Table 7. Cores in the group having the highest strength were characterized by a sandy feel, whereas those in the lower strength group were characterized by a soapy feel.

Hodges Hill Study

Concern over cracking in the Hodges Hill area (Fig. 3) in 1968 led to the drilling of several borings to investigate the subsurface, install piezometers and horizontal drains, and to obtain samples for limited

testing. Laboratory tests were conducted cooperatively by the WES and the PCC (PCC, 1969). Unconfined compression tests were conducted on 47 samples of Cucaracha at depths varying from near the ground surface to 370 ft. Also, five unconfined compression tests were conducted on samples of sandstone from the Cucaracha formation.

Atlantic-Pacific
Interoceanic Canal Study

During the most recent study of possible routes for a new sea level canal (APICSC, 1970), a boring was made through the East Culebra Slide (Figs. 3 and 48). Undisturbed 6-in.-diam samples were obtained and returned to the SADL for testing (SAD, 1969). The testing program consisted of determination of index values, grain-size analyses, densities, water contents and mineralogy, and limited strength tests.

Unconsolidated-undrained tests. Six specimens of full core diameter were tested under unconsolidated-undrained conditions. Confining loads ranged from 3.1 to 8.3 tsf. Times to failure ranged from 7 to 54 min.

Residual direct shear tests. A series of direct shear tests were run on precut specimens to determine the residual shear strength of the Cucaracha clay shale. Samples were 3 in. on the side and approximately 1 in. thick. The specimen was cut at midheight with a band saw to form a plane of weakness. The specimens were tested under normal stress varying from 4 to 12 tsf. The specimens were repeatedly sheared at a displacement rate of 0.001 in. per min until the minimum shear force was attained. Displacements under each normal stress generally reached 10 in. or more. The residual direct shear test results are shown in Fig. 52.

WES studies

Undisturbed 6-in. borehole samples of Cucaracha clay shale have been obtained by the WES at several locations during the five-year study of the behavior of clay shale slopes along the present Canal (Lutton and Banks, 1970; Banks et al, 1975). At the East Culebra Slide, samples have been taken from boring WEC-1 (Fig. 49). Additional samples have been taken from the Model Slope (Fig. 50), West Culebra Slide, and the South Cucaracha Slide (Fig. 51).

Laboratory strength tests consisted of unconfined compression tests on a few samples, drained direct shear of precut specimens (for

determination of residual strength), drained direct shear tests on intact and slickensided specimens (for determination of peak strength), and drained direct shear and consolidated-undrained tests (with pore pressure measurements) on slurry-consolidated specimens (for determination of strength of normally consolidated specimens).

Unconfined compression tests. Six specimens of full core diameter were tested. Times to failure ranged from 2 to 5 min. The sample descriptions and test results are given in Appendix A.

Direct shear tests - precut specimens. A series of direct shear tests were conducted on precut specimens to determine the residual strength of the Cucaracha clay shale. Test procedures and results are given in Appendix A. The test results are shown in Fig. 52 for comparison with residual test results obtained on Cucaracha clay shale by others. Several early tests were conducted to determine residual strengths. For example, an emphasis was made during the Isthmian Canal Study tests to continue straining both direct shear and triaxial compression tests beyond the peak strength to determine what was then termed "the residual strength." It is doubtful, however, that large enough displacements were obtained for the strength reported to be truly at a minimum. For that reason, the present generation of tests is relied upon to give the residual shear strength of the Cucaracha clay shale, since these tests were conducted explicitly for that purpose.

Approximately 100 test values are available from direct shear tests on precut specimens (SAD, 1969; Lutton and Banks, 1970; and PCC, 1969) and on remolded specimens in direct and annular shear tests (Herrmann and Wolfskill, 1966; and LaGatta, 1970). Test data from these sources are shown in Fig. 52.

The test data shown in Fig. 52 indicate a possible range of residual shear strength parameters from $c'_r = 0$, $\phi'_r = 11$ deg to $c'_r = 0$, $\phi'_r = 4$ deg. The best fitting straight line envelope indicates strength parameters of $c'_r = 0$, $\phi'_r = 7.5$ deg. It is noted that the best fitting straight line envelope is at a slight variance to the data points determined from tests on remolded samples. The data from Herrmann and Wolfskill (1966) and LaGatta (1970) indicate that the drained residual shear strength envelope may be slightly curved (Fig. A29).

Direct shear tests - intact specimens. During the preparation of

specimens for residual testing, it was noted at times that core samples evidenced no slickensides over small lengths. With reasonable precautions, specimens 3 in. on a side and 1 in. high could be formed for testing. Originally, it was decided to conduct direct shear tests on three specimens without forming a precut plane (Lutton and Banks, 1970). Later, 20 additional tests were conducted (Banks et al., 1975). Test details and test results are given in Appendix A.

The effective peak shear strength determined by direct shear tests on intact specimens is shown in Fig. 53. Test data in Appendix A indicate that for three specimens cut from a single sample, no systematic increase in strength resulted from an increase in the effective normal stress. This observation emphasizes the extreme variations that can be expected of Cucaracha clay shale at any depth. The variation of results is not so obvious in Fig. 53. Two limiting envelopes can be constructed to encompass the data. All specimens produced strengths in excess of a lower limiting envelope defined by $c'_p = 0.5$ tsf, $\phi'_p = 28$ deg. A curved line appeared to best describe the upper limiting envelope. The curve was approximated by a bilinear envelope defined by $c'_p = 5.0$ tsf, $\phi'_p = 28$ deg for $\sigma'_n > 3$ tsf and by $c'_p = 0$, $\phi'_p = 65$ deg for $\sigma'_n < 3$ tsf. The upper envelope is associated with samples that exhibited a brittle failure, i.e., the samples exhibited a large drop in shear strength after the peak shear strength was obtained. The lower envelope is associated with samples that exhibited a plastic failure, i.e., the samples exhibited little or no drop in shear strength after the peak shear strength was obtained.

Direct shear tests - slickensided specimens. Three series of direct shear tests were conducted on slickensided specimens. Specimen preparation and test procedures and results are given in Appendix A. The data obtained from these tests are shown in Fig. 54 to produce a curved effective peak strength envelope. The envelope passes through the origin and transitions at an effective normal stress of 2 tsf into an approximately linear envelope defined by strength parameters of $c'_p = 1.6$ tsf, $\phi'_p = 24$ deg.

It is observed that the strengths of the slickensided specimens are reproducible within narrow limits, with much of the variations noted on intact specimens being eliminated. Since a conscientious effort was made

to test specimens containing numerous randomly oriented slickensides, the data would suggest that the principal cause of the variations in the data from intact specimens results from variable cohesion offered by intact material. It is further observed that the strengths determined on slickensided specimens are comparable with those obtained from the intact specimens that exhibited plastic failure. This observation would suggest that, although seemingly intact specimens of Cucaracha clay shale can be found, some layers have undergone some form of weakening as evidenced by a reduction in the cohesion of the material.

It is also of interest to compare the results of field direct shear tests (Table 6) to the results of laboratory tests on slickensided specimens (Fig. 54). The field data exhibit considerable variation in the peak shear strength at the 7.5-tsf normal stress and, hence, the possibility of different interpretations of the strength parameters indicated by the test (Hirschfeld et al., 1965; Johnson, 1968). While it is not necessary here to offer yet another interpretation, it is interesting to note that a strength envelope drawn through the data parallel to that indicated by the laboratory tests appears to be reasonable. If such an envelope were constructed, the strength parameters would be $c = 0.3$ tsf, $\phi = 24$ deg.

Direct shear tests - slurry-consolidated specimens. The method of sample preparation and test results of slurry-consolidated specimens from Cucaracha clay shale specimens are given in Appendix A. The results of direct shear tests (Fig. 55) indicate that different strengths are obtained, depending upon whether the direct shear test is conducted on horizontal or vertical specimens. Most likely particle orientation causes the anisotropic effect. The direct shear test results are comparable to those obtained by LaGatta (1970) from annular shear tests. Curved effective strength envelopes are shown in Fig. 55. The initial portions of the envelopes are defined by the strength parameters: $c' = 0$, $\phi' = 17.5$ deg (horizontal shear plane); and $c' = 0$, $\phi' = 15$ deg (vertical shear plane).

Consolidated-undrained tests - slurry-consolidated specimens. Two slurry-consolidated specimens were tested under consolidated-undrained conditions, with pore pressure measurements being made during shear. The sample preparation and test procedure are discussed in Appendix A.

The test results are shown in Fig. 56. The effective strength is presented by a curved envelope. The initial portion of the envelope is given by strength parameters of $c' = 0$; $\phi' = 20$ deg. The strengths indicated by the consolidated-undrained tests are slightly higher than the strengths from direct shear tests on slurry-consolidated specimens.

Summary of strength data

The data presented and discussed above represent the present knowledge with respect to the strengths of the Cucaracha clay shale. The results may be summarized as follows:

a. No strength data exist from tests conducted on Cucaracha materials before the initial breaks.

b. Later strength tests are on materials taken from beneath the present depth of sliding or from sites located elsewhere within the Cucaracha formation.

c. A conscientious attempt has been made to test the weaker (most generally, slickensided) phases of the Cucaracha clay shale.

d. Strength tests conducted as part of the Third Locks Study (PCC, 1947), the Isthmian Canal Studies (PCC, 1947), or the Hodges Hill Study (PCC, 1969) either were inadequately described to allow a clear determination of their applicability to analyses of the initial breaks or were clearly described as being unconfined compression or unconsolidated-undrained triaxial tests. Possible exceptions were the field direct shear tests or the laboratory direct shear tests on polished surfaces conducted during the Third Locks Study (PCC, 1947) or the consolidated-undrained tests conducted by Casagrande and Shannon (1948) in connection with the Isthmian Canal Studies (PCC, 1947).

e. Strength tests conducted as part of more recent investigations (APICSC, 1970; and the WES) have, in addition to producing strength data for clay shale materials under different conditions (i.e., slurry-consolidated, slickensided, intact), concentrated on determining effective strength parameters.

f. Test techniques for effective strength parameters of the Cucaracha shale are given in Appendix A; individual test results have been summarized in previous discussions. The

individually determined strength envelopes are shown in Fig. 57. There it is shown that:

(1) First, the residual strength envelope is the lowest.

(2) Second, the effective strength envelope for slurry-consolidated specimens is somewhat higher than the residual strength envelope.

(3) Third, the effective peak strength of slickensided specimens is slightly higher than that determined for the slurry-consolidated specimens and, further, is comparable with test results from field direct shear tests on slickensided specimens and from laboratory direct shear tests on those intact specimens exhibiting plastic failure.

(4) Fourth, the effective peak strength of intact specimens that exhibited brittle failure is the highest.

Table 6. Results of Field Direct Shear Tests,
Slickensided Cucaracha Clay Shale, Third Locks Project (PCC, 1942)

Test Block No.	Normal Stress tsf	Shear Stress First Cycle tsf	Second Cycle tsf	Description of Specimen (Smith and Lutton, 1974)
1	7.64	3.11	2.12	Few minor slickensides visible at surface; failure plane below a lense of concretions, 3/8 in. in diameter; failure plane 30 percent slickensided
2	7.42	4.78	3.11	Pronounced slickensides visible; failure plane 65 percent slickensided and 35 percent crushed; failure surface rough
3	4.05	2.34	1.91	Two major slickensides visible near test block; failure surface 40 percent slickensided and 60 percent broken
4	7.42	2.68	2.02	Failure surface 90 percent slickensided
5	4.03	2.23	1.81	Few minor approximately horizontal slickensides visible; failure surface 90 percent slickensided and 10 percent crushed
6	7.42	4.03	2.29	Few minor slickensides, 1/4-in. concretions visible at surface; major slickensides near block nearly vertical; failure surface 20 percent slickensided and 80 percent broken and crushed

Table 7. Consolidated-Undrained Tests on Cucaracha Clay Shale, Harvard University 1948 (Second Series)*

Sample No.**	Depth Below Ground Surface, ft	Time of Loading, sec	Rate of Strain† %/sec	Compressive Strength $\sigma_1 - \sigma_3$, tsf	Strain of Compressive Strength, %	Description of Specimen
HP8-1A	151.5-151.9	8700.0	0.002	61††	1.74	Soupy, yet gritty; intact
HP8-1B	151.5-151.9	97.0	0.017	67††	1.65	
HP8-4A	159.2-159.7	88.0	0.016	94	1.42	Sandy; calcareous nodules, slightly fractured
HP8-7	57.7-58.2	31.0	0.011	59	0.33	Soupy, intact
HP8-8A	115.0-115.3	35.0	0.035	28	1.22	Soupy, intact; readily breakable along numerous slickensides
HP8-8B	115.3-115.6	0.035	31.0	39	1.08	
HP8-11C	Approx 99.0	35.0	0.031	29	1.09	Soupy, slightly fractured
HP8-13A	92.6- 93.0	330.0	0.0023	78	0.74	Soupy, yet gritty; intact
HP8-13B	93.0- 93.3	56.0	0.014	86	0.77	

* From Hirschfield et al., 1965.
** Harvard numbers.
† Strain at maximum compressive strength divided by time of loading.
†† Membrane punctured; bad air leak.

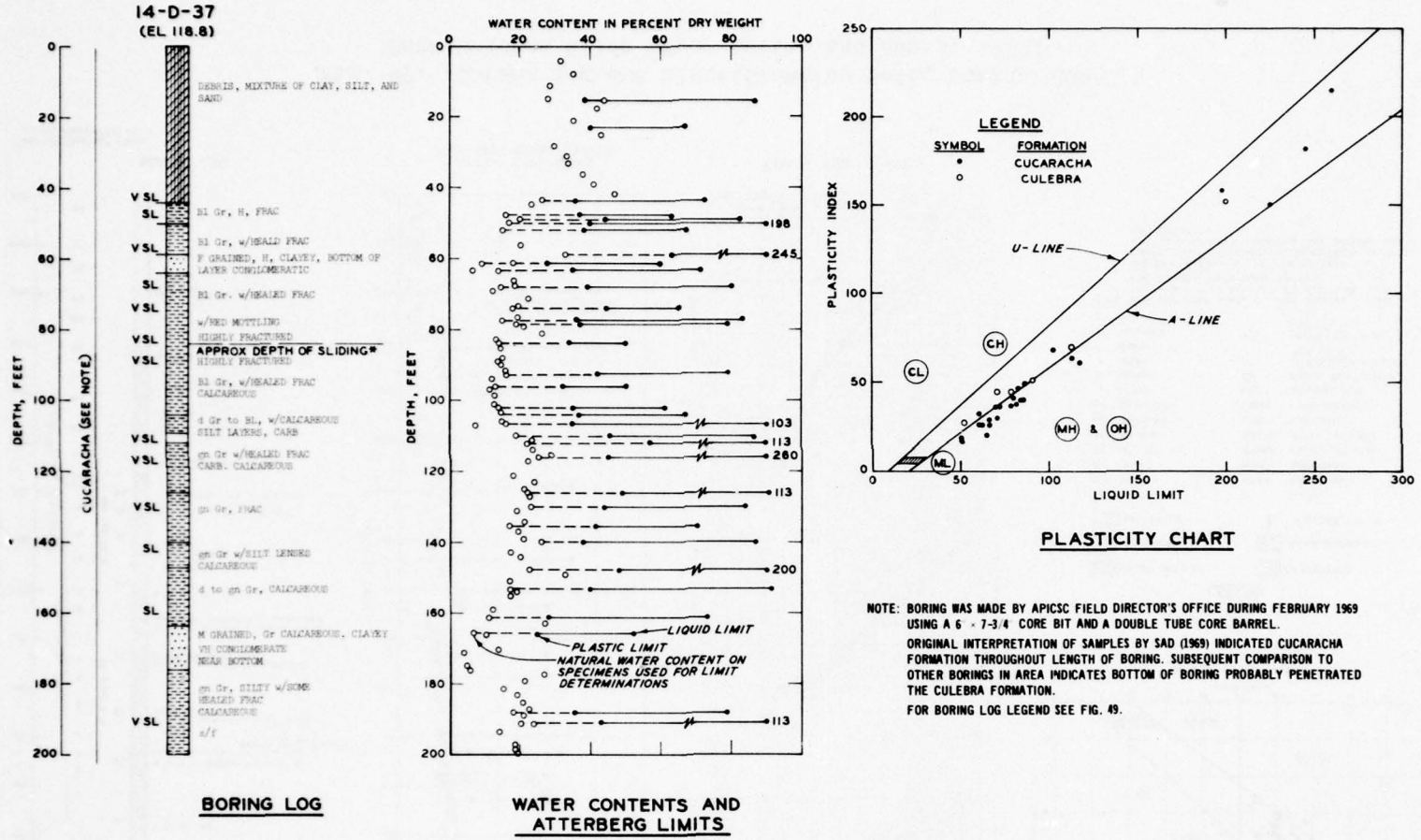

NOTE: BORING WAS MADE BY APICSC FIELD DIRECTOR'S OFFICE DURING FEBRUARY 1969 USING A 6 × 7-3/4 CORE BIT AND A DOUBLE TUBE CORE BARREL.
ORIGINAL INTERPRETATION OF SAMPLES BY SAD (1969) INDICATED CUCARACHA FORMATION THROUGHOUT LENGTH OF BORING. SUBSEQUENT COMPARISON TO OTHER BORINGS IN AREA INDICATES BOTTOM OF BORING PROBABLY PENETRATED THE CULEBRA FORMATION.
FOR BORING LOG LEGEND SEE FIG. 49.

Fig. 48. Boring log and classification data, boring 14-D-37, East Culebra Slide (from SAD, 1969)

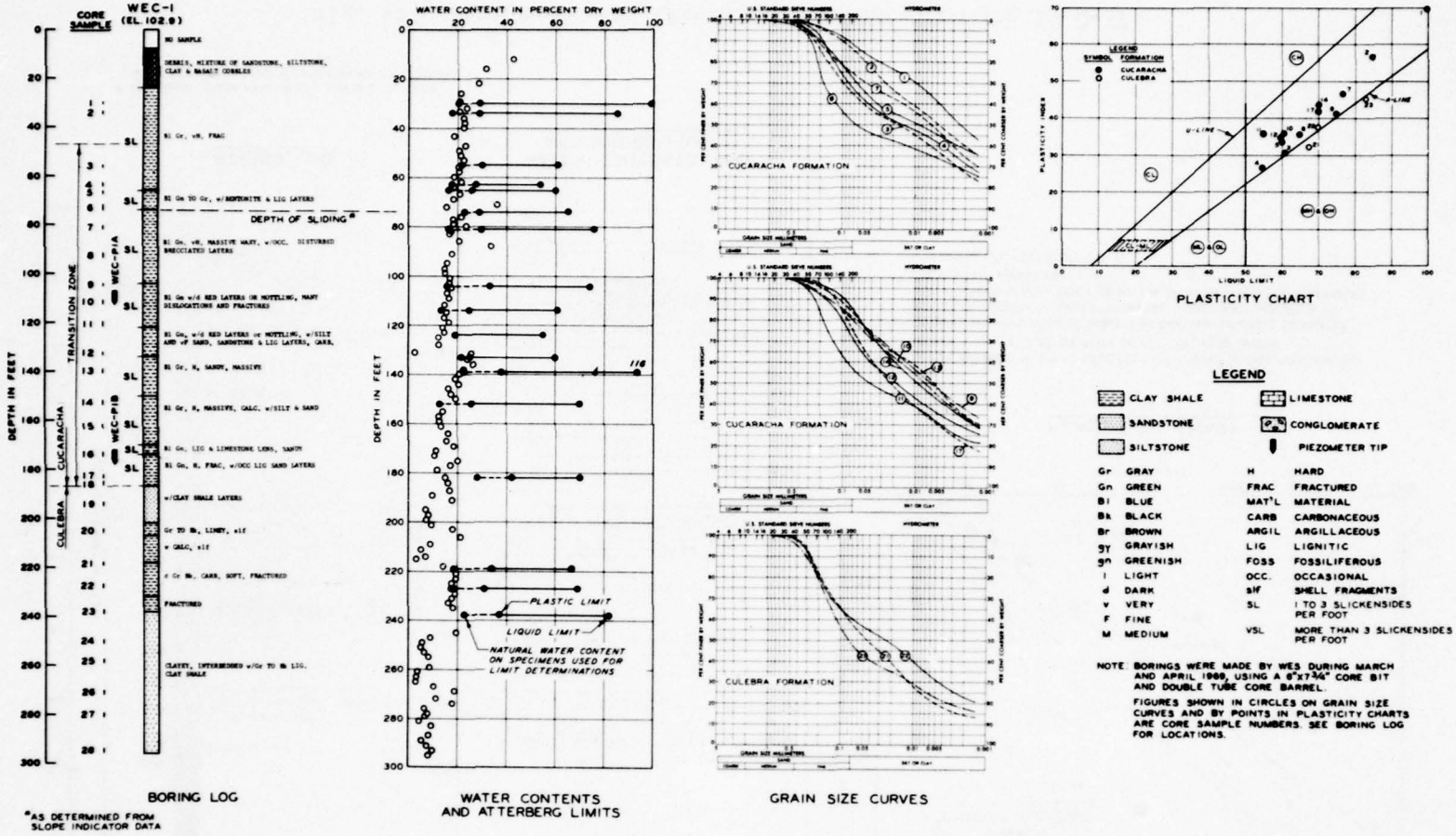

Fig. 49. Boring log and classification data, boring WEC-1, East Culebra Slide (from Lutton and Banks, 1970)

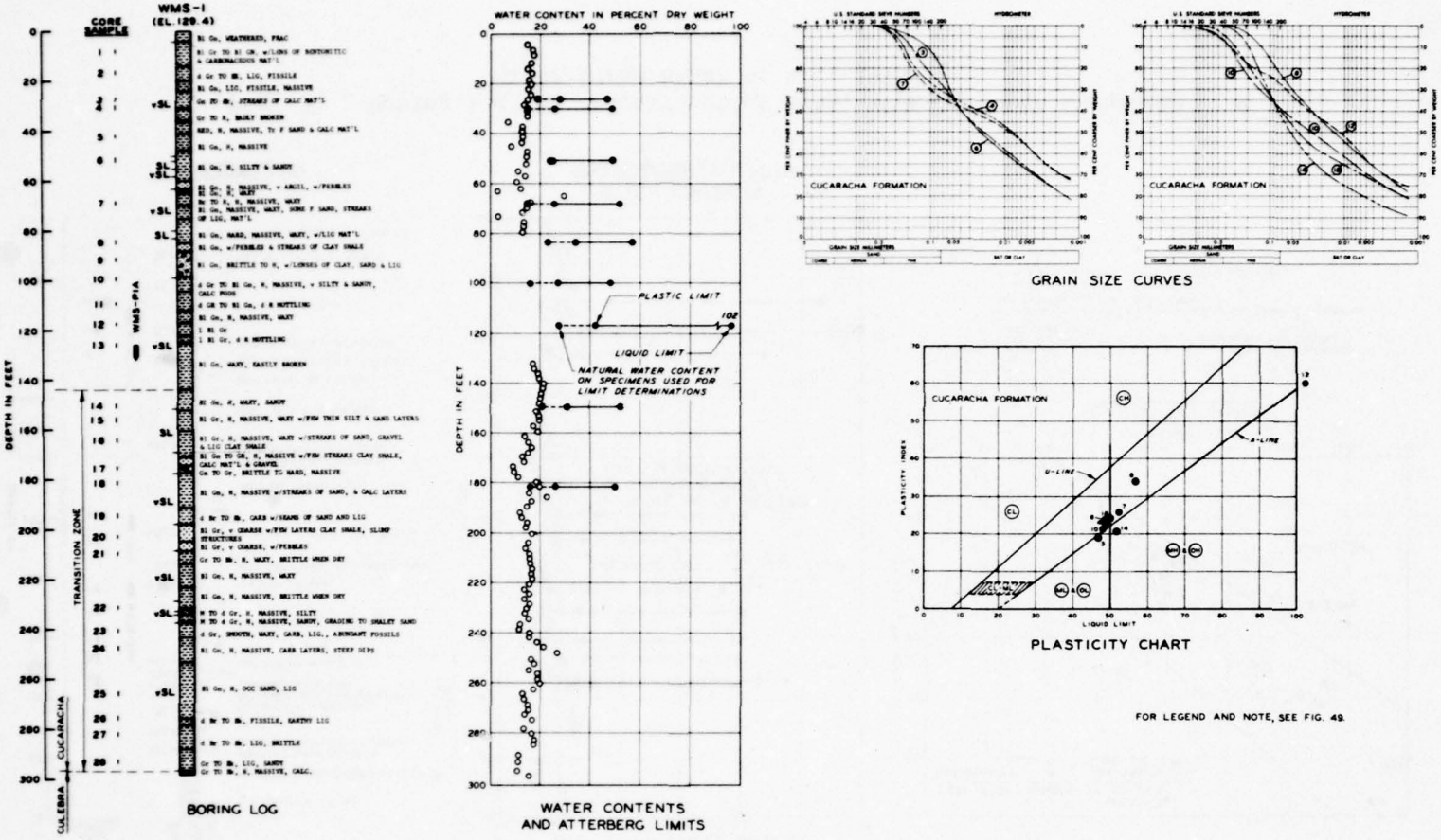

Fig. 50. Boring log and classification data, boring WMS-1, Model Slope (from Lutton and Banks, 1970)

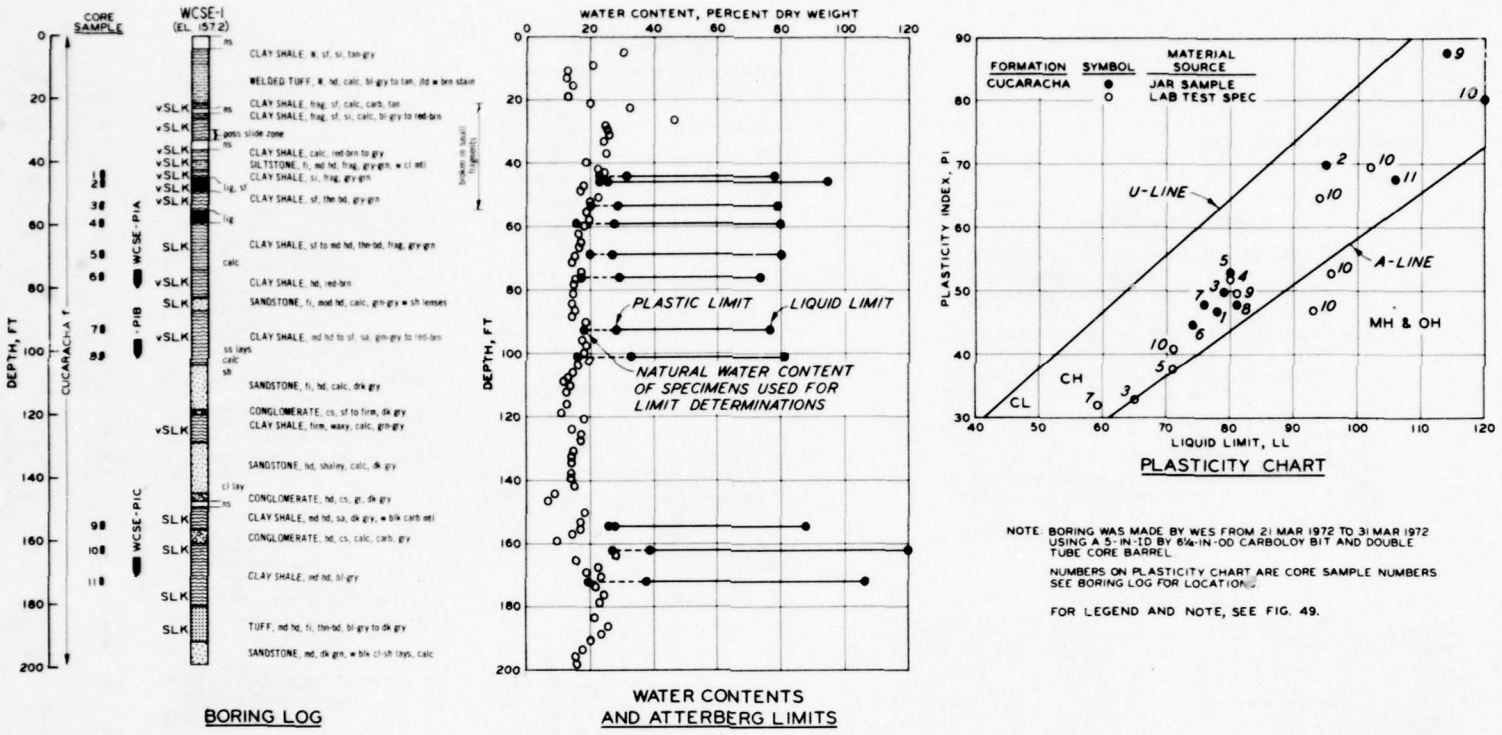

NOTE: BORING WAS MADE BY WES FROM 21 MAR 1972 TO 31 MAR 1972 USING A 5-IN-ID BY 6¼-IN-OD CARBOLOY BIT AND DOUBLE TUBE CORE BARREL.

NUMBERS ON PLASTICITY CHART ARE CORE SAMPLE NUMBERS. SEE BORING LOG FOR LOCATIONS.

FOR LEGEND AND NOTE, SEE FIG. 49.

Fig. 51. Boring log and classification data, WCSE-1, South Cucaracha Slide (from Banks et al., 1975)

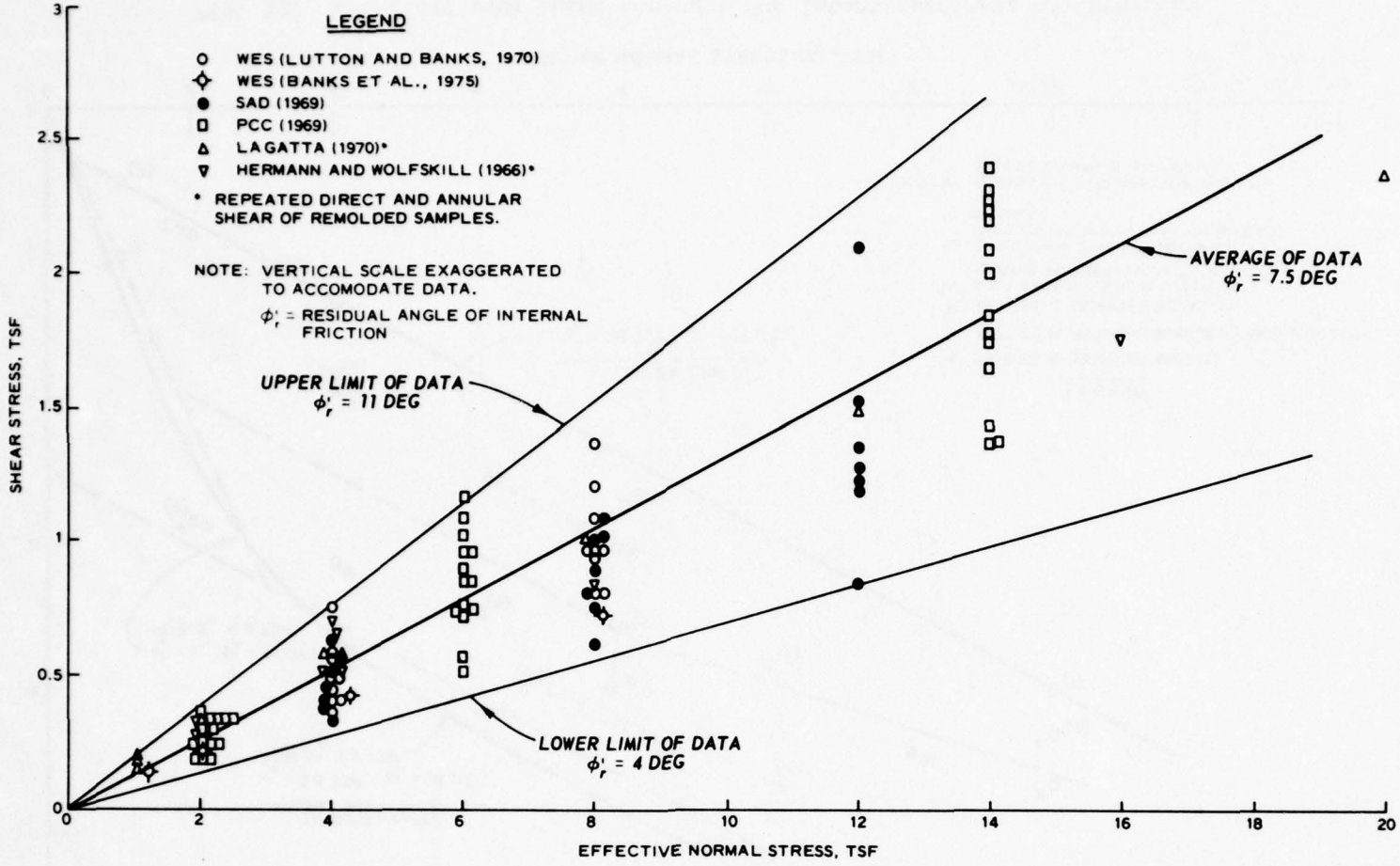

Fig. 52. Drained residual shear strength (from Banks et al., 1975)

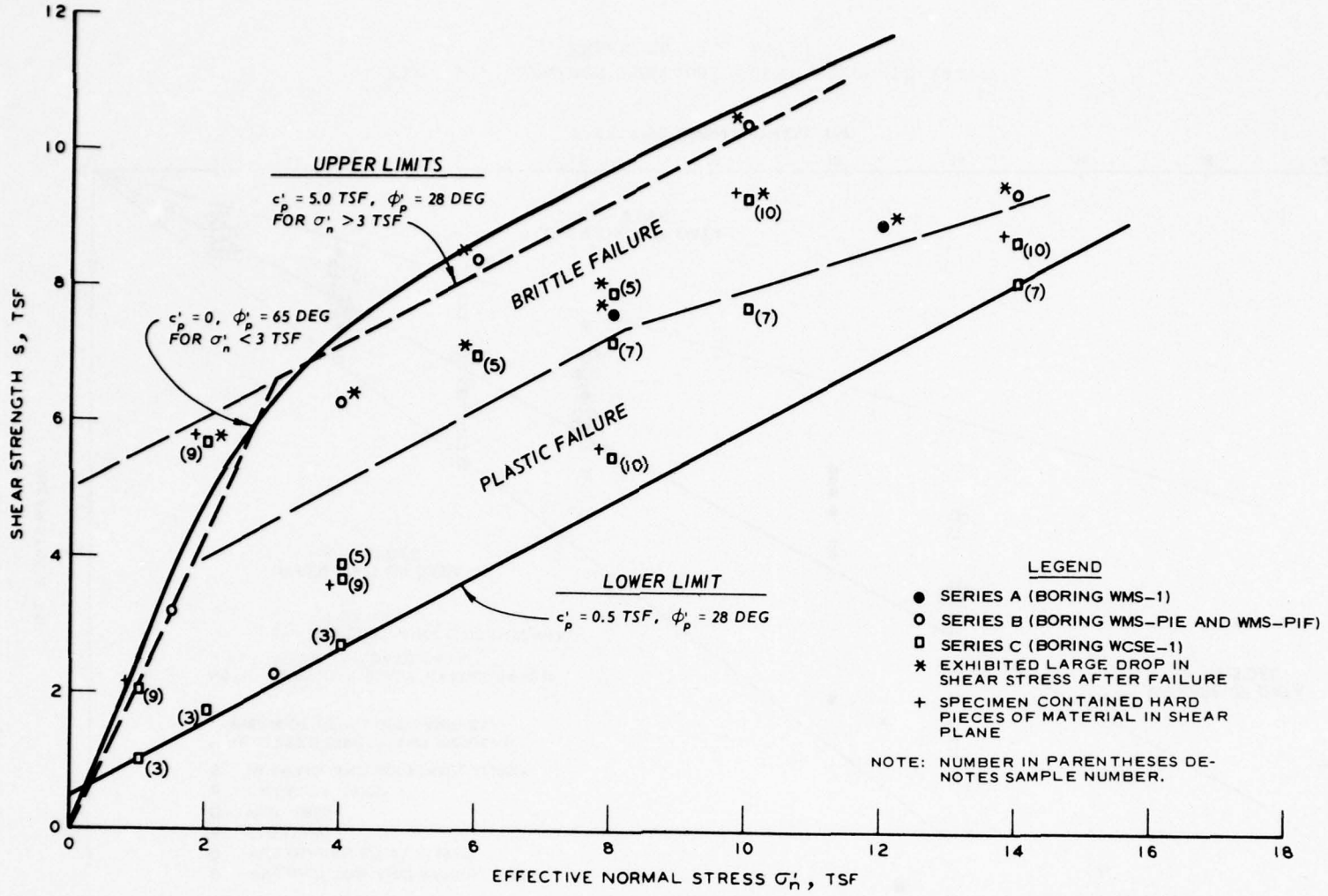

Fig. 53. Effective peak shear strength for intact specimens of Cucaracha clay shale (from Banks et al., 1975)

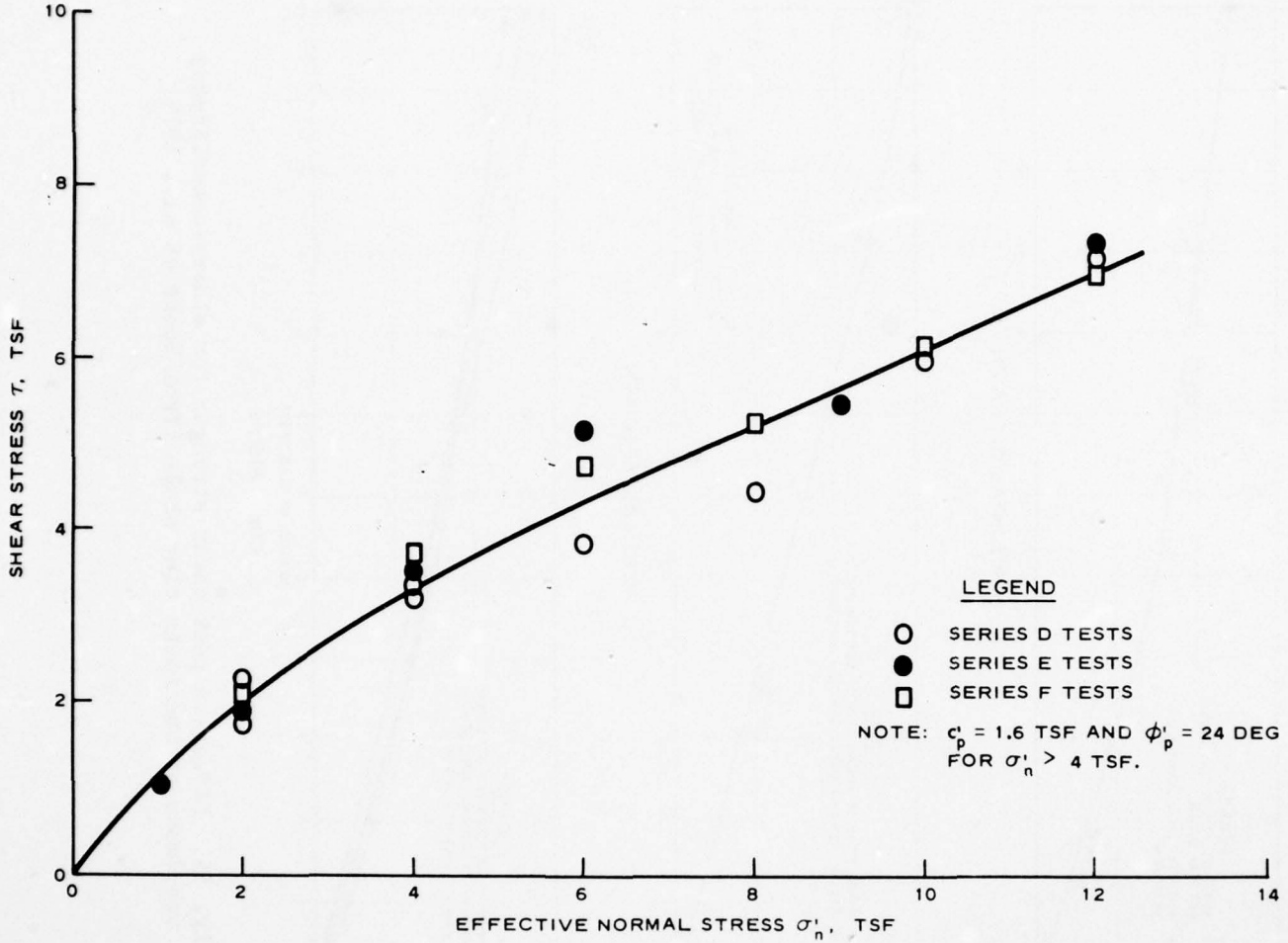

Fig. 54. Effective peak shear strength for slickensided specimens of Cucaracha clay shale (from Banks et al., 1975)

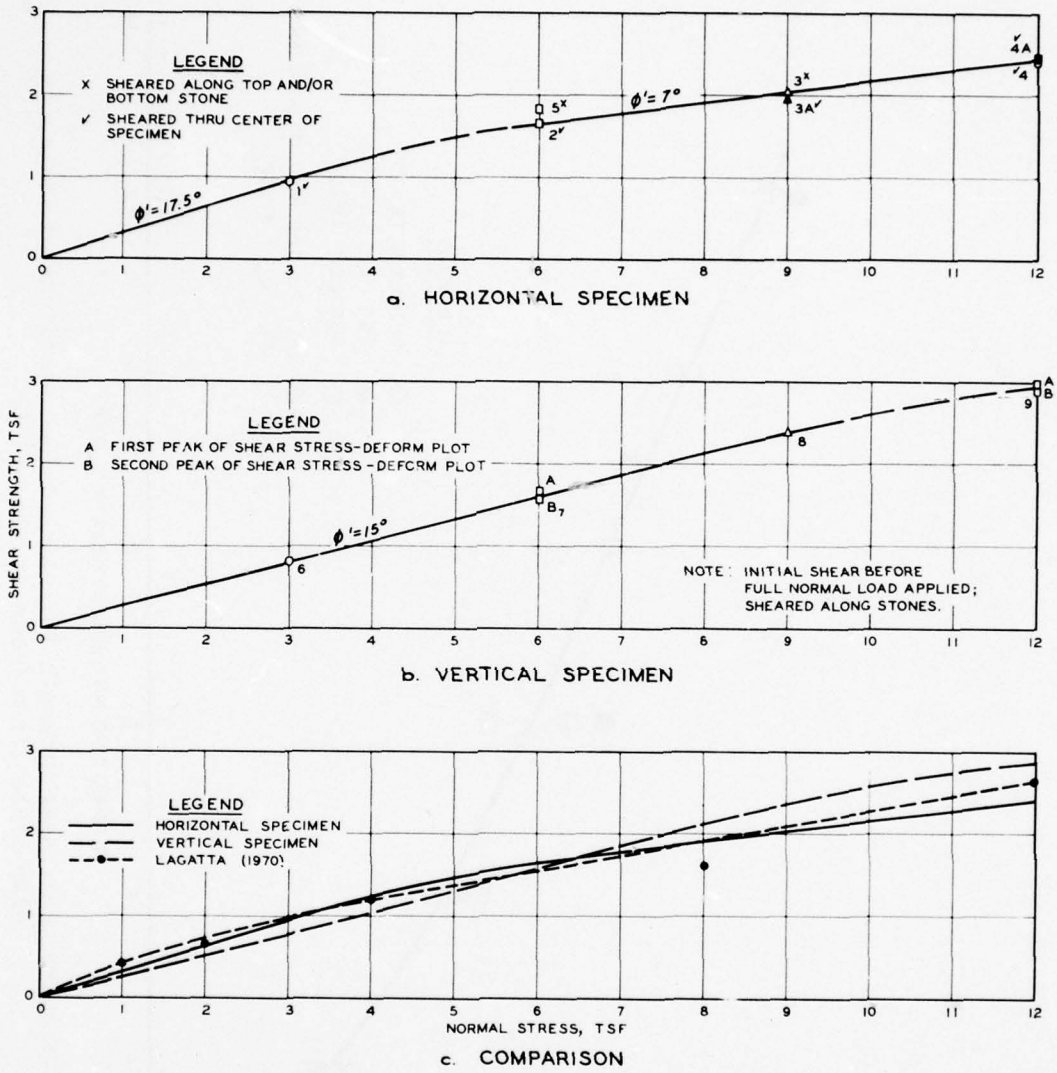

Fig. 55. Effective peak shear strength for slurry-consolidated specimens of Cucaracha clay shale (from Banks et al., 1975)

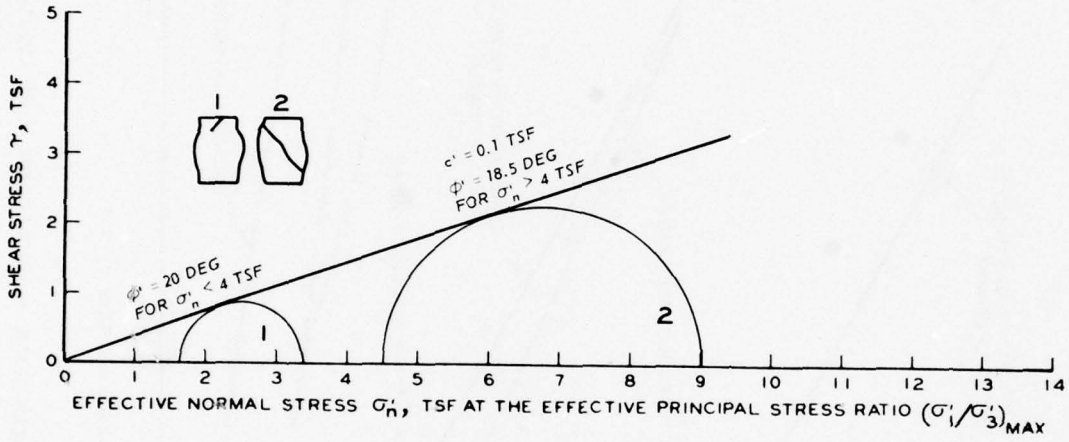

Fig. 56. Results of $\bar{R}$ triaxial compression tests for slurry-consolidated specimens of Cucaracha clay shale (from Banks et al., 1975)

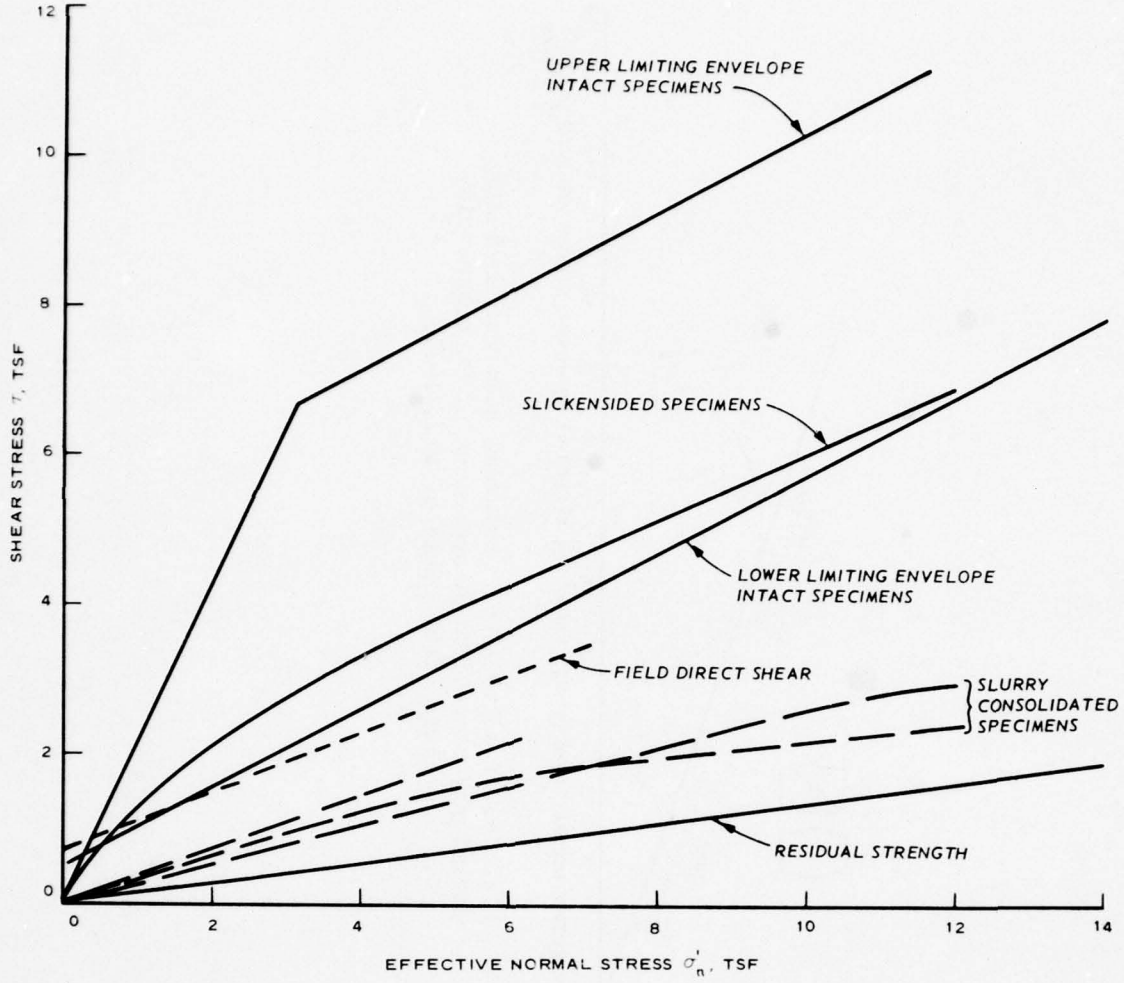

Fig. 57. Summary of strength data - Cucaracha clay shale

CHAPTER V: ANALYSES OF INITIAL BREAKS AT THE LOCATION OF THE EAST CULEBRA SLIDE

Stability analyses are routinely made to assess the ability of slopes to resist failure (as judged from computed factors of safety) after the stratigraphy, groundwater conditions, and physical properties have been determined and, in particular, applicable strength parameters have been established for the conditions of the analyses (e.g., short-term or long-term conditions). Such analyses of embankment slopes of compacted clay and cut slopes in normally consolidated or slightly overconsolidated clays are generally considered adequate for routine engineering practice. However, analyses made for slopes containing strata of highly overconsolidated clays and clay shales have generally propuced poor results. While the poor results have been attributed to the inability to properly assess various factors that contribute to failure of slopes in highly overconsolidated clays and clay shales (for example, Table 1), much attention has been focused on the inability to obtain and test representative samples of the weaker material contained within the slope and to perform significant tests on these samples. As a consequence, many investigators have analyzed failed slopes in highly overconsolidated clays and clay shales (i.e., for situations where, by definition, the factor of safety is equal to unity) to determine field strengths for conditions operative at the time of failure. Strengths so calculated or inferred can be compared with laboratory/field test results for a better understanding of proper test methods or used directly in subsequent analyses of unfailed slopes to determine their relative factors of safety.

Previous discussions have indicated that the East Culebra Slide developed as a consequence of several independent slides or breaks. In this chapter, those individual breaks are analyzed; the emphasis is on determining effective strength operative at times of failure. Once the strength is established, comparisons can be made with laboratory/field tests on samples from the Cucaracha clay shale strata.

Method of Analyses

While studies of methods of analyses (e.g., Wright, 1969) have shown that computed factors of safety for a given slope depend to some extent upon the chosen method, no detailed investigations were conducted as part of this thesis to determine the influence of the chosen method of analysis upon the calculated strength parameters. Rather, a single limit equilibrium method--a wedge analysis--was used.

A wedge analysis is considered suitable for this study since the description of the breaks (Chapter II) suggested that the failed masses were bounded by surfaces closely approximating a series of planes. The method actually employed follows that described by Morgenstern (1968). Figure 58 schematically shows failure masses comprised of both two wedges and three wedges; forces acting on the wedges and force ploygons are illustrated in the figure. In the following discussion of the method of analysis, the break is characterized by two wedges--an active or driving wedge and a resistive wedge. Some descriptions (mostly of breaks that occurred sometime after the initial breaks) speak of mounds of material at the toe of the slope suggesting the existence of a neutral block whose base was lower than the toe of the slope and, in turn, the existence of a passive wedge. In that case, the method of analysis employed can be extended to a three-plane geometry.

The resolution of forces shown in Fig. 58 follows recommendations made by Morgenstern (1968); that is, the total force acting between the active wedge and the resistive wedge is separated into two force components - first, a horizontal force, U_{a-n}, caused by the water pressure and second, an inclined effective force, E'_{a-n}. For a given slope configuration, stratigraphy, and groundwater condition, a trial failure surface can be established. For both wedges, then, the magnitudes and directions of the weight vectors, W_a and W_n, the interwedge water pressure force vector, U_{a-n}, and the water pressure force vectors acting along the bases of the wedges, U_a and U_n, can be calculated from the geometry of the problem. The method was formulated to determine the minimum factor of safety of a slope for known values of effective strength parameters c'_a and ϕ'_a acting along the base of the

active wedge and c'_n and ϕ'_n acting along the base of the resistive wedge. For that intended use, the direction of E'_{a-n} can be assumed and the factor of safety varied until a value is found that requires the magnitude of E'_{a-n} to be equal for both the active and resistive wedges. Other inclinations can be assumed and the process repeated until the smallest factor of safety is determined for the trial failure surface. Other failure surfaces are then assumed and the process repeated until the minimum factor of safety for the slope is determined.

The wedge method requires some modification when used, as in this thesis, to determine the shear strength acting at the time of failure. The factor of safety is known to be unity, but there exist four unknown shear strength parameters, c'_a, ϕ'_a, and c'_n, ϕ'_n. As a first assumption for all analyses, the effective cohesive components c'_a and c'_n were assumed to be zero. Thus the remaining two strength components ϕ'_a and ϕ'_n, rather than being effective angles of internal friction, become angles of obliquity α_a and α_n, respectively (Taylor, 1948). At this stage, two variables remain as unknowns. One approach to assess the two unknown angles of obliquity would be, as described above, to assume the direction of E'_{a-n} and assume a value of one of the angles of obliquity to determine the magnitude of E'_{a-n}; once determined, the resulting value of the other angle of obliquity can be found. Various directions of E'_{a-n} can be assumed until the largest value of the resulting angle of obliquity is determined. While sets of assumed angles of obliquity and largest resulting angles of obliquity can be generated by the analyses, a judgment, independent of the analyses, must be made to determine the most likely values acting at the time of failure. Several cross sections were analyzed using the above approach to investigate the nature of the solutions obtained. The detailed results obtained for the section at sta 1944+60 (1777+00) are described subsequently; the results are similar to those obtained for other sections. In particular, for apparently reasonable values of $\alpha_n = 24$ deg, the force E'_{a-n} was tensile to cause extremely large values of α_a. The existence of vertical cracks before the breaks occurred gives reasons, as subsequently discussed, to assume the magnitude of E'_{a-n} to be zero. With this condition or assumption placed on the analyses, the two

unknown angles of obliquity are no longer dependent upon each other and largest angles of obliquity can be independently determined along the bases of the active wedge and the resistive wedge. Several failure surfaces for each slope can be investigated to determine the maximum angles of obliquity.

Assumptions Involved in the Analyses

Slope geometry at time of individual break

Construction-day cross sections were maintained by PCC officials at 50-ft stations (for example, Fig. 6). Those records were originally used to compute excavation yardage but were reexamined in Chapter II to determine the dates and extent of individual breaks (Table 2). It was assumed that the geometry of the slope immediately prior to the individual break can be represented by the cross section depicted on those records. Furthermore, reviews of cross-sectional geometry were made to determine which cross sections through the break adequately represented the average cross-sectional geometry of the break; in cases of breaks extending over long distances or of radically varying slope geometry within the break, more than one cross section was analyzed.

Stratigraphy

Once cross sections existing before failure were established for each break, the elevations of marker beds (e.g., the welded tuff or the underlying conglomeratic sandstone layer) were established from information obtained during construction (Figs. 19 and 20). The composite stratigraphic column (Fig. 22) was superimposed on the cross sections to indicate the stratigraphic sequence of materials. The apparent dip of individual strata was assumed to be toward the Canal at approximately 4 deg. Individual strata were assumed to be continuous except where intersected by mapped major faults (Fig. 18).

Groundwater

Earlier descriptions indicated that the lowest position of the groundwater surface was at the base of the weathered soil or more particularly at the location of the change in color of the material from

yellow and red (i.e., oxidation zone) to greenish-gray. Seasonal variations caused the groundwater surface to be higher. Further study of water levels in open borings suggested that during the rainy season (May-December), the groundwater surface rises to near coincidence with the ground surface. Since the dates of the breaks (Table 2) occurred during or near the end of the rainy season, in all probability the groundwater surface was high and, for purposes of analysis, the groundwater surface was assumed to be coincident with the ground surface. Study of piezometer data indicated that the groundwater is communicative with the sandstone/siltstone strata by way of cracks, fissures, and joints. Thus for the analysis, full hydrostatic water pressures with respect to the overlying groundwater surface were assumed in all sandstone/siltstone strata. It was further assumed that seepage was parallel to bedding or approximately horizontal.

Unit weights

Earlier discussions indicated the average dry unit weight of the clay shale was about 110 pcf. Figure 49 shows that the water content varies, but in general, averages about 15 percent. On that basis, the saturated unit weight would be about 125 pcf. The geologic cross sections (Fig. 19) show materials other than clay shale existed at the site of the East Culebra Slide. Many of these strata are identified as sandstones, siltstones, conglomerates, etc., that would exhibit saturated unit weights in excess of 125 pcf. To account for this increased unit weight, an average saturated unit weight of 135 pcf was assumed for all materials.

Location of failure surfaces

Base of resistive wedge. This assumption is more fully described for each section in subsequent discussions. However, in general, the base of the resistive wedge was assumed to be parallel to bedding and to lie at (or, in some cases, near) the interface between the stronger, more permeable sandstone/siltstone strata and the weaker clay shale strata. By this assumption the water pressure acting on the base of the resistive wedge would be fully hydrostatic and the calculated strength parameters applicable to the clay shale materials.

Base of active wedge. This assumption is more fully described for

each section in subsequent discussions. However, in general, the base of the active wedge was assumed to be inclined from its intersection with the base of the resistive wedge to a location on the ground surface indicated by construction-day cross sections as the limit of breaks.

Approach of Analyses

Several sections were analyzed in detail to determine the nature of the wedge method employed and to establish a consistent approach to the analysis of each break. For the sake of brevity, only the detailed analysis of one section will be described here.

Discussion in Chapter II indicated that a break occurred in May 1908 between sta 1944+10 and 1947+60 (1776+50 and 1780+00) (Table 2). The center of the break was located at sta 1945+85 (1778+25). A review of cross sections through the break showed the section at sta 1946+10 (1778+50) best represented the break. Analysis of that section is presented subsequently. A second section at sta 1944+60 (1777+00) was chosen to illustrate in detail the approach taken to analyze each break.

Construction-day cross sections (PCC Vault File 288 and illustrated in Fig. 6) were reviewed to determine the slope geometry existing prior to the break (Fig. 59). Further interpretations were made to indicate the material excavated immediately before the break (January 1908) and material removed as a result of the break (Fig 59). For reference purposes, the planned Canal cross section (Fig. 7), original ground surface (Fig. 17), and thickness of French dumps (Fig. 18) are shown in Fig. 59. From the cross section, it would appear that the bulk of material removed because of the break was behind and above the construction bench at about el +172 ft. It would appear further that evidence of the May 1908 break at this section was manifested more by the lowering of the planned (and constructed) berm at el +245 ft than by encroachment of excavation upon the planned slope between el +172 and +245 ft. A review of information contained in Fig. 18 showed two faults crossing the section. Faults A3 and B are plotted in their respective positions in Fig. 59. Since the faults were apparently well removed from the area of the break, no estimate of the offset of strata across

the faults was necessary to indicate the stratigraphy in the volume of material affected by the break. Figure 20 indicates that the welded tuff marker bed daylighted to the south of sta 1944+60 (1777+00); therefore the stratigraphy depicted on the cross section was established with respect to the conglomeratic sandstone stratum at about el +100 ft.

While a conscientious attempt was made to assemble the available data into their proper spatial positions, it should be remembered that the data were taken from several sources. In turn the data were collected by different techniques with varying degrees of precision. It appears from the information shown in Fig. 59 that the base of the material removed because of the break was located entirely within clay shales. The closest interface between clay shale and sandstone layers is located about 8 ft below the bottom of the removed material. This interface, while not coinciding with the bottom of the removed materials, will be used as a trial failure surface. Also, it is apparent from Fig. 59 that after the break, a slope, quite steep (approximately 5V on 4H) and of moderate height (approximately 60 ft), was left in place. While it is impossible to determine the extent of the break from the records, it is assumed that the break encompassed material above the clay shale/sandstone interface and the back of the construction berm at el +245 ft.

In Fig. 60, results are shown of an investigation to determine the magnitude of the effective interwedge force E'_{a-n} and the resulting required angle of obliquity α_a acting on the base of the active wedge for the condition that the factor of safety equals unity. The trial failure surfaces were assumed to consist of two planes, one entering the slope at points marked A....E and one daylighting at points marked A'....G'. In this illustration of the method, the effective interwedge force E'_{a-n} was assumed to be inclined at an angle $\delta = 10$ deg (Fig. 58) with a trial angle of obliquity acting along the base of the resistive wedge, α_n, assumed to be 24 deg. (The angle of obliquity was chosen to equal the effective friction angle obtained from drained direct shear tests on slickensided specimens, Fig. 54.) The base of the resistive wedge was assumed to be inclined toward the Canal parallel to the bedding (about 4 deg); the base of the active wedge was assumed

to be inclined, as shown, at 45 deg above the horizontal.

The results of the investigation showed that for entrance points well beyond the crest of the slope (e.g., points A, B, C, D) the required angle of obliquity α_a increased as the assumed base of the resistive wedge was placed deeper. Only when surfaces entered the slope near the crest (and approximating the volume of material removed as a result of the break (e.g., surfaces E-E' or E-F')) did the required angle of obliquity α_a reach maximum values. Since only trial values of the angle of obliquity acting along the base of the resistive wedge (α_n = 24 deg) and inclination of the effective interwedge force (δ = 10 deg) were being used, the actual value of the required angle of obliquity acting along the base of the active wedge was not finally established. However, since reasonable assumptions had been made for α_n and δ, the maximum value of $\alpha_a \approx 82$ deg was surprisingly and unrealistically high. A clue to the calculated high value was given by an examination of the magnitude of E'_{a-n} (Fig. 60). As shown for many of the trial surfaces, tensile forces were required for equilibrium. This observation suggested that the trial value of $\alpha_n \approx 24$ deg was too low to maintain stability of the resistive wedge, causing E'_{a-n} to be tensile and in turn requiring a large value of α_a to maintain limit equilibrium. Before the obvious exercise of performing further analyses with $\alpha_n > 24$ deg was considered, the influence of the assumed angle of the base of the active wedge and the angle of inclination for effective interwedge force was investigated.

Figure 61 shows the results of one set of calculations with the base of the active wedge inclined at 30 deg above the horizontal. The required angles of obliquity did decrease to more realistic values (maximum $\alpha_a \approx 60$ deg) for failure surfaces approximating the base of the material removed as a result of the break, but, significantly, many of the solutions still indicated a tensile effective interwedge force. Figure 62 shows the results of one set of calculations in which the angle δ of the interwedge force was varied. For the single trial failure surface shown (surface E-F', Fig. 60), a variation in the angle δ from zero to 50 deg caused the required value of α_a to decrease from about 81.5 deg to about 79 deg.

Since varying the base angle of the active wedge and the angle of inclination of the effective interwedge force did not produce significant improvement in the results, the more obvious solution of increasing the value of the angle of obliquity acting on the base of the resistive wedge, α_n, was considered. It is noted that the large calculated values of the required angle of obliquity acting along the active wedge, α_a, and the tensile values of the effective interwedge force were caused by the relatively large water pressure forces being used in the problem. No attempt was made to investigate the influence of lowering the groundwater surface since a review of information presented in Chapter III indicated that a groundwater surface approximately equal in elevation to the ground surface was a realistic boundary condition.

In considering analyses with $\alpha_n > 24$ deg, an immediate dilemma arose--what value to assume for α_n. One solution would be to find the value of α_n such that $\alpha_n = \alpha_a$. In that case an average angle of obliquity mobilized along the entire failure surface would be determined. Such a solution was not desired. A second solution would be to assume values of α_n equal to effective friction angles determined from laboratory tests (as was the initial trial value of $\alpha_n = \phi'_p = 24$ deg). However, such an approach would have required, firstly, an assumption as to whether the laboratory tests on slickensided specimens or on intact specimens more nearly represented the field strength at the time of failure and, secondly, in view of the curved strength envelopes (Fig. 57), a trial-and-error solution to determine appropriate strength parameters. Moreover, an assumption of a value of α_n was not attractive since the basic purpose of the analysis was to determine the field strength operative at the time of the breaks. A solution to the dilemma was to assume that the magnitude of the effective interwedge force was equal to zero. The logic of this assumption follows from the description of the early stages of a break. In Chapter II, the appearance of vertical or near vertical cracks was described in the early stages of a break. As a crack was present, the effective interwedge force would decrease to zero, but with continued rainfall, the crack would fill with water to create a large horizontal water pressure force. Thus the way the breaks were visualized and used in the analyses was to assume a

vertical, water-filled crack and to calculate the required angle of obliquity acting along the base of the resistive wedge. Several trial locations of the crack and base of the resistive wedge were selected until the location was found that gave the maximum value of α_n. Once this location was determined, the inclination of the base of the active wedge was varied from the bottom of the crack until a surface indicating the maximum value of α_a was determined or α_a was calculated for the failure surface that intersected the ground surface at a position in close agreement with the material removed as a result of the break.

Figure 63 indicates the results of the first step in determining the critical location of the vertical crack and base of the resistive wedge. Several trial failure surfaces, daylighting at A'....G', were established. The failure surfaces were assumed to lie parallel to bedding and to constitute the base of the resistive wedge. Symbols on Fig. 63 indicate the assumed intersection of the failure surface and the water-filled vertical crack. The calculated value of α_n required for a factor of safety equal to unity is shown beside each intersection. The maximum value of α_n found was 48.8 deg at the intersection of a vertical crack and bedding surface daylighting at point F'. Actually a larger value of α_n was determined (along surface C'). This value was judged to be caused by local slope geometry and not representative of the overall stability problem being analyzed. For the section at sta 1944+60 (1777+00), as well as at other sections, such local values were ignored.

Once the location of the base of the resistive wedge and the vertical crack was located, then several active wedges were analyzed to determine the angle of obliquity α_a acting along the base to produce the maximum required value. Figure 64 illustrates the results of one such analysis. As shown for the trial surfaces, no maximum value was produced. Rather, the required value increased as the base angle increased. It is significant to note that the angle of obliquity varied only slightly for surfaces that entered the slope at the approximate location of material removed because of the break. The investigation showed that the solution would not produce a maximum value of the required value of α_a and that judgment will have to be applied.

In Figure 65, a trail failure surface daylighting at point F' and ending with a vertical crack is shown. Along this surface, the required value of α_n was calculated to be 48.8 deg. A surface along the base of the active wedge and entering the slope at the back of the original bench at approximate el +245 ft (surface A) was judged to best fit the problem. For that surface a required α_a of 60.3 deg was determined. When the results of the analysis were reviewed, it was seen that a second pair of planes could be established that closely approximated the bulk of the material removed as a result of the break (surface B). Analysis of that geometry indicated the required value of α_n was 41.0 deg; the corresponding required value of α_a was 71.5 deg. Required angles of obliquity, α_n and α_a, determined for both surfaces are shown in Table 8.

Once the angles of obliquity were determined, the force polygons used in the analyses (Fig. 58) were resolved to determine the value of the effective normal forces, N_n and N_a, acting on the bases of resistive and active wedges, respectively. These forces as well as others used in the final determination are shown on the insert in Fig. 65. The effective normal forces were divided by the lengths of the bases of the respective wedges to determine the average effective normal stresses acting along the bases of the wedges shown in Fig. 65. Forces, base lengths, and stresses so determined are shown in Table 8.

The determination of values of the average effective normal stresses and required angles of obliquity will allow the results of the analyses of individual sections to be plotted on a $\tau - \sigma'$ diagram for comparison with strength envelopes established from laboratory tests.

The discussion above outlines the reasoning used to perform the analysis of the section at sta 1944+60 (1777+00) at the time of the initial break. The procedure will be applied to the other sections to be analyzed; any variation will be described in the discussion of the analysis of the section. The basic procedure will be to:

a. Establish the cross section existing prior to the break.
b. Establish the extent of material removed because of the break.
c. Establish the location (elevation) of marker beds.
d. Establish the location (and offsets of strata, if appropriate) of major faults.

e. Establish the relative stratigraphic sequence.

f. Establish trial failure surfaces (base of resistive wedge). The surface must:
   (1) Daylight the surface of the slope.
   (2) Parallel the bedding.
   (3) Preferably, lie at the interface between weaker clay shale strata and stronger sandstone/siltstone strata.
   (4) End at the location of an assumed water-filled vertical crack.

g. Determine the location of the trial failure surface (base of resistive wedge) that requires the maximum value of an angle of obliquity α_n .

h. Determine the location of the base of the active wedge that best approximates the extent of material removed because of the break and determine the corresponding required value of an angle of obliquity α_a .

i. Review the analysis to see whether another surface equally approximates the material removed because of the break. If such a surface exists, determine the corresponding values of α_n and α_a .

j. Calculate the effective normal forces and average effective normal stresses acting along the failure surfaces.

Analysis of Initial Break - Sta 1938+10 to 1940+60

Data shown in Table 2 indicate that a break occurred in December 1909 between sta 1938+10 and 1940+60 (1770+50 and 1773+00). The center of the break was located at sta 1939+35 (1771+75). A review of the cross sections through the break indicated that the section at sta 1939+60 (1772+00) adequately represented the break. The cross section at sta 1939+60 (1772+00) (Fig. 66) indicates the original ground surface, thickness of French dumps, the prisms of material excavated immediately before the break (June 1909), and the material removed as a result of the break. Descriptions of the break (quoted in Chapter II) indicate the slope broke back about 90 ft, as illustrated by Fig. 66.

The welded tuff marker bed is not located within the section; however, Fig. 20 shows the conglomeratic sandstone stratum to have been present in the section at about el +160 ft along the French center line. Figure 18 shows that fault A3 crosses the section with an offset of strata by about 15 ft (lower to the east). Therefore the stratigraphic sequence of materials (Fig. 22) can be established for the cross section at sta 1939+60 (1772+00), as shown in Fig. 66.

Construction cross sections show that materials were excavated on three different levels following the break (Fig. 67). Although all prisms are labeled in Fig. 67 as being removed as a result of the break, the requirement for excavating the lower two prisms are questionable since they both lie within the planned Canal cross section (Fig. 66). Significantly, the upper prism extended well beyond the planned Canal cross section and was based at the interface between a weaker clay shale stratum and a stronger sandstone stratum. While preference is given to the break being represented only by the upper prism, the following analyses considers failure surfaces involving all the excavated prisms shown in Fig. 67.

Resistive wedges bounded by an assumed vertical water-filled crack with bases parallel to bedding were analyzed to determine the maximum required α_n (Fig. 67). Bases located at interfaces between clay shale and sandstone/siltstone strata approximately intersected the face of the slope near the toe of the materials excavated on the three different levels. As shown, the maximum values of α_n occurred along the interface that intersected the surface at the base of the upper volume of material removed because of the break. While a locally large value of α_n (48.8 deg) was found, a more appropriate value of α_n = 31.2 deg, near the heel of the break was chosen. The base of the active wedge was chosen to coincide with the back of the material removed because of the break. Along that surface (surface A) a value of α_a = 77.3 deg was calculated. A slightly flatter surface (surface B) constructed to enter the slope at the rear of the bench indicate a required α_a = 59.5 deg. Forces used in the final analysis are shown on the insert in Fig. 67. Values of α_n and α_a as well as calculated values of the average effective normal stresses acting along the bases of the failure surfaces are shown in Table 8.

Analysis of Initial Break - Sta 1940+60 to 1944+10

Data shown in Table 2 indicate that a break occurred in January 1909 between sta 1940+60 and 1944+10 (1773+00 and 1776+50). A review of cross-sectional data indicated that a single cross section at sta 1942+60 (1775+00) adequately represented the geometry of the break (Fig. 68). As shown, the break extended behind and above the construction berm at el +168 ft and caused complete removal of the construction berm at el +220 ft. The break occurred after the slope had apparently been made to conform to the planned Canal cross section. Evidently the break occurred after excavation along the face of the slope in May 1908 (Fig. 68). Although Fig. 20 shows the welded tuff marker bed daylighted to the south of sta 1942+60 (1775+00), the stratigraphic sequence of materials could be established with respect to the conglomeratic sandstone layer at about el +100 ft along the location of the French center line. Faults A3 and B are plotted in their respective positions in Fig. 68. Since the faults are well removed from the area of the break, no estimate of the offset of the strata was necessary.

A more detailed view of the cross section at sta 1942+60 (1775+00) is shown in Fig. 69. There it is shown that the material removed because of the break was entirely in a clay shale stratum. The nearest clay shale/sandstone interface was located about 6 ft beneath the base of the removed material. Resistive wedges bounded by an assumed vertical water-filled crack and with bases parallel to bedding were analyzed to determine the maximum required α_n ; Fig. 69 shows the results of those analyses. The maximum value of α_n was obtained on an upper surface. The value was influenced by the local geometry for that trial surface and was discounted in favor of the slightly lower value of $\alpha_n = 56.7$ deg that was required for the surface daylighting at the toe of slope. Values for α_n obtained by analyzing the surface at the interface of the sandstone and clay shale strata were all smaller.

Analysis of the active wedge extending from the base of the resisting wedge to the rear of the volume of material removed because of the break (surface A, Fig. 69) indicated a required value of α_a of 58.4 deg.

A second failure geometry (surface B, Fig. 69) was investigated to

determine required angles of obliquity and average effective normal stresses. This failure geometry was chosen to coincide as closely as possible with the volume of material removed because of the break. Forces used in the final analysis are shown on the insert in Fig. 69. The results of the analysis are shown in Table 8.

Analysis of Initial Break - Sta 1944+10 to 1947+60

Data shown in Table 2 indicated that a break occurred in May 1908 between sta 1944+10 and 1947+60 (1776+50 and 1780+00). The analysis of the section through the break at sta 1944+60 (1777+00) was previously given in detail to illustrate the approach taken for analyses at each section. The results of that analysis are shown in Table 8. The center of the break was located at sta 1945+85 (1778+25). A review of cross sections through the break indicated that the section at sta 1946+10 (1778+50) more nearly represented the geometry of the break (Fig. 70).

As shown in Fig. 70, the material removed because of the break was located behind and above the construction berm at about el +176 ft and extended to the crest of the slope, completely eliminating the construction berm at el +245 ft. Evidently the break occurred after excavation at the toe of the slope in January 1908 (Fig. 70). Figure 20 shows the welded tuff marker bed daylighted at about sta 1946+10 (1778+50). Both the welded tuff marker bed and the underlying conglomeratic sandstone layer (at about el +98 ft) along the French center line (refer to Fig. 20) were used to establish the stratigraphic sequence for the section. Fault B (Fig. 18) was plotted in its proper position on Fig. 70 with the strata shown as being downset to the east.

A more detailed view of the cross section at sta 1946+10 (1778+50) is shown in Fig. 71. There it is shown that the material removed because of the break was entirely in a clay shale stratum. The nearest clay shale/sandstone interface was located about 24 ft below the base of the removed materials; a lignitic clay shale layer was located about 8 ft above the base of the removed material.

Analyses were made of resistive wedges that were bounded by an assumed vertical water-filled crack and that had bases parallel to

bedding. The bases were located at the bottom of the lignitic clay shale stratum, at the bottom of a stratum that daylighted the toe of the material removed because of the break or at the toe of the next lower bench and at the clay shale/sandstone (Fig. 71). The maximum value of α_n (53.3 deg) was found for a surface daylighting at the toe of the material removed because of the break; values of α_n obtained for surfaces located along the clay shale/sandstone interface were considerably smaller.* Analysis of the active wedge extending from the base of the resisting wedge to the rear of the volume of material removed because of the break (surface A, Fig. 71) indicated a required value for α_a of 63.1 deg. A second failure geometry, surface B in Fig. 71, was investigated to determine angles of obliquity and average effective normal stresses. This failure geometry was chosen to correspond as closely as possible with the volume of material removed because of the break. Forces used in the final analysis are shown on the insert in Fig. 71. The results of the analyses are shown in Table 8.

Analysis of Initial Break - Sta 1947+60 to 1949+60

Data shown in Table 2 indicate that a break occurred in January 1909 between sta 1947+60 and 1949+60 (1780+00 and 1782+00). A single cross section located at sta 1948+60 (1781+00) was established to represent the conditions of the break (Fig. 72).

As shown in Fig. 72, the material removed because of the break was located behind and above a construction berm at about el +176 ft and extended to the crest of the slope. As a result of the break, the elevation of planned construction berm at et +295 ft was lowered to about

---

* Figure 70 shows that the interface of the clay shale/sandstone strata daylighted the excavated slope at a location well removed from the material removed because of the break. For the purposes of analyses, it was assumed that a vertical excavated face existed at a distance of about 240 ft from the present center line (Fig. 71). With the assumption of the vertical face, an analysis using the two wedges could be performed. If the base of the actual break were to be located along the clay shale/sandstone interface, the proper analysis would have to be made using the three-wedge formulation (Fig. 58). However, in that case, the passive wedge would offer resistance and cause the value of α_n on the neutral block to be even smaller than those values shown in Fig. 71.

el +266 ft. Evidently the break occurred after excavation at the toe and along the face of the slope in June 1908 (Fig. 72). Figure 20 shows that the welded tuff marker bed at sta 1948+60 (1781+00) was located at about el +200 ft along the French center line from which the stratigraphic sequence of material near the toe of the excavation could be established. Figure 18 indicates fault B crossed the section. The proper location of the fault with the strata downset to the east is shown in Fig. 72.

A more detailed view of the cross section is shown in Fig. 73. There it is shown that the material removed because of the break was entirely within a clay shale stratum. The nearest clay shale/sandstone interface was located about 40 ft below the base of the removed material; a lignitic clay shale layer was located at the approximate location of the base of the removed material.

Resistive wedges bounded by an assumed vertical water-filled crack and with bases parallel to bedding located at interfaces between clay shale and lignitic strata and between clay shale stratum and the welded tuff marker bed were analyzed (Fig. 73). The maximum calculated required value of α_n was 43.3 deg; a slightly smaller value $\alpha_n = 41.1$ deg located for a surface along the interface between a clay shale stratum and the welded tuff marker bed was considered more appropriate. A failure surface entering the slope to the rear of the material removed because of the break and joining the resisting wedge at the assumed vertical crack was assumed to bound the active wedge (Fig. 73). Along that surface, a required value of $\alpha_a = 39.4$ deg was calculated. These required values of α_n and α_a as well as calculated values of the average effective normal stresses acting along the base of the resisting and active wedges are shown in Table 8. Forces used in the final analyses are shown on the insert in Fig. 73.

Analysis of Initial Break - Sta 1949+60 to 1956+60

Data shown in Table 2 indicate that a break occurred in January 1912 between sta 1949+60 and 1956+60 (1782+00 and 1789+00). This break was perhaps the most dramatic of all those involved in the development of the East Culebra Slide. The break was the last to develop and is the one

most synonymous with the Slide. Historical analyses (e.g., Binger, 1948) have, as discussed in Chapters I and II, concentrated on this final break. Three cross sections were established to represent the conditions of the break. The sections are located at 1950+10 (1782+50), 1952+60 (1785+00), and 1955+10 (1787+50). These stations have been used in previous analyses of the East Culebra Slide (PCC, 1947; Binger, 1948; Lutton and Banks, 1970).

The slope geometry for the cross section at sta 1950+10 (1782+50) is shown in Fig. 74. There the large amount of material removed because of the break is shown. Since this break occurred late in the construction of the Canal, following numerous other breaks and slides, efforts were under way to remove material beyond the actual break to lighten the load on the slope. This practice was discussed in Chapter II. The exact extent of the break can only be established by referring to Canal Record (14 February 1912) where it was stated that cracks had opened along the old French 90-metre level (i.e., el +295 ft) and had carried the berm away. Excavation preceding the break was concentrated at the toe, March 1911 (Fig. 74). The welded tuff marker bed was present at the section, and the stratigraphic sequence of materials was established with respect to the bed. Fault B crosses the mass of material involved in the break; strata are shown to be offset by about 15 ft because of the fault (Fig. 74).

A more detailed view of the cross section of sta 1950+10 (1782+50) is shown in Fig. 75. There it is shown that in addition to the material removed because of the break (either directly or at positions behind the break to lighten the load), excavation was conducted at the toe to deepen the cut. Whether this material was removed because of the break or as a result of continued efforts to deepen the Canal cut is not known. In any event, trial resistive wedges were analyzed for deep failure surfaces. From the general configuration of the volume of material removed, a three-plane solution (Fig. 58) is indicated. However, before such a solution was attempted, the two-plane solution was used with the assumption of a vertical slope existing at a distance of 132 ft from the present center line (Fig. 75). The effect of a passive wedge would be to reduce the required angle of obliquity produced under the assumption of a vertical slope. Thus, it was desired to determine whether such an

assumption would produce larger required values of α_n than on other surfaces. As shown in Fig. 75, such was not the case. The largest required angle of obliquity was $\alpha_n = 46.7$ deg for a failure surface located along a contact between clay shale strata and a lignitic strata. A lower surface, depicted as surface A in Fig. 75, was chosen because the surface more nearly encompassed the break and daylighted more nearly to the toe of the break. Along this surface, the required value of α_n was 45.9 deg. The required value of α_a along a failure surface entering the slope behind the failed bench at the old French level of 90 metres (el +295 ft) was 69.1 deg. These values as well as the average effective normal stresses on the failure planes are shown in Table 8. Forces used in the final analyses are shown on the insert in Fig. 75.

A second cross section was established at sta 1952+60 (1785+00) (Fig. 76). The material removed in an attempt to reduce the overburden beyond the break is obvious. Excavation preceding the break (November 1911) is illustrated in Fig. 76. A detailed view of the cross section is shown in Fig. 77. There the maximum value of α_n required to produce a factor of safety of unity is shown to be 50.8 deg and occurs for a surface along the interface between sandstone/clay shale strata; the surface daylights the slope at the approximate position of the toe of the material removed because of the break. The corresponding value of the required α_a was 57.4 deg. Since a review of the section indicated a plausible failure surface (surface B, Fig. 77) in which the base of the resistive wedge coincided with the interface between sandstone/clay shale strata at a lower elevation, an additional analysis was made for the section at 1952+60 (1785+00). For that surface, an angle of obliquity $\alpha_n = 49.8$ deg and a related $\alpha_a = 60.1$ deg were determined. These values as well as the average effective normal stresses are presented in Table 8. Forces used in the final analyses are shown on the insert in Fig. 77.

A third cross section was established at sta 1955+10 (1787+50) (Fig. 78). Excavation preceding the break (November 1911) is also illustrated in Fig. 78. Again the material removed to reduce the overburden beyond the break is obvious (compare Fig. 78 with Fig. 76). A detailed view of the cross section is shown in Fig. 79. There the maximum value of α_n required to produce a factor of safety of unity is shown to be 57.6 deg; the maximum value of α_n was discounted, and

instead a slightly smaller value (α_n = 56.0 deg) was used to accommodate a sliding surface along the interface between the sandstone/clay shale strata. The interface daylights the surface slightly below the material removed because of the break. The corresponding value of the required α_a was 51.4 deg. As shown in Fig. 79, the amount of material removed because of the break was not as much at the section at sta 1955+10 (1787+50) as for other stations within the break (compare Fig. 79 with Figs. 75 and 77). As a consequence, the inclination of the base of the active wedge was determined by extending the base to the rear of the bench at el +295 ft. Such a positioning of the active wedge was based on descriptions of the break and on the analyses of sections at sta 1950+10 (1782+50) (Fig. 75) and at sta 1952+60 (1785+00) (Fig. 77). No alternate surfaces to closely approximate the removed material were attempted. The required angles of obliquity and average effective normal stresses for the section at sta 1955+10 (1787+50) are shown in Table 8. Forces used in the final analysis are shown on the insert in Fig. 79.

Analysis of Initial Break - Sta 1956+60 to 1960+60

Data shown in Table 2 indicate that a break occurred between September and November 1908 between sta 1956+60 and 1960+60 (1789+00 and 1793+00). A single cross section at sta 1958+60 (1791+00) was established to represent the conditions of the break (Fig. 80). As shown, the break extended behind and above the construction berm at about el +176 ft. At the time of the break, the excavation face was in approximate agreement with the planned Canal cross section. The break evidently occurred following excavation at the toe of the slope, in August 1908, as shown in Fig. 80. Figure 20 shows the welded tuff marker bed to dip in the vicinity of sta 1958+60 (1791+00) and to lie at approximately el +200 ft along the French center line; the figure also indicates some contortion of bedding at the same station. Thus, while the stratigraphy depicted in Fig. 80 was prepared with respect to the general sequence of materials (Fig. 22), that depiction should be considered approximate. Figure 18 indicates no major faults intersected the section in the vicinity of sta 1958+60 (1791+00).

Resistive wedges bounded by an assumed vertical water-filled crack

and with bases parallel to bedding that was located to intercept the slope at the base of the material that was removed because of the break and along the clay shale/lignitic shale interface were analyzed (Fig. 81). The largest required value of α_n (63.3 deg) was discounted in favor of α_n = 59.0 deg for a surface lying along the base of the material removed because of the break (surface A). The corresponding value of α_a was 64.9 deg. A failure geometry that closely approximated the entire volume of material removed because of the break (surface B, Fig. 81) was analyzed. For that surface, required values of α_n = 40.3 deg and α_a = 71.1 deg were determined. These values as well as values of the average effective normal stresses acting on the bases of the failure surfaces are shown in Table 8. Forces used in the final analysis are shown on the insert in Fig. 81.

Discussion of Results of Analyses

The evolution of the East Culebra Slide has occurred from early in construction activities (i.e., as early as 1885 in weathered surficial materials, Lutton et al. (1975)) to the present. The involvement of subsurface materials started about May 1908; by January 1912 the slope along the entire length of the Slide had experienced initial breaks. Construction cross sections have shown that the breaks occurred generally after materials were excavated at the toe of the slope, although in some instances, the excavation was additionally along the face of the cut. In general, the volume of materials excavated prior to the break was small in comparison with the volume of material removed because of the break.

As shown in the tabulation below, the breaks did not occur immediately upon excavation but usually after a period of one to ten months.

Section Station	Date of Preceding Excavation*	Date of Break	Elapsed Time, months
1939+60 (1772+00)	Jun 1909 (T)	Dec 1909	6
1942+60 (1775+00)	May 1908 (T & F)	Jan 1909	8
1944+60 (1777+00)	Jan 1908 (T)	May 1908	4

(Continued)

* (T) = excavation at toe of cut face.
(T & F) = excavation at toe and along face of cut.

Section Station	Date of Preceding Excavation	Date of Break	Elapsed Time, months
1946+10 (1778+50)	Jan 1908 (T & F)	May 1908	4
1948+60 (1781+00)	Jun 1908 (T & F)	Jan 1909	7
1950+10 (1782+50)	Mar 1911 (T)	Jan 1912	10
1952+60 (1785+00)	Nov 1911 (T)	Jan 1912	2
1955+10 (1787+50)	Nov 1911 (T)	Jan 1912	2
1958+60 (1791+00)	Aug 1908 (T & F)	Sep-Nov 1912	1

A review of the results of analyses indicates that within the accuracy of the assembled cross-sectional and stratigraphic data, weak layers of lignitic shales or interfaces between clay shale and sandstone/siltstone strata or a clay shale stratum and the welded tuff marker bed daylighted the cut face at or near the base of the material removed because of the break. This review serves to illustrate the important stratigraphic control on the development of the initial breaks. In general, the review indicated that the breaks did not develop as a result of excavation deepening the cut face and in the process causing the weak beds to daylight the face. Rather the excavation generally was along some previously established berm to cause, in effect, a loss of buttressing material at the toe. Since the volume of excavated material was small in comparison with the volume of material removed because of the break, any stability analysis made to assess the influence of the excavated volume of material would reflect only small, even if perceptible, decreases in computed factors of safety. The influence of the excavated volume of material was to prevent expansion of the toe, and the ensuing open vertical cracks that gave groundwater ready access to the slide mass.

Further review of the analyses indicated that the intersection of the vertical water-filled crack and the bedding plane that by calculations showed the maximum required angle of obliquity, α_n, generally occurred short distances from the face of the slope. In most cases, the geometry of the cut face controlled the critical location of the intersection. The maximum required value generally occurred under or slightly behind the crest of a prominent bench above or within the material removed because of the break. Because of this geometric control, most of

the resisting wedges had short base lengths. In the development of the break, however, just as the loss of material through excavation at the toe provided the opportunity for lateral displacement of the resisting wedge, so did the displacement of the resisting wedge provide the opportunity for the active wedge to develop.

By far the most important results of the analyses are in the nature of the strengths required for limit equilibrium of the initial breaks. The results of the previously discussed analyses were collected in Table 8. There required values of angles of obliquity acting along the bases of the resistive wedges, α_n, and the active wedges, α_a, were shown; in addition, the average effective normal stresses acting on the bases of the resistive wedges, σ'_n, and the active wedges, σ'_a, are tabulated. These results can be plotted on $\tau - \sigma'$ plots to indicate the comparison of calculated field strengths operating at the time of the initial breaks with strengths determined from laboratory or field shear tests.

Figure 82 shows the results of the analyses of the resistive wedge displayed on $\tau - \sigma'_n$ plots. Since only data points are shown for the resistive wedge (i.e., α_n, σ'_n) the relationships are applicable to strengths along bedding. The strength envelopes developed in Chapter IV for the Cucaracha clay shales are superimposed on Fig. 82. The data points shown in Fig. 82 (from Table 8) are not without scatter but show a well-established trend whether collected from analyses of surface A or surface B (see previous discussions of analyses of individual breaks). Envelopes such as for residual strength or the effective strength of slurry consolidated specimens indicate inadequate shear strength to have resisted failure. The data points are within the range of values determined from drained direct shear tests on intact specimens but do not approximate the two limiting strength envelopes from such tests. The data points show best agreement with the envelope derived from laboratory drained direct shear tests on slickensided specimens of Cucaracha clay shale material. The importance of this observation is discussed in Chapter VI.

Figure 83 shows results of analysis on the active wedges (i.e., α_a, σ'_a) displayed on $\tau - \sigma'_a$ plots. As such, the results are for

strengths across bedding. The strength envelopes developed in Chapter IV for the Cucaracha clay shales are superimposed on Fig. 83. The range in average effective normal stresses, σ_a, was small for the active wedges; all data points fall in a small area through which several strength envelopes pass. Therefore, the agreement of data with a single strength envelope is not as readily apparent as with agreement indicated above for failure along bedding. Nevertheless, the trend in data shows reasonable agreement with the upper strength envelope from drained direct shear tests on intact specimens. The importance of this observation is discussed in Chapter VI.

Table 8. Results of Stability Analyses, East Culebra Slide

Station	Surface	Resistive Wedge* α_n deg	N_n tons	L_n ft	σ'_n tsf	Active Wedge* α_a deg	N_a tons	L_a ft	σ'_a tsf
1939+60 (1772+00)	A	31.9	64.8	75	0.86	65.9	9.4	54	0.17
	B	31.9	64.8	75	0.86	56.4	17.2	59	0.29
1942+60 (1775+00)	A	56.0	26.2	39	0.67	64.8	12.7	61	0.21
	B	44.6	1.9	11	0.17	75.8	9.4	81	0.12
1944+60 (1777+00)	A	49.2	54.5	64	0.85	60.2	38.4	91	0.42
	B	40.5	21.1	40	0.53	78.8	14.3	96	0.15
1946+10 (1778+50)	A	53.5	8.6	25	0.34	63.2	47.1	159	0.30
	B	49.4	41.6	50	0.83	58.4	54.2	145	0.37
1948+60 (1781+00)	A	41.0	70.4	65	1.08	39.3	159.0	263	0.60
1950+10 (1782+50)	A	45.4	490.1	203	2.41	67.7	81.1	178	0.46
1952+60 (1785+00)	A	51.9	309.8	114	2.72	56.9	145.1	179	0.81
	B	49.9	421.1	224	1.88	62.0	128.3	191	0.67
1955+10 (1787+50)	A	56.9	179.6	105	1.71	49.9	157.1	165	0.95
1958+60 (1791+00)	A	61.5	21.3	26	0.83	65.2	82.6	188	0.44
	B	39.3	117.9	73	1.62	72.2	80.1	246	0.33

* α_n, α_a = required angle of obliquity, resistive and active wedges, respectively.

N_n, N_a = effective normal force acting on base of resistive and active wedges, respectively.

L_n, L_a = length of base of resistive and active wedges, respectively.

σ'_n, σ'_a = average effective normal stresses acting on base of resistive and active wedges, respectively.

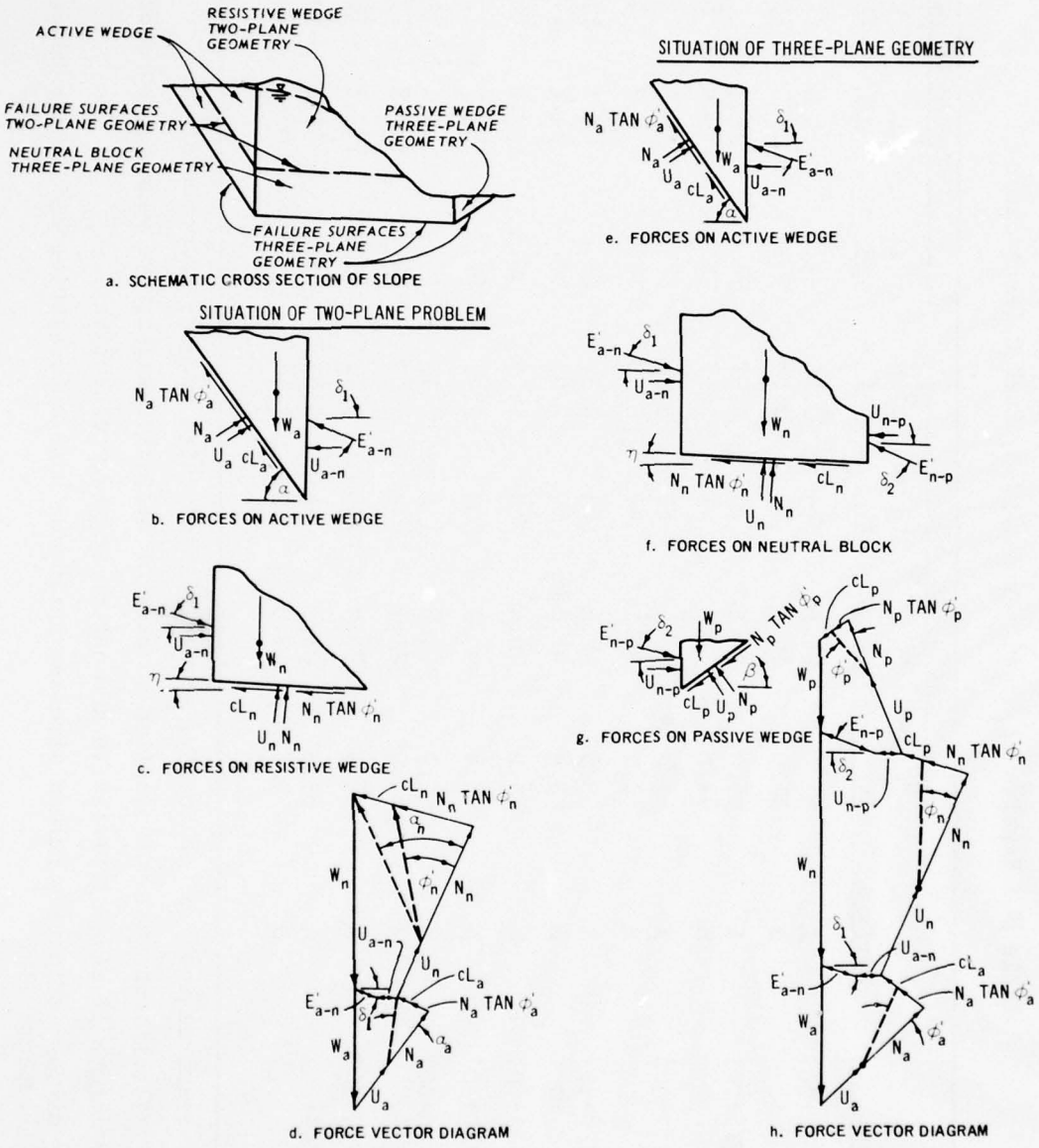

Fig. 58. Method of analyses for initial breaks

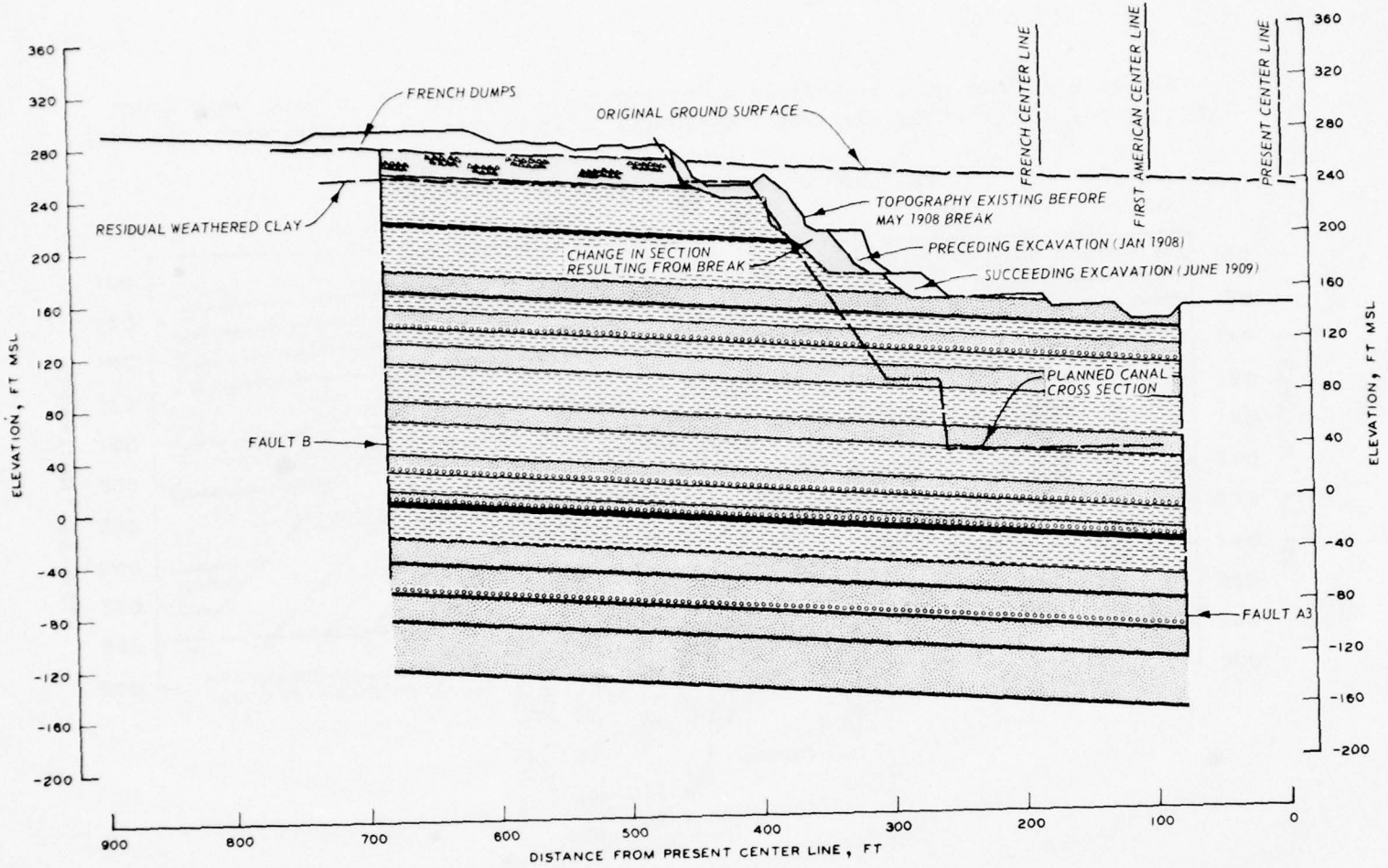

Fig. 59. Conditions surrounding the May 1908 break at sta 1944+60 (1777+00)

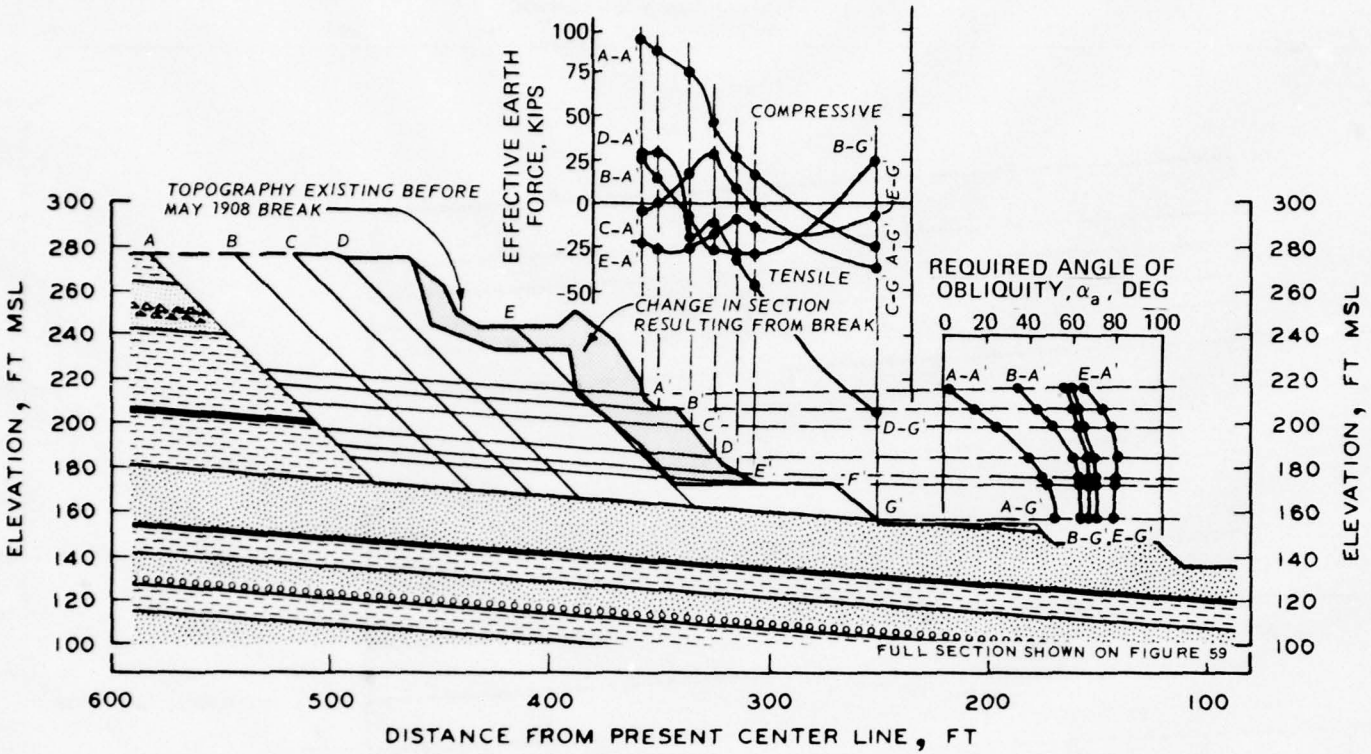

Fig. 60. Investigation of magnitude of effective interwedge force E'_{a-n} for initial break (May 1908) at sta 1944+60 (1777+00) (α_n = 24 deg; δ = 10 deg; α = 45 deg)

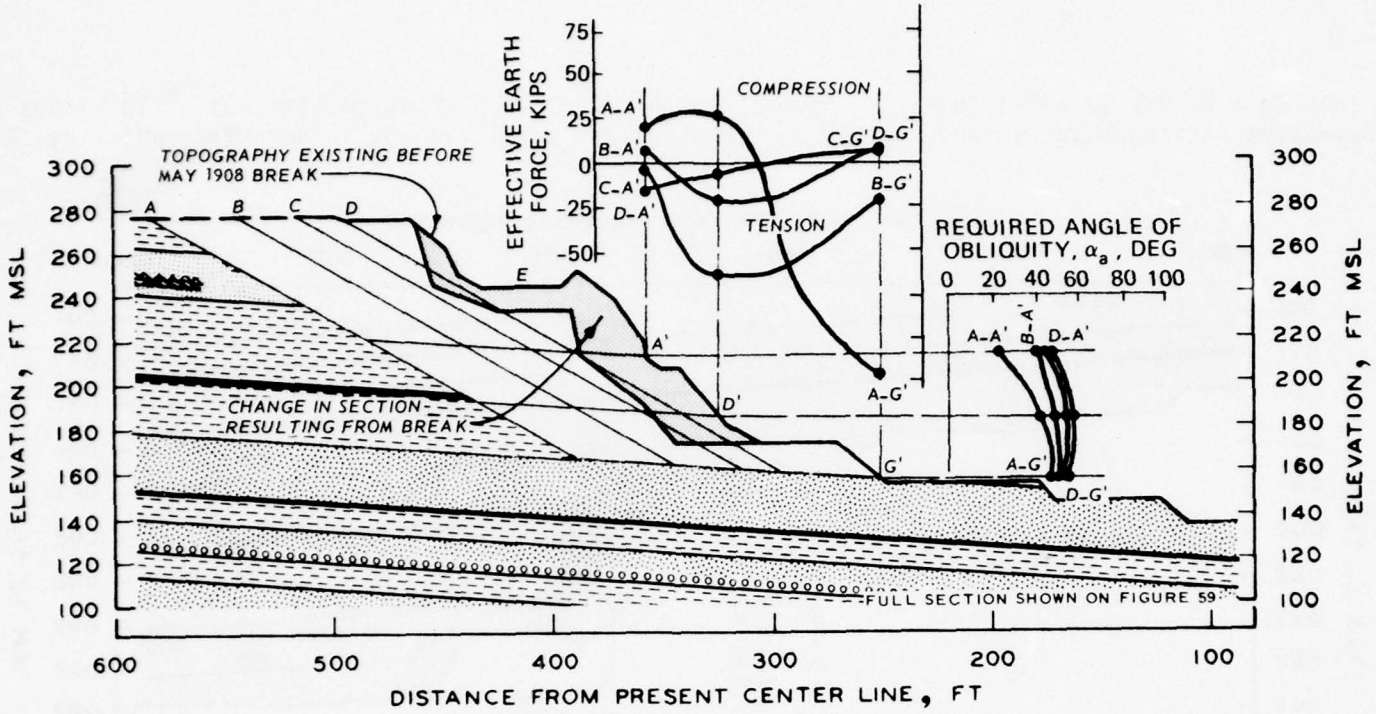

Fig. 61. Investigation of magnitude of effective interwedge force E'_{a-n} for initial break (May 1908) at sta 1944+60 (1777+00) (α_n = 24 deg; δ = 10 deg; α = 30 deg)

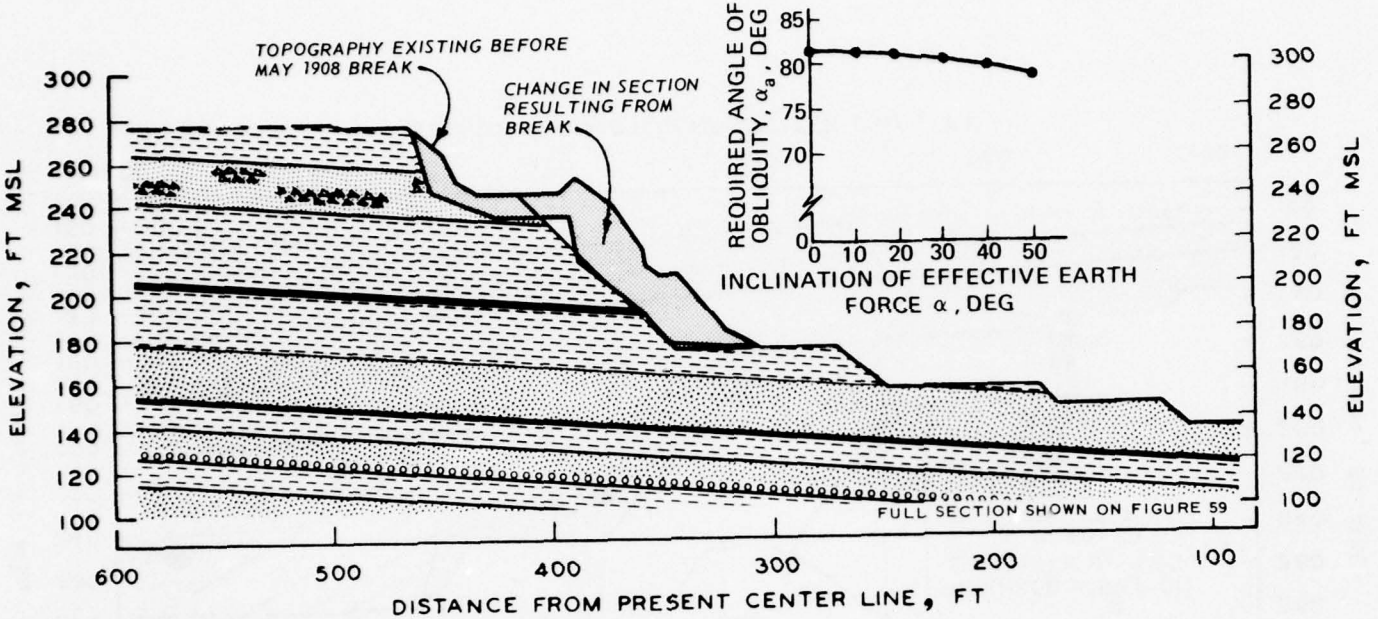

Fig. 62. Investigation of the effect of varying angle of inclination (δ) of effective interwedge force E'_{a-n} for initial break (May 1908) at sta 1944+60 (1777+00) (α_n = 24 deg; α = 45 deg)

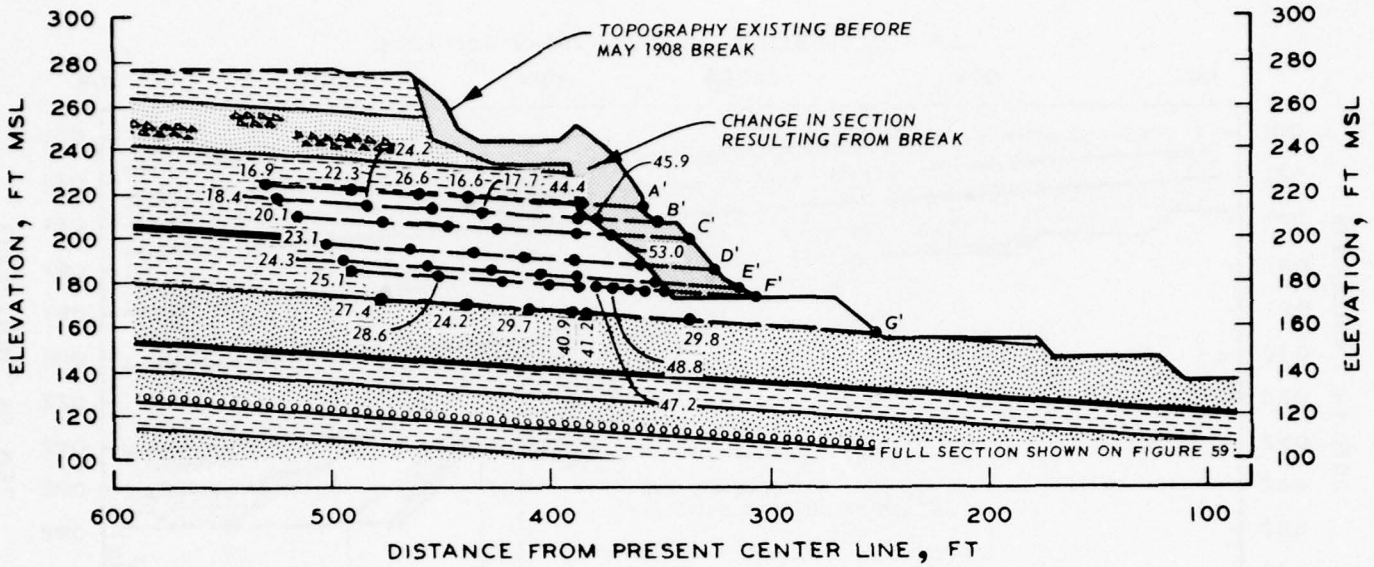

Fig. 63. Investigation to determine required angle of obliquity, α_n, assuming vertical water-fill cracks intersecting bedding planes for initial break (May 1908) at sta 1944+60 (1777+00)

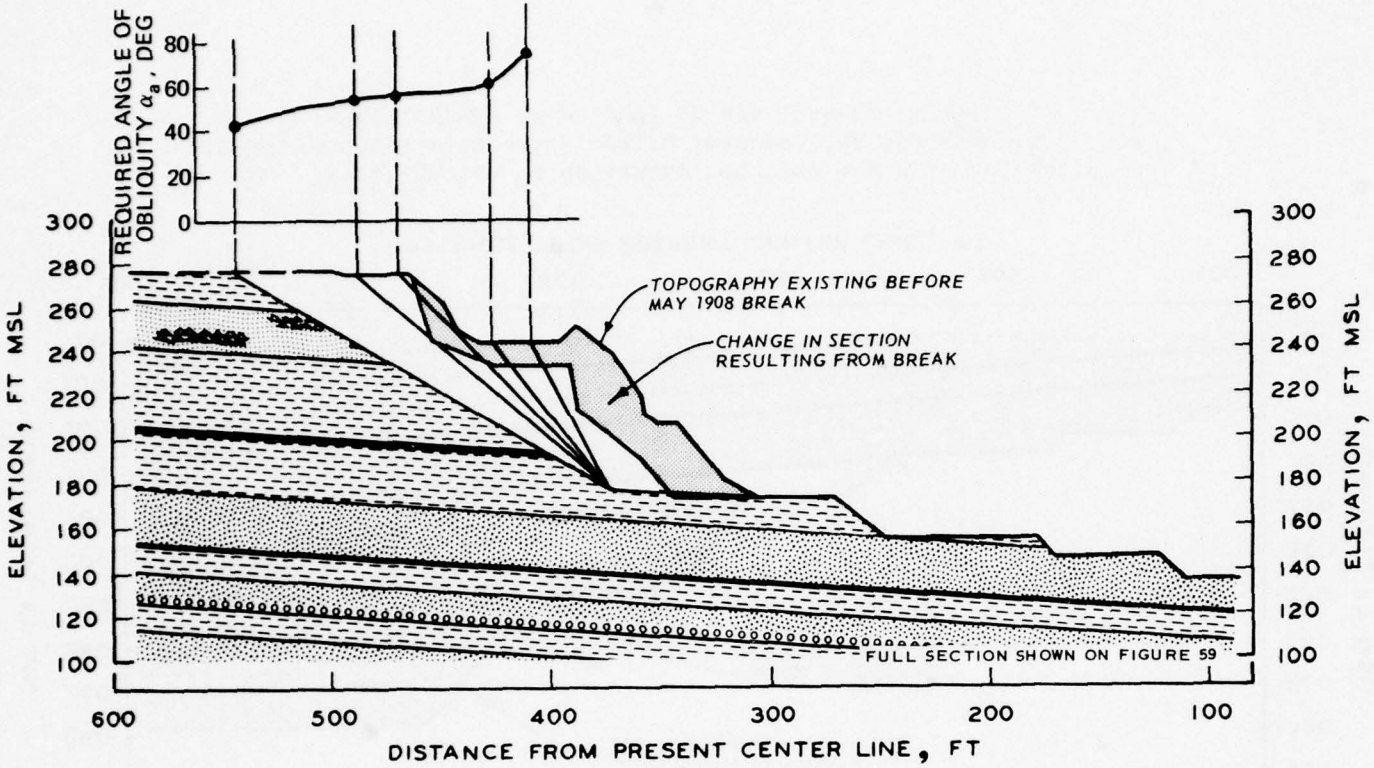

Fig. 64. Investigation to determine required angle of obliquity, α_a, for different base planes of active wedge for initial break (May 1908) at sta 1944+60 (1777+00)

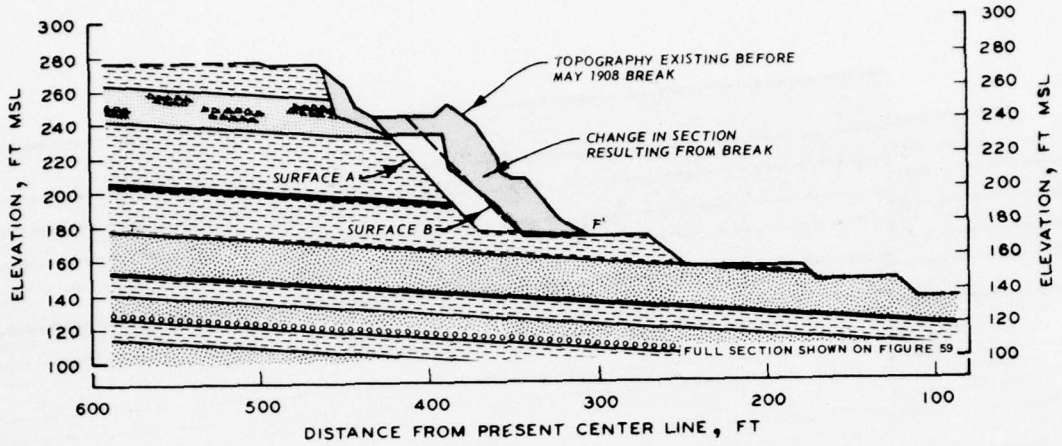

Fig. 65. Results of analyses for initial break (May 1908) at sta 1944+60 (1777+00)

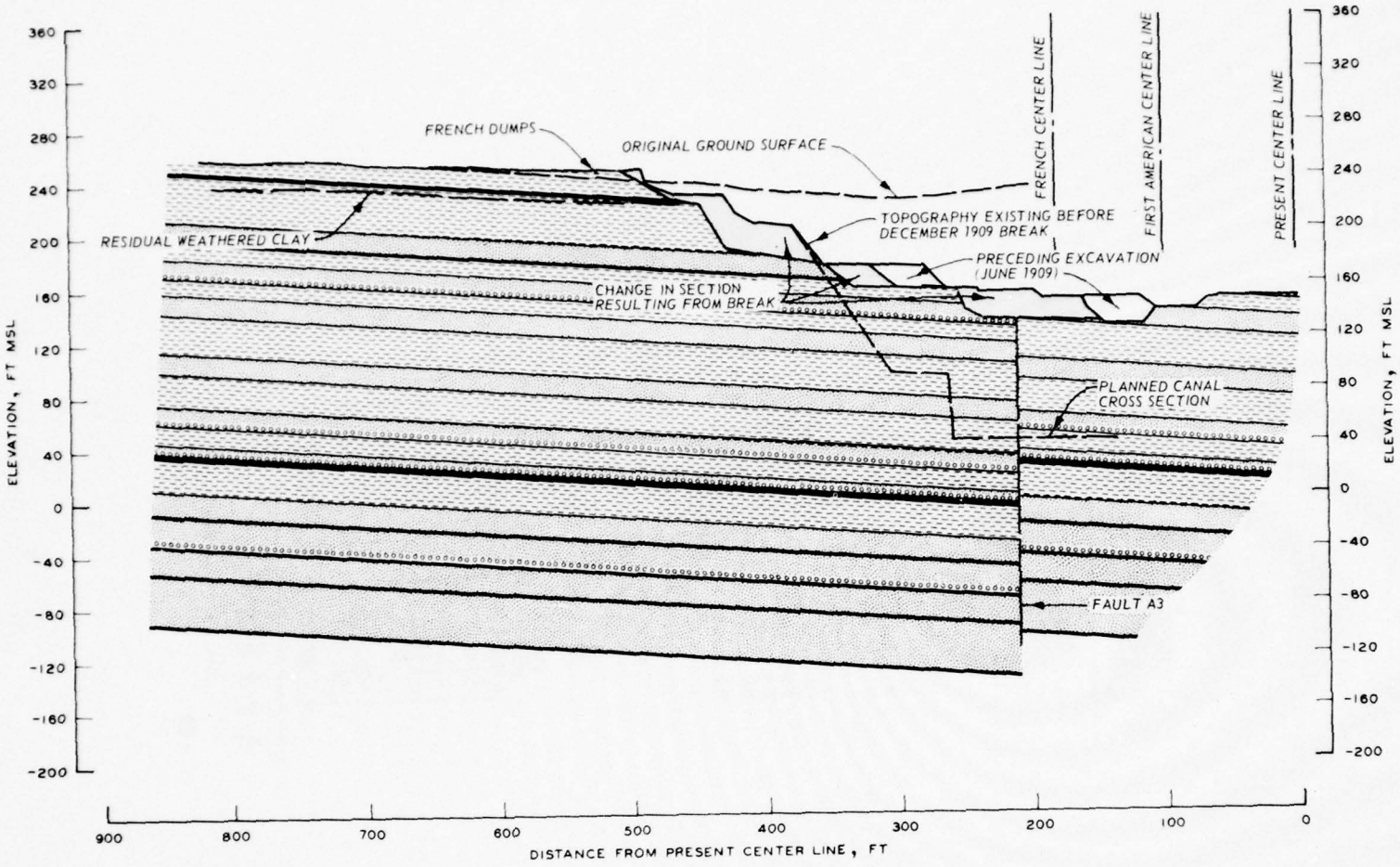

Fig. 66. Conditions surrounding the December 1909 break at sta 1939+60 (1772+00)

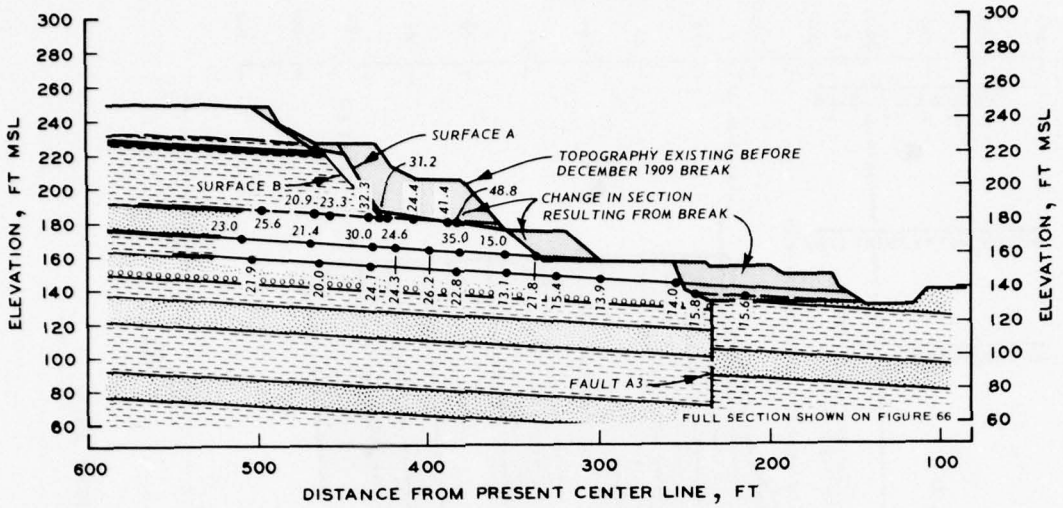

NUMERICAL VALUES FOR FINAL VECTOR DIAGRAM (FIG. 58d)

	SYMBOL	VALUE SURFACE A	VALUE SURFACE B	UNITS
COMMON	U_{a-n}	63.5	63.5	KIPS
	E'_{a-n}	0	0	KIPS
	δ_1	UNNECESSARY		--
RESISTIVE WEDGE	η	4.0	4.0	DEG
	c'_n	0	0	--
	L_n	75.0	75.0	FT
	W_n	251.0	251.0	KIPS
	U_n	116.3	116.3	KIPS
	N_n	129.6	129.6	KIPS
	α_n	31.9	31.9	DEG
ACTIVE WEDGE	α	60.0	52.0	DEG
	c'_a	0	0	--
	L_a	54.0	59.0	FT
	W_a	85.1	115.2	KIPS
	U_a	78.6	86.5	KIPS
	N_a	18.8	34.4	KIPS
	α_a	65.9	56.4	DEG

Fig. 67. Results of analyses for initial break (December 1909) at sta 1939+60 (1772+00)

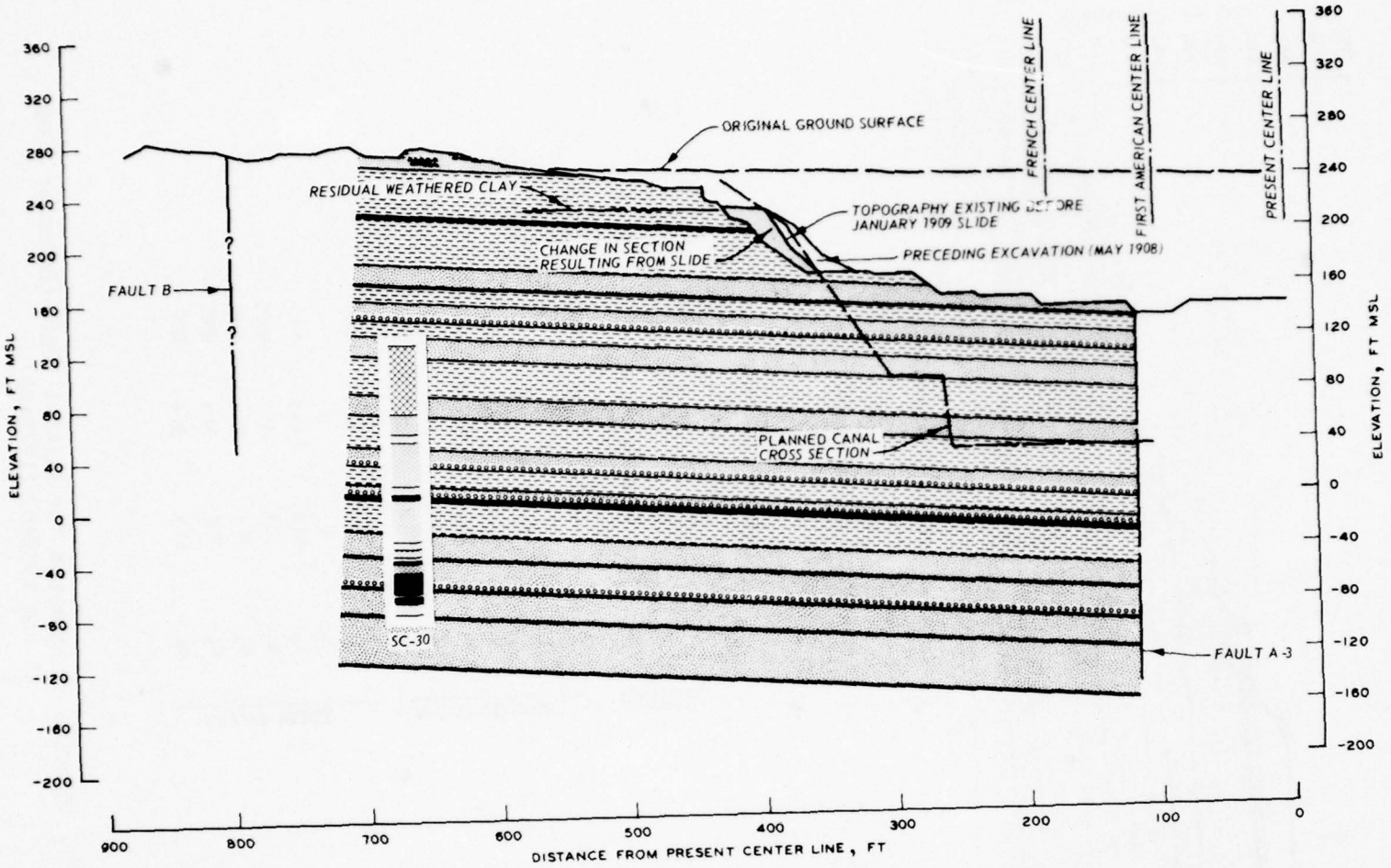

Fig. 68. Conditions surrounding the January 1909 break at sta 1942+60 (1775+00)

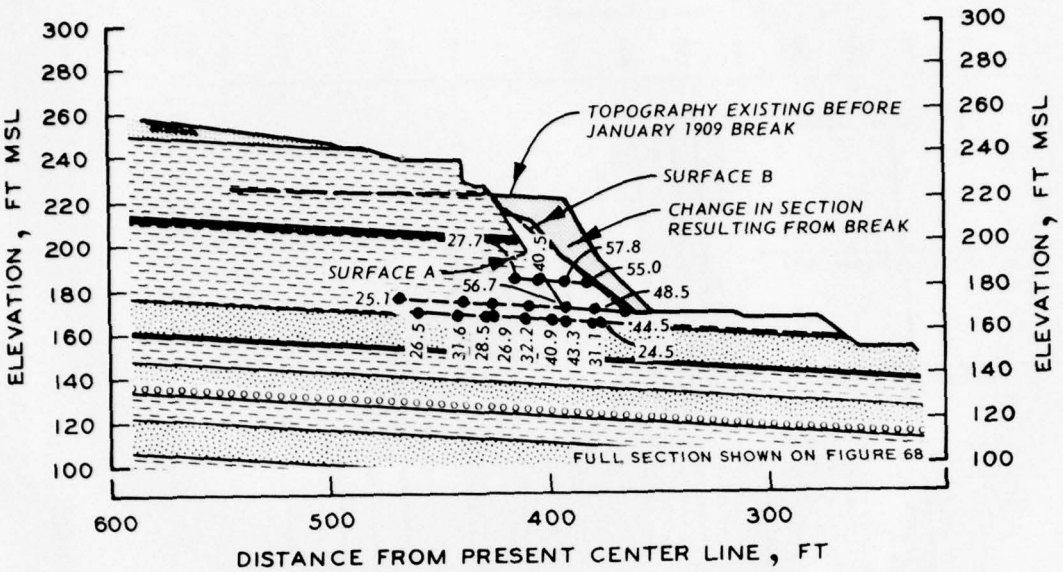

NUMERICAL VALUES FOR FINAL VECTOR DIAGRAM (FIG. 58d)

	SYMBOL	VALUE SURFACE A	VALUE SURFACE B	UNITS
COMMON	U_{a-n}	70.2	3.2	KIPS
	E'_{a-n}	0	0	KIPS
	δ_1	UNNECESSARY		--
RESISTIVE WEDGE	η	4.0	4.0	DEG
	c'_n	0	0	--
	L_n	39.0	11.0	FT
	W_n	107.1	7.6	KIPS
	U_n	49.6	3.5	KIPS
	N_n	52.3	3.8	KIPS
	α_n	56.0	44.6	DEG
ACTIVE WEDGE	α	57.0	41.0	DEG
	c'_a	0	0	--
	L_a	61.0	81.0	FT
	W_a	110.2	117.5	KIPS
	U_a	93.5	71.9	KIPS
	N_a	25.4	18.8	KIPS
	α_a	64.8	75.8	DEG

Fig. 69. Results of analyses for initial break (January 1909) at sta 1942+60 (1775+00)

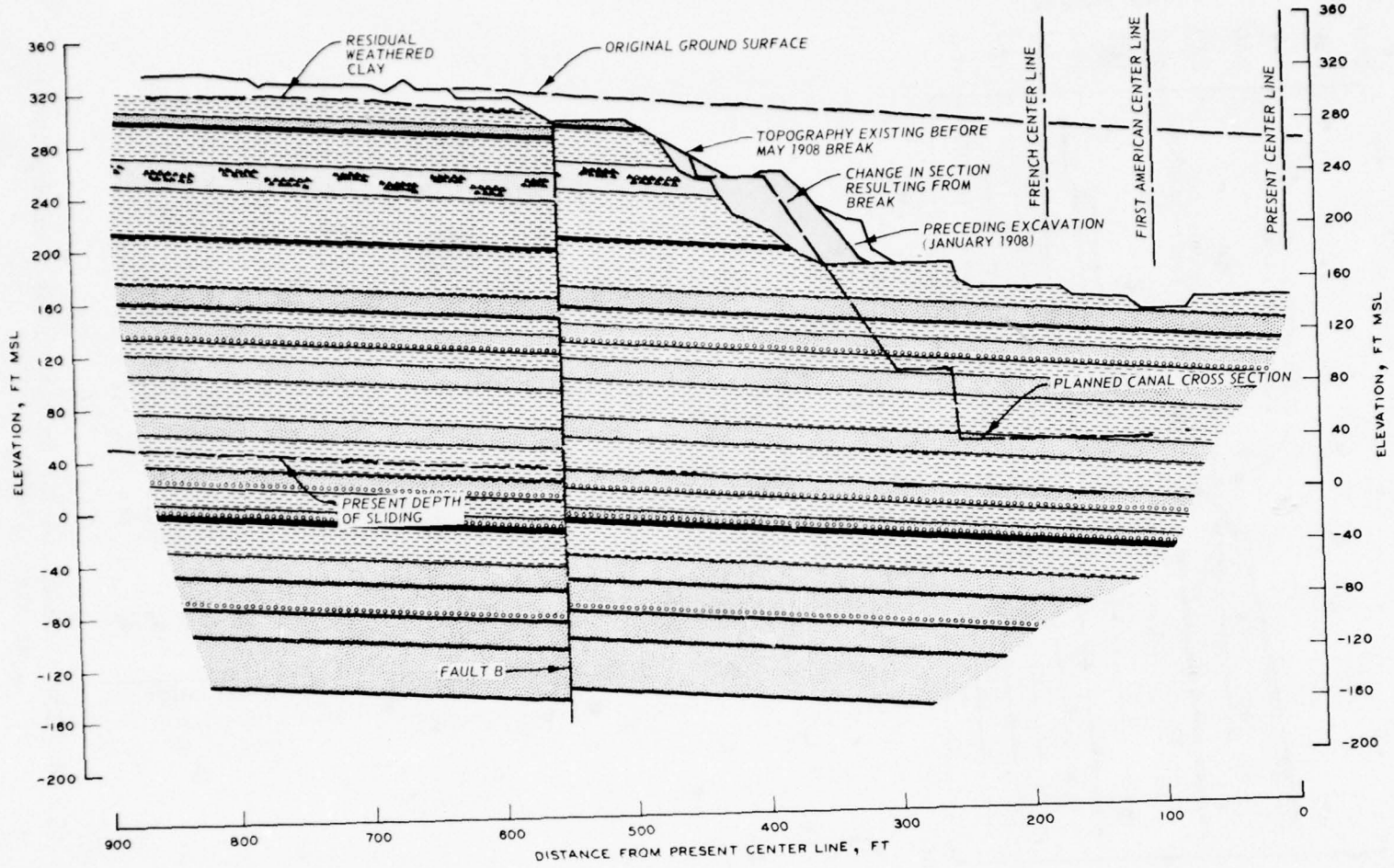

Fig. 70. Conditions surrounding the May 1908 break at sta 1946+10 (1778+50)

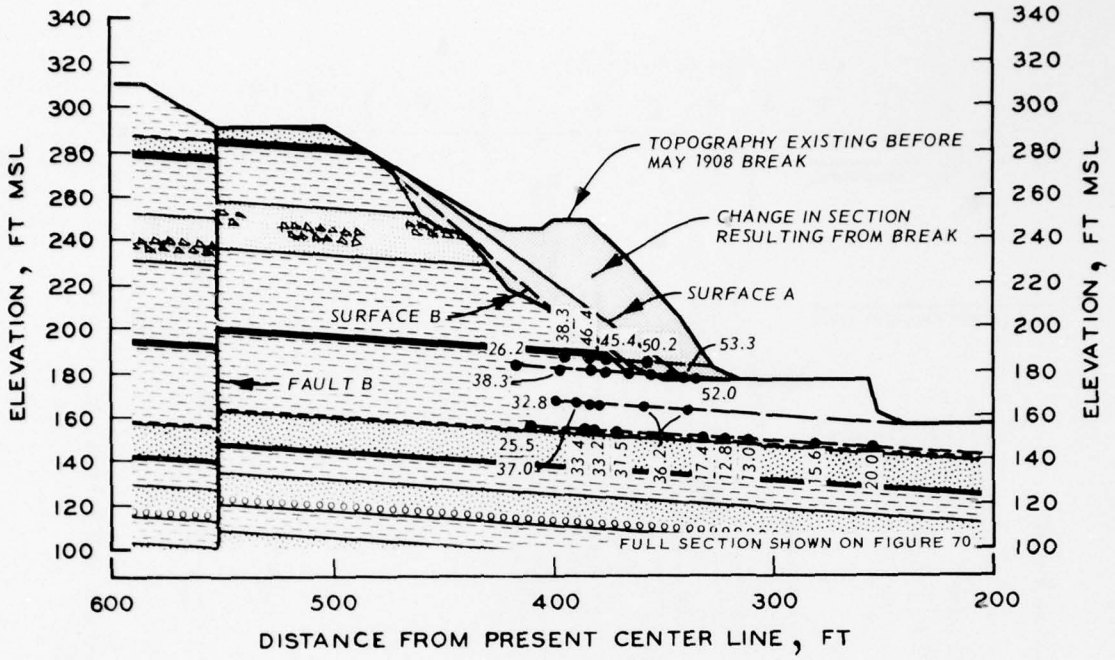

NUMERICAL VALUES FOR FINAL VECTOR DIAGRAM (FIG. 58d)

	SYMBOL	VALUE SURFACE A	VALUE SURFACE B	UNITS
COMMON	U_{a-n}	20.7	85.6	KIPS
	E'_{a-n}	0	0	KIPS
	δ_1	UNNECESSARY		--
RESISTIVE WEDGE	η	4.0	4.0	DEG
	c'_n	0	0	--
	L_n	25.0	50.0	FT
	W_n	34.9	167.0	KIPS
	U_n	16.1	77.4	KIPS
	N_n	17.2	83.2	KIPS
	α_n	53.3	49.4	DEG
ACTIVE WEDGE	α	36.0	41.0	DEG
	c'_a	0	0	--
	L_a	159.0	145.0	FT
	W_a	345.0	366.8	KIPS
	U_a	197.1	224.6	KIPS
	N_a	94.2	108.4	KIPS
	α_a	63.2	58.4	DEG

Fig. 71. Results of analyses for initial breaks (May 1908) at sta 1946+10 (1778+50)

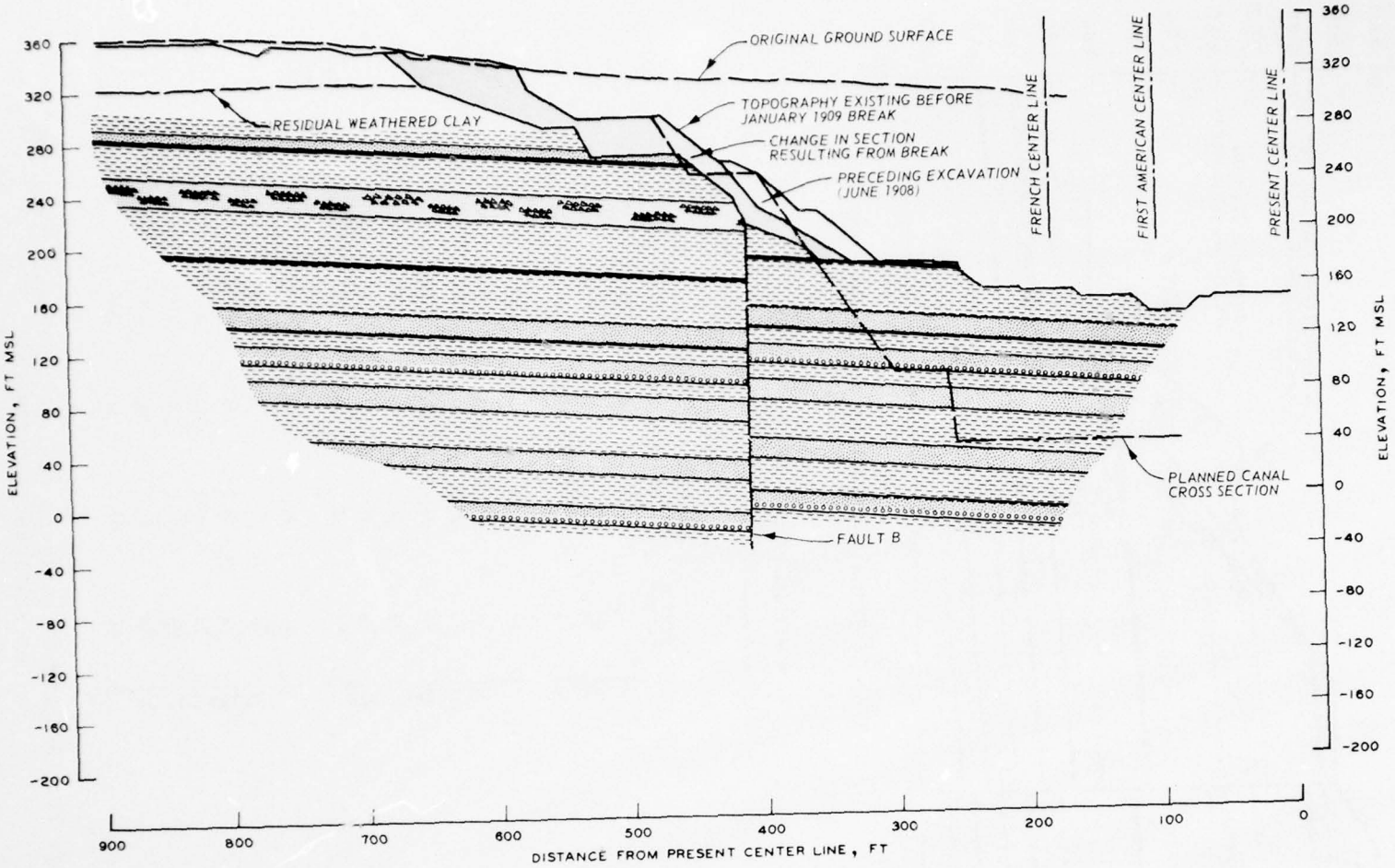

Fig. 72. Conditions surrounding the January 1909 break at sta 1948+60 (1781+00)

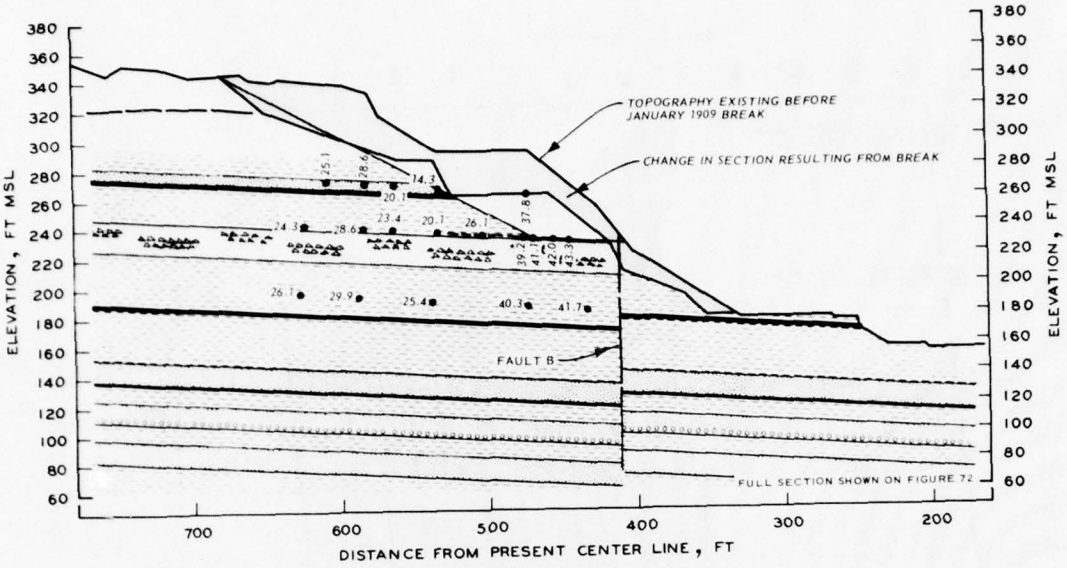

NUMERICAL VALUES FOR FINAL VECTOR DIAGRAM (FIG. 58d)

	SYMBOL	VALUE SURFACE A	VALUE SURFACE B	UNITS
COMMON	U_{a-n}	103.5	--	KIPS
	E'_{a-n}	0	--	KIPS
	δ_1	UNNECESSARY		--
RESISTIVE WEDGE	η	4.0	--	DEG
	c'_n	0	--	--
	L_n	65.0	--	FT
	W_n	277.3	--	KIPS
	U_n	128.5	--	KIPS
	N_n	140.9	--	KIPS
	α_n	41.0	--	DEG
ACTIVE WEDGE	α	28.0	--	DEG
	c'_a	0	--	--
	L_a	263.0	--	FT
	W_a	749.5	--	KIPS
	U_a	392.4	--	KIPS
	N_a	318.0	--	KIPS
	α_a	39.3	--	DEG

Fig. 73. Results of analyses for initial break (January 1909) at sta 1948+60 (1781+00)

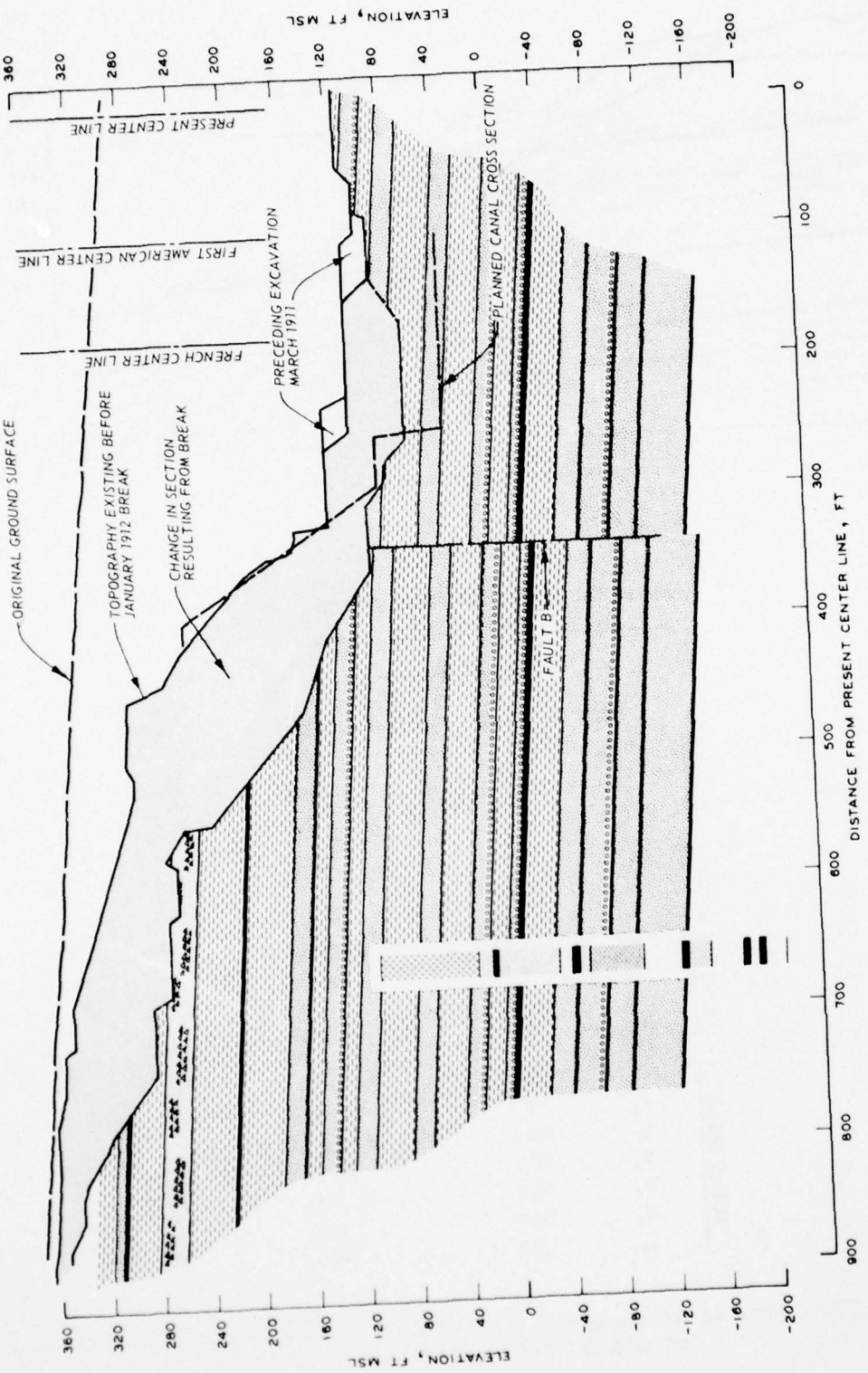

Fig. 74. Conditions surrounding the January 1912 break at sta 1950+10 (1782+50)

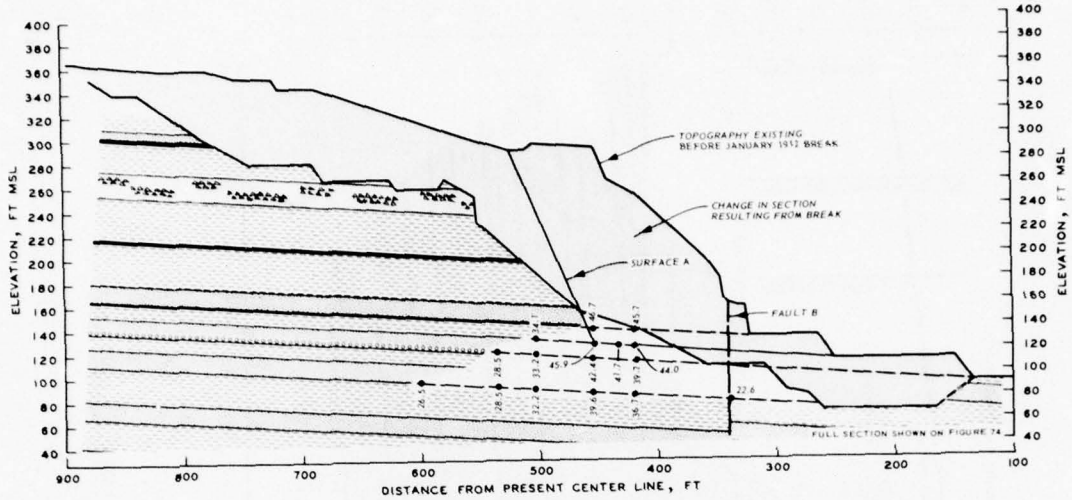

NUMERICAL VALUES FOR FINAL VECTOR DIAGRAM (FIG. 58d)

	SYMBOL	VALUE SURFACE A	VALUE SURFACE B	UNITS
COMMON	U_{a-n}	859.5	--	KIPS
	E'_{a-n}	0	--	KIPS
	δ_1	UNNECESSARY		--
RESISTIVE WEDGE	η	4.0	--	DEG
	c'_n	0	--	--
	L_n	203.0	--	FT
	W_n	1946.8	--	KIPS
	U_n	902.1	--	KIPS
	N_n	980.1	--	KIPS
	α_n	45.4	--	DEG
ACTIVE WEDGE	α	67.0	--	DEG
	c'_a	0	--	--
	L_a	178.0	--	FT
	W_a	794.6	--	KIPS
	U_a	940.0	--	KIPS
	N_a	162.2	--	KIPS
	α_a	67.7	--	DEG

Fig. 75. Results of analyses for initial break (January 1912) at sta 1950+10 (1782+50)

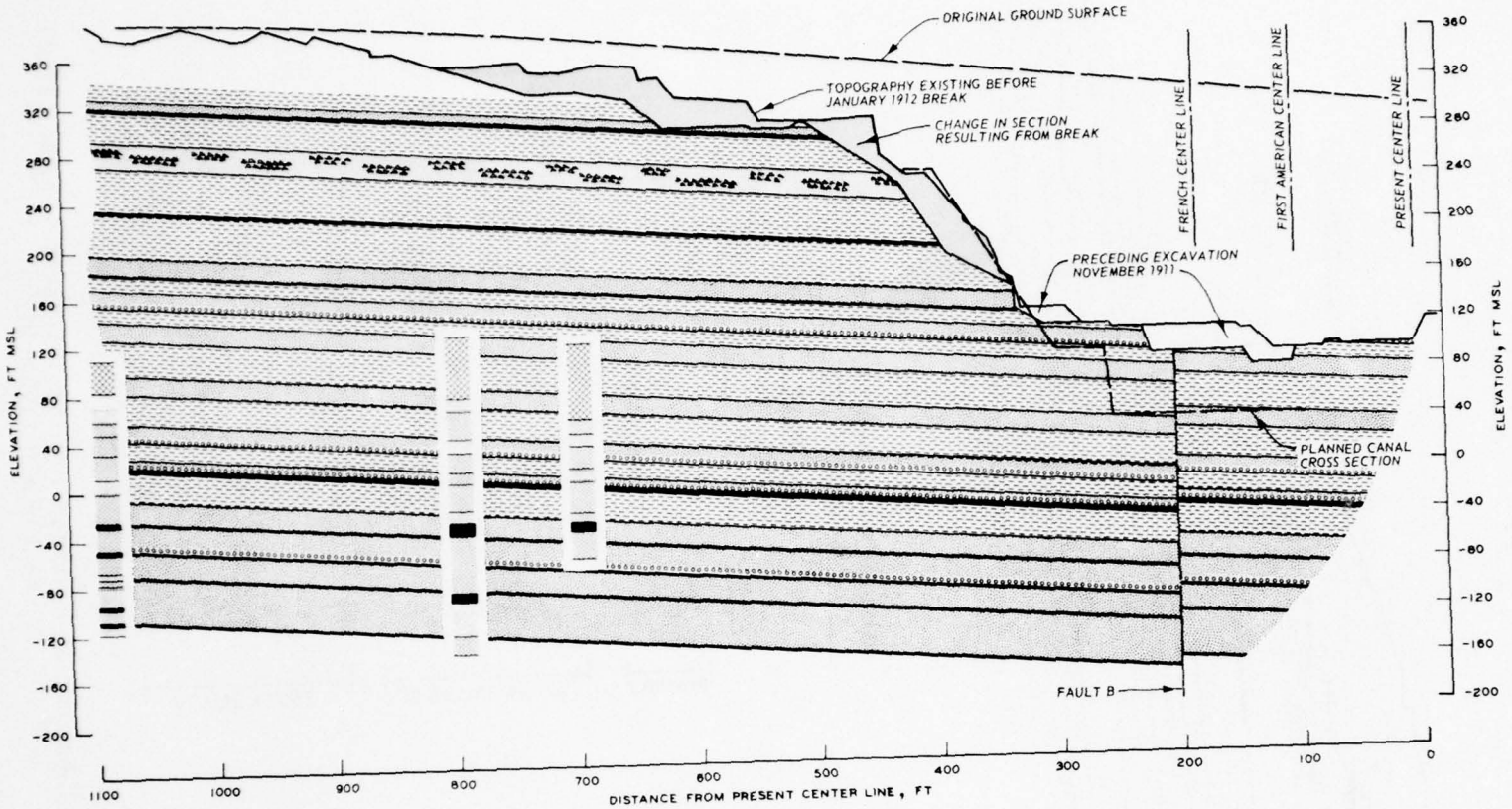

Fig. 76. Conditions surrounding the January 1912 break at sta 1952+60 (1785+00)

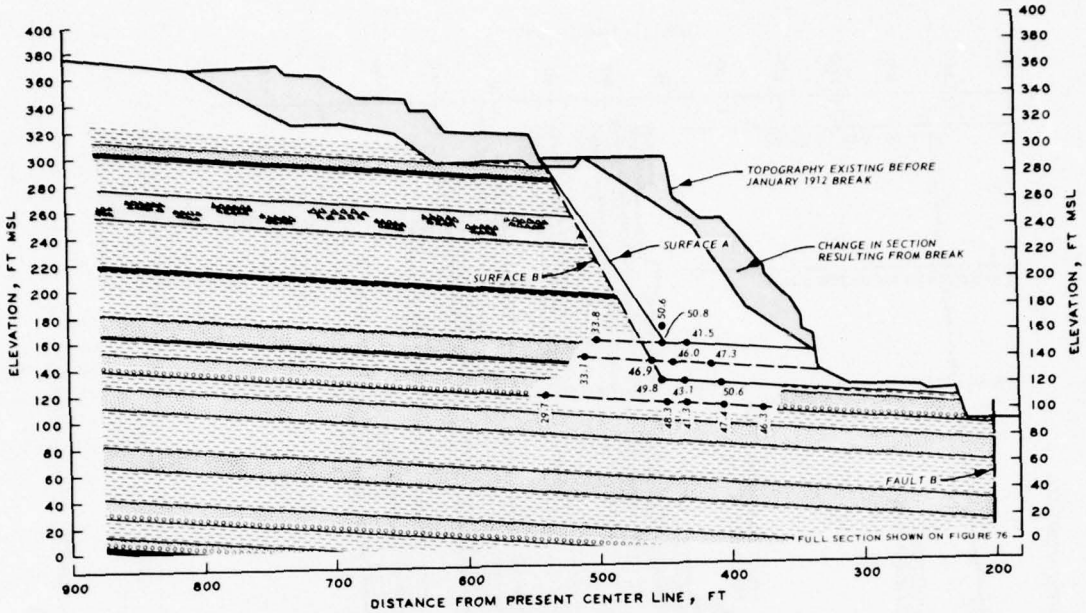

NUMERICAL VALUES FOR FINAL VECTOR DIAGRAM (FIG. 58d)

	SYMBOL	VALUE: SURFACE A	VALUE: SURFACE B	UNITS
COMMON	U_{a-n}	703.3	884.5	KIPS
	E'_{a-n}	0	0	KIPS
	δ_1	UNNECESSARY		--
RESISTIVE WEDGE	η	4.0	4.0	DEG
	c'_n	0	0	--
	L_n	114.0	224.0	FT
	W_n	1251.3	1691.9	KIPS
	U_n	579.8	794.0	KIPS
	N_n	619.5	842.1	KIPS
	α_n	51.9	49.9	DEG
ACTIVE WEDGE	α	57.0	62.0	DEG
	c'_a	0	0	--
	L_a	179.0	191.0	FT
	W_a	988.2	1017.5	KIPS
	U_a	838.7	1001.8	KIPS
	N_a	290.3	256.6	KIPS
	α_a	56.9	62.0	DEG

Fig. 77. Results of analyses for initial break (January 1912) at sta 1952+60 (1785+00)

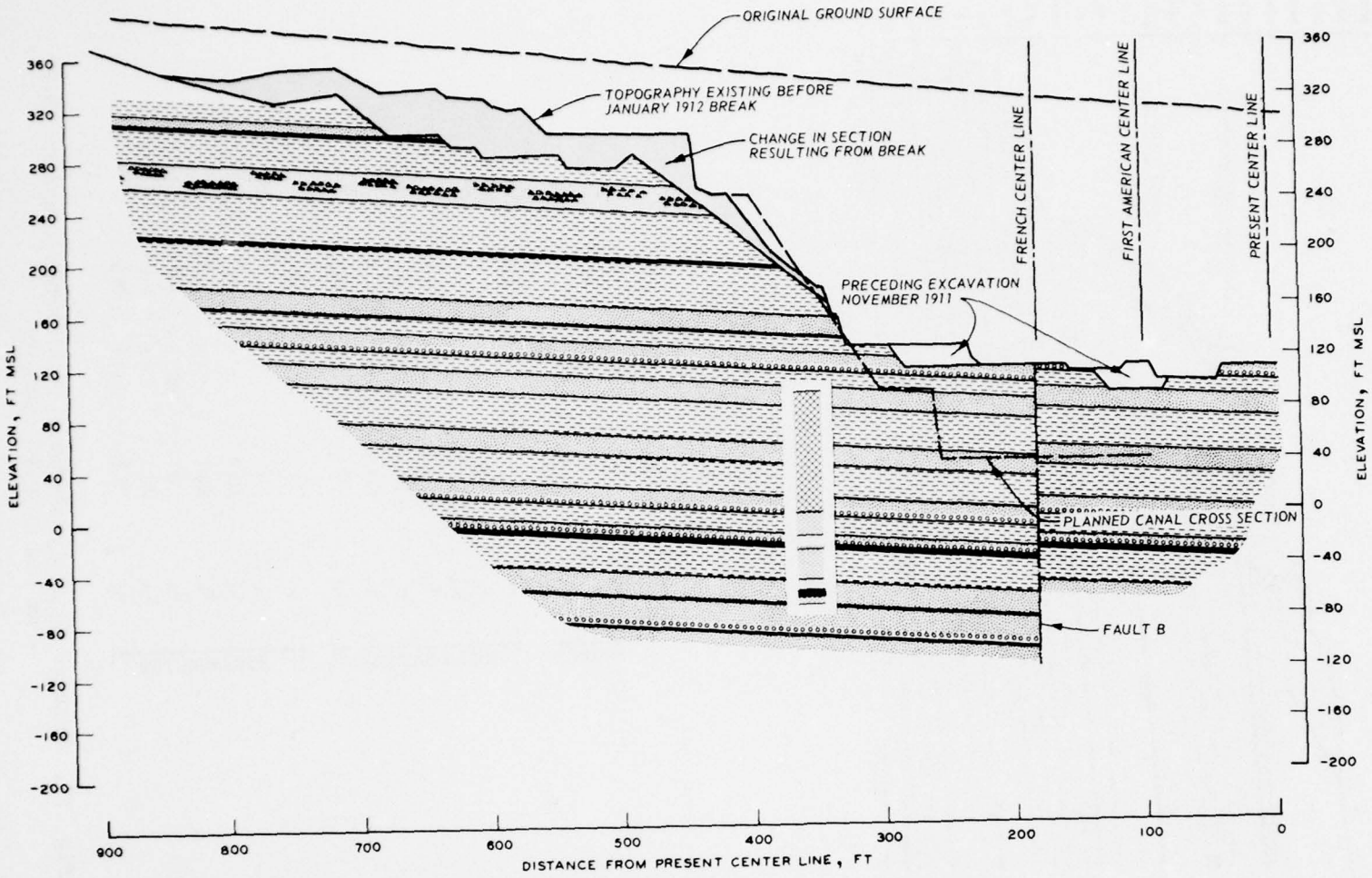

Fig. 78. Conditions surrounding the January 1912 break at sta 1955+10 (1787+50)

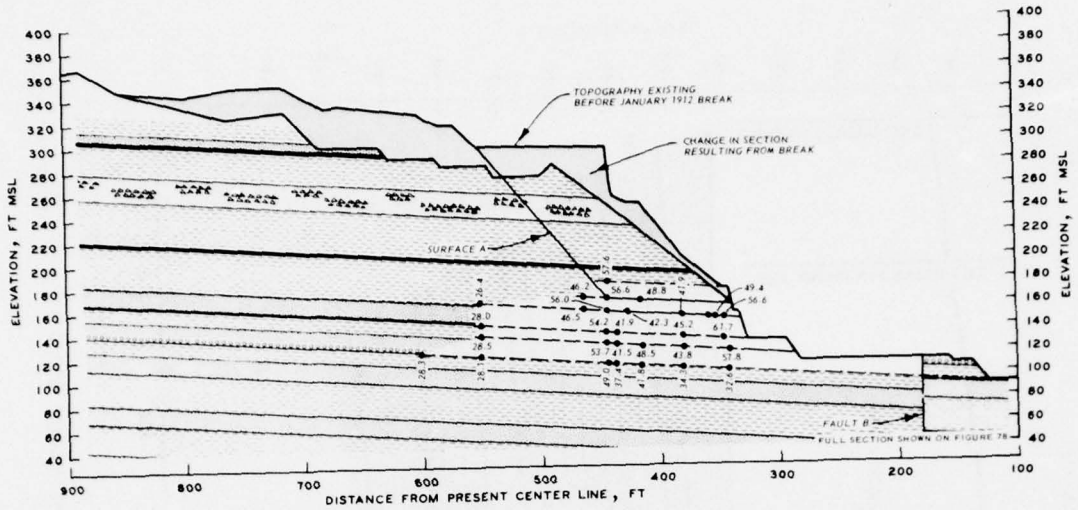

NUMERICAL VALUES FOR FINAL VECTOR DIAGRAM (FIG. 58d)

	SYMBOL	VALUE SURFACE A	VALUE SURFACE B	UNITS
COMMON	U_{a-n}	499.7	--	KIPS
	E'_{a-n}	0	--	KIPS
	δ_1	UNNECESSARY		--
RESISTIVE WEDGE	η	4.0	--	DEG
	c'_n	0	--	--
	L_n	105.0	--	FT
	W_n	737.5	--	KIPS
	U_n	341.7	--	KIPS
	N_n	359.3	--	KIPS
	α_n	56.9	--	DEG
ACTIVE WEDGE	α	50.0	--	DEG
	c'_a	0	--	--
	L_a	165.0	--	FT
	W_a	907.1	--	KIPS
	U_a	652.3	--	KIPS
	N_a	314.3	--	KIPS
	α_a	49.9	--	DEG

Fig. 79. Results of analyses for initial break (January 1912) at sta 1955+10 (1787+50)

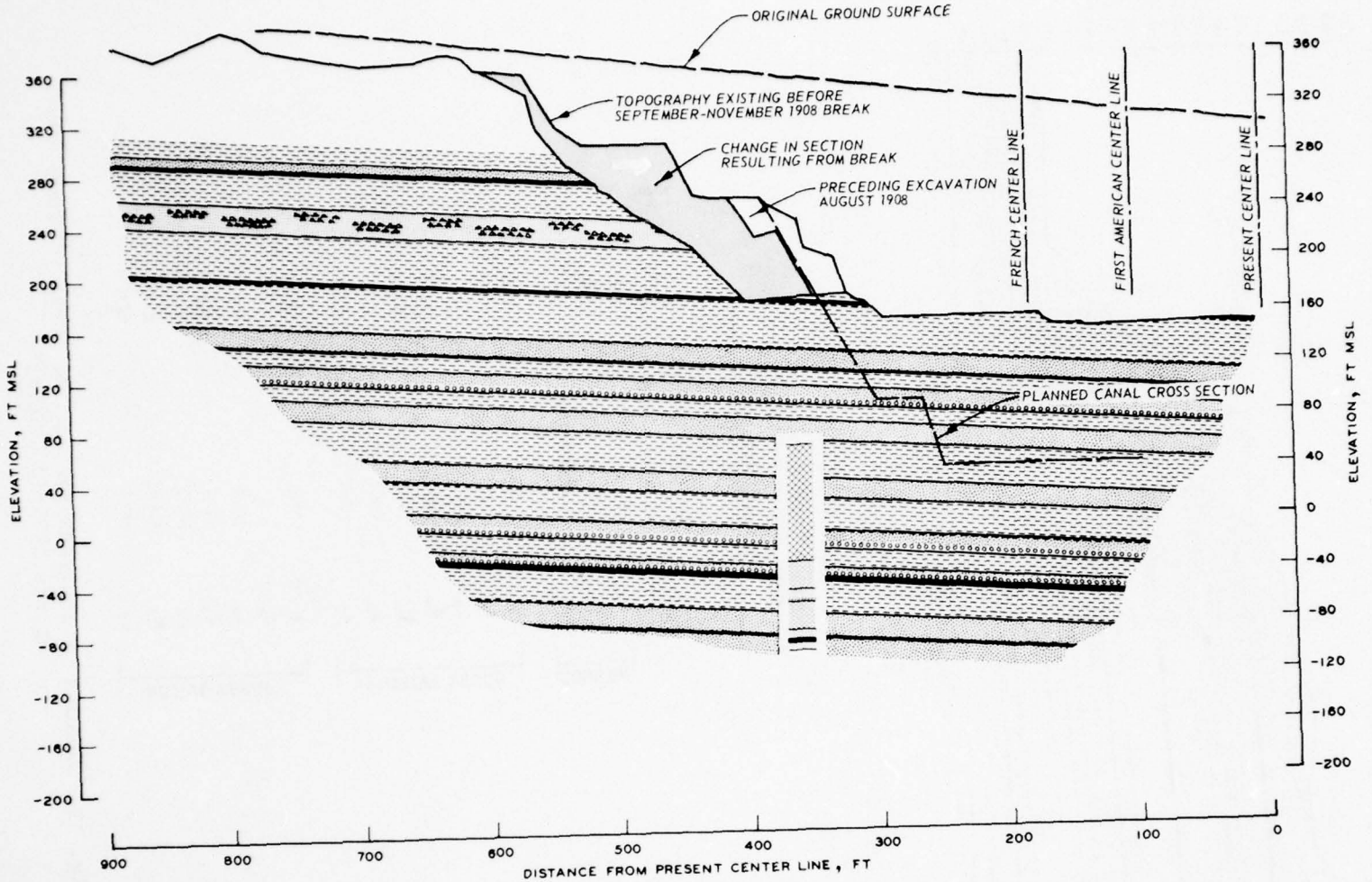

Fig. 80. Conditions surrounding the September-November 1908 break at sta 1958+60 (1791+00)

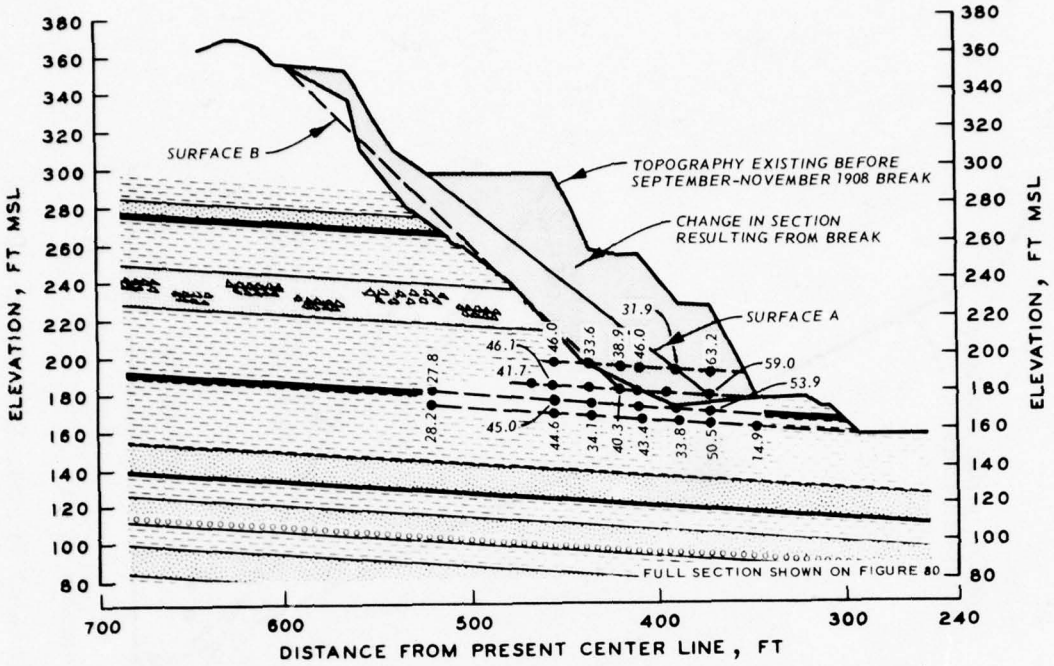

NUMERICAL VALUES FOR FINAL VECTOR DIAGRAM (FIG. 58d)

	SYMBOL	VALUE SURFACE A	VALUE SURFACE B	UNITS
COMMON	U_{a-n}	72.6	161.4	KIPS
	E'_{a-n}	0	0	KIPS
	δ_1	UNNECESSARY		--
RESISTIVE WEDGE	η	4.0	4.0	DEG
	c'_n	0	0	--
	L_n	26.0	73.0	FT
	W_n	89.2	462.5	KIPS
	U_n	41.3	214.3	KIPS
	N_n	42.6	235.8	KIPS
	α_n	61.5	39.3	DEG
ACTIVE WEDGE	α	39.0	45.0	DEG
	c'_a	0	0	--
	L_a	188.0	246.0	FT
	W_a	656.5	865.4	KIPS
	U_a	390.5	565.7	KIPS
	N_a	165.3	160.2	KIPS
	α_a	65.2	72.2	DEG

Fig. 81. Results of analyses for initial break (September-November 1908) at sta 1958+60 (1791+00)

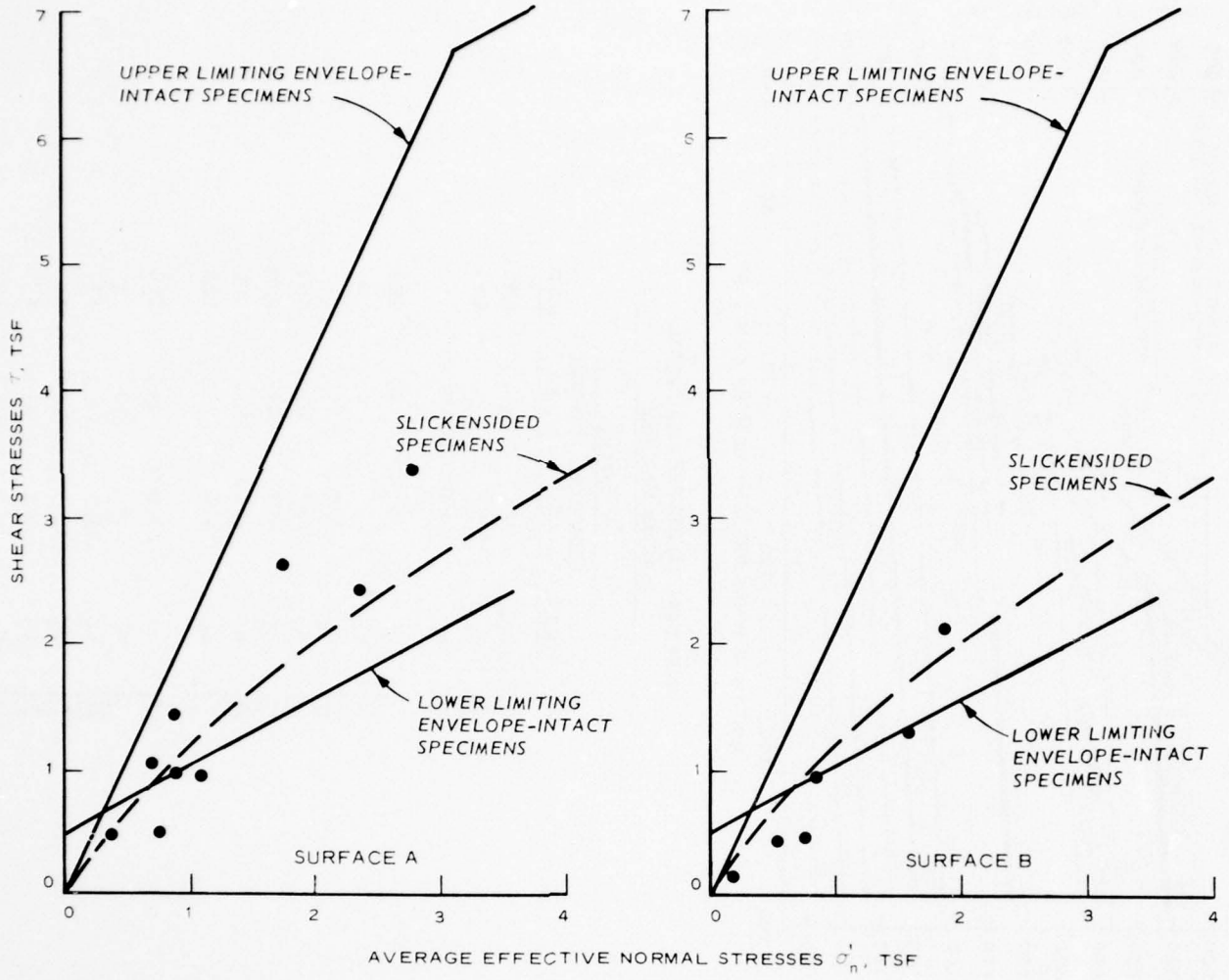

Fig. 82. Required shear strength along bedding, initial breaks, East Culebra Slide

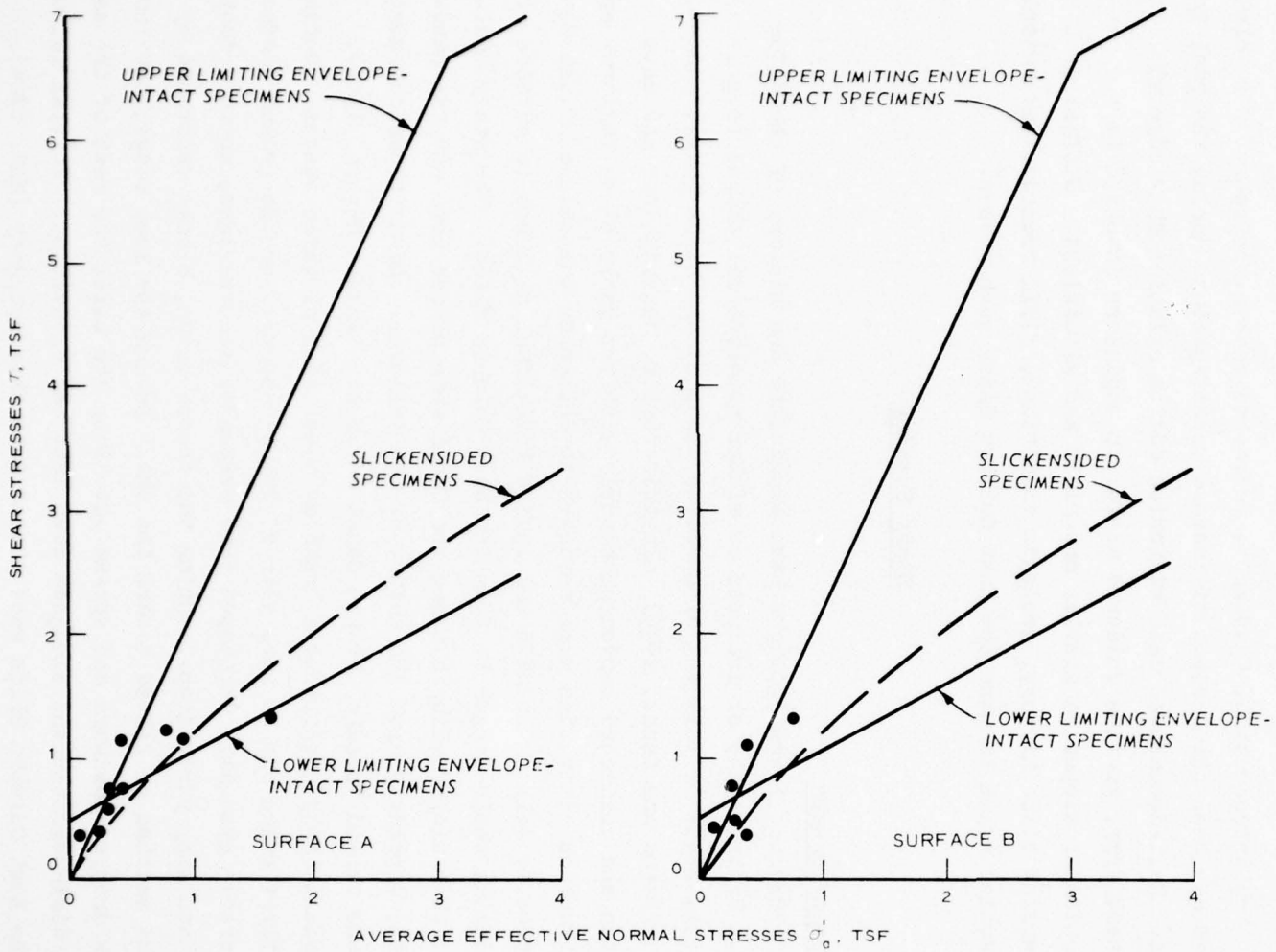

Fig. 83. Required shear strength across bedding, initial breaks, East Culebra Slide

CHAPTER VI: STUDY SUMMARY, CONCLUSIONS, AND RECOMMENDATIONS

The introduction, Chapter I, indicated that slope behavior in clay shales has been the subject of intense investigations during the past few years. Well-documented case histories add to existing knowledge and, at the same time, provide guidance useful to engineers involved in the construction of slopes in similar materials and situations. Sufficient data concerning slide history, geologic conditions, field records, and material properties exist to make the East Culebra Slide such a case.

Study Summary

Nature of breaks

Previous investigations have emphasized the history of the Slide (e.g., Cross, 1924) or analyses of either hypothetical slopes (e.g., Collins, 1942) or failures of specific areas of the Slide (e.g., Binger, 1948; Lutton and Banks, 1970). In this thesis, descriptions and data written and collected contemporaneously with the early slope failures and construction activities were reviewed to determine the nature of the slope failures as well as to date and locate individual failures in advance of and during their merger to form the East Culebra Slide. The study indicated that slope failures along the Canal were placed into several categories, depending upon the nature of the failures. Among these categories was one termed "breaks" by the Canal engineers (Annual Report, 1912). MacDonald (1915) described a break as consisting of three stages. During the first stage one or more sets of cracks appeared on the ground surface. The cracks gradually developed into perpendicular crevices, up to a foot wide and many yards deep. During the second stage, blocks separated by cracks settled or tilted toward the cut. During the last stage, the front block dropped downward and spread out along its base; the rest of the mass then disintegrated and sloughed down into the excavation. Initial failures at the East Culebra Slide were placed into this category (NAS, 1924).

Any sliding that occurred prior to 1908 was surficial, involving only the upper weathered, residual clay. The first slide to involve subsurface materials (i.e., the first break) occurred in May 1908 at the East

Culebra Slide. This break involved only a small length along the face of the future slide. By January 1912 these individual breaks had united to involve the entire length of the Slide. Following 1912, the Slide increased in size by incorporating additional areas further back in the slope. While the dating and positioning of the individual breaks cannot be made exactly, reasonable approximations were established from cross sections made during Canal construction.

A study of the cross sections indicated that the breaks occurred generally after materials were excavated at the toe of the slope, although in some instances, excavation was additionally along the face of the cut. The breaks occurred within a period of one to ten months after the excavation. While the volume of material excavated prior to the break was small in comparison to the volume of material removed because of the break, the excavated material acted to prevent expansion at the toe and the ensuing, open vertical cracks that gave groundwater ready access to the slide mass.

Geology of the East Culebra Slide

The general structure of the Isthmus is anticlinal with local intrusions of igneous rock. In the study area a downfold, or syncline, trends across the Gaillard Cut to take the stronger, limy sandstone beds of the underlying Culebra formation below the bottom of the Canal for a horizontal distance of more than a mile and to leave the weaker Cucaracha formation to form the sides of the Canal near its deepest point. The bedding in the area dips gently toward the Cut but is intersected by local faults to produce graben-horst features. The East Culebra Slide presently extends from near a fault zone on the north to fault planes on the south and east. The intruded mass of Gold Hill to the southeast is separated from the East Culebra Slide by a fault. The influence of the faults on the initiation of sliding cannot be ascertained, although it was noted that the first breaks occurred in areas where faults intersected the face of the cut. However, strength data obtained from analyses of the breaks are not commensurate with residual shear strength data such as would normally be expected in areas of tectonic movements or large shear displacements. Apparently, the intruded mass at Gold Hill produced drag features, but they only extended for a few tens of feet before beds again become nearly horizontal (Lutton and Banks, 1970). The clay shale strata within the Cucaracha formation contain numerous slickensides but without pattern of

AD-A061 404 ARMY ENGINEER WATERWAYS EXPERIMENT STATION VICKSBURG MISS F/G 8/6
STUDY OF CLAY SHALE SLOPES ALONG THE PANAMA CANAL. SUPPLEMENTAL--ETC(U)
AUG 78 D C BANKS

UNCLASSIFIED WES-TR-S-70-9 NL

3 OF 3
ADA
061404

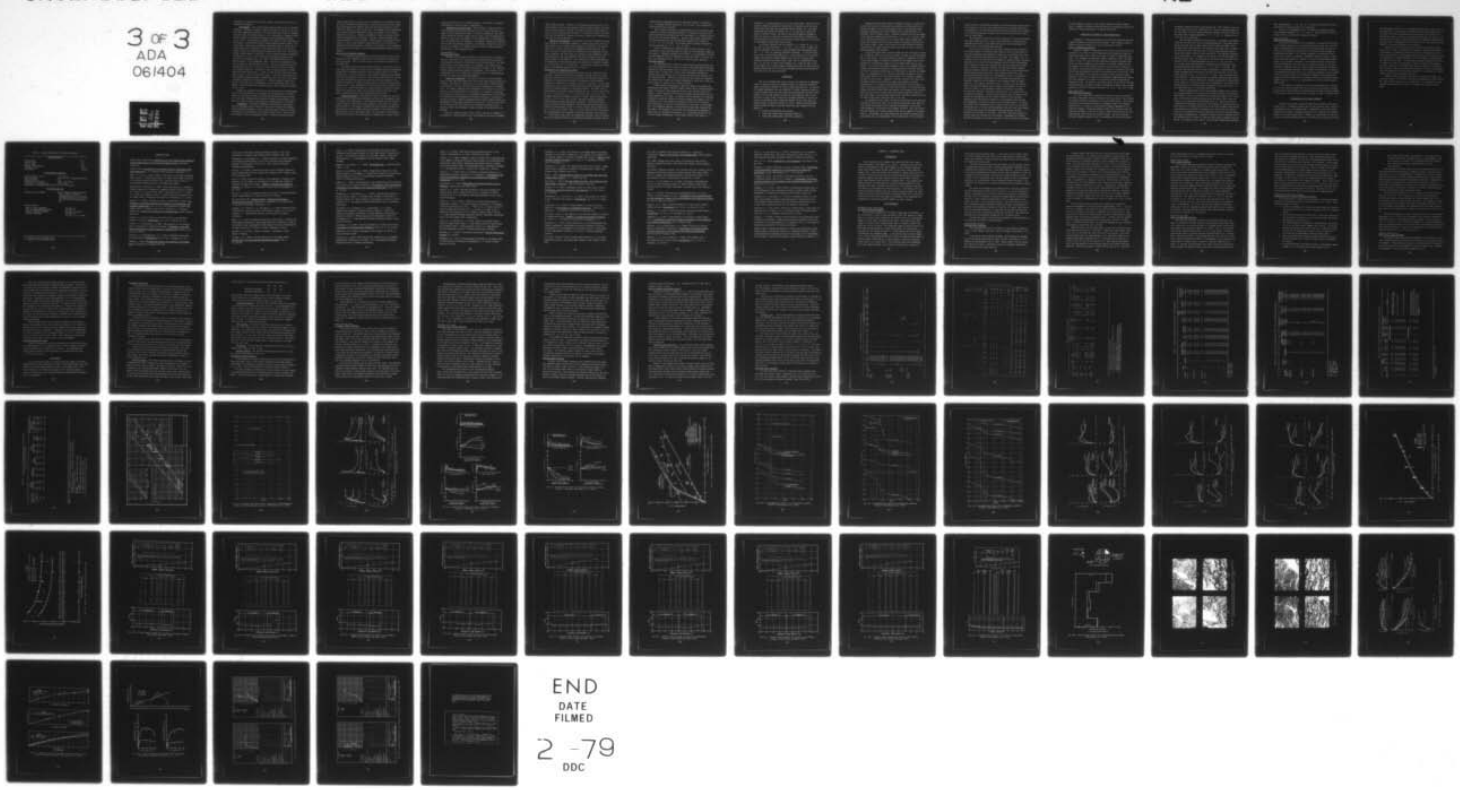

END
DATE
FILMED
2-79
DDC

orientation or appreciable continuity, except locally where they were influenced by faulting.

Stratigraphy. Four recent borings have been made into the Cucaracha formation. Although the ground surface elevations at the top of the borings were comparable, faulting in the area caused the borings to encounter the same strata at different depths. As a consequence, a composite stratigraphic column of the Cucaracha formation can be established (Lutton et al., 1975). Corroborative information was obtained from French and old PCC borings. During construction, geologic mapping along the center line of the Canal allowed the stratigraphic sequence within the breaks to be established by the correlation of important marker beds in the stratigraphic column with corresponding beds along the center line. The stratigraphic column showed the upper part of the Cucaracha formation (generally the upper 20 to 30 ft) to be altered by near-surface weathering into a yellow and red residual clay. The base of the weathered clay is the lowest position of the groundwater table. Beneath the groundwater table, the clay shale is greenish-gray in color. A hard and resistant layer of welded tuff, from 10 to 20 ft thick, lies about 300 ft above the base of the Cucaracha formation. Beneath the tuff, alternating layers of sandstone and shale layers exist. A brown or black lignitic shale layer commonly occurs at the top of each shale layer. Grain size increases more or less gradually downward through a sedimentary cycle of shale, silty shale, siltstone, sandstone, and conglomerate. A marked change in grain size exists at the base of the conglomerate, and the sedimentary cycle is repeated. At least eight such sedimentary cycles can be identified (Lutton et al., 1975).

Within the accuracy with which the cross-sectional and stratigraphic data could be established, it was shown that the weak layers of lignitic shales, or interfaces between clay shale and sandstone/siltstone strata, or a clay shale stratum and the welded tuff marker bed daylighted the cut face at or near the base of the materials removed because of the breaks.

Groundwater. No detailed information concerning the groundwater data was determined from a review of construction accounts and contemporarily recorded information. Hence, inferences must be drawn from recent observations in areas adjacent to the East Culebra Slide. Those observations indicate that the groundwater table is high and, during the rainy

season, approximately coincides with the elevation of the ground surface. The initial breaks developed during or shortly following the rainy season. Recent piezometer data indicate that deep clay shale layers are slow to respond to changes in stress conditions. For example, several piezometers still indicate reduced piezometric levels with respect to the present Canal water elevation. However, piezometers in upper clay shale strata indicate responsiveness to rainfall. The data indicated further that clayey sandstone or siltstone layers readily respond to groundwater fluctuations. Since failure surfaces along interfaces of clay shale and sandstone/siltstone strata were assumed in the analyses, full hydrostatic water pressure with respect to the overlying groundwater surface was also assumed.

Nature of the Cucaracha formation

It is generally accepted that the East Culebra Slide involved only materials in the Cucaracha formation; this thesis does not produce any other conclusion. Thus, only the nature of the Cucaracha formation is discussed here.

The study indicated that the ground surface at the time of the initial breaks was lowered in excess of 250 ft through sliding and subsequent excavation or unloading activities over the present extent of the East Culebra Slide. During construction, only general information was recorded concerning the materials involved in the initial breaks; specific information comes from borings and tests conducted on the clay shales of the Cucaracha formation at depths presently below the initial breaks and from adjacent areas. This information is considered valid since studies (e.g., Lutton et al., 1975) have shown that strata presently existing in nearby areas, but separated by faults from the East Culebra Slide area, have direct correlations with strata existing before the breaks.

General description. The Cucaracha formation consists of strata of highly overconsolidated, greenish-gray clay shale with subordinate strata of sandstone and conglomerate. The Cucaracha formation is lower Miocene in age (Woodring, 1957) and has been regarded as terrestrial in origin, mainly because of the presence of mammal and plant remains, although the lower portion has been termed transitional because of the presence of marine fossils (Lutton and Banks, 1970). The clay shale strata resulted from the alteration of very fine-grained, somewhat basic, volcanic ash to

clay-sized particles rich in montmorillonite. The presence of numerous slickensides in certain strata is significant.

Properties of the clay shale. While average or typical values of index parameters and physical properties can be cited to describe the nature of the Cucaracha clay shale, it should be emphasized that considerable variations from the values shown in Table 9 can be determined for different strata and, for example, in the determination of index parameters, by varying the test techniques. Furthermore, parameters relating to strength and consolidation properties are strongly influenced by the condition of the sample, for example, whether the test specimen contained slickensides or was reasonably intact.

Slickensiding in the clay shale strata

Sliding in the Cucaracha formation was facilitated by the numerous strata of clay shale with a high content of montmorillonite and by the well-developed network of slickensides within the clay shales. The weakening effect of the slickensides on the strength of the materials was noted by Thompson (1947) and was qualitatively assessed in this thesis by testing samples containing numerous slickensides. The presence of the slickensides may be the single most important feature in controlling the failure of slopes in the Cucaracha formation.

Origin of slickensides. The smooth, striated, polished surfaces found in many clays and clayey rocks result from shear failures within the material. The origin of slickensides is, in most cases, speculative but is attributed to several factors acting either singularly or in combination. For example, Thompson (1947) thought that the origin of the slickensides in the Cucaracha could be attributed to a change in volume when the original ashy materials in the formation underwent hydration and chemical alteration with accompanying differential swelling. A process described by Terzaghi (1962) and demonstrated by Yudhbir (1969) involves the development of shear during unloading or erosion at a time when the ratio of the effective vertical stress to the effective horizontal stress reaches a lower limit, causing the shear strength of the material to be exceeded.

While no attempt was made in this study to ascribe the formation of slickensides to one particular cause, the explanation offered by Terzaghi

(1962) seems plausible. Whether the slickensides presently seen in the deep borings at the site were caused by Canal excavation and/or unloading of the slopes because of sliding or whether they were created from the erosion of the estimated 2500 to 3000 ft of overburden leads to the inference that the materials involved in the early breaks were slickensided no less than the present material.

Extent of slickensides. Slickensides are found throughout the clay shale strata of the Cucaracha formation. Borings reveal that some clay shale layers do not contain readily apparent slickensides; other strata contain one to three prominent or throughgoing slickensides per foot. While the logs of borings typically describe only the prominent slickensides, experience has shown that upon exposure to the atmosphere, even for short periods of time, many samples check and disintegrate into small chunks bounded by slickensides. This experience is further amplified by the difficulty of obtaining integral test specimens from samples thought to be relatively free of slickensides. In many cases, samples will break apart on slickensides spaced from 1/10 to 3/10 in.

Strengths of the Cucaracha clay shale

Samples of relatively intact clay shales can be formed into test specimens. Whether these materials represent stronger portions of the clay shale strata that were not failed during the unloading process and formation of slickensides or whether they represent intact material bounded by a network of slickensides or joints is not known. At any rate, drained direct shear tests on intact materials indicate variable strengths that can be bounded between two limiting envelopes. The upper limit is approximated by a bilinear envelope defined by $c'_p = 5.0$ tsf, $\phi'_p = 28$ deg for $\sigma'_n > 3$ tsf and by $c'_p = 0$, $\phi'_p = 65$ deg for $\sigma'_n < 3$ tsf. All specimens indicated strengths in excess of a lower limiting envelope defined by $c'_p = 0.5$ tsf, $\phi'_p = 28$ deg. Specimens containing numerous slickensides were formed by special techniques. Drained direct shear tests on these materials indicated a curved envelope transitioning at an effective normal stress of about 2 tsf into a linear portion defined by $c'_p = 1.6$ tsf, $\phi'_p = 24$ deg. Thus, it is shown that the effect of including slickensides in test specimens reduces the strength of the material.

Field direct shear tests on slickensided specimens, while not duplicating the laboratory results on slickensided specimens, indicate that an

interpretation commensurate with the laboratory results is plausible; i.e., a strength envelope defined as $c'_p = 0.3$ tsf, $\phi'_p = 24$ deg can be developed from the field data.

Some variation occurred in the determination of the effective peak strength of slurry-consolidated specimens of Cucaracha clay shale (normally consolidated) depending upon the test method, i.e., whether from direct shear or triaxial compression. However, when viewed collectively, the data indicated that the peak drained strength can be defined by $c' = 0$, $\phi' = 15$ to 20 deg. The average drained residual strength envelope is defined by $c'_r = 0$, $\phi'_r = 7.5$ deg.

Tests to determine the undrained shear strength indicate a wide scattering of data, depending upon the quantity of slickensides present in the samples. Undrained strengths varied from 0.3 to approximately 40 tsf. The data suggested that the undrained strength was about 5.5 tsf for the more slickensided and about 16.5 tsf for the more intact specimens.

Stability analyses

Data developed from a review of cross sections prepared during construction indicated that at least six distinct individual breaks occurred between May 1908 and January 1912 to involve the entire length of the East Culebra Slide. Single cross sections were established through four breaks; two cross sections, for one break; and three cross sections, for the remaining break. These nine cross sections were chosen for analysis. The construction records gave enough information to allow each of the sections chosen for analysis to be studied in detail.

A wedge analysis (Morgenstern, 1968) was chosen as the method for determining the average effective normal stresses and the maximum required angles of obliquity acting along the bases of the resistive and active wedges. Several analyses were made to investigate characteristics of the method employed in the study. In general, when an analysis of a break was attempted in which the active and resistive wedges were assumed to be interreactive, the force between the wedges was found to be in tension. This observation, as well as the description of the nature of the breaks, led to an assumption whereby a vertical water-filled crack separated the two wedges. The analysis of each break then determined the maximum required value of the angle of obliquity α_n acting along the base of the resistive wedge independently of the required value of the angle of

obliquity α_a acting along the base of the active wedge. The base of the resistive wedge was assumed to lie parallel to bedding and at the interface between clay shale and sandstone/siltstone strata, or a clay shale stratum and the welded tuff marker bed, or, in some cases, along weak layers of lignitic shale. The base of the active wedge was assumed to enter the slope at a position in keeping with the extent of material removed because of the break and to join the resistive wedge at the location of the assumed vertical water-filled crack.

The results obtained from the analysis (i.e., values of σ'_n, α_n, σ'_a, and α_a) were plotted on $\tau - \sigma'_n$ and $\tau - \sigma'_a$ plots. Strength envelopes determined from various testing programs were superimposed upon the $\tau - \sigma'$ plots to determine comparable strengths. It was found that in the case of shear along bedding (i.e., along the base of the resistive wedge), the required strength compared best with the effective peak strength obtained from drained direct shear tests on slickensided specimens. In the case of shear across bedding (i.e., along the base of the active wedge), the required strength compared best with the upper limiting envelope describing the effective peak strength obtained from drained direct shear tests on intact specimens.

Conclusions

The use of standard approaches to assess the stability of embankment slopes of compacted clays and excavated slopes in normally consolidated clays is generally adequate for routine engineering practice. The success of standard approaches, when the stability of slopes containing strata of overconsolidated clays and clay shales are being assessed, has been poorer. Because of the poorer success in assessing the stability, much use has been made of case records in which the strength operating at the time of failure is determined from a stability analysis of the slope under the condition that the factor of safety was unity. Skempton and Hutchinson (1969) considered several cases and placed them into categories as examples of:

a. Slides on preexisting slip surfaces.

b. First-time slides under long-term conditions.

c. First-time slides under short-term conditions.

Skempton and Hutchinson (1969) illustrated by means of several case studies that slides on preexisting slip surfaces are controlled by the residual strength of the overconsolidated clay or clay shale materials. Confirming conclusions have been reached by other investigators, e.g., Palladino (1971) and Hamel (1973). Residual strengths for the clay shales of the Cucaracha formation are defined by $c'_r = 0$, $\phi'_r = 7.5$ deg. Analysis of the East Culebra Slide in this thesis shows that strengths much larger than residual would have been required to maintain equilibrium of the initial breaks. Study of the nature of the East Culebra Slide additionally does not suggest that the Slide falls into the case of failure along preexisting slip surfaces.

First-time slides under long-term conditions are controlled, according to Skempton (1970), by the fully softened strength of overconsolidated clay or clay shales. The fully softened strength is comparable to the effective peak strength of normally consolidated clay samples derived from remolded (or resedimented) samples of the overconsolided clays or clay shales. In the cases described by Skempton (1970), the strengths have decreased from values associated with overconsolidated clay shale through processes of swelling, weathering, or softening by the presence of groundwater. A determination of the effective peak shear strength of slurry-consolidated material from clay shale strata of the Cucaracha formation was made for this thesis. Analysis of the East Culebra Slide showed that strengths larger than the effective peak shear strength of slurry-consolidated (i.e., normally consolidated) material would have been required to maintain equilibrium of the initial breaks. The conditions surrounding the East Culebra Slide additionally do not suggest that the Slide falls into the case of a first-time failure under long-term conditions since the breaks occurred during construction, following excavation at the toe (and in some cases, along the face) of the cut.

As indicated by this study, the relief was moderate in the area, the influence of faults was local, the intrusions caused only local drag features within the strata, and the observed slickensides in clay shale strata appeared to be pervasive but randomly oriented. Thus, the conclusion was reached that the East Culebra Slide was an example of first-time failure. Furthermore, the study showed that the breaks occurred during construction and, in consideration of the permeability of the clay shale

strata, should be considered an example of first-time failure under short-term conditions. As such, the close agreement of strengths determined from analysis of the initial breaks with the effective peak shear strength of slickensided specimens obtained from laboratory drained direct shear tests is significant.

The comparison shows that for field situations in which slickensided clay shale strata occur, but without deep weathering or softening, the strength-controlling initial short-term failure can be determined from drained tests on the slickensided material.

It should be cautioned that the study conclusions may be unique to the initial breaks at the East Culebra Slide in that the conclusions result from inferences and assumptions required by the existing body of information concerning the initiation of the Slide. For example, the conclusions result from inferences and assumptions regarding dates, locations, and extent of the initial breaks; geologic factors such as stratigraphy, fault locations, joints, and slickensides; and most importantly groundwater conditions. The heavy reliance upon locating failure surfaces along an interface between a clay shale stratum and a siltstone/sandstone stratum was previously described. That reliance allowed full pore water pressures with respect to the groundwater level to be assumed for the siltstone/sandstone materials and at the same time permitted the required strength to be attributed to that available from clay shale materials. Two important questions arise: firstly, does the existing body of information support such a reliance; and secondly, if such a situation exists, is the strength to which the results of the back-analyses were compared adequately represented by direct shear tests on slickensided specimens. A second concern centers upon the severe consequences of assuming that the pore water pressure in the siltstone/sandstone layer was directly related to the groundwater level and that the groundwater level was coincident with the ground surface. No parameter studies were conducted as part of this thesis, but it can be easily recognized that, if in fact, the groundwater level was lower than assumed, the calculations would have produced accordingly smaller required strengths for stability of the Slide. With these cautions, perhaps the results should be considered at the present as semiempirical findings and only be applied in the future to cases in which conditions are similar

to those assumed to exist for the initial breaks at the East Culebra Slide. Guidance is offered in the next section in applying the study conclusions to future excavations, in similar situations.

Application of Results to Future Excavations

Designers of future excavations in the Cucaracha formation must distinguish between two possible field conditions. The conditions involve whether extensive sliding has or has not previously occurred.

Slides on preexisting surfaces

Results of studies of existing slides by Lutton and Banks (1970) and by Banks et al. (1975) in the Cucaracha and other formations along the Panama Canal agree with results of studies of slides in formations elsewhere, e.g., Skempton and Hutchinson (1969), Palladino (1970), and Hamel (1973), in that for areas that have experienced previous extensive movements, the shear strength has been reduced to residual strength values. For example, at the East Culebra Slide the initial breaks, described in this thesis, were followed by progressive failures to involve an area that by 1916 was approximately as large as the present area of the Slide. From 1916 to the present, the Slide has continued to move toward the Canal. Analysis of the Slide for conditions prevailing in 1969 showed the governing field strength to be equal to the residual strength determined by laboratory tests. The design of any future slopes at the site of the East Culebra Slide must be based on properly determined residual shear strength parameters, which for Cucaracha clay shale are $c'_r = 0$ and $\phi'_r = 7.5$ deg.

First-time slides under long-term conditions

If, on the other hand, excavations are made in areas that have not previously experienced failure, recognition must be given to the reduction in strength caused by slickensides in the clay shale strata. Little doubt exists that for excavations leading to permanent slopes, the long-term stability will of course be controlled by strengths commensurate with long-term strength. Studies by Skempton (1970, 1977) indicated that the long-term strengths at the time of failure tended toward and did not fall significantly below the fully softened strength. The fully softened strength, Skempton reasoned, could be represented by the effective peak

strength of remolded normally consolidated clay. While extensive data are not available upon which to judge the fully softened strength parameters for clay shales of the Cucaracha formation, available laboratory data suggest that shear strength parameters of $c' = 0$ and ϕ' varying from 15 to 20 deg may be applicable.

Some information supporting these choices of seemingly low-strength parameters has been given from a preliminary analysis of the Model Slope across the Canal from the East Culebra Slide (Lutton and Banks, 1970). The Model Slope, which involved the Cucaracha clay shale, did not experience failure during construction and is still stable although surface cracks and fissures occurred in the late 1960's. The analysis indicated that in March 1911, i.e., roughly in the period of active development of the East Culebra Slide, the stability of the Model Slope could have been accounted for by strength parameters as low as $c' = 0.4$ tsf and $\phi' = 19$ deg; upon reinterpretation (unreported and preliminary), those strength parameters are equivalent to $c' = 0$ and $\phi' = 26$ deg. The slope has been modified from its 1911 configuration. Reinterpretation (again unreported and preliminary) indicates that stability can be presently accounted for by $c' = 0$ and $\phi' = 24$ deg. Thus, the Model Slope, in the absence of deep weathering but with strata containing many slickensides (Fig. 50), requires small shear strength parameters for equilibrium. In the absence of a detailed study, such as presented in this thesis, the agreement between the unreported and preliminary results and the results from laboratory tests is considered significant.

Further substantiation of the low-strength parameters that control the long-term stability of slopes in the Cucaracha formation is given by the analysis of the so-called 1925 East Problem Area (Banks et al., 1975). Deep, open vertical cracks were observed in the early 1970's along the surface of the previously unfailed slope (Fig. 2). The cracks were instrumented and observed to widen with the occurrence of ensuing rainy seasons, until on 10 October 1974 the toe of the Slide suddenly broke away to cause shoaling in the Canal at distances up to 500 ft from its initial position; the remainder of the mass broke into two blocks that experienced much smaller displacements. Volumes of material were not computed, but it was estimated that in excess of a million cubic yards of material were involved. An analysis of the slide at the 1925 East Problem Area indicated

that the parameters, $c' = 0$ and $\phi' = 16$ deg, were required for static equilibrium of the slide before its occurrence.

Thus, it is recommended that for the design of permanent slopes, shear strength parameters of $c' = 0$ and ϕ' varying from 15 to 20 deg should be used to ensure safe long-term stability.

First-time slides
under short-term conditions

In the case illustrated by the reanalysis of the East Culebra Slide in this thesis, failure can occur during construction and can, in the absence of weathering and large, previous shear displacement but with the presence of slickensides, be related to the effective peak strength of slickensided specimens. Such strength parameters as reported in this thesis may be used in the design of temporary excavated slopes or slopes under short-term conditions. However, in view of the seemingly variable nature of the cohesion intercept, it would appear prudent to reduce the cohesion parameter to zero and to use a friction component of the shear strength in agreement with the effective peak shear strength of either intact or slickensided specimens. While further investigations are needed to adequately define the value of the frictional component of the strength of the clay shale strata in the Cucaracha formation, particularly from properly conducted field tests, the guidance offered by this thesis would suggest that $c'_p = 0$ and ϕ'_p varying from 24 to 28 deg would be applicable values.

In the absence of laboratory data, the slope-height chart developed for the first-time failures (Fig. 15) can be used for guidance in design. Since the chart was developed by determining the average slope and heights at the time of failure, no data exist to extend the chart to higher slopes.

Recommendations for Future Research

Broad conclusions have been made based on the analysis of the East Culebra Slide. A somewhat similar case, the West Culebra Slide, exists on the opposite side of the Panama Canal. A reanalysis of the West Culebra Slide may be in order to provide similar data for comparison with that obtained for the East Culebra Slide. However, in consideration of the difficulty in obtaining definitive data on such factors as geologic structure

and groundwater conditions, it is recommended that unfailed areas, such as the Model Slope (to the south of the West Culebra Slide), Hodges Hill (to the north of the West Culebra Slide), and the area to the north of the East Culebra Slide, as well as all present-day failures, be studied to determine factors leading to their stability and to determine whether their stability would be maintained if the strength of the clay shales were commensurate with values presented in this thesis.

Conclusions were based on test data obtained from drained direct shear tests on intact or slickensided specimens. Additional work needs to be performed to determine the validity of the use of such direct shear tests, particularly on slickensided specimens and for the inference of the correspondence of laboratory strength to field strength of slickensided but unsoftened clay shale. In particular, questions regarding the effects of sample size, time of consolidation, rates of loading, and changes in pore water chemistry to distilled water should be studied. A comprehensive, carefully controlled field testing program on slickensided specimens should be conducted for corroborative evidence of the influence of slickensides upon the shear strength parameters.

Finally, since conclusions regarding the applicable strength for first-time failure in Cucaracha clay shale are comparable to those reached for other similar materials, e.g., London clay, it is of benefit to the engineering profession to continue to document case records in other areas.

Table 9. Average Properties of Cucaracha Clay Shale

Index Properties	
Liquid limit	86
Plastic limit	32
Plastic index	54
Natural water content	15%
Liquidity index	-0.18
Dry density	110 pcf
Consolidation Properties	
Preconsolidation load*	11 to 98 tsf
Swell pressure*	(0.8 to 1.3) × overburden pressure
Swelling index*	0.05
Coefficient of swelling	0.24×10^{-4} cm^2/sec
Coefficient of permeability*	10^{-10} cm/sec
Coefficient of permeability (field)**	10^{-9} to 10^{-6} cm/sec
Strength Properties	
Undrained shear strength	Highly variable ranging from near zero to about 40 tsf but averaging about 5.5 tsf for more slickensided specimens and about 16.5 tsf for more intact specimens
Drained strength	
Peak on intact specimens	See Fig. 53
Peak on slickensided specimens	See Fig. 54
Peak on remolded specimens	See Figs. 55 and 56
Residual (average)	See Fig. 52 ($c'_r = 0$; $\phi'_r = 7.5$ deg)

* Determined from laboratory data.
** Determined from piezometric data.

LITERATURE CITED

Annual Report (1905-1916); Annual Report of the Isthmian Canal Commission and the Panama Canal for the Fiscal Year Ended 30 June (published annually).

APICSC (1970); Final Report of the Atlantic-Pacific Interoceanic Canal Study Commission, U. S. Government Printing Office, Washington, D. C.

Banks, D. C, et al. (1975); "Study of Clay Shale Slopes Along the Panama Canal, Report 3: Engineering Analyses of Slides and Strength Properties of Clay Shales Along the Gaillard Cut," Technical Report S-70-9, U. S. Army Engineers Waterways Station, Vicksburg, Mississippi.

Bertrand, M., and Zurcher, P. (1899); "Etude géologique sur l'Isthme de Panama," Rapport de la Commission, Campagnie Nouvelle du Canal de Panama etc., Annex I, pp. 85-120, Paris 1899. (Translated by CPT J. C. Oakes, U. S. Army in the Report of the U. S. Board of Consulting Engineers for the Panama Canal, Government Printing Office, Washington, D. C., 1906.)

Binger, W. V. (1948); "Analytical Studies of Panama Canal Slides," Proceedings of the Second International Conference on Soil Mechanics and Foundation Engineering, Vol. 2, p. 54. Also published in Panama Canal Company (1947). "Isthmian Canal Studies, Appendix 12: Slopes and Foundations," Report of the Governor of the Panama Canal, Diablo Heights, Canal Zone.

Bishop, A. W. (1955); "The Use of the Slip Circle in the Stability Analysis of Slopes," Geotechnique, Vol. 5, No. 1, March, pp. 7-17.

Bishop, A. W., and Bjerrum, L. (1960); "The Relevance of the Triaxial Test to the Solution of Stability Problems," Proceedings of the ASCE Research Conference on Shear Strength of Cohesive Soils, Boulder, Colorado, pp. 437-501.

Bishop, A. W., and Morgenstern, N. R. (1960); "Stability Coefficients for Earth Slopes," Geotechnique, Vol. 10, No. 4, December, p. 129.

Cameron, I. (1971); The Impossible Dream - The Building of The Panama Canal, William Morrow & Company, New York.

Canal Record (1907-1932); Weekly information bulletin, Vols. 1-26, published by the Panama Canal Company, Balboa Heights, Canal Zone.

Casagrande, A., and Shannon, W. L. (1948); "Research on Stress-Deformation and Strength Characteristics of Soils and Soft Rocks Under Transient Loading," Soil Mechanics Series No. 31, June, Harvard University, Cambridge, Massachusetts.

Collins, L. D. (1942); "Excavation Slopes for the Cucaracha Formation," Special Engineering Division, Panama Canal Company, Diablo Heights, Canal Zone (reprinted 1947).

Cross, W. (1924); "Historical Sketch of the Landslides of Gaillard Cut," Appendix A to the "Report of the Committee of the National Academy of Sciences on Panama Canal Slides," Memoirs of the National Academy of Sciences, Vol. XVIII, U. S. Government Printing Office, Washington, D. C., pp. 22-43.

DeLory, F. A. (1957); "Long-Term Stability of Slopes in Over-Consolidated Clays," unpublished Ph. D. thesis, University of London.

EM 1110-2-1906 (1970); Engineer Manual: Engineering and Design - Laboratory Soils Testing, Headquarters, Department of the Army, Office of the Chief of Engineers, Washington, D. C.

Fleming, R. W., Spencer, G. S., and Banks, D. C. (1970); "Empirical Study of Behavior of Clay Shale Slopes," NCG Technical Report No. 15 (in two volumes), U. S. Army Engineer Nuclear Cratering Group, Livermore, California.

Gamble, J. C. (1971); "Durability-Plasticity Classification of Shales and Other Argillaceous Rocks," unpublished dissertation submitted in partial fulfillment of the requirements for the degree of Doctor of Philosophy in Geology, University of Illinois at Urbana, Champaign, Illinois.

Geothals, G. W. (1916a); "Slides at Panama," Supplement to Canal Record, 5 January.

Goethals, G. W. (1916b); "The Dry Excavation of the Panama Canal," Transactions of the International Engineering Congress, Vol. 1, pp. 335-385.

Hamel, J. V. (1973); "Final Report, Rock Strength from Failure Cases: Powerhouse Slope Stability Study, Fort Peck Dam, Montana," Technical Report No. 1-73, May 1973, prepared at South Dakota School of Mines and Technology for U. S. Army Engineer Division, Missouri River, Omaha, Nebraska.

Hammond, R., and Lewin, C. J. (1966); The Panama Canal, Frederick Muller, London, p. 253.

Heley, W., and MacIver, B. N. (1971); "Engineering Properties of Clay Shales, Report 1: Development of Classification Indexes for Clay Shales," Technical Report S-71-6, U. S. Army Engineer Waterways Experiment Station, Vicksburg, Mississippi.

Henkel, D. J. (1957); "Investigations of Two Long-Term Failures in London Clay Slopes at Wood Green and Northolt," Proceedings, Fourth International Conferences on Soil Mechanics and Foundation Engineering, London, Vol. 2, pp. 315-370.

Herrmann, H. G., and Wolfskill, L. A. (1966); "Engineering Properties of Nuclear Craters, Report 5: Residual Shear Strength of Weak Shales," Technical Report No. 3-699, prepared by Massachusetts Institute of Technology for U. S. Army Engineer Waterways Experiment Station, Vicksburg, Mississippi.

Hirschfeld, R. C., Whitman, R. V., and Wolfskill, L. A. (1965); "Engineering Properties of Nuclear Craters, Report 3: Review and Analysis of Available Information on Slopes Excavated in Weak Shales," Techanical Report No. 3-699, prepared at Massachusetts Institute of Technology for U. S. Army Engineer Waterways Experiment Station, Vicksburg, Mississippi.

Hutchinson, J. N. (1967); "The Free Degradation of London Clay Cliffs," Proceedings of the Geotechnical Conference, Oslo, Vol. 1, pp. 113-118.

Hutchinson, J. N. (1970); Unpublished review comments for report by Lutton and Banks (1970).

Hvorslev, M. J. (1951); "Time Lag and Soil Permeability in Groundwater Observations," Bulletin No. 36, April, U. S. Army Engineer Waterways Experiment Station, Vicksburg, Mississippi.

James, P. M. (1970); "Time Effects and Progressive Failure in Clay Slopes," unpublished Ph. D. thesis, University of London.

Johnson, S. J. (1968); "Summary of Report of 1968 Corps of Engineers Task Force (CETAF) to Evaluate Excavation Slope Criteria for Atlantic-Pacific Interoceanic Canal Study," Engineering Feasibility Studies, Atlantic-Pacific Interoceanic Canal, IOCS Memorandum JAX-61, JAX-1998-1, November, U. S. Army Engineer District, Jacksonville, Jacksonville, Florida.

Johnson, S. J. (1969); Report of Chairman of Specialty Session No. 10, Engineering Properties and Behavior of Clay-Shales," Proceedings of the Seventh International Conference of Soil Mechanics and Foundation Engineering, Vol. 3, p. 483.

Krinitzsky, E. L. (1970); Radiography in the Earth Sciences and Soil Mechanics, Plenum Press, New York, 163 pp.

LaGatta, D. P. (1970); "Residual Strength of Clay and Clay-Shales by Rotation Shear Tests," Contract Report S-70-5, prepared at Harvard University for U. S. Army Engineer Waterways Experiment Station, Vicksburg, Mississippi.

Lutton, R. J. et al. (1975); "Study of Clay Shale Slopes Along the Panama Canal, Report 2: History, Geology, and Mechanics of Development of Shales in Gaillard Cut," Vol. 1: "Text" by R. J. Lutton, and Vol. 2: "Plates of Maps and Sections" by R. J. Lutton, R. W. Hunt, and W. L. Murphy with contributions by R. H. Stewart, Technical Report S-70-9, U. S. Army Engineer Waterways Experiment Station, Vicksburg, Mississippi, April 1975 and December 1974, respectively.

Lutton, R. J., and Banks, D. C. (1970); "Study of Clay Shale Slopes Along the Panama Canal, Report 1: East Culebra and West Culebra Slides and the Model Slope." Technical Report S-70-9, U. S. Army Engineer Waterways Experiment Station, Vicksburg, Mississippi, November.

MacDonald, D. F. (1913); "Excavation Deformations," Twelfth International Congress, pp. 779-792.

MacDonald, D. F. (1915); "Some Engineering Problems of the Panama Canal in Their Relation to Geology and Topography," U. S. Bureau of Mines Bulletin 86, 88 pp.

MacDonald, D. F. (1924); "The Geology of the Panama Canal with Special Reference to the Slides," Appendix B to the "Report of the Committee of the National Academy of Sciences on Panama Canal Slides," Memoirs of the National Academy of Sciences, Vol. XVIII, U. S. Government Printing Office, Washington, D. C.

MacDonald, D. F. (1947); "The Panama Canal Third Locks Project: Panama Canal Slides," Department of Operation and Maintenance, Panama Canal Company, Diablo Heights, Canal Zone.

Mack, G. (1944); Land Divided; A History of the Panama Canal and Other Isthmian Canal Projects. A. A. Knopf, New York.

McCullough, D. (1977); The Path Between the Seas: The Creation of the Panama Canal: 1870-1914. Simon and Schuster, New York.

Mitchell, J. K. (1961); "Fundamental Aspects of Thixotropy in Soils," Transactions, American Society of Civil Engineers, Vol. 126, Part I, pp. 1586-1620.

Morgenstern, N. R., and Price, V. E. (1965); "The Analysis of the Stability of General Slip Surfaces," Geotechnique, Vol. 15, No. 1, March, p. 79.

Morgenstern, N. R. (1968); "Ultimate Behavior of Rock Structures," Chapter 10 of Rock Mechanics in Engineering Practice. Edited by K. G. Stagg and O. C. Zienkiewicz, John Wiley & Sons, New York.

NAS (1924); "Report of the Committee of the National Academy of Sciences on Panama Canal Slides," Memoirs of the National Academy of Sciences, Vol. XVIII, U. S. Government Printing Office, Washington, D. C.

Palladino, D. J. (1971); "Slope Failures in an Over-Consolidated Clay, Seattle, Washington," unpublished dissertation submitted in partial fulfillment of the requirements for the degree of Doctor of Philosophy in Civil Engineering, University of Illinois at Urbana, Champaign, Illinois.

PCC (1942); "Report of Tests in Pedro Miguel Test Pit No. 3," Special Engineering Division, The Panama Canal Company, Diablo Heights, Canal Zone.

PCC (1947); "Isthmian Canal Studies, Appendix 12: Slopes and Foundations," Report of the Governor of the Panama Canal, Diablo Heights, Canal Zone.

PCC (1969); "Hodges Hill Study, Report of Laboratory Tests on Rock Samples," unpublished report, The Panama Canal Company, Balboa Heights, Canal Zone.

SAD (1969); "Laboratory Results, East Culebra Slide Area, Boring 14-D-37," Engineering Feasibility Studies, Atlantic-Pacific Interoceanic Canal, Route 14, Panama, IOCS Memorandum JAX-80, JAX 1803.10-P, August, U. S. Army Engineer District, Jacksonville, Jacksonville, Florida.

Scott, J. S., and Brooker, E. W. (1968); "Geological and Engineering Aspects of Upper Cretaceous Shales in Western Canada," Paper 66-37, Geological Survey of Canada, Department of Energy, Mines, and Resources, Ottowa.

Seed, H. B. (1968); "Landslides During Earthquakes Due to to Liquefaction" (Fourth Terzaghi Lecture), Proceedings of the American Society of Civil Engineers, Journal of the Soil Mechanics and Foundations Division, Vol. 94, No. SM5, pp. 1053-1122.

Skempton, A. W. (1964); "Long-Term Stability of Clay Slopes" (Fourth Rankine Lecture), Geotechnique, Vol. 14, No. 2, June, pp. 77-101.

Skempton, A. W. (1970); "First-Time Slides in Over-Consolidated Clays," Geotechnique, Vol. 20, No. 3, September, pp. 320-324.

Skempton, A. W. (1977); "Slope Stability of Cuttings in Brown London Clay," Proceedings of the Ninth Internation Conference on Soil Mechanics and Foundations Engineering, Vol. 3, Tokoyo, Japan.

Skempton, A. W., and Hutchinson, J. N. (1969); "Stability of Natural Slopes and Embankment Foundations," Proceedings of the Seventh International Conference on Soil Mechanics and Foundations Engineering. State-of-the-Art Volume, p. 291.

Skempton, A. W., and La Rochelle, P. (1965); "The Bradwell Slip: A Short-Term Failure in London Clay," Geotechnique, Vol. 15, No. 3, September, pp. 221-242.

Smith, C. K., and Lutton, R. J. (1974); "Field Tests of the Cucaracha Formation, Panama Canal, 1942-1946," Miscellaneous Paper S-74-16, U. S. Army Engineers Waterways Experiment Station, Vicksburg, Mississippi.

Taylor, D. W. (1948); Fundamentals of Soil Mechanics, John Wiley & Sons, New York.

Terzaghi, K. (1936); "Stability of Slopes in Natural Clay," Proceedings, First International Conference on Soil Mechanics and Foundations Engineering, Boston, Massachusetts, Vol. 1, pp. 161-165.

Terzaghi, K. (1962); "Discussion of Horizontal Stresses in an Overconsolidated Eocene Clay' by A. W. Skempton," Proceedings, Fifth International Conference on Soil Mechanics and Foundations Engineering, Paris, France, Vol. 3, p. 144.

Thompson, T. F. (1947); "Origin, Nature, and Engineering Significance of the Slickensides in the Cucaracha Clay Shales," Isthmian Canal Studies Memorandum 245, Panama Canal Company, Diablo Heights, Canal Zone.

Townsend, F. C., and Banks, D. C. (1974); "Preparation Effects on Clay Shale Classification Indexes," paper presented at American Society of Civil Engineers Natural Meeting on Water Resources Engineering, 21-25 January 1974, Meeting Preprint 2140, Los Angeles, California.

Woodring, W. P. (1957, 1964); "Geology and Paleontology of Canal Zone and Adjoining Parts of Panama," U. S. Geological Survey Professional Paper 306-4-a, -c, U. S. Government Printing Office, 297 pp.

Wright, S. G. (1969); "A Study of Slope Stability and the Undrained Shear Strength of Clay Shales," unpublished dissertation submitted in partial fulfillment of the requirements for the degree of Doctor of Philosophy in Engineering, University of California, Berkeley.

Yudhbir (1969); "Engineering Behavior of Heavily Overconsolidated Clays and Clay Shales with Special Reference to Long-Term Stability," unpublished dissertation submitted in partial fulfillment of the requirements for the degree of Doctor of Philosophy, Cornell University, Ithaca, N. Y.

APPENDIX A: LABORATORY TESTS

Introduction

Data contained in this appendix were taken from WES test results (Lutton and Banks, 1970; Banks et al., 1975). Laboratory tests were conducted on representative clay shale samples of the Cucaracha formation taken from borings during the WES study of clay shale slopes along the Panama Canal. Since few results are available on samples taken only from the East Culebra Slide area, data are additionally presented from tests on Cucaracha samples from other boring locations, specifically the Model Slope, West Culebra Slide, and South Cucaracha Slide. This appendix primarily addresses the determination of shear strength parameters of the Cucaracha clay shale, although descriptions of tests methods, along with test results, are presented for other properties. Test methods were conducted in general accordance with the Corps of Engineers Manual for Laboratory Soils Testing (EM 1110-2-1906, 30 November 1970) with certain modifications for use of the high capacity consolidation test apparatus and preparation of slurry-consolidated samples for shear testing.

Test Procedures

Atterberg limits, grain-size, and specific gravity analyses

Two general procedures were followed in preparing the materials. In the first series of tests (Lutton and Banks, 1970), the sample was broken down at its natural water content by the shaving action of a salad grater, spread in a flat tray, and air-dried for 48 hr. The material was then ground in a mortar with a rubber-tipped pestle to produce a powder that would pass the No. 40 sieve. The powder was slaked in distilled water for 48 hr and then dried back to a water content above the liquid limit. A thin layer of the slurry was worked on a glass plate with a steel spatula to break down any remaining lumps. In the second series of tests (Banks et al., 1975), after being air-dried for 48 hr, the material was slaked in distilled water (sufficient for a water content of twice the estimated liquid limit) for at least 48 hr. The resulting slurry was blenderized for 10 min, washed through a No. 40 sieve, and drained in a plaster of

paris dish lined with filter paper. A thin layer of the drained slurry, at a water content above the liquid limit, was worked on a glass plate with a steel spatula. Both the liquid and plastic limits were determined by working from the wet side.

The first method (the air-dried procedure) was used during a period of experimental testing by WES to develop standardized procedures for determining the Atterberg limits of clay shale materials. The work leading to the three standardized procedures for the Corps of Engineers to use, as contained in EM 1110-2-1906, is described by Heley and MacIver (1971). As a result of the experimental work, the first method is not a recommended procedure; the second method is the recommended primary procedure. Discussion of the differences in methods has been given by Townsend and Banks (1974).

The grain-size analyses were performed only on material processed as described above for the first series of tests, i.e., the air-dried procedure. Approximately 150 gm of the slurry were selected. The material was split into two portions; one portion of approximately 75 gm was oven-dried for a water content determination for use in computation of the weight of solids in the grain-size analyses. The other portion was used for a hydrometer analysis described in EM 1110-2-1906 to determine the particle size distribution between 0.074 mm (No. 200 sieve) and 0.001 mm. After the hydrometer analysis, the specimen was wet-sieved through the No. 200 sieve, and the material retained was oven-dried. The oven-dried material was then dry-sieved through the Nos. 40 and 80 sieves.

The specific gravity of solids was determined on slurry material by the procedures described in EM 1110-2-1906.

Consolidation and swell
pressure tests (combined)

Two techniques were used to determine the consolidation characteristics of the Cucaracha clay shale (Lutton and Banks, 1970; Banks et al., 1975).

In the first series (Lutton and Banks, 1970) material was trimmed into a thick-walled consolidation ring to produce a specimen 2.50 in. in diameter by approximately 0.75 in. high. Porous stones, 0.25 in. thick, were used in the tests. Calibration curves for equipment deformations were obtained and all data corrected.

A small seating load (0.02 tsf) was initially placed on each specimen for about 30 min. The load was then increased to three-fourths the estimated effective overburden pressure (based on groundwater level at the ground surface), followed by inundation of the specimen with distilled water. The load was slowly increased in 0.25- to 0.50-tsf increments until the specimen showed no more tendency to swell. The final load was allowed to remain on the specimen for a minimum of 48 hr, but more commonly about 168 hr (one week), to verify that no more swelling was occurring. The load at this stage was designated as the swelling pressure p_s. The consolidation portion of the test was begun by application of additional loads in increments to a maximum of 200 tsf. Each load was left on the specimen until the time-compression curve indicated that primary consolidation was complete (generally 24 to 48 hr). Unloading was accomplished in increments with 64-, 16-, and 0.02-tsf loads maintained until the time-expansion curve indicated that primary swelling was complete. Generally, rebound was allowed to proceed for at least 48 hr at the higher rebound loads; at the final rebound load (0.02 tsf), specimens continued to increase in height at a decreasing rate even for periods up to five to seven days.

For the second series, material was trimmed into a fixed-ring, sealed consolidometer to produce specimens approximately 0.82 in. high and 4.44 in. in diameter. The height of the trimmed specimens was less than the 1.0-in. height of the ring to accommodate the top porous stone. The specimens were loaded by a hydraulically controlled, high-capacity loading apparatus with an electronic measuring system. Vertical load and compression (or expansion) measurements were continuously recorded on a strip chart. Calibration measurements for equipment deformations were obtained, and changes in height data were corrected.

Specimens were intially placed under a 5-tsf load, flooded with distilled water, and allowed to consolidate. Additional consolidation loads of 10, 20, 50, 100, 200, 300, 400, and 500 tsf were applied. Each load was maintained until the time-compression curve indicated completion of primary consolidation (generally 50 hr). Specimens were allowed to rebound at 300, 100, 50, 20, 10, and 0.07 tsf. Each load was maintained until the time-expansion curve indicated completion of primary swelling. Generally, rebound was allowed to proceed for at least 50 hr. Under the

final rebound load (0.07 tsf), specimens continued to swell at a decreasing rate for periods of as long as 10 to 12 days.

Drained direct shear tests, intact specimens

The effective peak shear strength of intact Cucaracha clay shale was determined in three series of drained direct shear tests, using 3-in.-square and 1-in.-thick specimens in a standard direct shear device. Series A test results were reported by Lutton and Banks (1970); Series B and C test results were reported by Banks et al. (1975). In all, 23 specimens under normal effective stresses ranging from 1 to 14 tsf were tested. Specimens were trimmed from undisturbed 6-in. core samples and placed in the shear box for testing. After positioning the shear box in the test machine, the desired normal stress was applied; after 2 min the sample was inundated with distilled water. The changes in height of the specimens were observed for 48 hr, although all tendency for change apparently ceased within 24 hr. Shear was accomplished by displacing the top half of the shear box. The shear rate for Series A was 7.7×10^{-6} in. per min; for Series B, 1.5×10^{-6} in. per min was used; and for Series C, 30×10^{-6} in. per min was used. The tests were terminated at approximately 0.5-in. displacement, i.e., before the residual strength was obtained. Inspection of the test specimens indicated that failure did not always occur entirely along the midheight plane and that many specimens contained hard pieces interbedded in a soft matrix.

Drained direct shear tests, slickensided specimens

The effective peak shear strength of slickensided Cucaracha clay shale was determined in three series of drained direct shear tests using 3-in.-square and 1-in.-thick specimens in a standard direct shear device. Test results were reported by Banks et al. (1975). In all, 20 specimens under normal stresses ranging from 1 to 12 tsf were tested. Initially, attempts were made to trim the specimens from undisturbed 6-in. core samples. However, the nature of the slickensides was such that once the material was unrestrained and exposed to the atmosphere, the specimen would check, begin to crumble, and in a matter of minutes, completely fall apart. To overcome this difficulty, 1-in.-thick slices were prepared by sawing through the cardboard sample tubes with a falling-arm metal band

saw. The slices were then placed in a press and a 3-in.-square cutting device was pushed through the specimen. The confinement afforded the specimen by the cardboard ring and the encapsulating paraffin/wax mixture was sufficient to maintain the integrity of the specimen. Porous stones were placed on top and bottom of the specimen before pushing the specimen from the cutting box into the shear box. After the shear box was placed in the testing machine, the desired normal stress was applied to the specimen, followed after 2 min by inundation with distilled water. The changes in the height of the specimens were observed throughout the soaking stage. In Test Series D and E, the soaking period was 10 days; in Test Series F, the specimens were soaked for 70 days. The top half of the shear box was displaced at the rate of 36×10^{-6} in. per min. The tests were terminated after the shear stress-displacement data indicated the effective peak shear strength had been obtained. Inspection of the test specimens indicated that failure occurred along the midheight plane.

Drained direct shear and triaxial
compression tests, slurry-consolidated specimens

The effective shear strength was determined on slurry-consolidated specimens of Cucaracha clay shale materials (Banks et al., 1975). Preparation proceeded as follows:

a. Unused core segments were broken into small chunks and soaked in distilled water for 24 hr, then oven-dried at 50°C to a constant weight.
b. The oven-dried material was mixed with a sufficient quantity of distilled water to produce a water content of about 300 percent and allowed to slake for 48 hr.
c. The soupy mixture was blenderized in approximately 2-qt batches for 10 min and then passed through a No. 40 sieve. The sieved material was placed in an oven at 50°C for a sufficient length of time for the evaporation of excess water to result in a water content of approximately twice the liquid limit.
d. After the desired water content had been achieved, the slurry was again placed in the blender for about 3 min to homogenize the slurry.
e. A sufficient quantity of slurry to obtain a consolidated sample height of 6 in. was pulled slowly under vacuum into an

8-in.-diam by 18-in.-high consolidometer. The slurry was consolidated under small increases in load to approximately 3 tsf over a period of 55 days. The consolidation load was removed over a 24-hr period and the sample pushed out of the consolidometer.

Nine specimens for direct shear tests were trimmed and placed in the test apparatus within one-half day of sample recovery. Portions of the sample were used in the determination of Atterberg limits, water contents, and specific gravity of solids; hydrometer analyses; and for study using scanning electron microscope and X-radiography techniques. Remaining parts of the sample were coated with a paraffin/wax mixture and stored in a humid room. Two additional direct shear test specimens were prepared from the stored material after about two weeks; two triaxial compression test specimens were prepared after about three months.

The direct shear specimens were 3 in. square and varied in height from 0.5 to 0.75 in. After placing in the shear box, consolidation stresses were applied to the specimens in 3-tsf increments until the desired normal stress for shear testing was reached. The changes in height of the specimens were observed during each consolidation increment to ensure that primary consolidation was completed before additional stresses were applied. The specimens were sheared at the rate of 60×10^{-6} in. per min.

Consolidated-undrained triaxial compression tests with pore pressure measurements (i.e., $\overline{R}$ test) were performed on two specimens trimmed from a remaining section of the slurry-consolidated sample. The two specimens (1.4 in. in diam by 3.0 in. high) were saturated in the triaxial apparatus under a final back pressure of 5.0 tsf and then consolidated isotropically under chamber pressures of 3 and 9 tsf, respectively. The specimens were failed at the rate of 7×10^{-4} in./in. per min.

Repeated drained direct
shear tests, precut specimens

The residual shear strength was determined on 3-in.-square by 1-in.-thick specimens that had been precut by a band saw to form a shear surface at midheight. Porous stones were placed on top and bottom of each specimen and the shear box halves adjusted to leave a 1/16-in. gap. Specimens were submerged in distilled water throughout the test.

Tests were conducted under stage loading (i.e., the same specimen was tested more than once under differing normal stresses). After an initial normal stress was applied, shearing was immediately started by pulling the upper half of the shear box, the lower half being fixed. The initial rate of deformation varied from 50×10^{-6} to 15×10^{-6} in. per min. Some tests were conducted on equipment incapable of producing a reversible shear load. Consequently, after approximately 0.3 in. of displacement, the normal stress was reduced to approximately 0.25 tsf, and the specimen manually returned to its initial position. The normal stress for the test was restored and the shearing cycle repeated. In other tests, double acting equipment was used. For these tests, the specimens were repeatedly sheared to a displacement of 0.25 in. on either side of the centered position until the ratio of shear resistance to normal stress indicated that a constant value had been reached (generally in excess of 5 in. of accumulated displacement).

When a minimum shear stress had been reached for a given stage or under a given normal stress, the specimen was returned to its initial or centered position, the normal stress was changed for the next stage, and the shearing process was repeated. Deformation rates varied throughout the tests; in general, rates of approximately 30×10^{-6} in. per min were used for the final pull for each stage. After testing, the halves were separated and the shear surfaces inspected and photographed.

Unconfined compression tests

Unconfined compression tests were performed on full-sized core samples (approximately 6 in. in diameter) with the ends trimmed to provide a length-to-diameter ratio slightly in excess of 2. The specimens were tested under controlled strain conditions; the loading rate was about 1×10^{-4} in./in. per min.

Test Results

Only one WES boring (WEC-1) was made within the bounds of the East Culebra Slide to obtain samples for testing. Additional borings were made by WES into the Cucaracha formation as part of the ongoing work. Test results obtained at the WES are described in the following sections. Table A1 indicates the site, boring designation, sample number and depth, and test assignments.

Descriptive properties

The general material description of the Cucaracha materials presently found at the East Culebra Slide is shown on the log for boring WEC-1 (Fig. 49, main text). The detailed descriptions of samples showed the Cucaracha clay shale to be medium hard to hard and capable of being polished along cut surfaces, indicating a high clay content (Lutton and Banks, 1970). The material indicated no reaction to HCl at natural water content, but insoluble residue tests indicated 9 to 13 percent loss on immersion in HCl. The material slaked to grains very rapidly when immersed in distilled water in an air-dried condition. Slower rates and less complete breakdown occurred as specimens in an air-dried condition were slaked in ethylene glycol and at natural water content in both distilled water and ethylene glycol.

Material from the transitional zone at the bottom of the Cucaracha formation was hard and capable of being polished to a dull gloss, indicating possibly a clay content lower than in other portions of the Cucaracha. The samples indicated some slight amount of reaction to HCl at natural water content, mostly on material in the form of small concretions; insoluble residue tests indicated from 10 to 16 percent loss on immersion in HCl. The slaking behavior was similar to that noted on the other Cucaracha clay shale.

On the basis of the similarity of the clay shales in the transition zone with clay shales from the remaining portions of the Cucaracha formation, no further distinction will be made in discussing the test results.

Table A2 shows values obtained on samples of Cucaracha clay shale for the Atterberg limit determination, percent material smaller than 0.002 mm (<2μ), specific gravity, field water content and water content, dry density, void ratio, and percent saturation determined as part of other laboratory tests.

Atterberg limits. The results obtained from the Atterberg limit determinations are shown in Table A2 to vary significantly from sample to sample and even within a sample. The range of values is shown in Fig. A1. Although the two different procedures produce liquid limits (LL) and plastic index (PI) values that plot near and in most cases slightly above the A-line, the blenderized procedure apparently causes a large increase in the liquid limits with only a small increase in the plastic limits (PL).

These changes are shown below by values averaged from Table A2.

	LL	PL	PI
Air-dried procedure	68	29	39
Blenderized procedure	86	32	54

The Atterberg limits for samples taken from boring WEC-1 in the East Culebra Slide were all determined by use of the air-dried procedure. These values are plotted with depth in Fig. 49, main text.

Grain-size analyses. Grain-size distributions obtained from samples in boring WEC-1 are shown in Fig. 49, main text. All determinations were made on material that was broken down with the air-dried procedure. As shown by values contained in Table A2, on the average, 37 percent of the material (boring WEC-1) is smaller than 0.002 mm; by comparison, materials from other borings indicated an average of only 22 percent to be smaller than 0.002 mm. No grain-size distributions were obtained for samples broken down by the blenderized procedure.

Water content. The water content was typically about 2 percent higher on field samples than was reported from undisturbed samples in the laboratory. The differences could reflect some drying of undisturbed samples during storage but more likely indicate drying during preparation of test specimens. In any case, the water content was about 10 percentage points lower than the plastic limit for all material tested. The overall variation of water content suggests only a slight decrease with depth (Fig. 49, main text).

Dry density. The dry densities ranged from 90.3 to 131.4 pcf; the average value (Table A2) was 110 pcf.

Specific gravity. The specific gravity ranged from 2.73 to 2.85; the average value (Table A2) was 2.78.

Consolidation characteristics

Consolidation test results, using loads up to 200 tsf, were given by Lutton and Banks (1970). Test results obtained with the high capacity consolidation test apparatus (loads up to 500 tsf) were reported by Banks et al. (1975). Results from both test series are shown in Table A3.

The swell pressures, determined on the first series of tests, appear to be approximately equal to or slightly greater than the existing overburden. For the second series (boring WCSE-1), no significant swelling

occurred under the 5-tsf seating load, indicating the swelling pressure must be less than 5 tsf. Since the pressure-void ratio curves for the first series of tests exhibited considerable curvature at the maximum applied stress of 200 tsf, the preconsolidation load could not be defined. On the second series (maximum applied stress of 500 tsf) the preconsolidation load was well defined but did not show a consistent trend to increase with depth (Banks et al., 1975).

Since materials in the study area are in the rebound stage, the swelling index, C_s, time at 50 percent rebound, t_{50}, the coefficient of swelling, c_s, and coefficient of permeability, k, were all computed from the unloading portion of the consolidation curves. For the first series, data were computed between the 16- and 0.02-tsf loads; for the second series, data were computed between the 20- and 10-tsf loads. Values for the parameters listed above are shown for individual tests in Table A3.

Effective peak shear
strengths, intact specimens

The results of drained direct shear tests on intact specimens of Cucaracha clay shale are shown in Figs. A2-A6; a summary of results is shown in Table A4. Insufficient data were collected during the consolidation phase of Series A tests to develop time-consolidation curves (Lutton and Banks, 1970). Those data collected from Series B (Fig. A2) are similar to Series C tests and are thought to be typical of the behavior of Series A specimens (Banks et al, 1975). Initially, the specimens compressed in an amount proportional to the magnitude of the normal stress. Only slight additional compression of the specimens was noted during the 2 min before the specimens were inundated. The addition of water caused an immediate increase in the compression, followed by an expansion phase. Expansion continued for periods up to about one day (1440 min), after which the specimens appeared to be in equilibrium.

Data collected during shear are shown in Figs. A3-A5. The specimens compressed during initial stages of shear until, approximately at the attainment of peak strength, expansion was noted. The expansion was dramatic for specimens of small normal stresses (less than about 4 tsf); for large normal stress, the expansion appeared to level off and to become fairly constant for displacements beyond the peak shear strength.

Interpretation of effective peak shear strength parameters is difficult because of the scatter in test data (Table A4, Fig. A6). After testing, observations indicated that about one-half of the specimens contained hard pieces of material in the shear plane, and some exhibited an unusually high peak shear stress. Because of the wide scatter in peak shear stress for specimens of individual samples, only the presentation of an upper and lower limiting strength envelope appeared appropriate. All specimens indicated strengths in excess of a lower limiting envelope defined by $c'_p = 0.5$ tsf, $\phi'_p = 28$ deg. Specimens in this range exhibited a plastic-type failure with little or no drop in shear strength after peak (Figs. A3-A5). A curved line appeared to best describe the upper limiting envelope. The curve was approximated by a bilinear envelope defined by $c'_p = 5.0$ tsf, $\phi'_p = 28$ deg for $\sigma'_n > 3$ tsf and by $c'_p = 0$, $\phi'_p = 65$ deg for $\sigma'_n < 3$ tsf. Specimens in this upper range exhibited a brittle failure with a large drop in shear strength after peak (Figs. A3-A5).

Effective peak shear
strengths, slickensided specimens

The results of drained direct shear tests on slickensided Cucaracha clay shale specimens are shown in Figs. A7-A14 and summarized in Table A5. In all, 20 specimens were tested under normal stresses ranging from 1 to 12 tsf. The tests were conducted on samples obtained from boring WEC-1 at the East Culebra Slide and piezometer borings adjacent to WES boring WMS-1 at the Model Slope (refer to Tables A1 and A2). Time-compression behavior of specimens is shown in Figs. A7-A9. As indicated, compression was nominal under the applied normal stress. The specimens continued to compress until they were inundated with distilled water, whereupon the rate of compression increased significantly. The compression continued at a decreasing rate until, after 24 hr, generally only small changes in specimen heights were being recorded. Shearing was started on specimens in Test Series D and E after immersion for 10 days. Although by that length of time the rate of compression was less than 0.0001 in. per day, specimens in Test Series F were sheared after being immersed for 70 days.

The time-compression behavior of the slickensided specimens (Figs. A7-A9) were in opposition to that observed for the intact specimens (Fig. A2) in that no specimen exhibited any net tendency to expand. It is envisioned that the slickensides gave the water access to the interior of

the specimens and, while expansion may have occurred internally, the net effect was to cause softened material to fill spaces created by slickensides. The weakening effect was indicated by the shear tests following the soaking period.

Figures A10-A12 show the shear test data for Series D, E, and F, respectively. At low normal stresses (generally less than about 6 tsf), the specimens compressed during the initial shear phase but exhibited a tendency to expand at displacements near the peak strength and beyond. At higher normal stresses, the specimens generally exhibited compression throughout the test, although the rate usually decreased significantly when the peak shear stress was reached.

Figure A13 shows the effective peak shear strengths obtained from tests on slickensided specimens. The data are consistent among the series with the only significant scatter being indicated at the 6- and 8-tsf normal load. It was anticipated that the additional consolidation time allowed during Test Series F might produce lower peak shear strengths; however, no reduction was evidenced. As interpreted, the average strength envelope is strongly curved for normal stresses less than about 4 tsf. At higher stresses, the approximate linear strength envelope is defined by parameters of c'_p = 1.6 tsf, ϕ'_p = 24 deg.

All slickensided specimens increased in water content during testing (Table A5 and Fig. A14). The increase at an effective normal stress of 2 tsf amounted to about 6 percent; at an effective normal stress of 12 tsf, the increase ranged from 2.5 to 4.5 percent. By comparison, the intact specimens increased in water content from about 0.4 to 0.8 percent (Fig. A14). The relatively larger increase in water content for the slickensided specimens reflects the ability of the water to penetrate through slickensides to the interior of the specimen.

Residual shear strengths

Residual shear strength parameters were determined from test data from repeated drained direct shear tests on specimens with precut planes. Test data are shown in Figs. A15-A23. On the respective figures, the ratio of the minimum shear stress to the effective normal stress is plotted for each pull. Each specimen was repeated sheared until the ratio reached a minimum. Thus the strength envelope shown on each figure reflects the minimum strength obtained. The data indicated zero cohesion

intercepts and friction angles, ϕ'_r, varying from 4 to 11 deg with an average of about 7.5 deg.

Tests on slurry-consolidated samples

Remaining portions of Samples 3, 5, 7, and 8 from boring WCSE-1 were used to prepare a slurry-consolidated sample of the Cucaracha clay shale. The details of sample preparation have been described above. After consolidation, the resulting 6-in.-high specimen exhibited only a small variation in water content over the height of the sample (Fig. A24), with an average value of about 50 percent. The liquid limit was 74; the plastic limit was 31, and the specific gravity of solids was 2.74. Hydrometer analyses of 1-in.-high increments from one segment of the sample and an isodensity scan of a 1/2-in.-thick segment, 4.5 in. high, indicated uniform particle size and density over the height of the sample.

A small specimen of the slurry-consolidated sample was observed under the scanning electron microscope and showed a marked textural difference, indicating general horizontal orientation of clay platelets. Figures A25 and A26 show photographs of a horizontal and a vertical surface within the consolidated specimen. Careful study of Fig. A25 reveals flat platelets lying in the photograph, which indicates an orientation of flat faces parallel to the horizontal plane. Similarly, Fig. 26 shows the edges of platelets stacked vertically. Since all samples of clay shales examined had a high percentage of montmorillonite, flat lying particles would be expected.

Drained direct shear tests. Five horizontal direct shear specimens (1-5) were trimmed from the central segment (Fig. A24), with specimen numbers indicating location sequence from bottom to top of the sample. Specimens 3A and 4A were taken from the top of the specimen for use in check tests two weeks after initial testing was started. Four vertical direct shear specimens (6-9) were trimmed from sections adjacent to the central section, as shown in Fig. A24.

Results of the drained direct shear tests are shown in Figs. A27 and A28 and summarized in Table A6. The shear strength versus effective normal stress shown in Fig. A28 indicates curved effective strength envelopes with horizontal specimens having a slightly higher shear strength (ϕ' = 17.5 deg) than the vertical specimens (ϕ' = 15 deg) at normal loads less than about 6 tsf. At effective normal stresses greater than 6 tsf, the

reverse occurred. The effective shear strength envelopes shown in Fig. A28 compare closely with results obtained by LaGatta (1970) on normally consolidated specimens of slaked-crushed Cucaracha clay shale from Hodges Hill.

Clay platelet orientation may explain the difference in strength results between vertical and horizontal direct shear test specimens. In the horizontal specimens, shear was parallel to clay platelet orientation, while in vertical specimens shear was across clay platelets. Under increasing normal loads, the vertical clay platelets in vertical specimens may have been pushed closer together or bent and offered more resistance to shearing.

Triaxial tests. Consolidated-undrained triaxial compression tests with pore pressure measurements ($\overline{R}$ tests) were performed on two specimens trimmed from a remaining section of the slurry-consolidated sample (Fig. A24). The test was conducted on material that had been sealed in a paraffin/wax mixture following consolidation and stored in a humid room for three months before testing. The results of the tests are shown in Fig. A29 and pertinent specimen data are summarized in Table A7.

The shear stress versus effective normal stress shown in Fig. A29 indicates a slightly curved drained strength envelope that can be approximated by two linear segments. For effective normal stresses less than about 4 tsf, the effective shear strength envelope is defined by $c' = 0$ tsf, $\phi' = 20$ deg; and above 4 tsf, by $c' = 0.1$ tsf, $\phi' = 18.5$ deg. These values are slightly higher than the value of $\phi' = 17.5$ deg indicated by the direct shear tests on horizontally cut specimens. The higher effective strength indicated by the triaxial tests may have been caused by a slight gain in strength or thixotropic hardening (Mitchell, 1961) over the three-month storage period. Since the initial water contents of the triaxial specimens (Table A7) were the same as the direct shear specimens (Table A6), the increased strength cannot be attributed to a change in water content.

Undrained shear strengths

No clear trend was evidenced by undrained shear strengths from unconfined compression tests. Apparently, quite low values (0.45 to 0.77 tsf) can occur at shallow depths, whereas values ranging from 2.18 to 8.10 tsf were measured on deeper specimens (Figs. A30 and A31).

Table A1. Test Assignments for Cucaracha Clay Shale Specimens

Site	Boring	Sample No.	Depth ft	Atterberg Limits	Grain Size	Specific Gravity	Dry Density	Consolidation Test	Direct Shear Tests: Intact Specimen	Direct Shear Tests: Slickensided Specimen	Direct Shear Tests: Precut Specimen	Direct Shear Tests: Slurry-Consolidated Specimen	Triaxial Compression R	Unconfined Compression
East Culebra Slide	WEC-1	1	29.8-30.4	x	x									
		2	33.7-34.8	x	x	x								
		3	54.9-56.0	x	x									
		4	62.0-63.2	x	x		x							
		5	65.0-66.4	x	x	x	xx	x		x	x			
		6	72.4-74.2	x	x		xx				x			x
		7	80.2-81.4	x	x									
		9	104.1-104.8	x	x	x								
		10	112.3-114.1	x	x	x	xx	x			x			
		11	121.2-123.1	x	x	x								
		12	132.5-133.6	x	x									
		13	139.0-140.2	x	x		x							x
		14	151.7-153.6	x	x	x	xx	x						x
		17	181.7-183.5	x	x									
West Culebra Slide	WWC-1	1	14.1-14.7	x	x									
		4	52.7-53.9	x	x	x	x	x						
Model Slope	WMS-1	3	26.1-27.5	x	x		x							x
		4	29.3-30.8	x	x	x	xx	x			x			
		6	49.1-52.8	x	x		x				x			
		7	67.9-69.2	x	x		x							x
		8	83.4-85.0	x	x		xxx		xxx					
		10	98.1-99.8	x	x	x	xxx	x			x			x
		12	116.3-117.3	x	x	x	x				x			
		14	149.1-150.6	x	x		x	x			x			
		18	180.0-181.5	x	x		x							
	WMS-P1E	4	22.8-25.3	x						xxxxxx				
		8	137.7-140.2	x		x	xxxx		xxxx					
	WMS-P1F	4	22.7-25.1	x						xxxxxx				
		5	65.0-66.4	x						**xxxxxxx**				
		7	142.0-142.7	x		x	x		x					
South Cucaracha Slide	WCSE-1	1	43.5-44.5	x										
		2	45.0-46.0	x										
		3	52.5-53.6	xx		x	xxxx	**x**	xxx					
		4	58.4-59.2	x										
		5	68.5-69.6	xx		x	xxx		xxx					
		6	75.8-76.7	x										
		7	91.9-92.9	xx		x	xxx		xxx					
		8	100.9-101 9	x		x	xx	x			x			
		9	154.7-155.7	x		x	xxxx	x	xxx					
		10	162.3-163.2	xxxxxx		x	xxx		xxx					
		11	171.9-173.1	xx		x	x	x						
		3,5,7,8	See above for WCSE-1	x	x	x						xxxxxxxxxx	xx	

Table A2. General Properties of Cucaracha Clay Shale

Site	Boring	Sample No.	Depth ft	Atterberg Limits LL	PL	PI	<2μ percent	G_s	Field w percent	Laboratory w percent	Dry Density pcf	e_o	Saturation percent
East Culebra Slide	WEC-1	1	29.8-30.4	99	29	70	47		20.5	20.1			
		2	33.7-34.8	85	29	56	40	2.82	20.5	17.7			
		3	54.9-56.0	61	30	31	28		21.0	21.6			
		4	62.0-63.2	54	28	26	32		19.5	18.2			
										19.0	97.2	0.760	68.5
		5	65.0-66.4	60	26	34	38	2.85	19.1	16.0			
										14.1	116.5	0.528	76.1
										16.9	111.0	0.603	79.9
				73	26	47				17.0			
		6	73.4-74.2	65	29	36	28		20.5	23.1			
										22.1	95.9	0.777	77.6
										21.0	113.2	0.506	100+
		7	80.2-81.4	76	30	46	35		17.0	16.7			
		9	104.1-104.8	74	33	41	37	2.80	16.2	15.8			
		10	112.3-114.1	61	25	36	33	2.79	15.7	13.9			
										15.4	117.5	0.482	89.0
										13.8	111.0	0.569	67.7
		11	121.2-123.1	55	19	36	23	2.73	14.1	13.6			
		12	132.5-133.6	60	25	35	28		23.0	21.8			
		13	139.0-140.2	116	38	78	35		22.1	22.7			
										22.3	99.2	0.731	83.9
		14	151.7-153.6	70	26	44	32	2.80	16.0	13.1			
										17.6	115.0	0.519	95.1
										12.1	120.5	0.451	75.1
		17	181.7-183.5	70	28	42	21						
West Culebra Slide	WWC-1	1	14.1-14.7	49	30	19	12		18.3	17.8			
		4	52.7-53.9	56	33	23	13	2.74	25.1	21.3			
										22.8	103.3	0.657	95.3
Model Slope	WMS-1	3	26.1-27.5	47	28	19	23		14.5	13.3			
										10.5	117.2	0.465	62.1
		4	29.3-30.8	49	26	23	33	2.75	14.4	15.4			
										16.6	114.8	0.496	92.0
										15.6	113.5	0.513	83.6
		6	49.1-52.8	49	25	24	22		14.0	12.3			
										12.6	121.0	0.419	82.7
		7	67.9-69.2	52	26	26	31		15.7	15.0			
										13.9	131.4	0.306	100+
		8	83.4-85.0	57	23	34	26			17.6			
										16.9	115.1	0.492	94.5
										17.0	113.1	0.518	90.2
										16.1	114.1	0.499	88.7
		10	98.1-99.8	48	27	21	22	2.75		16.1			
										16.7	115.7	0.484	95.0
										16.3	111.2	0.544	82.4
										15.6	121.7	0.411	100+
		12	116.3-117.3	102	42	60	27	2.75		27.2			
										31.3	90.3	0.901	95.5
		14	149.1-150.6	52	31	21	13		19.3	18.7			
										17.6	109.4	0.569	85.1
		18	180.0-181.5	50	26	24	22		18.9	15.8			
										19.7	110.6	0.551	98.1
	WMS-P1E	4	22.8-25.3	89	28	61				17.5			
		8	137.7-140.2	92	36	56		2.83		20.5	106.3	0.662	87.6
										23.6	104.0	0.699	95.5
										23.1	105.8	0.670	97.6
										22.4	106.6	0.657	96.5
	WMS-P1F	4	22.7-25.1	69	27	42				15.3			
		5	65.0-66.4	78	30	48				16.8			
		7	142.0-142.7	90	41	49		2.83		22.8	106.1	0.665	97.0
South Cucaracha Slide	WCSE-1	1	43.5-44.5	78	31	47			23.8	23.3			
		2	45.0-46.0	95	25	70			23.8	23.7			
		3	52.5-53.6	79	29	50			19.6	19.7			
				65	32	33		2.80		22.7	104.1	0.679	93.5
										24.6	100.5	0.739	93.2
										24.7	100.5	0.739	93.6
										20.8	98.6	0.773	75.6
		4	58.4-59.2	80	28	52			19.7	15.9			
		5	68.5-69.6	80	27	53			15.1	20.0			
				71	33	38		2.74		17.2	109.0	0.556	84.8
										16.6	113.0	0.514	88.5
										16.7	114.9	0.489	93.6
		6	75.8-76.7	74	29	45			15.5	17.0			
		7	91.9-92.9	76	28	48			17.5	17.5			
				59	27	32		2.80		16.1	111.4	0.569	79.2
										17.0	102.6	0.704	67.6
										16.2	111.9	0.562	80.7
		8	100.9-101.9	81	33	48			19.1	15.9			
								2.75		20.2	109.4	0.569	97.8
										18.2	115.6	0.485	100.0
		9	154.7-155.7	114	26	88			16.7	27.5			
				81	30	51		2.75		16.4	115.3	0.489	92.5
										15.6	121.1	0.418	100.0
										16.0	117.4	0.463	95.0
										15.4	116.1	0.479	88.4
		10	162.3-163.2	120	39	81			27.4	27.2			
				71	30	41		2.81					
				102	32	70				24.7	100.5	0.628	100.0
				96	43	53				23.5	103.0	0.588	100.0
				93	46	47				26.0	98.9	0.801	92.5
				94	29	65							
		11	171.9-173.1	106	38	68			23.4	19.2			
								2.76		22.0	101.9	0.691	87.9

Table A3. Results of Consolidation Tests

Site	Boring	Sample No.	Depth ft		LL	PI	Effective Overburden Pressure tsf	Preconsolidation Pressure tsf	Swell Pressure tsf		C_s		t_{50} sec		$c_s \times 10^{-4}$ cm^2/sec		$k \times 10^{-10}$ cm/sec	
East Culebra Slide	WEC-1	5	65.0-66.4	Note 1	60	34	3.0	>50	2.3	Note 3	0.043	Note 5	15,000	Note 7	0.38	Note 9	1.9
		10	112.3-114.1		61	36	4.8	>25	4.1		0.049		7,800		0.09		0.5
		14	151.7-153.6		70	44	6.3	>50	5.4		0.060		7,200		0.06		0.3
West Culebra Slide	WWC-1	4	52.7-53.9		56	23	2.6	>30	2.8		0.050		9,000		0.09		0.6
Model Slope	WMS-1	4	29.3-30.8		49	23	2.0	>30	2.1		0.018		7,200		1.22		2.3
		10	98.1-99.8		48	21	5.1	>60	6.5		0.040		6,900		0.15		0.8
		18	180.0-181.5		50	24	8.2	>40	12.8		0.052		16,800		0.50		3.2
South Cucaracha Slide	WCSE-1	3	52.5-53.6	Note 2	79	50	3.4	11	--	Note 4	0.09	Note 6	700	Note 8	0.04	Note 10	0.05
		8	100.9-101.9		81	48	6.6	76	--		0.07		700		0.05		0.07
		9	154.7-155.7		114	88	9.2	98	--		0.05		700		0.05		0.05
		11	171.9-173.1		106	68	11.1	26	--		0.05		500		0.06		0.04

Notes
1. Atterberg limits determined by air-dried procedure.
2. Atterberg limits determined by blenderized procedure.
3. Swelling index computed from slope of rebound curve between 16 and 0.02 tsf.
4. Swelling index computed from slope of rebound curve between 20 and 10 tsf.
5. Time of 50 percent rebound for the 16-tsf load.
6. Time of 50 percent rebound for the 20-tsf load.
7. Coefficient of swelling computed between the 16- and 0.02-tsf rebound loads.
8. Coefficient of swelling computed between the 20- and 10-tsf rebound loads.
9. Coefficient of permeability computed between the 16- and 0.02-tsf rebound loads.
10. Coefficient of permeability computed between the 20- and 10-tsf rebound loads.

Table A4. Results of Drained Direct Shear Tests, Intact Specimens

Boring	Sample No.	Specimen	Water Content Initial percent	Water Content Final percent	Void Ratio	Saturation percent	Dry Density pcf	Effective Normal Stress tsf	Peak Shear Stress tsf	Displacement at Peak Shear Stress in.
WMS-1*	8	1	16.9	17.3	0.492	94.5	115.1	4.0	6.27	0.0618
		2	17.0	17.6	0.518	90.2	113.1	8.0	7.62	0.0919
		3	16.1	14.0	0.499	88.7	114.1	12.0	8.85	0.1460
WMS-P1E**	8	1	20.5	24.1	0.662	87.6	106.3	3.0	2.26	0.0618
		2	23.6	24.4	0.699	95.5	104.0	6.0	8.40	0.0459
		3	23.1	23.5	0.670	97.6	105.8	10.0	10.39	0.0313
		4	22.4	23.3	0.657	96.5	106.6	14.0	9.40	0.0376
WMS-P1F**	7	1	22.8	22.4	0.665	97.0	106.1	1.5	3.19	0.0352
WCSE-1†	3	1	24.6	25.5	0.739	93.2	100.5	1.0	1.03	0.0904
		2	24.7	28.8	0.739	93.6	100.5	2.0	1.69	0.0904
		3	20.8	24.8	0.773	75.3	98.6	4.0	2.74	0.0904
	5	1	17.2	21.6	0.556	84.8	109.9	4.0	3.90	0.0368
		2	16.6	19.4	0.514	88.5	113.0	6.0	7.00	0.0354
		3	16.7	18.4	0.489	93.6	114.9	8.0	7.90	0.0382
	7	1	16.1	18.0	0.569	79.2	111.4	8.0	7.16	0.1049
		2	17.0	24.8	0.704	67.6	102.6	10.0	7.74	0.0320
		3	16.2	24.3	0.562	80.7	111.9	14.0	8.09	0.0617
	9	1	15.6	16.0	0.418	100.0	121.1	1.0	2.05	0.0150
		2	16.0	18.0	0.463	95.0	117.4	2.0	5.71	0.0690
		3	15.4	16.8	0.479	88.4	116.1	4.0	3.93	0.0138
	10	1	24.7	28.9	0.628	100.0	100.5	8.0	5.47	0.0981
		2	23.5	27.9	0.588	100.0	103.0	10.0	9.34	0.0526
		3	26.0	28.8	0.801	92.5	98.9	14.0	8.68	0.0928

* Series A tests.
** Series B tests.
† Series C tests.

Table A5. Results of Drained Direct Shear Tests, Slickensided Specimens

Boring	Sample No.	Specimen	Water Content Initial percent	Water Content Final percent	Effective Normal Stress tsf	Peak Shear Stress tsf	Displacement at Peak Shear Stress in.
WEC-1*	5	1	17.0	22.1	4**	3.34	0.1550
WMS-P1E†	4	1	17.5	22.0	2	2.01	0.1330
		2		22.8	4	3.73	0.0699
		3		22.7	6	4.79	0.1287
		4		21.8	8	5.27	0.1060
		5		19.8	10	6.18	0.1060
		6		20.0	12	7.21	0.3540
WMS-P1F††	4	1	15.3	21.8	1	1.04	0.1149
		2		21.1	2	1.90	0.2230
		3		19.8	4	3.54	0.1966
		4		19.4	6	5.18	0.1334
		5		20.1	9	5.48	0.1820
		6		19.8	12	7.37	0.1388
WMS-P1F††	5	1	16.8	23.9	2**	1.82	0.1635
		2		23.8	2‡	2.24	0.2787
		3		21.5	4‡	3.36	0.0868
		4		21.9	6	3.84	0.1495
		5		21.2	8	4.50	0.1999
		6		21.5	10	5.99	0.2326
		7		19.4	12	7.14	0.0980

* Series D tests.
** Specimen A.
† Series F tests.
†† Series E tests.
‡ Specimen B.

Table A6. Results of Drained Direct Shear Tests, Slurry-Consolidated Specimens

Specimen	Height H_o, in.	Water Content w_o %	Water Content w_c %	Void Ratio e_o	Saturation S_o, %	Dry Density pcf	Effective Normal Stress tsf	Peak Shear Stress tsf	Displacement at Peak Shear Stress in.	Remarks
						Horizontal Specimens				
1	0.500	50.0*	46.8	1.348*	101.0*	72.7*	3	0.94	0.173	Undulating, highly polished failure surface through center of specimen
2	0.623	50.0*	39.6	1.374*	99.5*	71.9*	6	1.65	0.110	
5	0.623	50.0*	41.1	1.382	98.9	71.7*	6	1.82	0.114	Sheared up to and along topstone
3	0.623	50.0*	35.4	1.371	99.8*	72.0*	9	2.03	0.202	
3A	0.623	48.7	36.2	1.377	96.7	71.8	9	1.98	0.087	
4	0.750	50.0*	33.5	1.366*	100.0*	72.1*	12	2.40	0.268	Planar failure surface, highly polished
4A	0.750	49.8	35.9	1.388	98.1	71.6	12	2.42	0.104	
						Vertical Specimens				
6	0.500	46.9	--	1.319	97.2	73.6	3	0.81	0.210	Shear planes from center to top stone and bottom stone of opposite ends
7	0.623	49.2	39.6	1.373	98.0	71.9	6	1.65	0.256	Failure surface on both sides of specimen
8	0.623	53.4	36.8	1.443	101.0	69.9	9	2.39	0.120	Apparently planar failure surface
9	0.750	51.0	34.5	1.394	100.0	71.3	12	2.97	0.239	Apparently planar failure surface; semiglossy

Note: LL - 74; PL = 30; PI = 44; and G_s = 2.74.
* Estimated.

Table A7. Results of Consolidated-Undrained Triaxial Tests, Slurry-Consolidated Specimens

Consolidated Stress, $\bar{\sigma}_{3c}$	Water Content		Saturation		Void Ratio		Dry Density		Strain Rate	Effective Stress at $(\sigma'_1/\sigma'_3)_{max}$		
	w_o	w_c	S_o	S_c	e_o	e_c	γd_o	γd_c		$\sigma_1 - \sigma_3$	σ'_3	σ'_1
tsf	%	%	%	%			pcf	pcf	%/min	tsf	tsf	tsf
3.0	49.8	46.0	100	100	1.35	1.23	72.7	76.7	0.061	1.78	1.61	3.39
9.0	50.1	37.3	100	100	1.36	0.95	72.5	87.8	0.063	4.53	4.50	9.03

Notes: 1. $\bar{\sigma}_{3c}$ = effective minor principal stress after consolidation;
o (subscript) = initial; c (subscript) = after consolidation;
$\sigma_1 - \sigma_3$ = deviator stress;
$(\sigma'_1/\sigma'_3)_{max}$ = maximum principal stress ratio;
σ'_3 = minor principal effective stress; and
σ'_1 = major principal effective stress.
2. LL = 74; PL = 30; PI = 44; and G_s = 2.74.

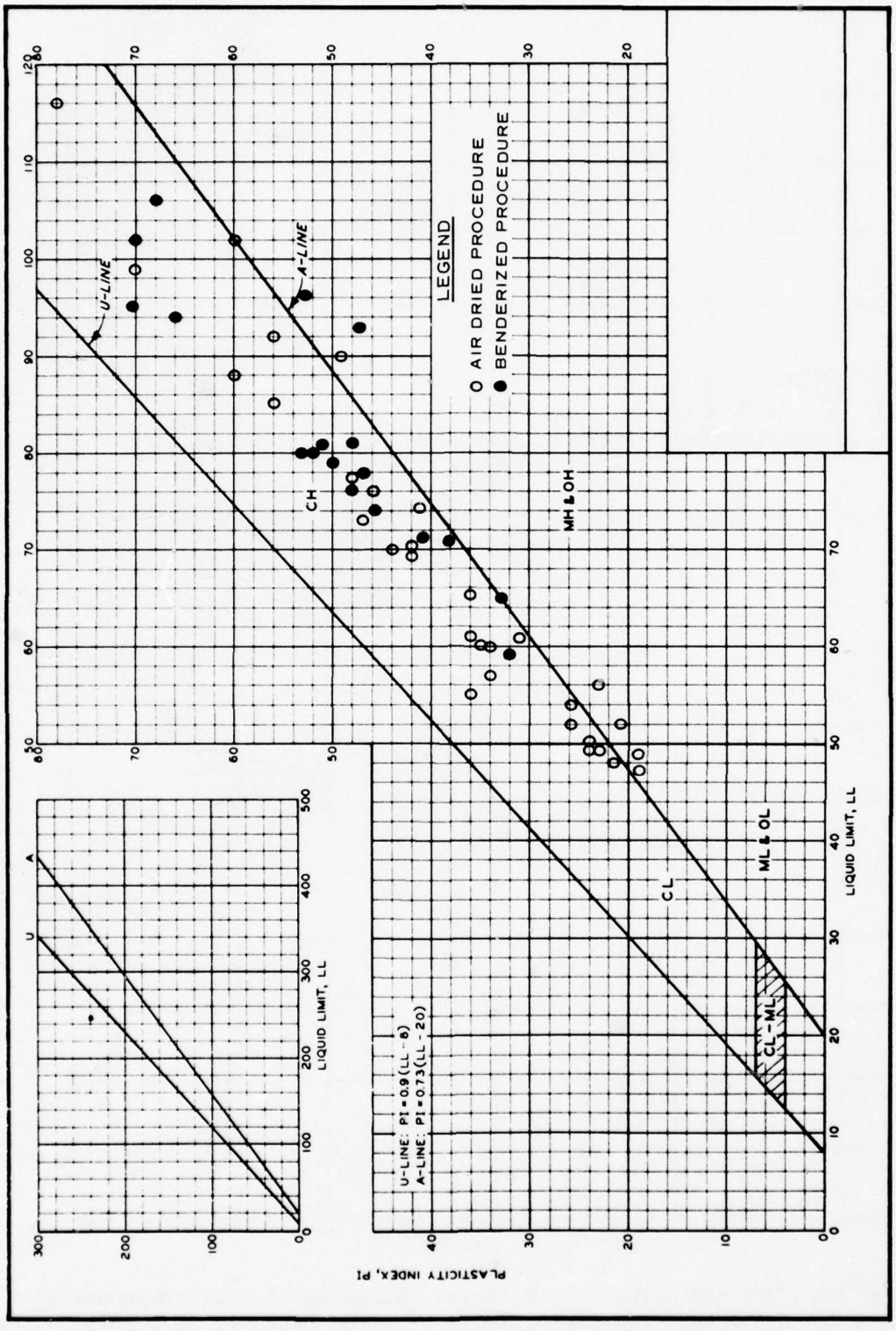

Fig. A1. Plasticity chart

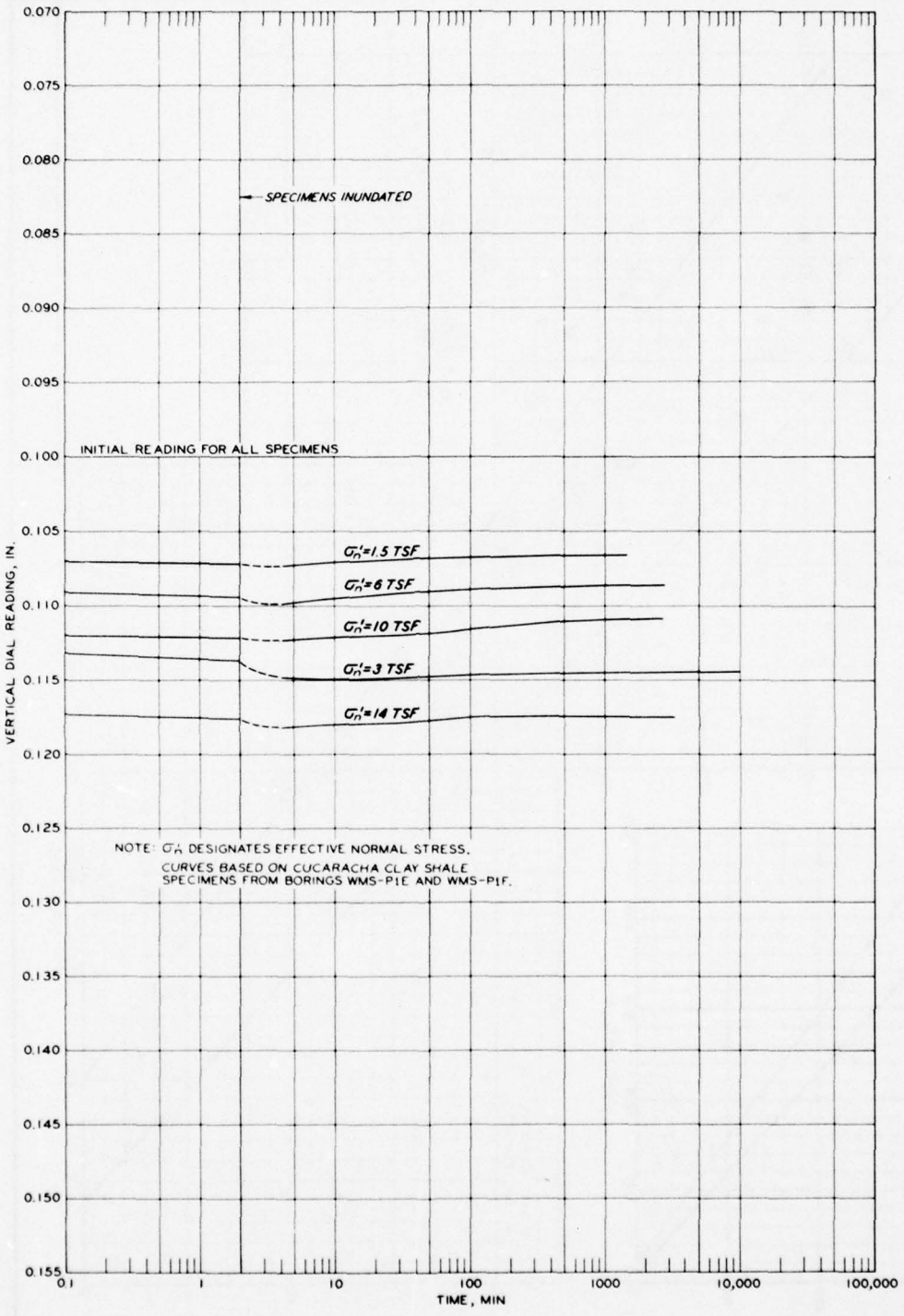

Fig. A2. Drained direct shear tests: examples of time-compression curves for intact specimens, Series B (from Banks et al., 1975)

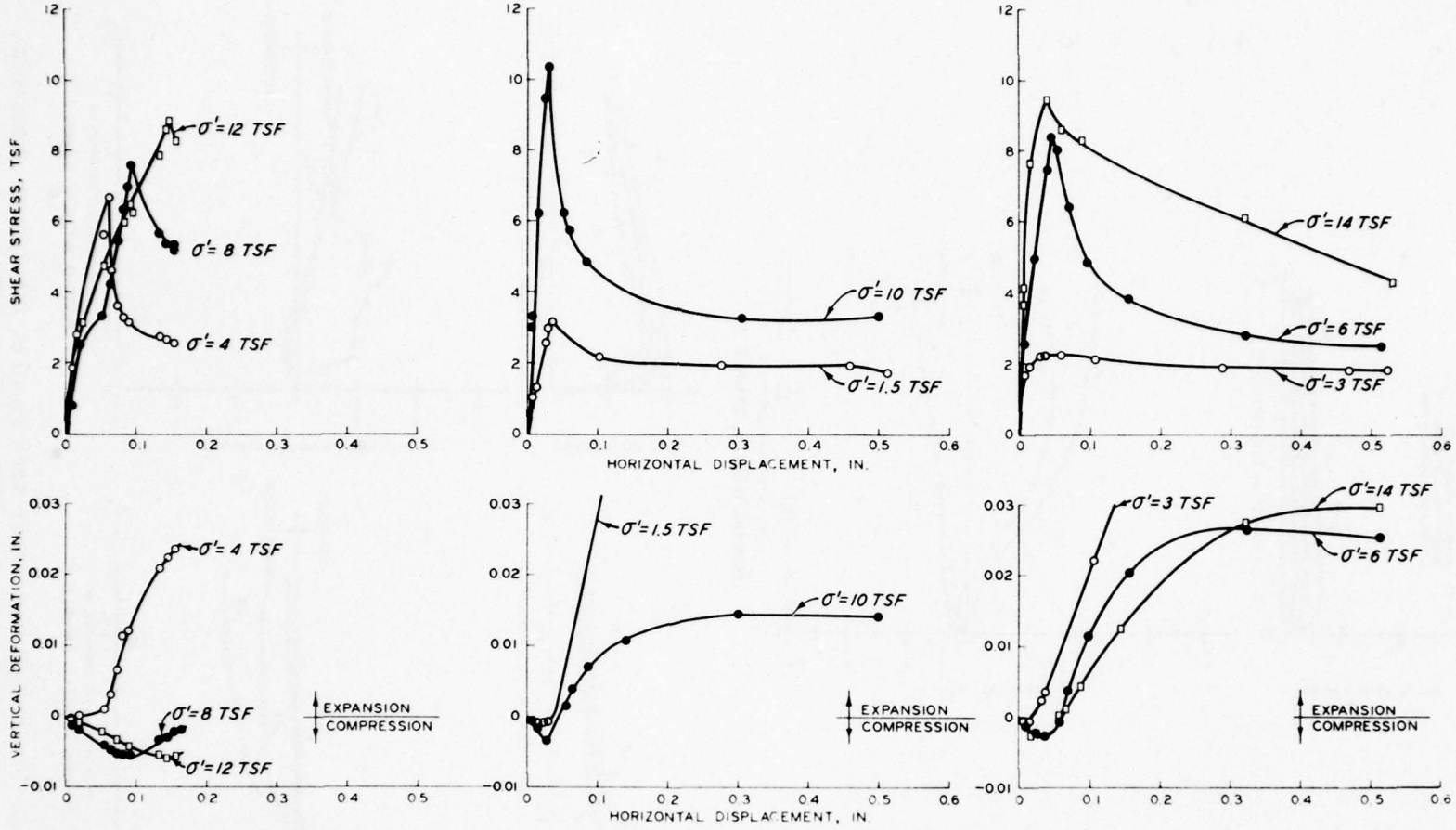

a. Test results--Series A

b. Test results--Series B

Fig. A3. Drained direct shear test results for intact specimens, Series A and B (from Banks et al., 1975)

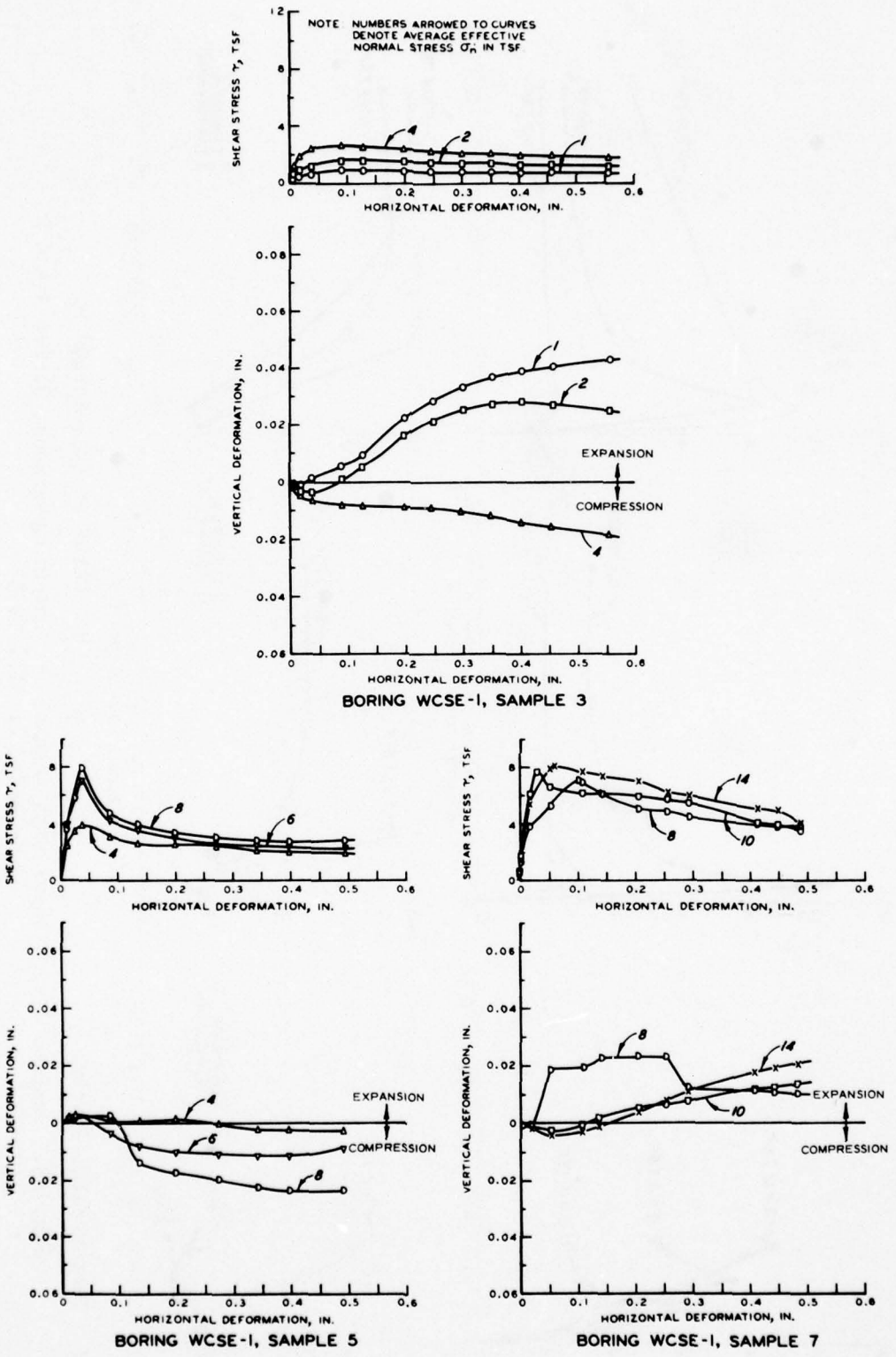

Fig. A4. Drained direct shear test results for intact specimens, Series C (from Banks et al., 1975)

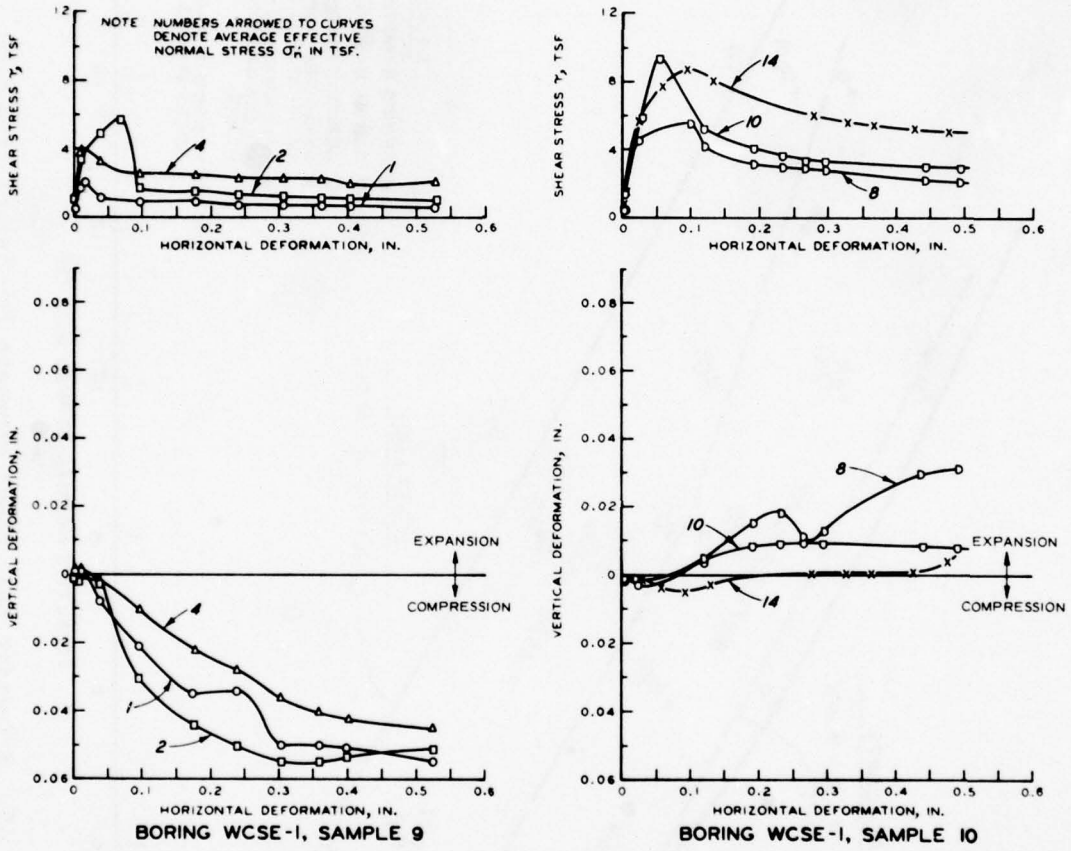

Fig. A5. Drained direct shear test results for intact specimens, Series C, concluded (from Banks et al., 1975)

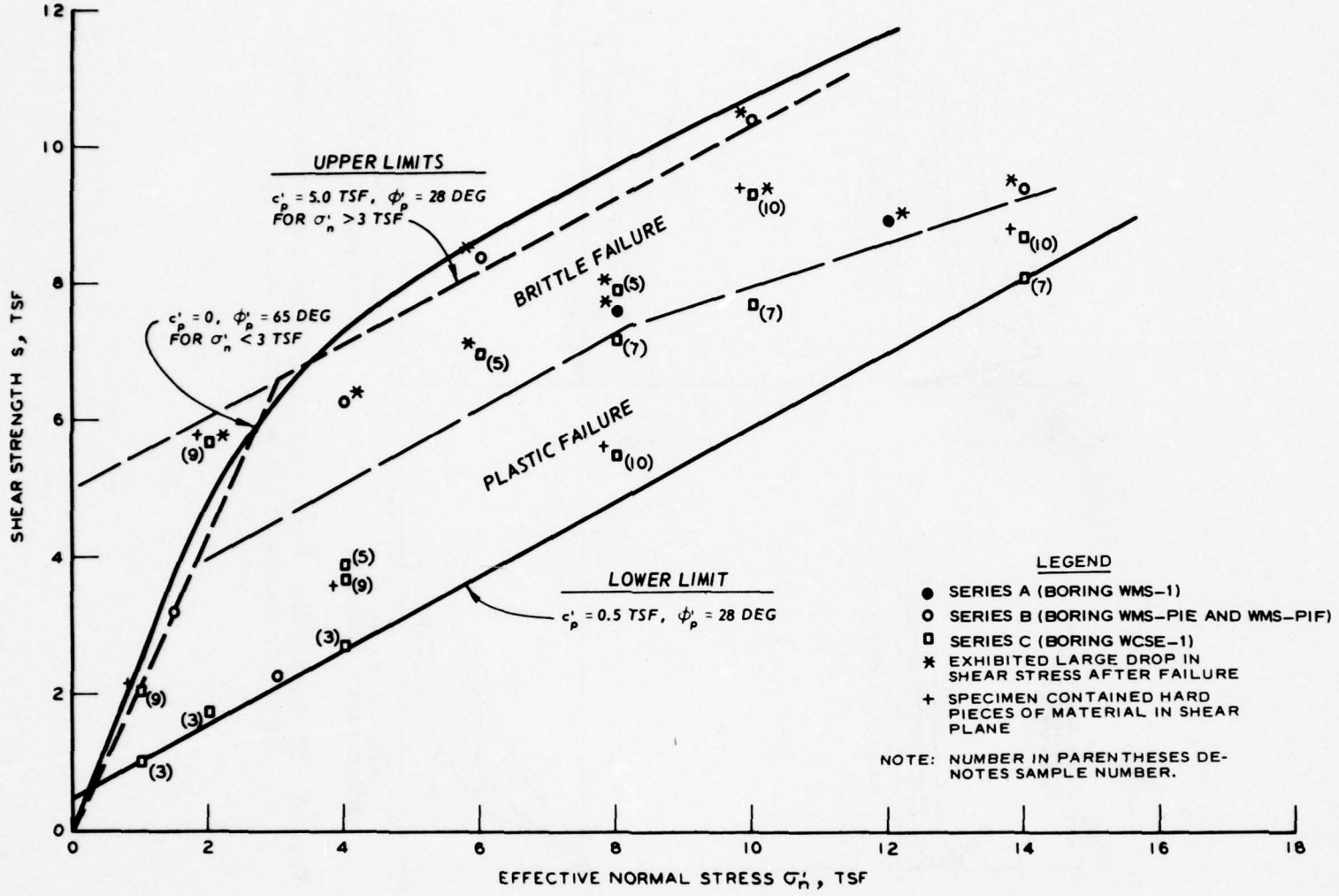

Fig. A6. Effective peak shear strength for intact specimens

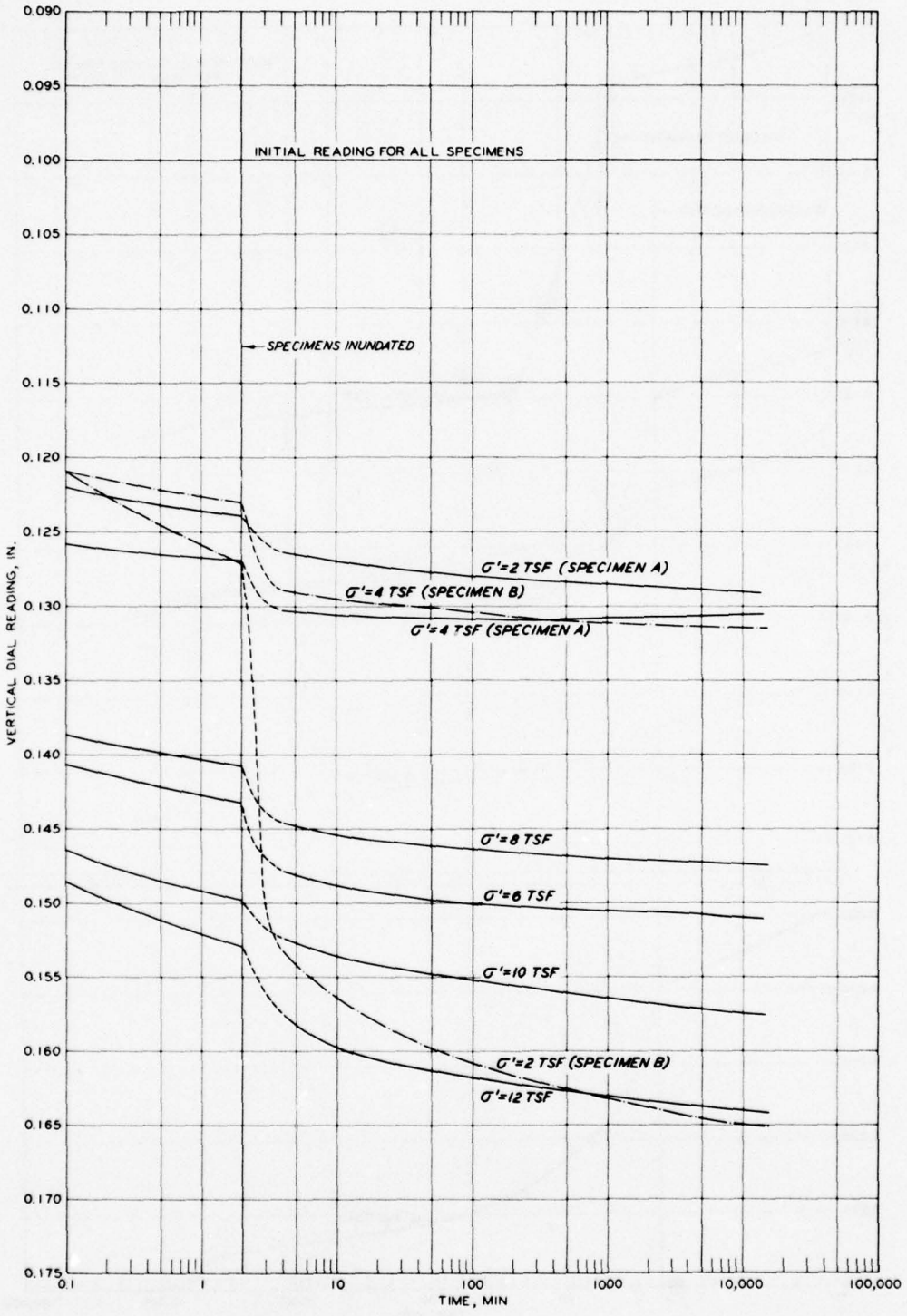

Fig. A7. Time-compression curves for slickensided specimens, Series D (from Banks et al., 1975)

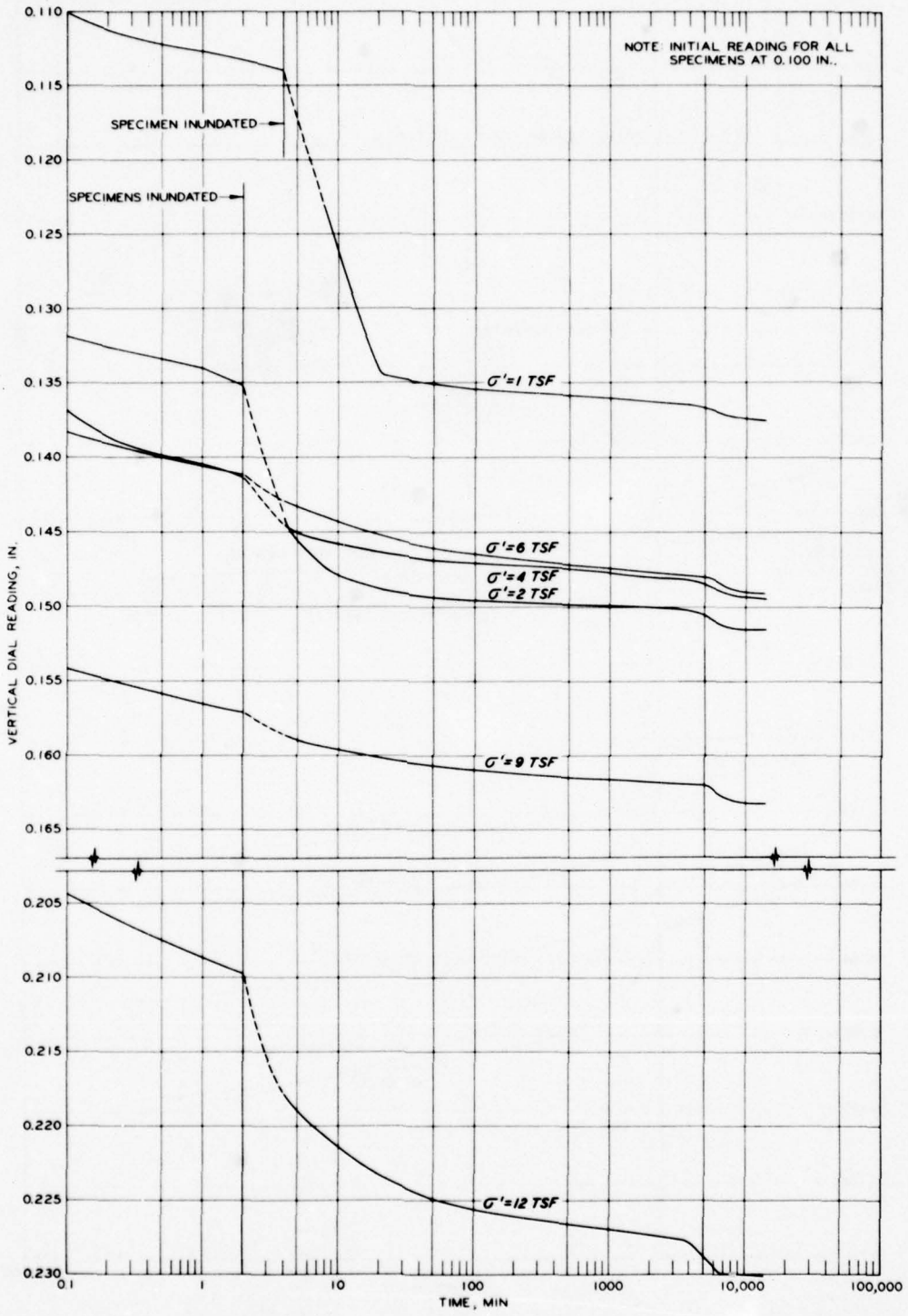

Fig. A8. Time-compression curves for slickensided specimens, Series E (from Banks et al., 1975)

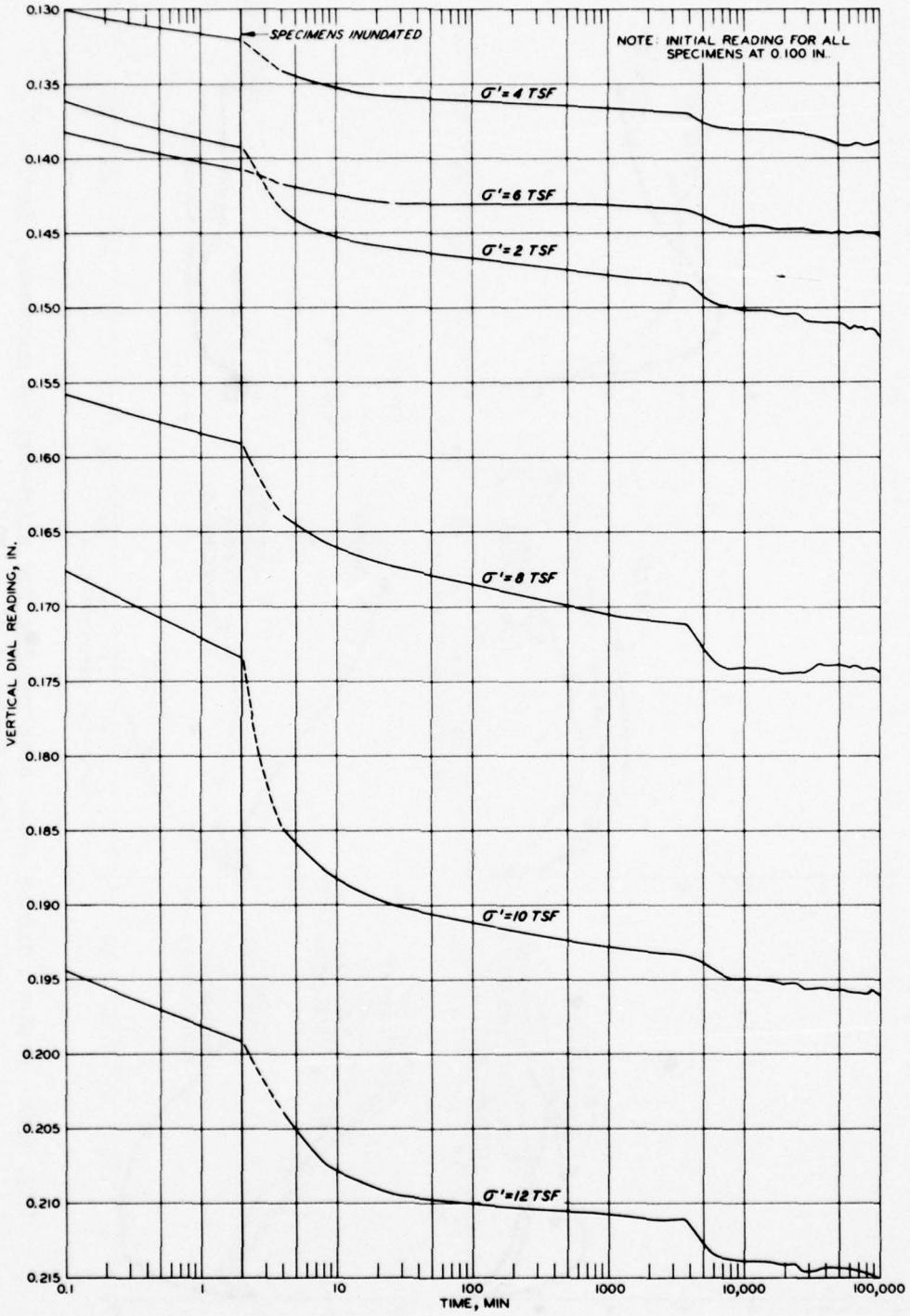

Fig. A9. Time-compression curves for slickensided specimens, Series F (from Banks et al., 1975)

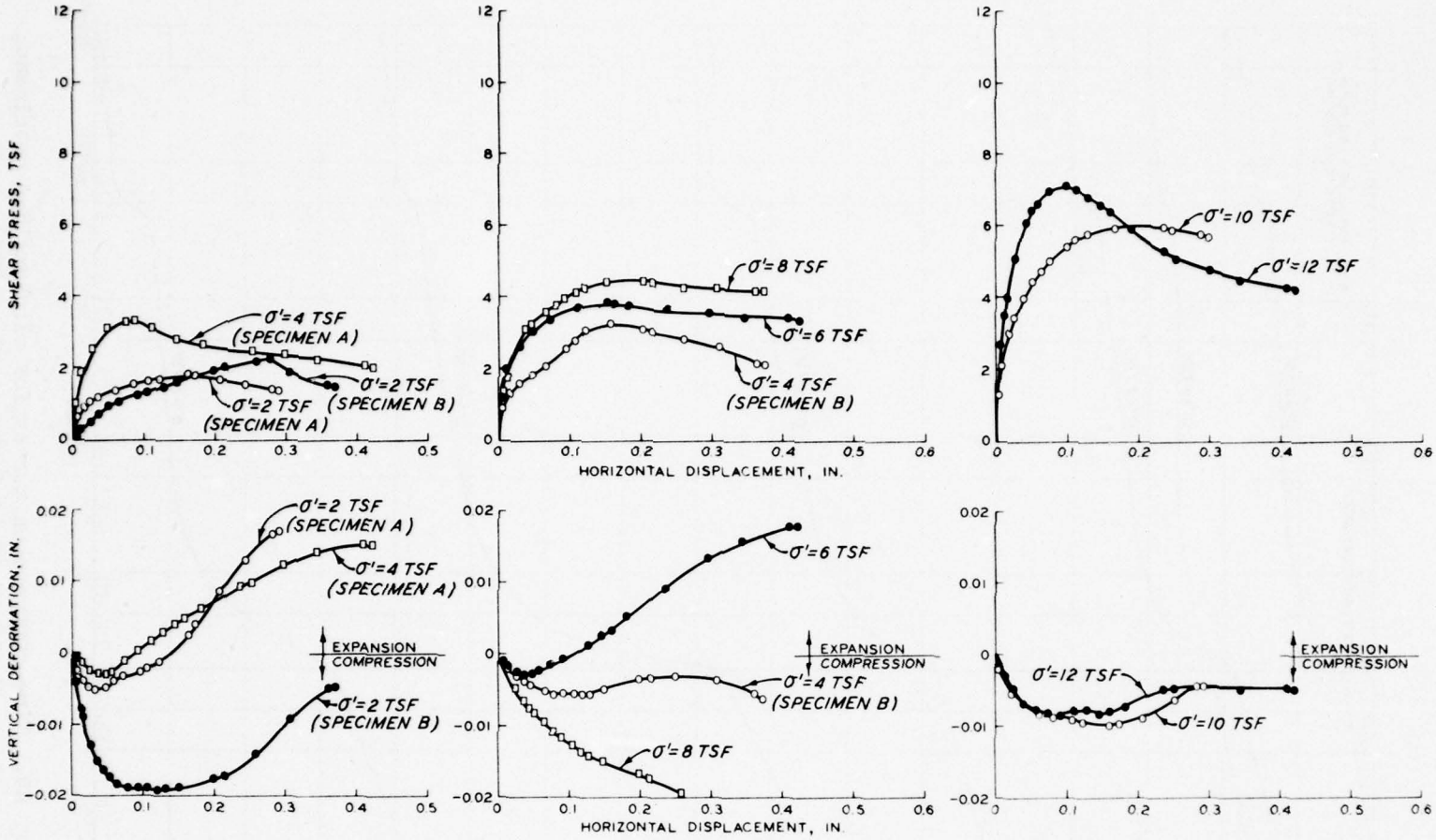

Fig. A10. Drained direct shear test results for slickensided specimens, Series D (from Banks et al., 1975)

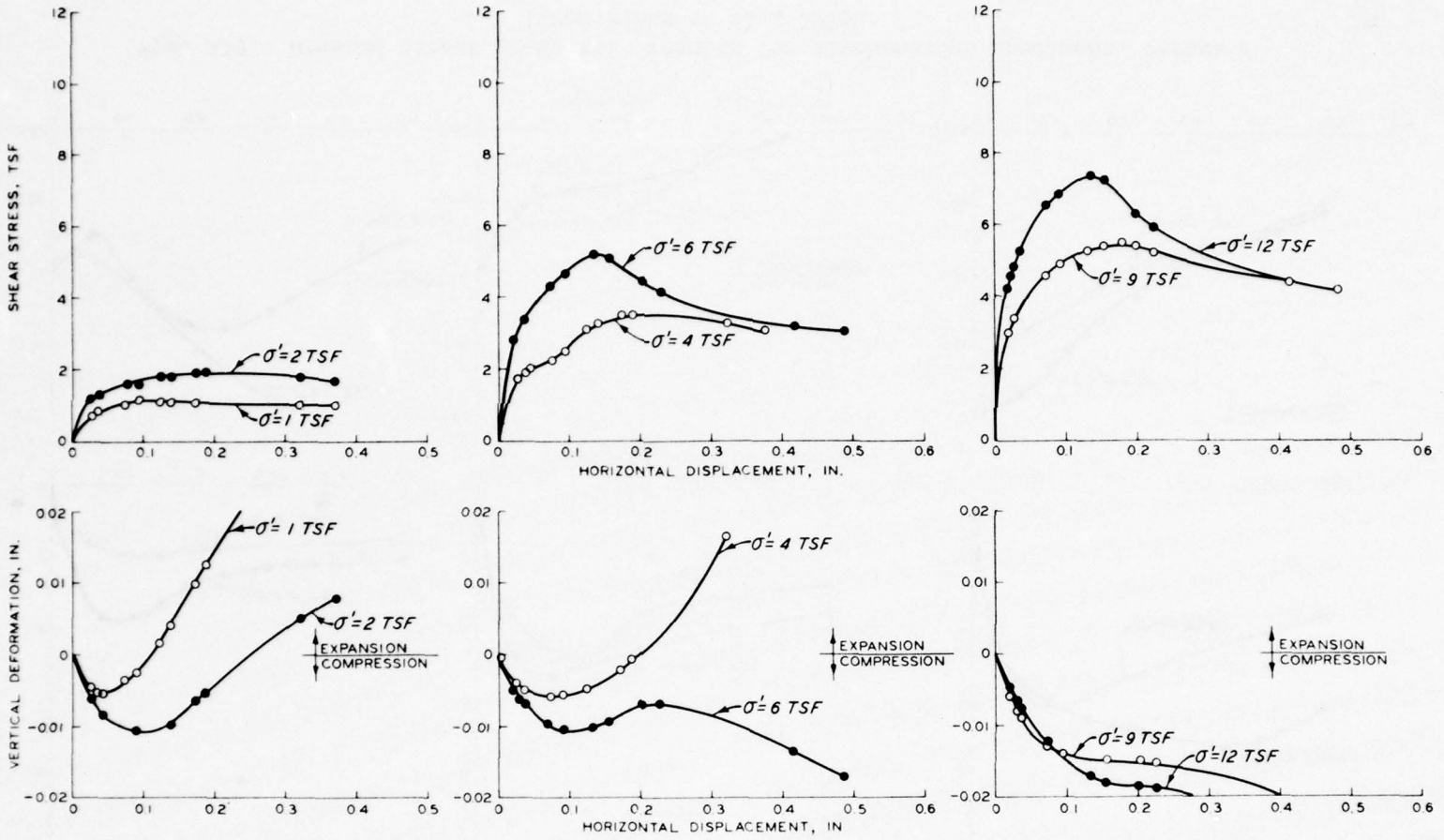

Fig. All. Drained direct shear test results for slickensided specimens, Series E (from Banks et al., 1975)

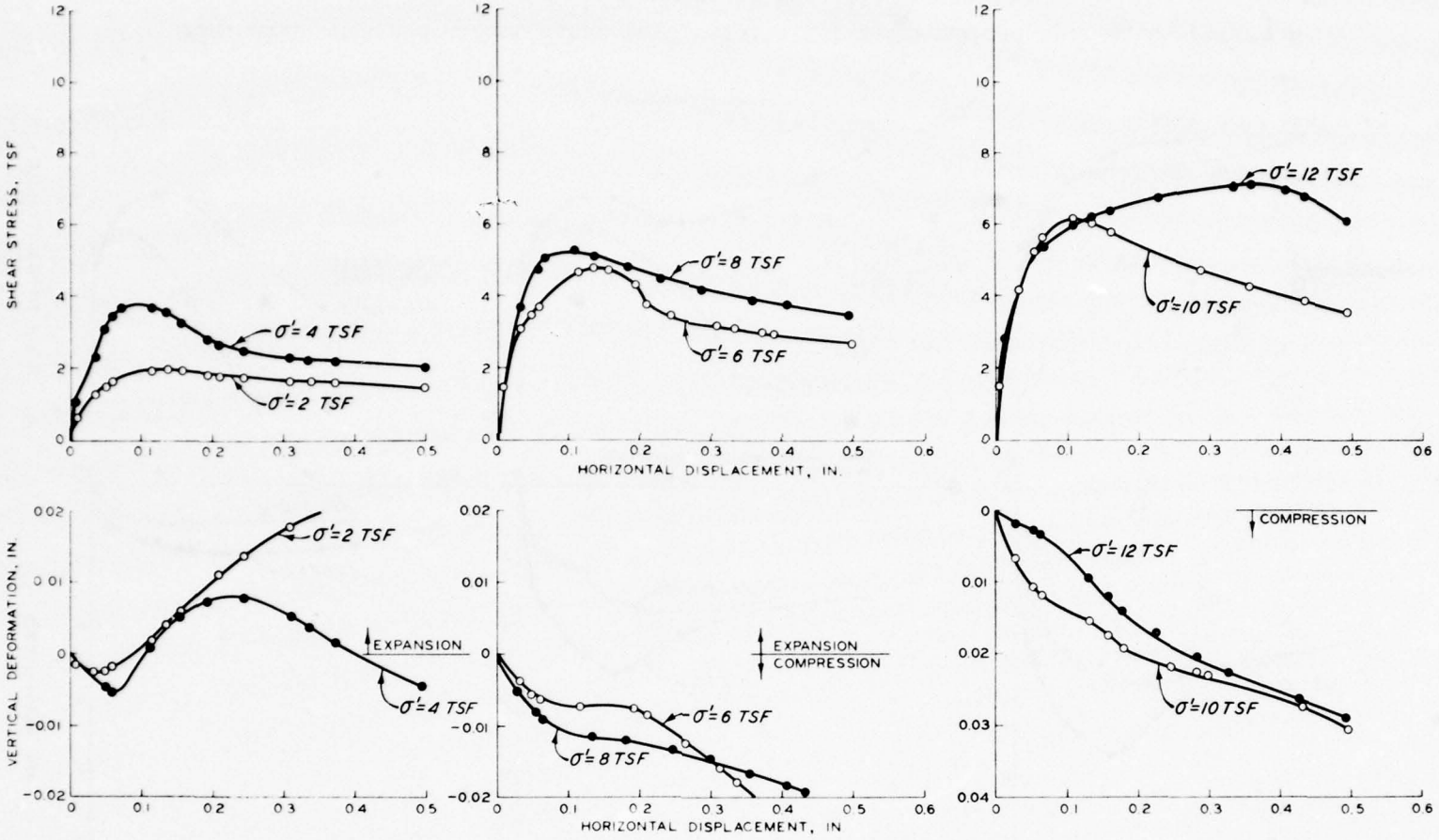

Fig. A12. Drained direct shear test results for slickensided specimens, Series F (from Banks et al., 1975)

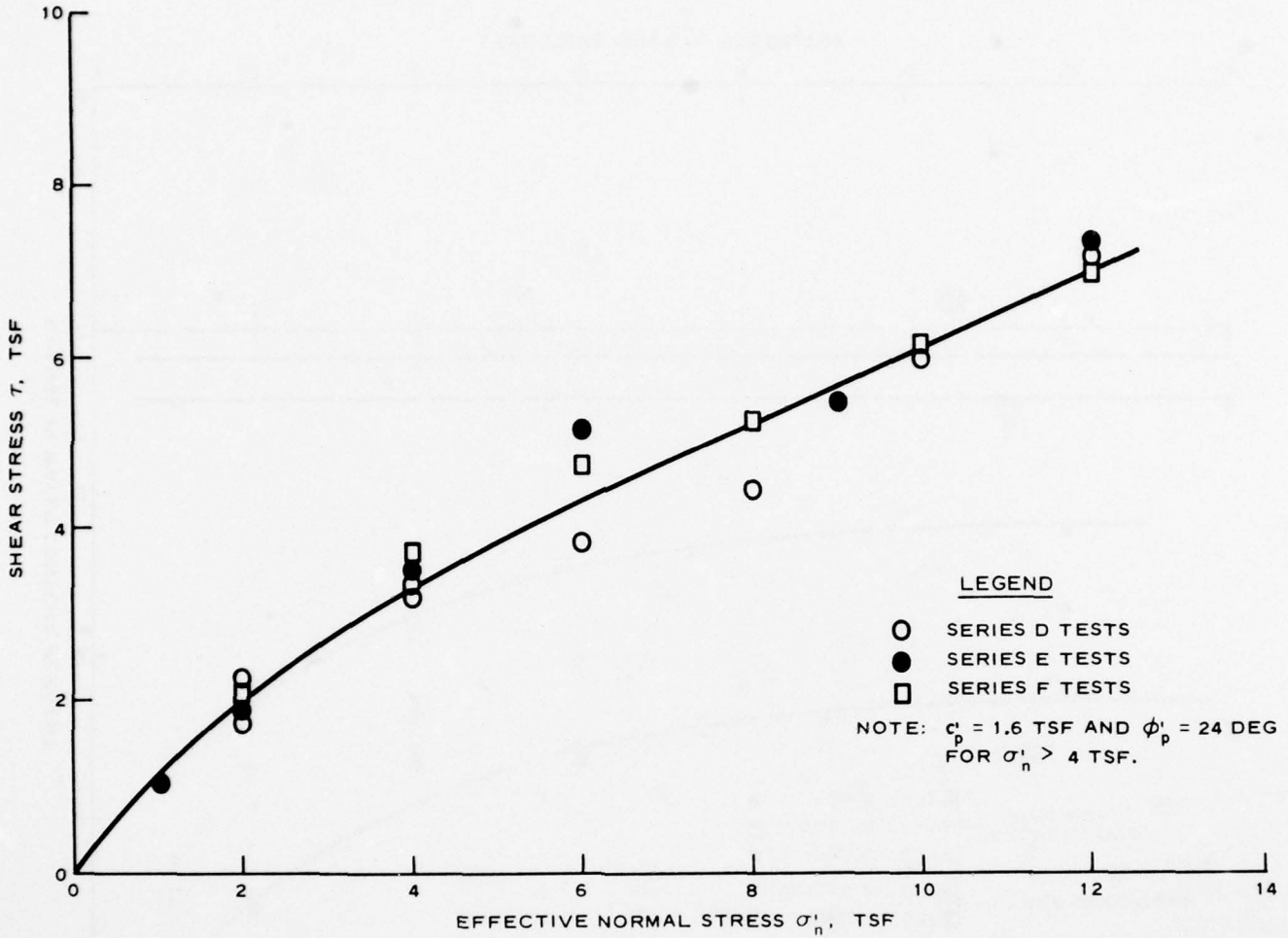

Fig. A13. Effective peak shear strength for slickensided specimens

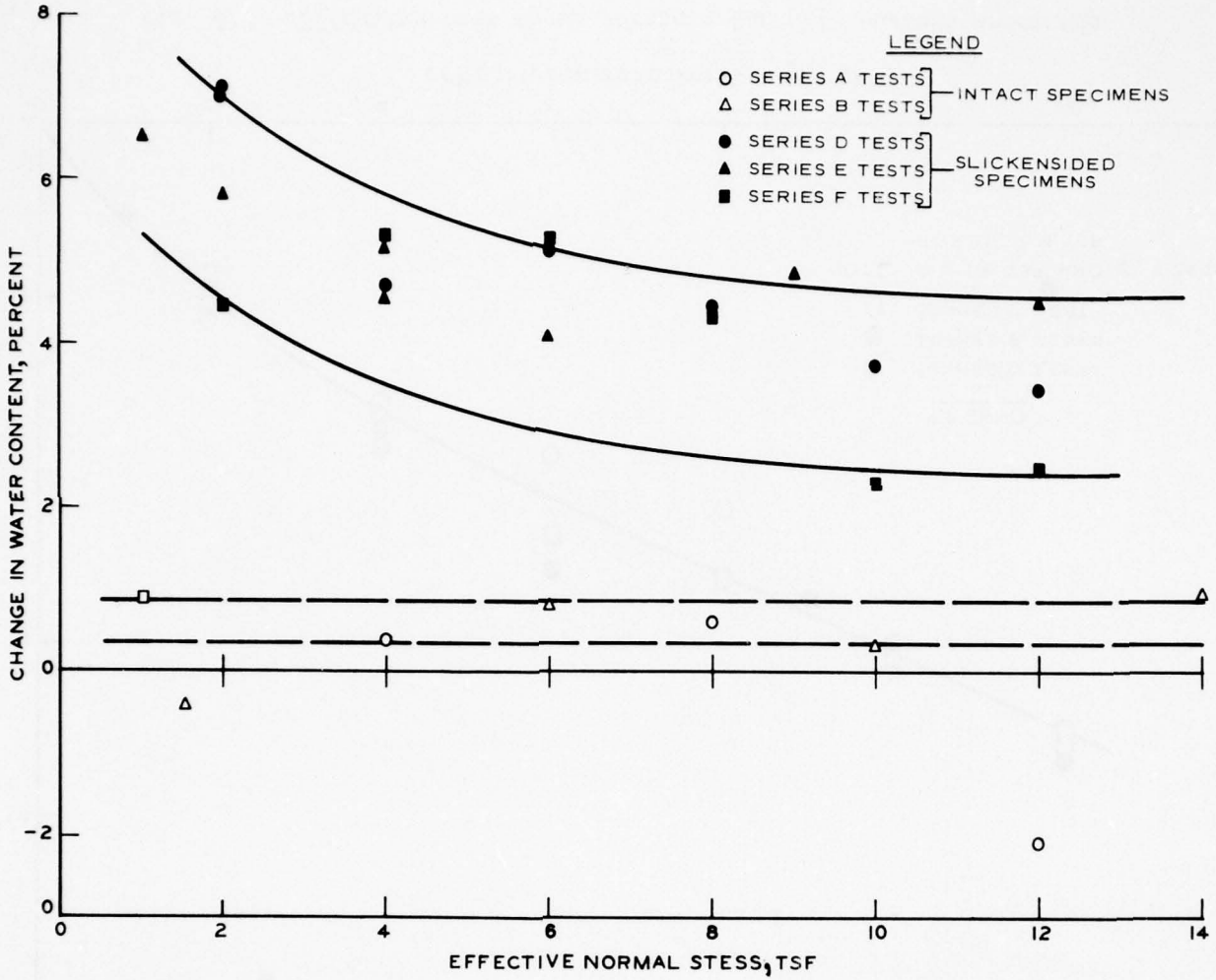

Fig. A14. Change in water content during direct shear tests

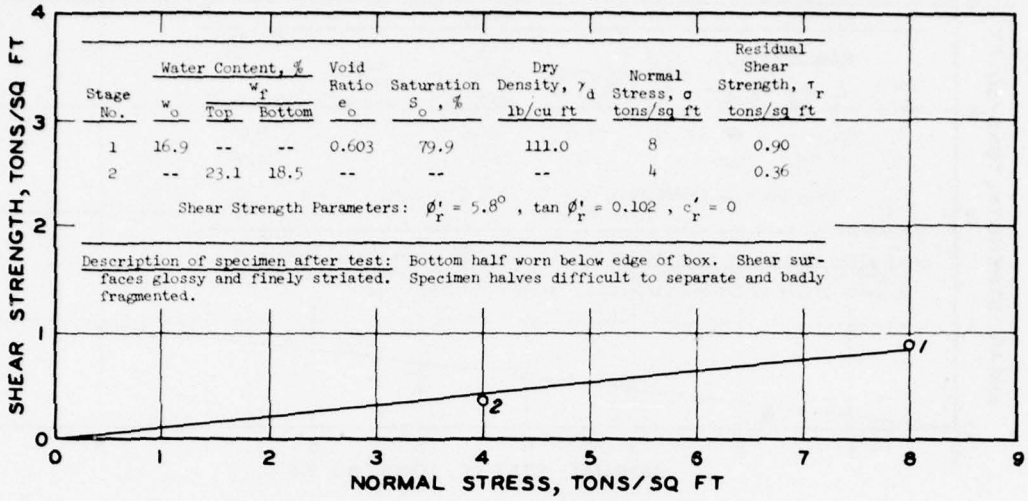

Stage No.	Water Content, % w_o	Water Content, % w_f Top	Water Content, % w_f Bottom	Void Ratio e_o	Saturation S_o, %	Dry Density, γ_d lb/cu ft	Normal Stress, σ tons/sq ft	Residual Shear Strength, τ_r tons/sq ft
1	16.9	--	--	0.603	79.9	111.0	8	0.90
2	--	23.1	18.5	--	--	--	4	0.36

Shear Strength Parameters: $\phi_r' = 5.8^\circ$, $\tan \phi_r' = 0.102$, $c_r' = 0$

Description of specimen after test: Bottom half worn below edge of box. Shear surfaces glossy and finely striated. Specimen halves difficult to separate and badly fragmented.

Run No.	σ tons/sq ft	Rate of Strain 10^{-2} in./hr	Horizontal Displacement: Per Run in.	Horizontal Displacement: Accumulated in.	Horizontal Displacement: Per Run at τ min in.	Horizontal Displacement: Accumulated at τ min in.	τ min tons/sq ft	Ratio $\frac{\tau}{\sigma}$
1	8	0.31	0.28	0.28	0.25	0.25	1.47	0.18
2		4.31	0.28	0.56	0.10	0.38	0.84	0.10
3		1.94	0.31	0.87	0.12	0.68	0.84	0.10
4		4.83	0.29	1.16	0.11	0.98	0.80	0.10
5		1.81	0.29	1.45	0.08	1.24	0.81	0.10
6		5.00	0.30	1.75	0.15	1.60	1.00	0.13
7		2.00	0.32	2.07	0.13	1.88	0.83	0.10
8		4.83	0.29	2.36	0.15	2.22	1.07	0.13
9		1.88	0.30	2.66	0.13	2.49	0.80	0.10
10		5.00	0.30	2.96	0.07	2.73	0.90	0.11
11		0.50	0.32	3.28	0.07	3.03	0.82	0.10
12		4.83	0.29	3.57	0.04	3.32	0.84	0.10
13		2.00	0.32	3.89	0.03	3.60	0.92	0.12
14		5.80	0.29	4.18	0.03	3.92	1.00	0.12
15		2.00	0.32	4.50	0.04	4.22	0.86	0.11
16	4	4.67	0.28	4.78	0.03	4.53	0.43	0.11
17		2.25	0.36	5.14	0.02	4.80	0.37	0.09
18		4.83	0.29	5.43	0.02	5.16	0.41	0.10
19		1.94	0.31	5.74	0.03	5.46	0.41	0.10
20		4.67	0.28	6.02	0.04	5.78	0.35	0.09
21		0.53	0.34	6.36	0.02	6.04	0.35	0.09

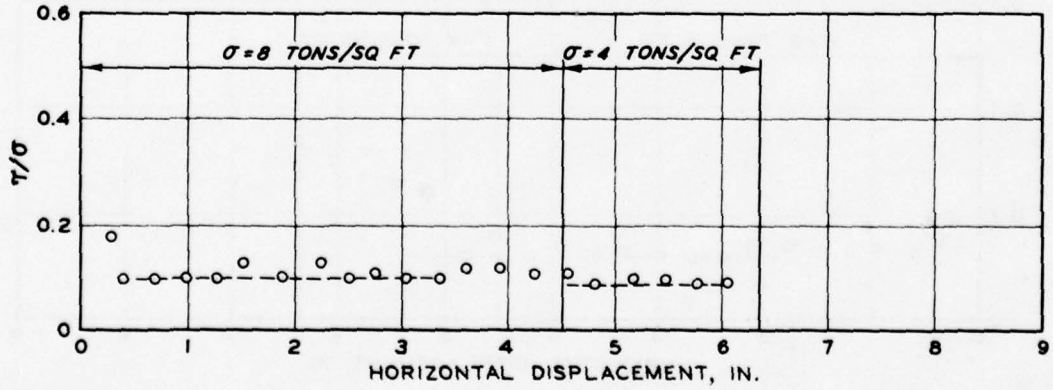

Fig. A15. Residual shear strength test results, boring WEC-1, Sample 5 (from Lutton and Banks, 1970)

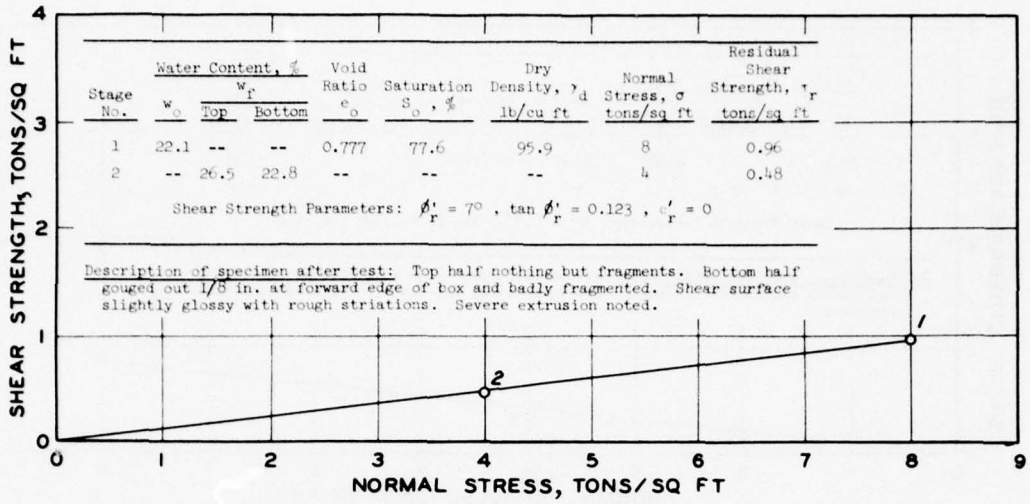

Stage No.	Water Content, % w_o	Water Content, % w_f Top	Water Content, % w_f Bottom	Void Ratio e_o	Saturation S_o, %	Dry Density, γ_d lb/cu ft	Normal Stress, σ tons/sq ft	Residual Shear Strength, τ_r tons/sq ft
1	22.1	--	--	0.777	77.6	95.9	8	0.96
2	--	26.5	22.8	--	--	--	4	0.48

Shear Strength Parameters: $\phi'_r = 7°$, $\tan \phi'_r = 0.123$, $c'_r = 0$

Description of specimen after test: Top half nothing but fragments. Bottom half gouged out 1/8 in. at forward edge of box and badly fragmented. Shear surface slightly glossy with rough striations. Severe extrusion noted.

Run No.	σ tons/sq ft	Rate of Strain 10^{-2} in./hr	Horizontal Displacement: Per Run in.	Horizontal Displacement: Accumulated in.	Horizontal Displacement: Per Run at τ min in.	Horizontal Displacement: Accumulated at τ min in.	τ min tons/sq ft	Ratio $\frac{\tau}{\sigma}$
1	8	0.31	0.28	0.28	0.26	0.26	1.61	0.20
2		4.31	0.28	0.56	0.06	0.34	1.29	0.16
3		1.94	0.31	0.87	0.03	0.59	1.02	0.13
4		4.83	0.29	1.16	0.06	0.93	1.14	0.14
5		1.81	0.29	1.45	0.03	1.19	1.04	0.13
6		5.00	0.30	1.75	0.03	1.48	1.07	0.13
7		2.00	0.32	2.07	0.04	1.79	1.13	0.14
8		4.83	0.29	2.36	0.04	2.11	1.11	0.14
9		1.88	0.30	2.66	0.03	2.39	0.92	0.12
10		5.00	0.30	2.96	0.03	2.69	1.00	0.12
11		0.50	0.32	3.28	0.03	2.99	1.00	0.12
12		4.83	0.29	3.57	0.03	3.31	1.04	0.13
13		2.00	0.32	3.89	0.02	3.59	1.05	0.13
14		5.80	0.29	4.18	0.02	3.91	1.13	0.14
15		2.00	0.32	4.50	0.02	4.20	1.00	0.12
16	4	4.67	0.28	4.78	0.02	4.52	0.64	0.16
17		2.25	0.36	5.14	0.02	4.80	0.46	0.12
18		4.83	0.29	5.43	0.29	5.43	1.04	0.26
19		1.94	0.31	5.74	0.31	5.74	1.27	0.32
20		4.67	0.28	6.02	0.28	6.02	1.20	0.30
21		0.53	0.34	6.36	0.34	6.36	1.28	0.32

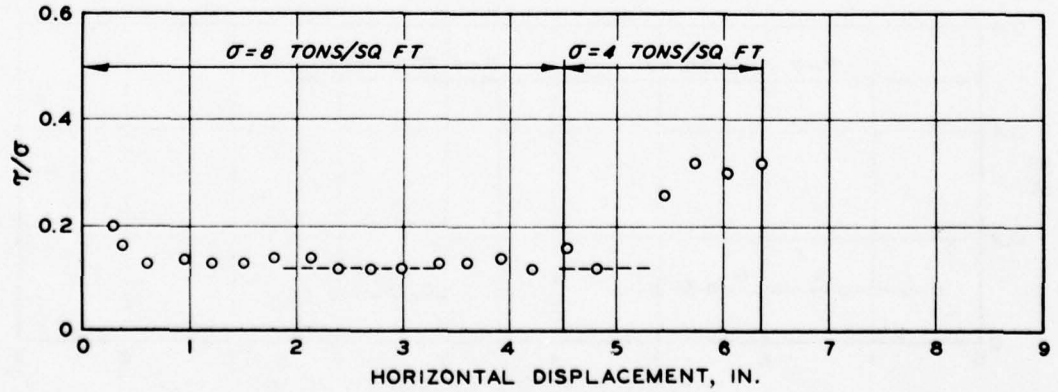

Fig. A16. Residual shear strength test results, boring WEC-1, Sample 6 (from Lutton and Banks, 1970)

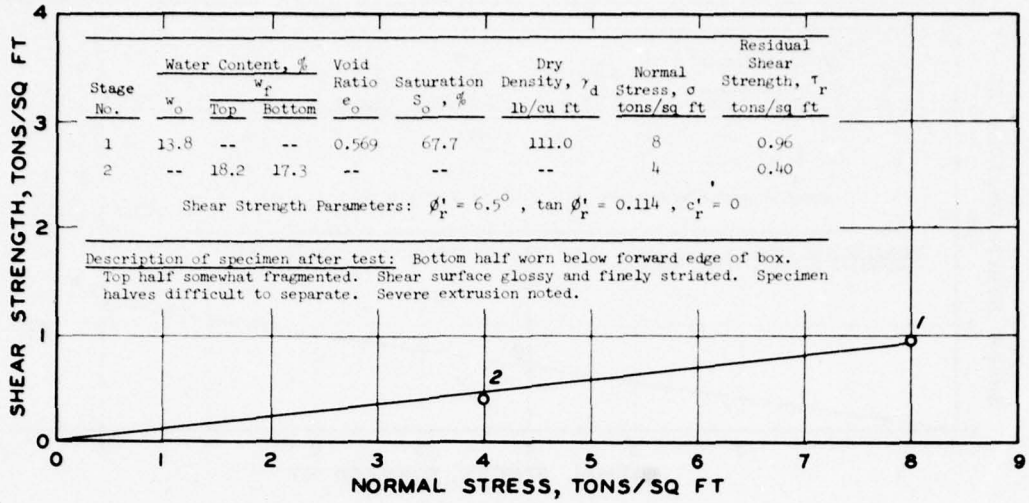

Stage No.	Water Content, % w_o	Water Content, % w_f Top	Water Content, % w_f Bottom	Void Ratio e_o	Saturation S_o, %	Dry Density, γ_d lb/cu ft	Normal Stress, σ tons/sq ft	Residual Shear Strength, τ_r tons/sq ft
1	13.8	--	--	0.569	67.7	111.0	8	0.96
2	--	18.2	17.3	--	--	--	4	0.40

Shear Strength Parameters: $\phi'_r = 6.5^\circ$, $\tan \phi'_r = 0.114$, $c'_r = 0$

Description of specimen after test: Bottom half worn below forward edge of box. Top half somewhat fragmented. Shear surface glossy and finely striated. Specimen halves difficult to separate. Severe extrusion noted.

Run No.	σ tons/sq ft	Rate of Strain 10^{-2} in./hr	Horizontal Displacement: Per Run in.	Horizontal Displacement: Accumulated in.	Horizontal Displacement: Per Run at τ min in.	Horizontal Displacement: Accumulated at τ min in.	τ min tons/sq ft	Ratio $\frac{\tau}{\sigma}$
1	8	0.31	0.28	0.28	0.28	0.28	1.92	0.24
2		4.31	0.28	0.56	0.10	0.36	1.72	0.22
3		1.94	0.31	0.87	0.10	0.66	1.60	0.20
4		4.83	0.29	1.16	0.09	0.96	1.32	0.16
5		1.81	0.29	1.45	0.09	1.25	0.96	0.12
6		5.00	0.30	1.75	0.09	1.54	1.25	0.16
7		2.00	0.32	2.07	0.06	1.81	0.99	0.12
8		4.83	0.29	2.36	0.06	2.13	1.30	0.16
9		1.88	0.30	2.66	0.12	2.48	0.88	0.11
10		5.00	0.30	2.96	0.06	2.72	1.04	0.13
11		0.50	0.32	3.28	0.12	3.08	1.12	0.14
12		4.83	0.29	3.57	0.09	3.37	0.76	0.10
13		2.00	0.32	3.89	0.08	3.65	0.81	0.10
14		5.80	0.29	4.18	0.02	3.91	1.16	0.14
15		2.00	0.32	4.50	0.04	4.22	0.96	0.12
16	4	4.67	0.28	4.78	0.10	4.60	0.43	0.11
17		2.25	0.36	5.14	0.06	4.84	0.39	0.10
18		4.83	0.29	5.43	0.05	5.19	0.40	0.10
19		1.94	0.31	5.74	0.03	5.46	0.42	0.10
20		4.67	0.28	6.02	0.10	5.84	0.40	0.10
21		0.53	0.34	6.36	0.03	6.05	0.51	0.13

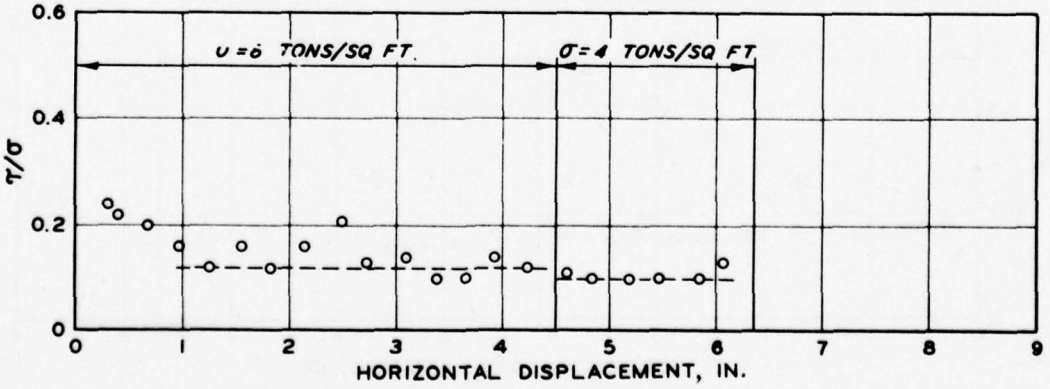

Fig. A17. Residual shear strength test results, boring WEC-1, Sample 10 (from Lutton and Banks, 1970)

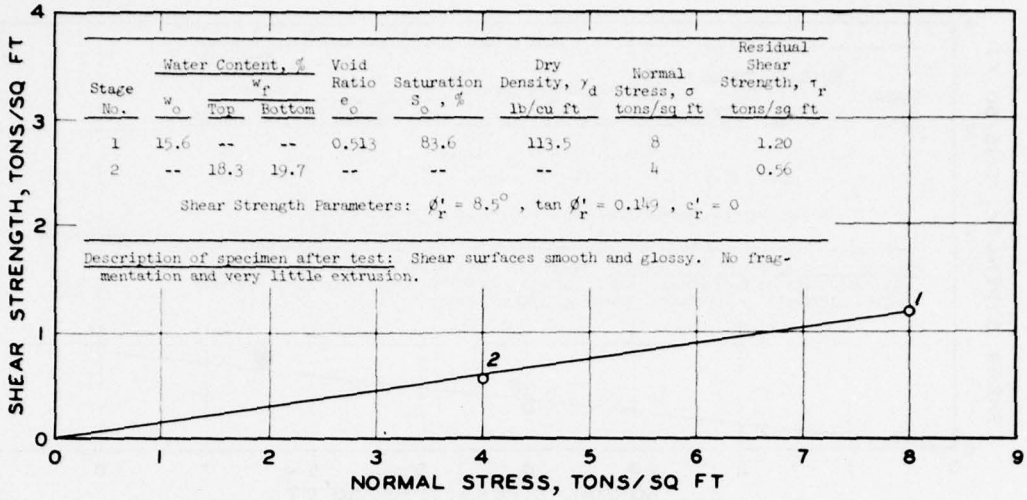

Stage No.	Water Content, % w_o	Water Content, % w_f Top	Water Content, % w_f Bottom	Void Ratio e_o	Saturation S_o, %	Dry Density, γ_d lb/cu ft	Normal Stress, σ tons/sq ft	Residual Shear Strength, τ_r tons/sq ft
1	15.6	--	--	0.513	83.6	113.5	8	1.20
2	--	18.3	19.7	--	--	--	4	0.56

Shear Strength Parameters: $\phi'_r = 8.5^\circ$, $\tan \phi'_r = 0.149$, $c'_r = 0$

Description of specimen after test: Shear surfaces smooth and glossy. No fragmentation and very little extrusion.

Run No.	σ tons/sq ft	Rate of Strain 10^{-2} in./hr	Horizontal Displacement: Per Run in.	Horizontal Displacement: Accumulated in.	Horizontal Displacement: Per Run at τ min in.	Horizontal Displacement: Accumulated at τ min in.	τ min tons/sq ft	Ratio τ/σ
1	8	9.33	0.28	0.28	0.28	0.28	1.43	0.18
2		2.25	0.36	0.64	0.28	0.56	1.45	0.18
3		9.33	0.28	0.92	0.28	0.92	1.42	0.18
4		1.81	0.29	1.21	0.19	1.11	1.29	0.16
5		4.83	0.29	1.50	0.19	1.40	1.34	0.17
6		1.94	0.31	1.81	0.18	1.68	1.37	0.17
7		4.67	0.28	2.09	0.20	2.01	1.26	0.16
8		0.48	0.31	2.40	0.10	2.19	1.25	0.16
9		5.00	0.30	2.70	0.18	2.58	1.19	0.15
10		2.00	0.32	3.02	0.14	2.84	1.18	0.15
11		4.67	0.28	3.30	0.16	3.18	1.26	0.16
12		1.88	0.30	3.60	0.15	3.45	1.22	0.15
13		4.83	0.29	3.79	0.21	3.81	1.24	0.16
14		2.00	0.32	4.11	0.18	3.97	1.18	0.15
15	4	5.00	0.30	4.41	0.14	4.25	0.61	0.15
16		0.29	0.28	4.71	0.11	4.62	0.63	0.16
17		2.06	0.33	5.04	0.17	4.88	0.60	0.15
18		4.83	0.29	5.33	0.16	5.20	0.56	0.14
19		1.94	0.31	5.64	0.16	5.49	0.58	0.14
20		4.83	0.29	5.93	0.14	5.78	0.62	0.16
21		1.81	0.32	6.25	0.13	6.06	0.64	0.16
22		4.83	0.29	6.54	0.19	6.44	0.62	0.16
23		1.94	0.31	6.86	0.20	6.74	2.41	0.17
24		4.67	0.28	7.13	0.24	7.09	2.20	0.16
25		0.64	0.41	7.69	0.12	7.25	2.18	0.16

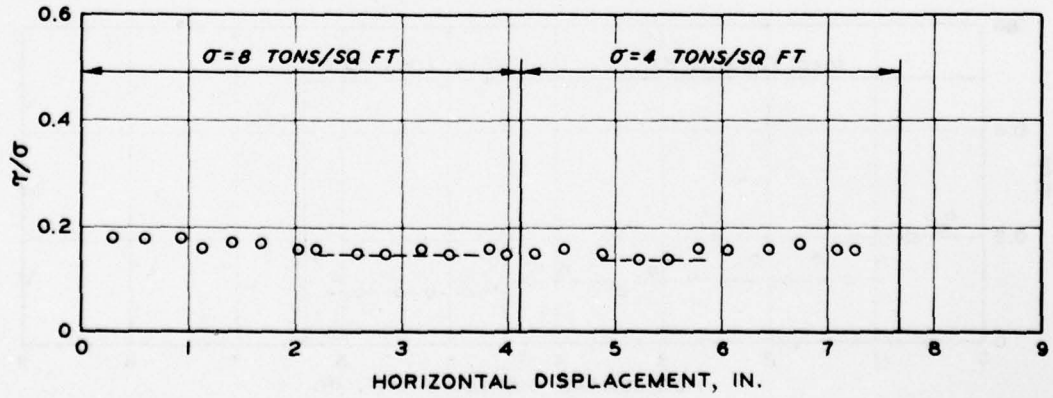

Fig. A18. Residual shear strength test results, boring WMS-1, Sample 4 (from Lutton and Banks, 1970)

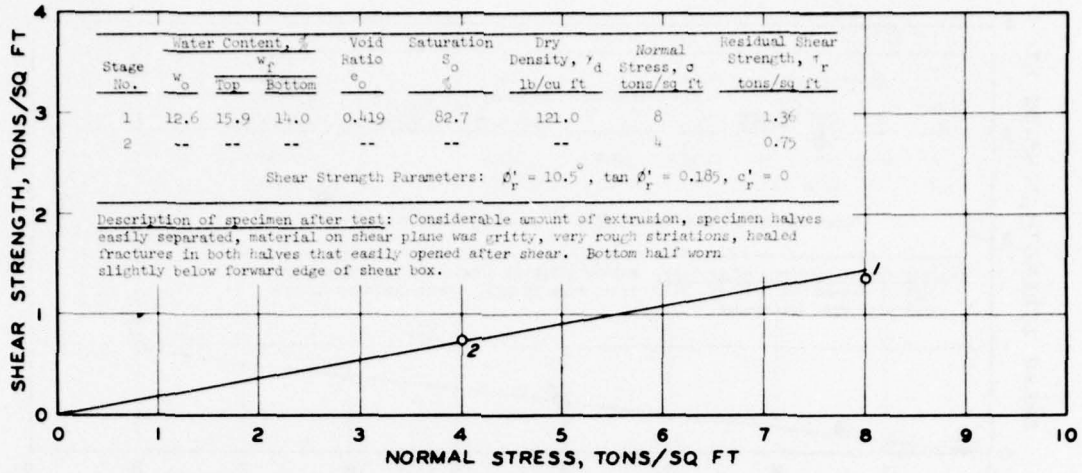

Stage No.	Water Content, % w_o	w_f Top	w_f Bottom	Void Ratio e_o	Saturation S_o %	Dry Density, γ_d lb/cu ft	Normal Stress, σ tons/sq ft	Residual Shear Strength, τ_r tons/sq ft
1	12.6	15.9	14.0	0.419	82.7	121.0	8	1.36
2	--	--	--	--	--	--	4	0.75

Shear Strength Parameters: $\phi_r' = 10.5°$, $\tan \phi_r' = 0.185$, $c_r' = 0$

Description of specimen after test: Considerable amount of extrusion, specimen halves easily separated, material on shear plane was gritty, very rough striations, healed fractures in both halves that easily opened after shear. Bottom half worn slightly below forward edge of shear box.

Run No.	σ tons/sq ft	Rate of Strain 10^{-2} in./hr	Horizontal Displacement: Per Run in.	Accumulated in.	Per Run at τ min in.	Accumulated at τ min in.	τ min tons/sq ft	Ratio τ/σ
1	8	0.25	0.24	0.24	0.24	0.24	1.91	0.24
2		1.56	0.25	0.49	0.20	0.44	1.72	0.22
3		4.33	0.26	0.75	0.15	0.64	1.50	0.19
4		1.81	0.29	1.04	0.19	0.94	1.48	0.18
5		4.83	0.29	1.33	0.13	1.17	1.48	0.18
6		5.16	0.31	1.64	0.15	1.48	1.39	0.17
7		1.94	0.31	1.95	0.14	1.78	1.40	0.18
8		4.83	0.29	2.24	0.13	2.08	1.44	0.18
9		0.35	0.25	2.49	0.15	2.32	1.41	0.18
10		2.31	0.37	2.86	0.08	2.57	1.38	0.17
11		3.47	0.26	3.12	0.05	2.91	1.18	0.15
12		5.00	0.30	3.42	0.10	3.22	1.37	0.17
13		2.00	0.32	3.74	0.12	3.54	1.40	0.18
14		4.50	0.27	4.01	0.11	3.85	1.41	0.18
15		2.25	0.36	4.37	0.10	4.11	1.26	0.16
16		4.67	0.28	4.65	0.19	4.56	1.49	0.19
17		0.44	0.28	4.93	0.12	4.77	1.39	0.17
18		4.16	0.25	5.18	0.12	5.05	1.38	0.17
19		2.06	0.33	5.51	0.12	5.30	1.43	0.18
20		4.50	0.27	5.78	0.13	5.43	1.36	0.17
21		1.81	0.29	6.07	0.11	5.89	1.42	0.18
22		4.17	0.25	6.32	0.11	6.28	1.47	0.18
23		1.81	0.29	6.61	0.14	6.46	1.50	0.19
24		4.17	0.25	6.86	0.13	6.74	1.44	0.18
25		1.94	0.31	7.17	0.16	7.02	1.50	0.19
26	4	4.33	0.26	7.43	0.06	7.23	0.75	0.19
27		0.45	0.29	7.72	0.11	7.54	0.77	0.19
28		4.17	0.25	7.97	0.10	7.82	0.78	0.19
29		2.06	0.33	8.30	0.04	8.01	0.72	0.18
30		5.00	0.30	8.60	0.08	8.38	0.84	0.21
31		2.00	0.32	8.92	0.07	8.67	0.80	0.20
32		5.00	0.30	9.22	0.06	8.98	0.85	0.21
33		1.94	0.31	9.53	0.07	9.29	0.89	0.22

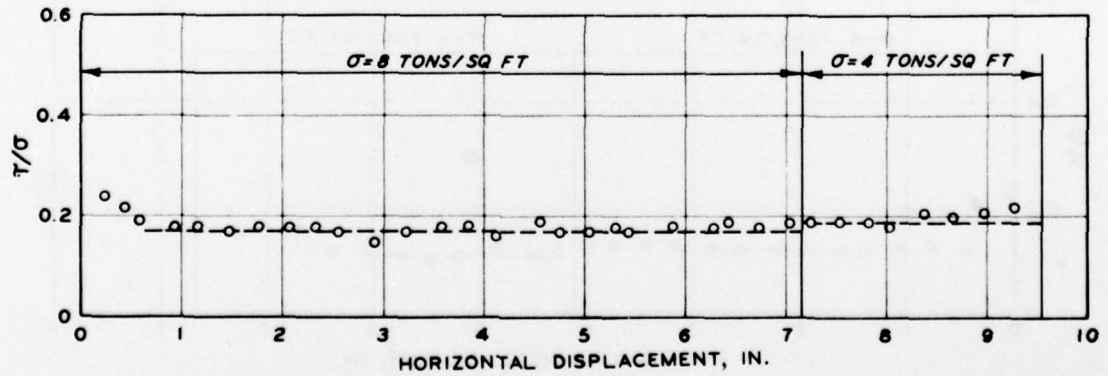

Fig. A19. Residual shear strength test results, boring WMS-1, Sample 6 (from Lutton and Banks, 1970)

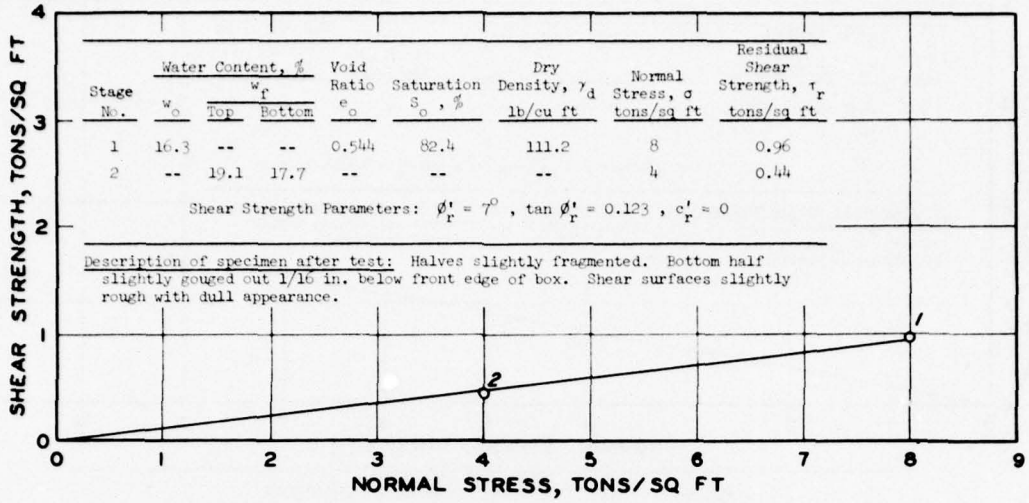

Stage No.	Water Content, % w_o	Water Content, % w_f Top	Water Content, % w_f Bottom	Void Ratio e_o	Saturation S_o, %	Dry Density, γ_d lb/cu ft	Normal Stress, σ tons/sq ft	Residual Shear Strength, τ_r tons/sq ft
1	16.3	--	--	0.544	82.4	111.2	8	0.96
2	--	19.1	17.7	--	--	--	4	0.44

Shear Strength Parameters: $\phi_r' = 7^\circ$, $\tan \phi_r' = 0.123$, $c_r' = 0$

Description of specimen after test: Halves slightly fragmented. Bottom half slightly gouged out 1/16 in. below front edge of box. Shear surfaces slightly rough with dull appearance.

Run No.	σ tons/sq ft	Rate of Strain 10^{-2} in./hr	Horizontal Displacement: Per Run in.	Horizontal Displacement: Accumulated in.	Horizontal Displacement: Per Run at τ min in.	Horizontal Displacement: Accumulated at τ min in.	τ min tons/sq ft	Ratio $\frac{\tau}{\sigma}$
1	8	4.67	0.28	0.28	0.02	0.02	1.81	0.23
2		2.25	0.36	0.64	0.13	0.41	0.97	0.12
3		4.67	0.28	0.92	0.16	0.80	1.02	0.13
4		1.81	0.29	1.21	0.12	1.04	0.96	0.12
5		4.83	0.29	1.50	0.19	1.40	0.96	0.12
6		1.94	0.31	1.81	0.12	1.62	0.94	0.12
7		4.67	0.28	2.09	0.14	1.95	0.96	0.12
8		0.48	0.31	2.40	0.13	2.22	0.94	0.12
9		5.00	0.30	2.70	0.17	2.57	0.99	0.12
10		2.00	0.32	3.02	0.14	2.84	0.94	0.12
11		4.67	0.28	3.30	0.16	3.18	1.01	0.13
12		1.88	0.30	3.60	0.14	3.44	1.05	0.13
13		4.83	0.29	3.79	0.15	3.75	1.06	0.13
14		2.00	0.32	4.11	0.18	3.97	1.00	0.12
15	4	5.00	0.30	4.41	0.14	4.25	0.48	0.12
16		0.29	0.28	4.71	0.11	4.52	0.43	0.11
17		2.06	0.33	5.04	0.15	4.86	0.49	0.12
18		4.83	0.29	5.33	0.16	5.20	0.44	0.11
19		1.94	0.31	5.64	0.14	5.47	0.41	0.10
20		4.83	0.29	5.93	0.12	5.76	0.44	0.11
21		2.00	0.32	6.25	0.12	6.05	0.46	0.12
22		4.83	0.29	6.54	0.13	6.38	0.50	0.12
23		1.94	0.31	6.85	0.15	6.69	2.22	0.16
24		4.67	0.28	7.13	0.17	7.02	2.21	0.16
25		0.64	0.41	7.69	0.12	7.25	2.03	0.15

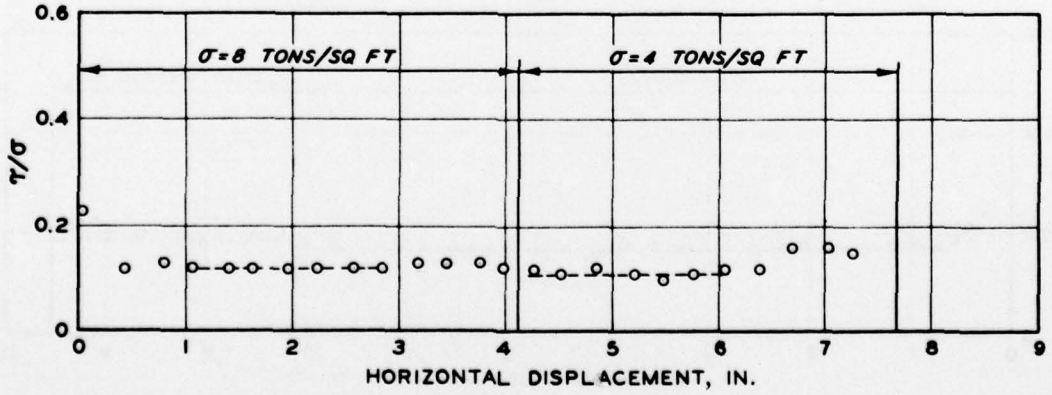

Fig. A20. Residual shear strength test results, boring WMS-1, Sample 10 (from Lutton and Banks, 1970)

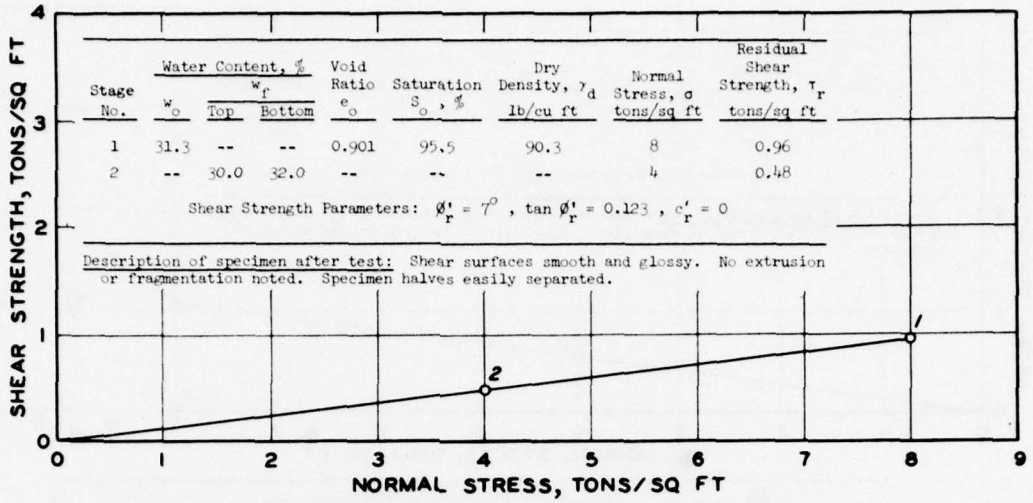

Stage No.	Water Content, % w_o	Water Content, % w_f Top	Water Content, % w_f Bottom	Void Ratio e_o	Saturation S_o, %	Dry Density, γ_d lb/cu ft	Normal Stress, σ tons/sq ft	Residual Shear Strength, τ_r tons/sq ft
1	31.3	--	--	0.901	95.5	90.3	8	0.96
2	--	30.0	32.0	--	--	--	4	0.48

Shear Strength Parameters: $\phi'_r = 7^\circ$, $\tan \phi'_r = 0.123$, $c'_r = 0$

Description of specimen after test: Shear surfaces smooth and glossy. No extrusion or fragmentation noted. Specimen halves easily separated.

Run No.	σ tons/sq ft	Rate of Strain 10^{-2} in./hr	Horizontal Displacement: Per Run in.	Horizontal Displacement: Accumulated in.	Horizontal Displacement: Per Run at τ min in.	Horizontal Displacement: Accumulated at τ min in.	τ min tons/sq ft	Ratio $\frac{\tau}{\sigma}$
1	8	9.33	0.28	0.28	0.28	0.28	1.00	0.12
2		2.25	0.36	0.64	0.28	0.56	0.96	0.12
3		9.33	0.28	0.92	0.28	0.92	1.01	0.13
4		1.81	0.29	1.21	0.14	1.06	0.96	0.12
5		4.83	0.29	1.50	0.19	1.40	0.96	0.12
6		1.94	0.31	1.81	0.23	1.73	0.92	0.12
7		7.00	0.28	2.09	0.28	2.09	0.94	0.12
8		0.48	0.31	2.40	0.19	2.28	0.91	0.11
9		5.00	0.30	2.70	0.30	2.70	0.96	0.12
10		2.00	0.32	3.02	0.28	2.98	0.93	0.12
11		9.33	0.28	3.30	0.28	3.30	0.92	0.12
12		1.88	0.30	3.60	0.25	3.55	0.92	0.12
13		4.83	0.29	3.79	0.26	3.86	0.93	0.12
14		2.00	0.32	4.11	0.30	4.09	0.96	0.12
15	4	5.00	0.30	4.41	0.14	4.25	0.48	0.12
16		0.29	0.28	4.71	0.11	4.52	0.43	0.11
17		2.06	0.33	5.04	0.15	4.86	0.50	0.12
18		4.83	0.29	5.33	0.16	5.20	0.47	0.12
19		1.94	0.31	5.64	0.14	5.47	0.45	0.11
20		4.83	0.29	5.93	0.12	5.76	0.46	0.12
21		2.00	0.32	6.25	0.12	6.05	0.46	0.12
22		4.83	0.29	6.54	0.13	6.38	0.50	0.12
23		1.94	0.31	6.85	0.22	6.76	1.82	0.13
24		4.67	0.28	7.13	0.17	7.02	1.83	0.13
25		0.64	0.41	7.69	0.12	7.25	2.03	0.14

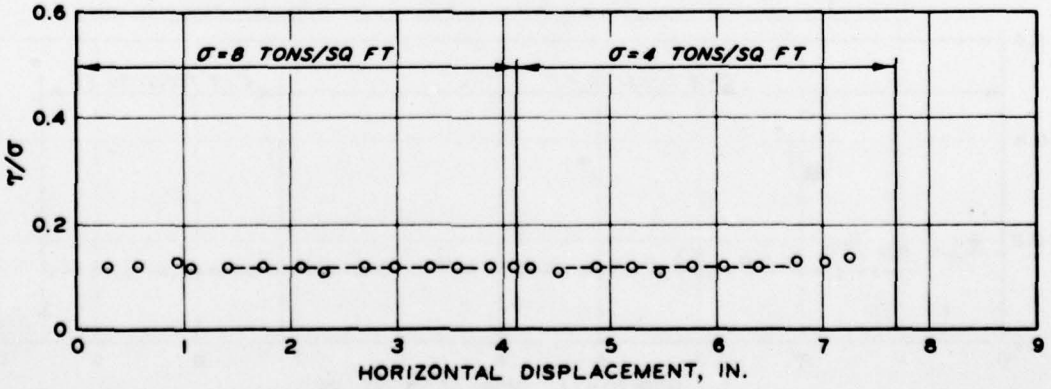

Fig. A21. Residual shear strength test results, boring WMS-1, Sample 12 (from Lutton and Banks, 1970)

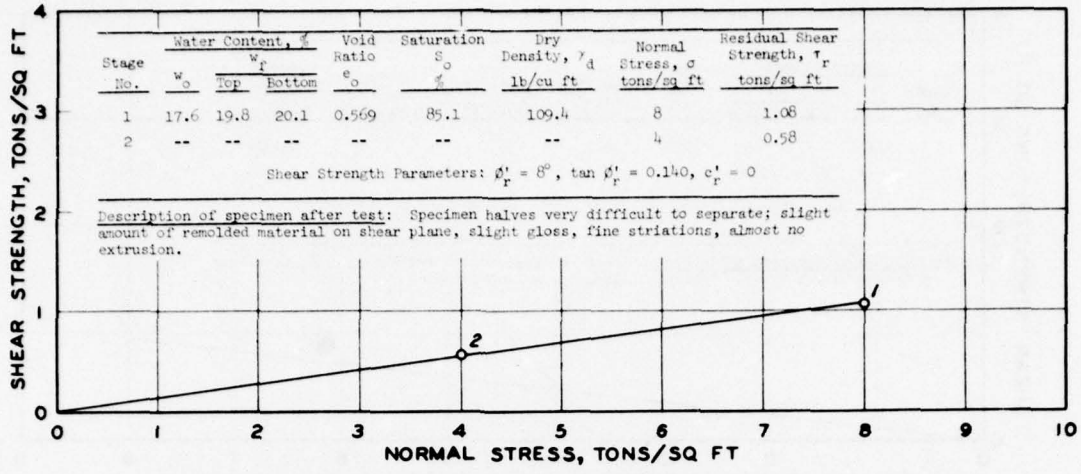

Stage No.	Water Content, % w_o	Water Content, % w_f Top	Water Content, % w_f Bottom	Void Ratio e_o	Saturation S_o %	Dry Density, γ_d lb/cu ft	Normal Stress, σ tons/sq ft	Residual Shear Strength, τ_r tons/sq ft
1	17.6	19.8	20.1	0.569	85.1	109.4	8	1.08
2	--	--	--	--	--	--	4	0.58

Shear Strength Parameters: $\phi'_r = 8°$, $\tan \phi'_r = 0.140$, $c'_r = 0$

Description of specimen after test: Specimen halves very difficult to separate; slight amount of remolded material on shear plane, slight gloss, fine striations, almost no extrusion.

Run No.	σ tons/sq ft	Rate of Strain 10^{-2} in./hr	Horizontal Displacement: Per Run in.	Horizontal Displacement: Accumulated in.	Per Run at τ min in.	Accumulated at τ min in.	τ min tons/sq ft	Ratio τ/σ
1	8	0.25	0.24	0.24	0.24	0.24	1.43	0.18
2		1.56	0.25	0.49	0.25	0.49	1.28	0.16
3		4.33	0.26	0.75	0.19	0.68	1.45	0.18
4		1.81	0.29	1.04	0.21	0.96	1.42	0.18
5		4.83	0.29	1.33	0.14	1.18	1.48	0.18
6		5.17	0.31	1.64	0.20	1.53	1.50	0.19
7		1.94	0.31	1.95	0.09	1.73	1.44	0.18
8		4.83	0.29	2.24	0.08	2.03	1.37	0.17
9		0.35	0.25	2.49	0.11	2.35	1.28	0.16
10		2.31	0.37	2.86	0.06	2.55	1.28	0.16
11		3.47	0.26	3.12	0.03	2.89	1.04	0.13
12		5.00	0.30	3.42	0.09	3.21	1.29	0.16
13		2.00	0.32	3.74	0.12	3.54	1.27	0.16
14		4.50	0.27	4.01	0.10	3.84	1.19	0.15
15		2.25	0.36	4.37	0.10	4.11	1.21	0.15
16		4.67	0.28	4.65	0.09	4.46	1.22	0.15
17		0.44	0.28	4.93	0.07	4.72	1.21	0.15
18		4.17	0.25	5.18	0.08	5.01	1.22	0.15
19		2.06	0.33	5.51	0.10	5.28	1.23	0.15
20		4.50	0.27	5.78	0.09	5.60	1.20	0.15
21		1.81	0.29	6.07	0.06	5.84	1.15	0.14
22		4.17	0.25	6.32	0.06	6.13	1.15	0.14
23		1.81	0.29	6.61	0.08	6.40	1.10	0.14
24		4.17	0.25	6.86	0.06	6.67	1.08	0.14
25		1.94	0.31	7.17	0.06	6.92	1.20	0.15
26	4	4.33	0.26	7.43	0.10	7.27	0.58	0.14
27		0.45	0.29	7.72	0.06	7.49	0.58	0.14
28		4.17	0.25	7.97	0.09	7.81	0.58	0.14
29		2.06	0.33	8.30	0.04	8.01	0.58	0.14
30		5.00	0.30	8.60	0.06	8.36	0.57	0.14
31		1.94	0.32	8.92	0.08	8.68	0.58	0.14
32		5.00	0.30	9.22	0.08	9.00	0.57	0.14
33		1.94	0.31	9.53	0.04	9.26	0.59	0.15

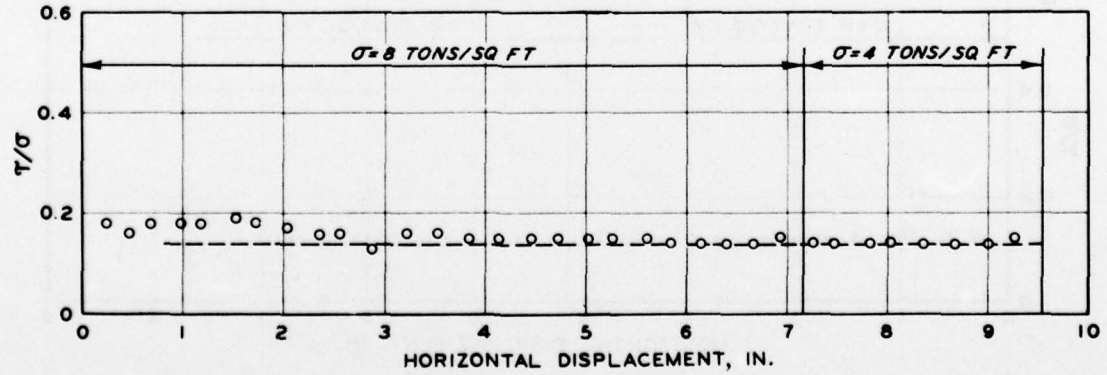

Fig. A22. Residual shear strength test results, boring WMS-1, Sample 14 (from Lutton and Banks, 1970)

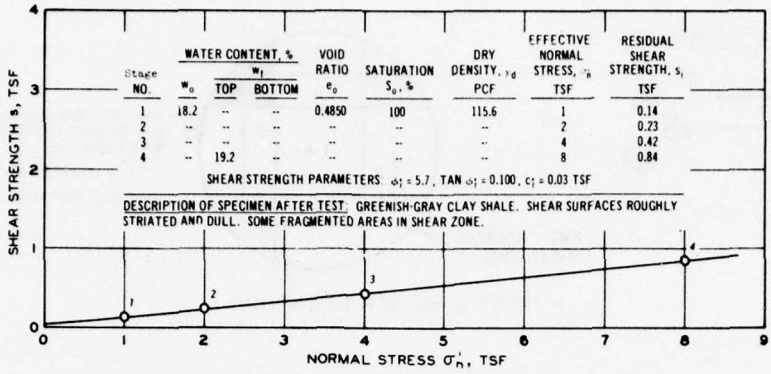

Stage NO.	WATER CONTENT, % w_o	WATER CONTENT, % w_f TOP	WATER CONTENT, % w_f BOTTOM	VOID RATIO e_o	SATURATION S_o, %	DRY DENSITY, γ_d PCF	EFFECTIVE NORMAL STRESS, σ'_n TSF	RESIDUAL SHEAR STRENGTH, s_r TSF
1	18.2	--	--	0.4850	100	115.6	1	0.14
2	--	--	--	--	--	--	2	0.23
3	--	--	--	--	--	--	4	0.42
4	--	19.2	--	--	--	--	8	0.84

SHEAR STRENGTH PARAMETERS: ϕ'_r = 5.7°, TAN ϕ'_r = 0.100, c'_r = 0.03 TSF

DESCRIPTION OF SPECIMEN AFTER TEST: GREENISH-GRAY CLAY SHALE. SHEAR SURFACES ROUGHLY STRIATED AND DULL. SOME FRAGMENTED AREAS IN SHEAR ZONE.

RUN NO.	EFFECTIVE NORMAL STRESS, σ'_n TSF	ACCUMULATED HORIZONTAL DISPLACEMENT IN.	SHEAR STRESS TSF	τ/σ'_n	RUN NO.	EFFECTIVE NORMAL STRESS, σ'_n TSF	ACCUMULATED HORIZONTAL DISPLACEMENT IN.	SHEAR STRESS TSF	τ/σ'_n
1	1	0.5	0.24	0.24	45	4	22.5	0.42	0.10
2		1.0	0.19	0.19	46		23.0	0.44	0.11
3		1.5	0.20	0.20	47		23.5	0.42	0.10
4		2.0	0.15	0.15	48		24.0	0.44	0.11
5		2.5	0.18	0.18	49		24.5	0.41	0.10
6		3.0	0.15	0.15	50		25.0	0.44	0.11
7		3.5	0.17	0.17	51		25.5	0.41	0.10
8		4.0	0.14	0.14	52		26.0	0.44	0.11
9		4.5	0.17	0.17	53		26.5	0.40	0.10
10		5.0	0.14	0.14	54		27.0	0.44	0.11
11		5.5	0.16	0.16	55		27.5	0.41	0.10
12		6.0	0.14	0.14	56		28.0	0.43	0.11
13		6.5	0.16	0.16	57		28.5	0.41	0.10
14		7.0	0.13	0.13	58	8	29.0	0.90	0.11
15		7.5	0.16	0.16	59		30.0	0.85	0.11
16		8.0	0.13	0.13	60		30.5	0.89	0.11
17	2	8.5	0.28	0.14	61		31.0	0.85	0.11
18		9.0	0.24	0.12	62		31.5	0.88	0.11
19		9.5	0.26	0.13	63		32.0	0.85	0.11
20		10.0	0.23	0.12	64		32.5	0.88	0.11
21		10.5	0.25	0.12	65		33.0	0.85	0.11
22		11.0	0.23	0.12	66		33.5	0.87	0.11
23		11.5	0.25	0.12	67		34.0	0.84	0.10
24		12.0	0.22	0.11	68		34.5	0.87	0.11
25		12.5	0.24	0.12	69		35.0	0.84	0.10
26		13.0	0.22	0.11	70		35.5	0.86	0.11
27		13.5	0.24	0.12	71		36.0	0.84	0.10
28		14.0	0.22	0.11	72		36.5	0.87	0.11
29		14.5	0.24	0.12	73		37.0	0.84	0.10
30		15.0	0.22	0.11	74		37.5	0.87	0.11
31		15.5	0.24	0.12	75		38.0	0.84	0.10
32		16.0	0.22	0.11	76		38.5	0.87	0.11
33		16.5	0.24	0.12	77		39.0	0.84	0.10
34		17.0	0.22	0.11	78		39.5	0.85	0.11
35		17.5	0.24	0.12	79		40.0	0.86	0.11
36	4	18.0	0.52	0.13	80		40.5	0.84	0.10
37		18.5	0.45	0.11	81		41.0	0.87	0.11
38		19.0	0.48	0.12	82		41.5	0.84	0.10
39		19.5	0.44	0.11	83		42.0	0.86	0.11
40		20.0	0.46	0.12	84		42.5	0.84	0.10
41		20.5	0.46	0.12	85		43.0	0.86	0.11
42		21.0	0.48	0.12	86		43.5	0.84	0.10
43		21.5	0.43	0.11	87		44.0	0.86	0.11
44		22.0	0.46	0.12	88		44.5	0.84	0.10

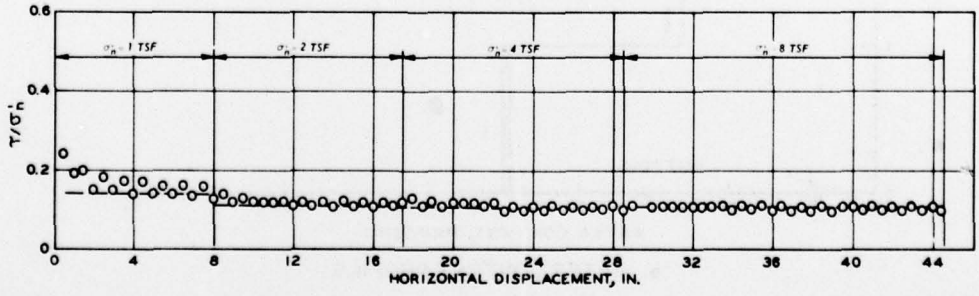

Fig. A23. Residual shear strength test results, boring WCSE-1, Sample 8 (from Banks et al., 1975)

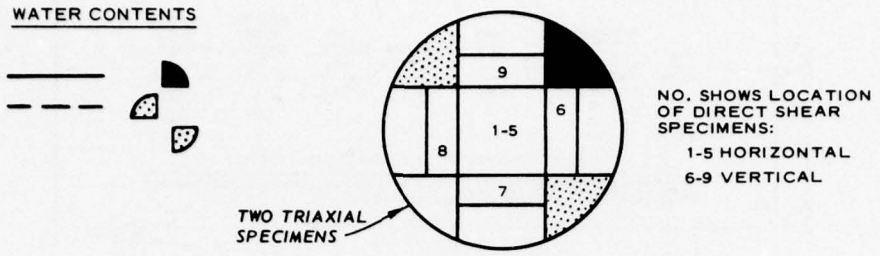

a. TEST SPECIMEN LOCATIONS

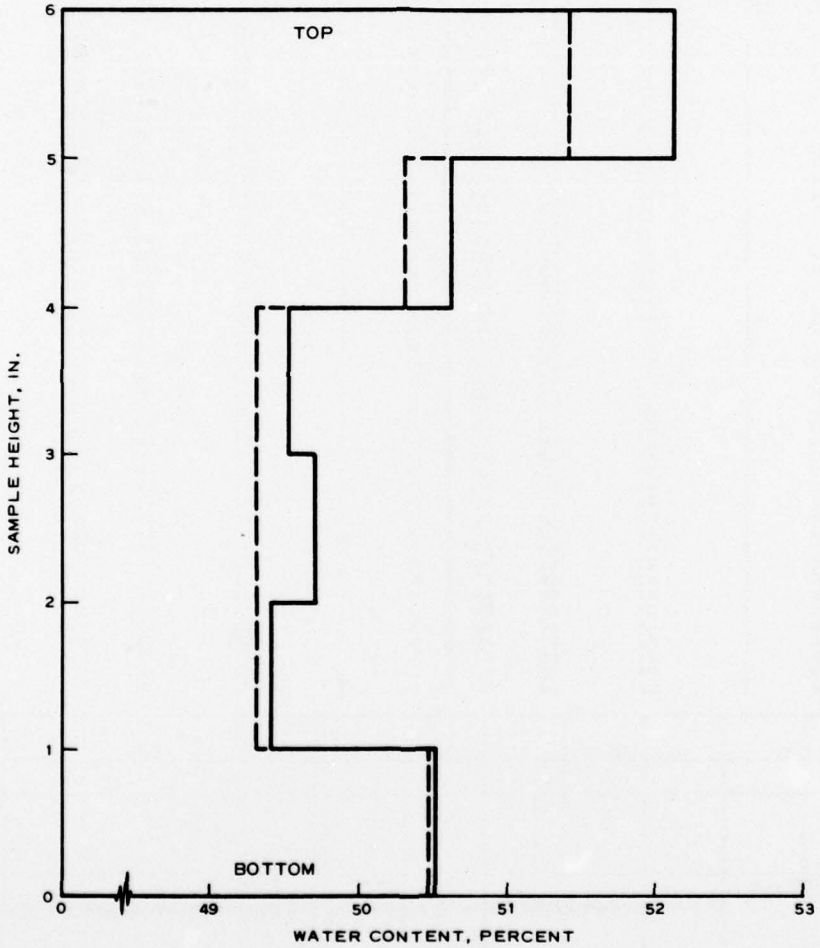

b. WATER CONTENT PROFILE

Fig. A24. Water content profile for slurry-consolidated sample (from Banks et al., 1975)

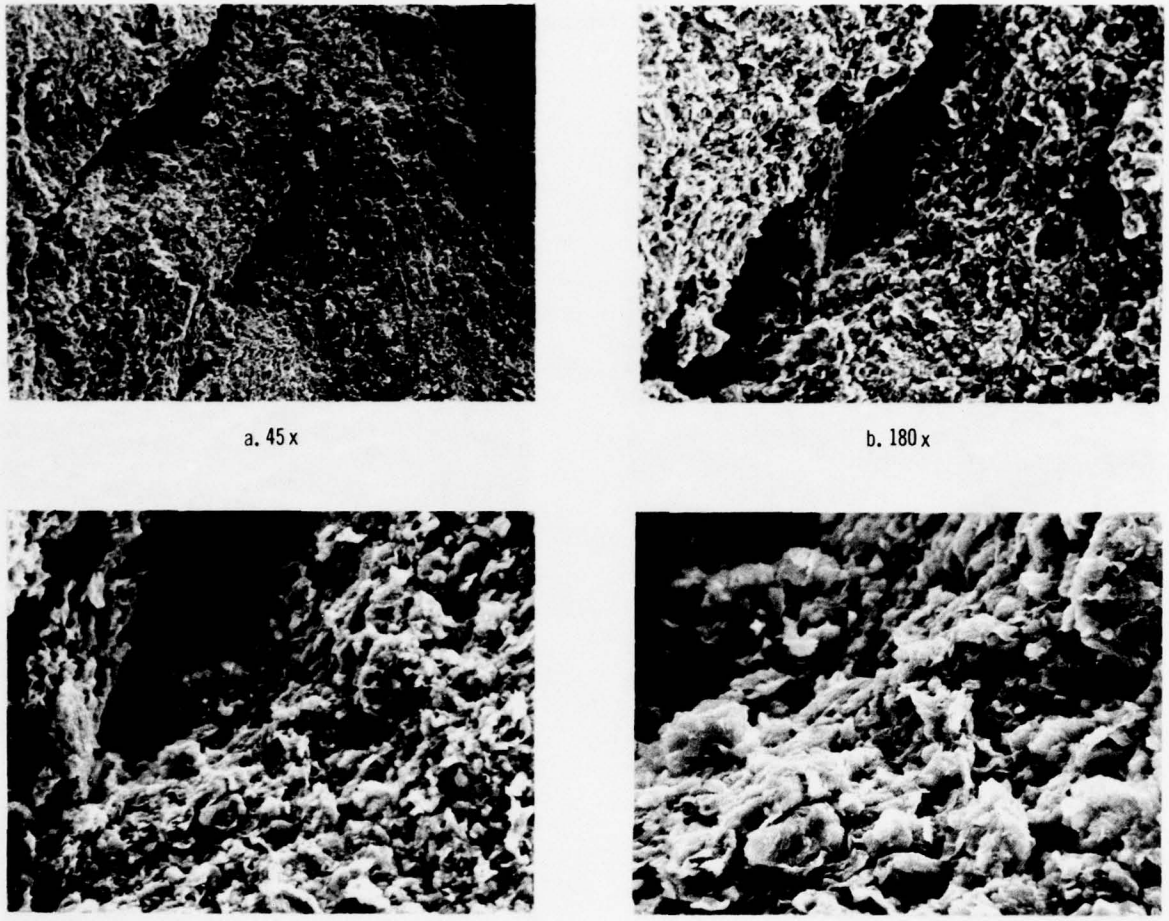

a. 45x

b. 180x

c. 450x

d. 900x

Fig. A25. Scanning electron microscope photograph of horizontal surface of slurry-consolidated sample (from Banks et al., 1975)

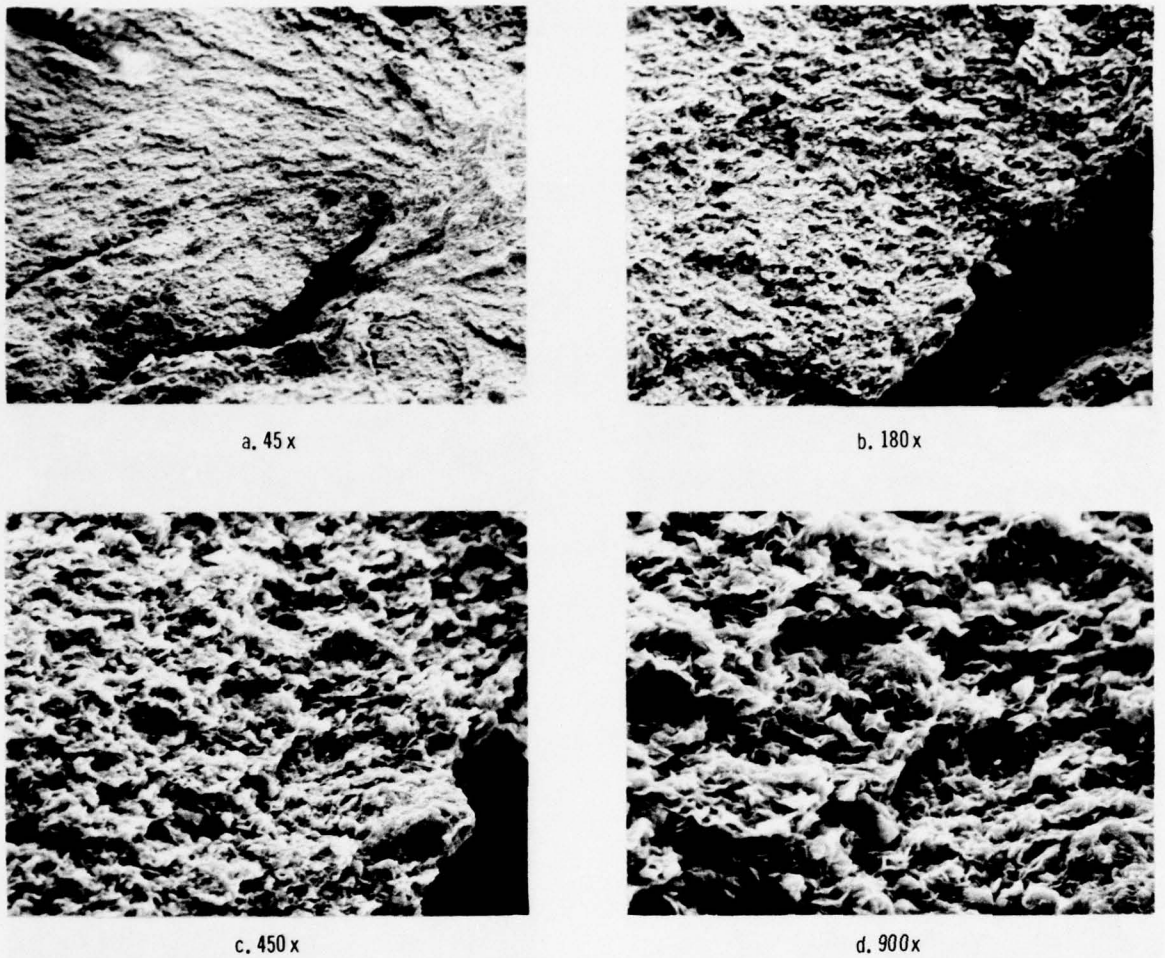

Fig. A26. Scanning electron microscope photograph of vertical surface of slurry-consolidated sample (from Banks et al., 1975)

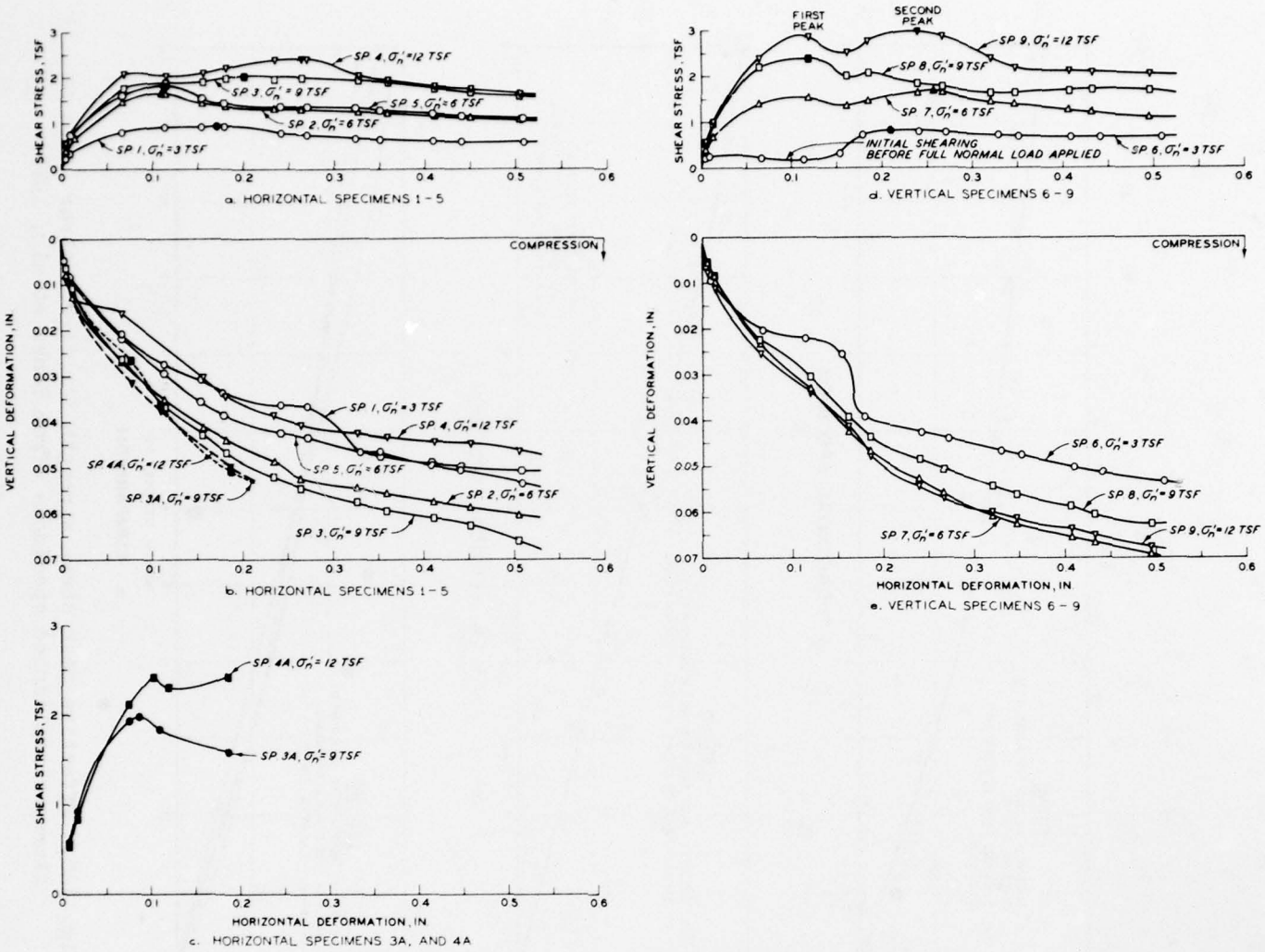

Fig. A27. Drained direct shear test results for slurry-consolidated specimens (from Banks et al., 1975)

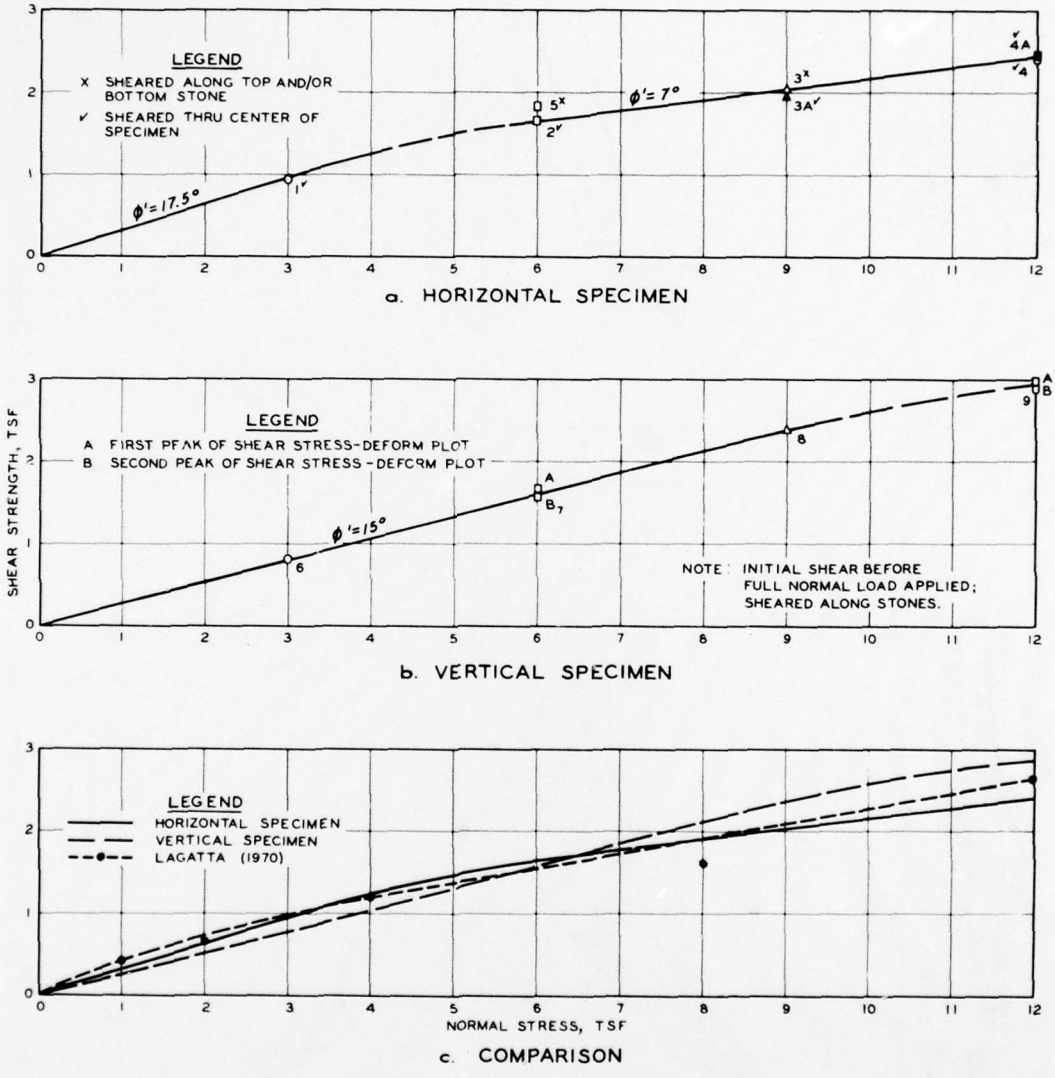

Fig. A28. Effective peak shear strength for direct shear tests on slurry-consolidated specimens (from Banks et al., 1975)

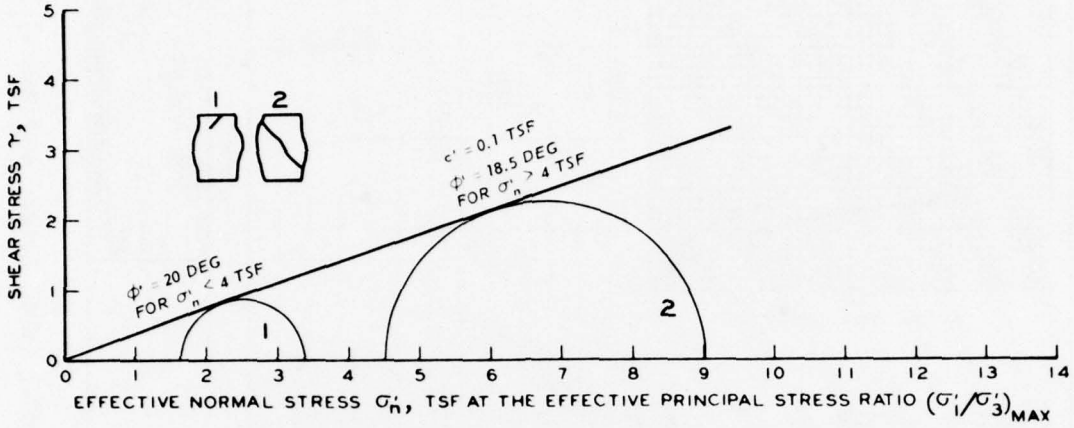

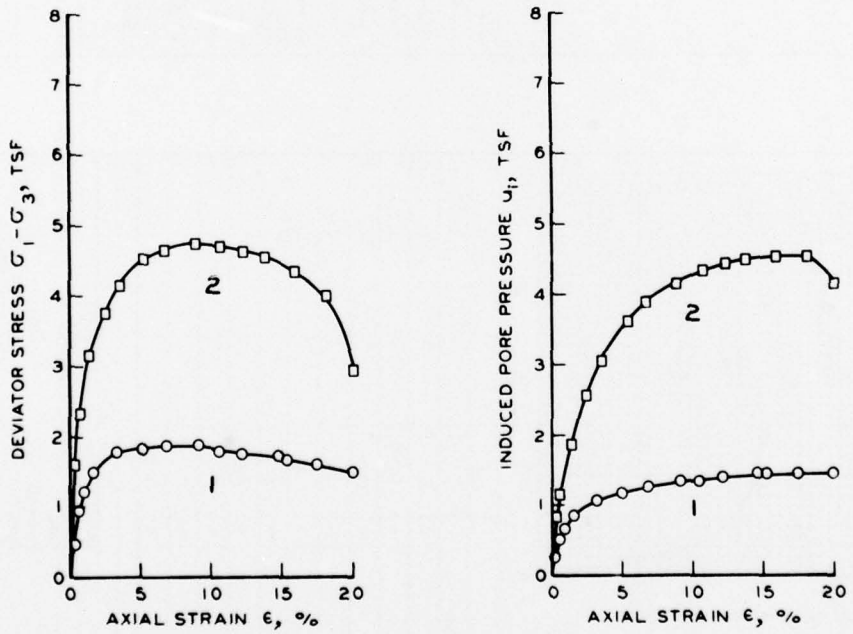

Fig. A29. Triaxial compression test ($\bar{R}$) results for slurry-consolidated specimens (from Banks et al., 1975)

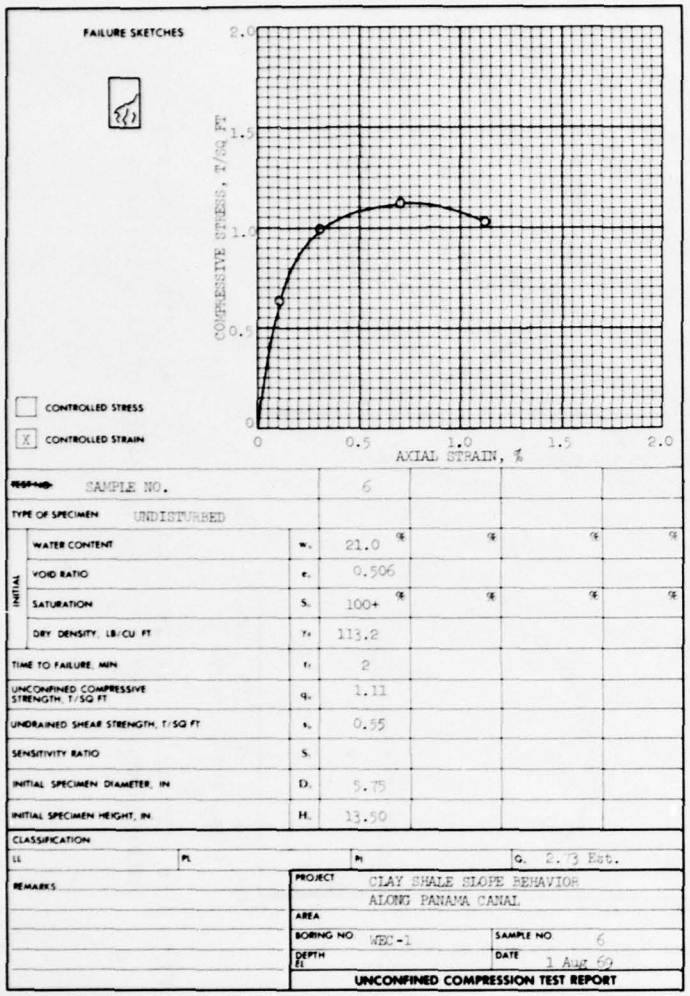

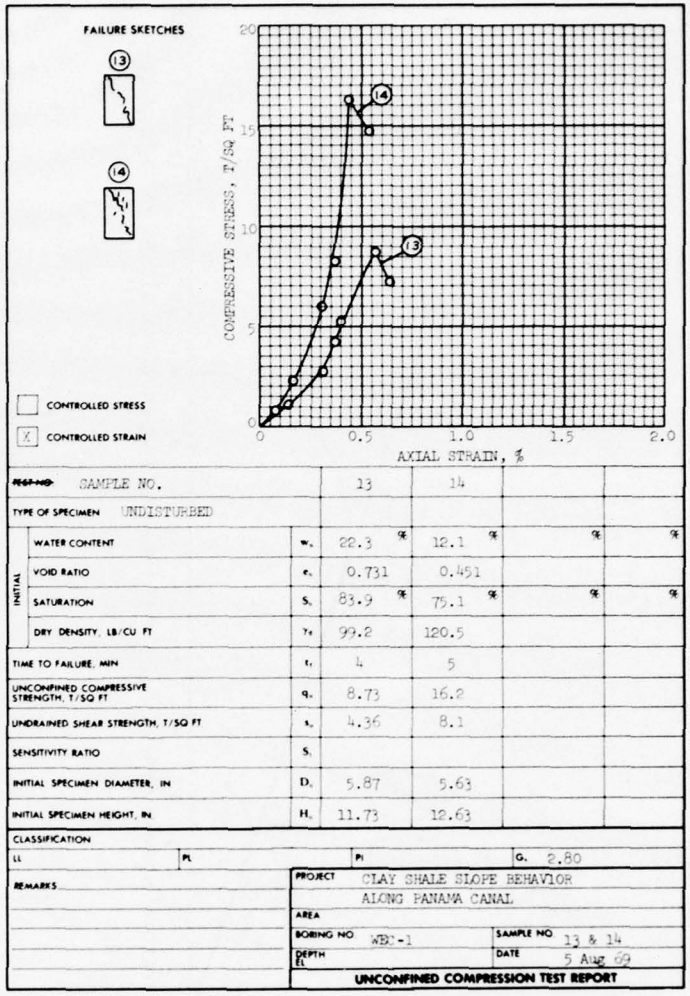

Fig. A30. Unconfined compression test results, boring WEC-1 (from Lutton and Banks, 1970)

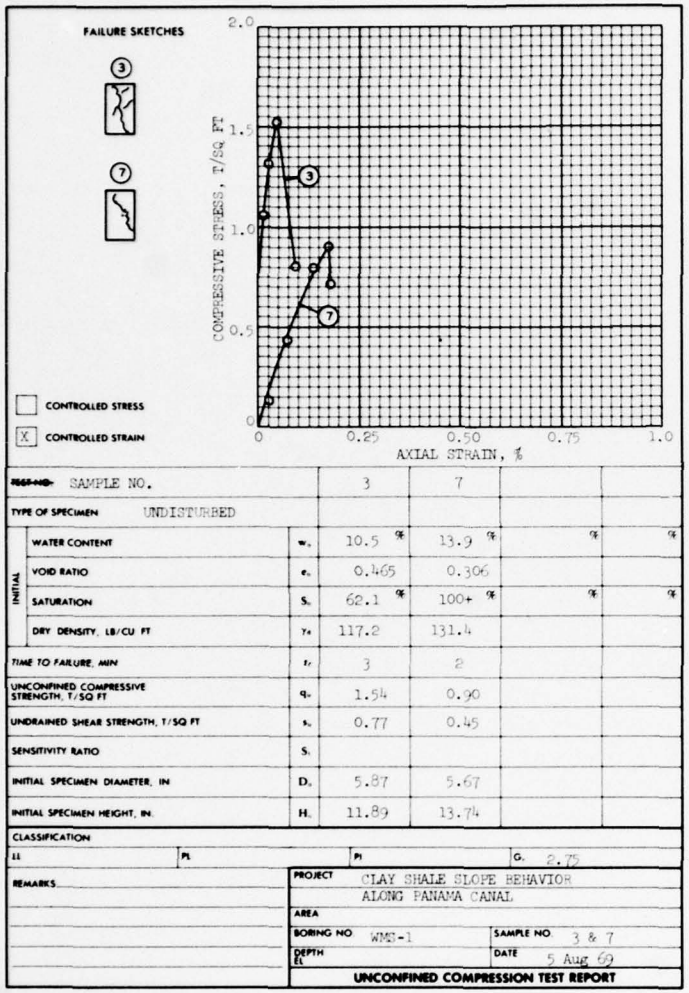

~~REG NO~~ SAMPLE NO.		3	7		
TYPE OF SPECIMEN UNDISTURBED					
INITIAL WATER CONTENT	w_o	10.5 %	13.9 %	%	%
INITIAL VOID RATIO	e_o	0.465	0.306		
INITIAL SATURATION	S_o	62.1 %	100+ %	%	%
INITIAL DRY DENSITY, LB/CU FT	γ_d	117.2	131.4		
TIME TO FAILURE, MIN	t_f	3	2		
UNCONFINED COMPRESSIVE STRENGTH, T/SQ FT	q_u	1.54	0.90		
UNDRAINED SHEAR STRENGTH, T/SQ FT	s_u	0.77	0.45		
SENSITIVITY RATIO	S_t				
INITIAL SPECIMEN DIAMETER, IN	D_o	5.87	5.67		
INITIAL SPECIMEN HEIGHT, IN.	H_o	11.89	13.74		

CLASSIFICATION
LL | PL | PI | G. 2.75

REMARKS

PROJECT: CLAY SHALE SLOPE BEHAVIOR ALONG PANAMA CANAL
AREA
BORING NO. WMS-1 SAMPLE NO. 3 & 7
DEPTH EL DATE 5 Aug 69

UNCONFINED COMPRESSION TEST REPORT

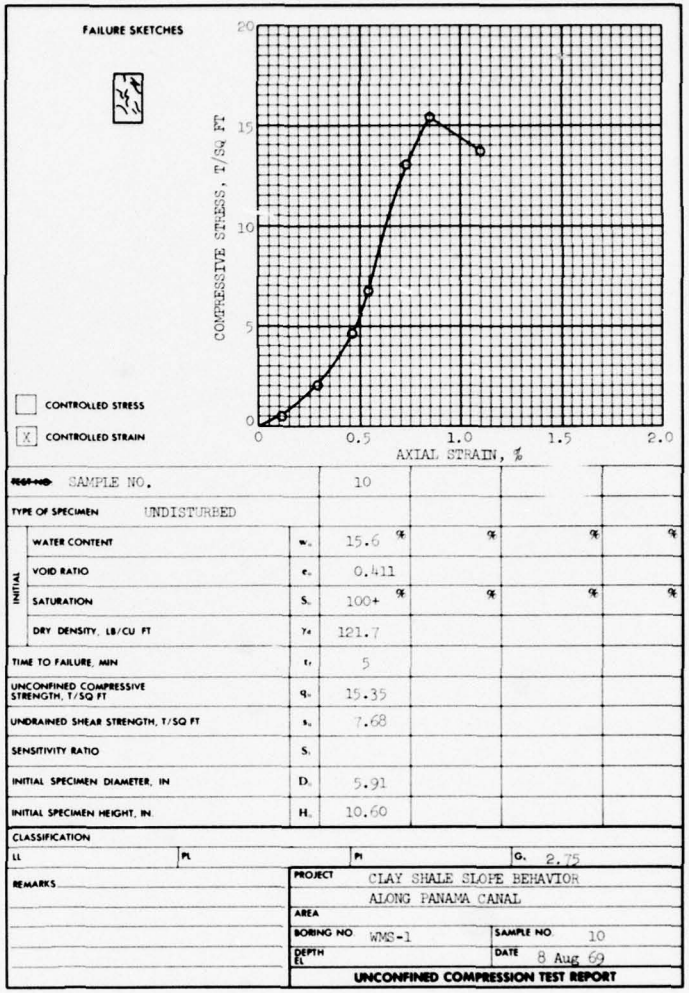

~~REG NO~~ SAMPLE NO.		10			
TYPE OF SPECIMEN UNDISTURBED					
INITIAL WATER CONTENT	w_o	15.6 %	%	%	%
INITIAL VOID RATIO	e_o	0.411			
INITIAL SATURATION	S_o	100+ %	%	%	%
INITIAL DRY DENSITY, LB/CU FT	γ_d	121.7			
TIME TO FAILURE, MIN	t_f	5			
UNCONFINED COMPRESSIVE STRENGTH, T/SQ FT	q_u	15.35			
UNDRAINED SHEAR STRENGTH, T/SQ FT	s_u	7.68			
SENSITIVITY RATIO	S_t				
INITIAL SPECIMEN DIAMETER, IN	D_o	5.91			
INITIAL SPECIMEN HEIGHT, IN.	H_o	10.60			

CLASSIFICATION
LL | PL | PI | G. 2.75

REMARKS

PROJECT: CLAY SHALE SLOPE BEHAVIOR ALONG PANAMA CANAL
AREA
BORING NO. WMS-1 SAMPLE NO. 10
DEPTH EL DATE 8 Aug 69

UNCONFINED COMPRESSION TEST REPORT

Fig. A31. Unconfined compression test results, boring WMS-1 (from Lutton and Banks, 1970)

In accordance with letter from DAEN-RDC, DAEN-ASI dated 22 July 1977, Subject: Facsimile Catalog Cards for Laboratory Technical Publications, a facsimile catalog card in Library of Congress MARC format is reproduced below.

Banks, Don Charles
Study of clay shale slopes along the Panama Canal; supplemental report: A reanalysis of the East Culebra Slide, Panama Canal / by Don C. Banks. Vicksburg, Miss. : U. S. Waterways Experiment Station ; Springfield, Va. : available from National Technical Information Service, 1978.
xiii, 249 p. : ill. ; 27 cm. (Technical report - U. S. Army Engineer Waterways Experiment Station ; S-70-9, Supplemental report)
Prepared for Office, Chief of Engineers, U. S. Army, Washington, D. C., and The Panama Canal Company, Balboa Heights, Canal Zone.
Literature cited: p. 191-197.

1. Clay shales. 2. East Culebra Slide. 3. Panama Canal. 4. Shear strength. 5. Slides. 6. Slope failures. I. Panama Canal Company. II. United States. Army. Corps of Engineers. III. Series: United States. Waterways Experiment Station, Vicksburg, Miss. Technical report ; S-70-9, Supplemental report.
TA7.W34 no.S-70-9 Supplemental report